# Reservoir quality determination and modelling of unconsolidated Canadian Oil Sands reservoir following analytical techniques


Kanad Kulkarni

School of Engineering

University of Portsmouth

This Dissertation is submitted for the degree of

Doctor of Philosophy

February 2018

I would like to dedicate this thesis to my loving parents, late grandparents, my wife and my in-laws…….

# Declaration

Declaration I Kanad Sadashiv Kulkarni hereby declare that except where specific reference is made to the work of others, the contents of this dissertation are original and have not been submitted in whole or in part for consideration for any other degree or qualification in this, or any other university. This dissertation is my own work and contains nothing which is the outcome of work done in collaboration with others, except as specified in the text and Acknowledgements. This dissertation contains fewer than 65,000 words including appendices, bibliography, footnotes, tables and equations and has fewer than 250 figures.

Kanad Sadashiv Kulkarni

February 2018

# Acknowledgements

First and Foremost, I want to thank my supervisor Dr Mohamed Hassan. It has been an honour to be his Ph.D. student. He has taught me, both consciously and unconsciously, how a Ph.D. thesis can be completed. I appreciate all time, efforts and support he has provided me through this research. His invaluable contribution has helped me complete this Ph.D. It has been great joyous working with you and debating on several important topics within this Ph.D. It would have been extremely difficult to complete this project.

I would like to extend my special thanks for Dr Richard Wheaton for his wealth of knowledge and support provided to me in completing chapter 6 of this Ph.D. I would like to further extend my gratitude to Dr David Franklin for his support through this Ph.D. at the University of Portsmouth your timely feedback and continuous guidance has been of immense importance. Your support in assisting me to secure funding for this research at the University of Portsmouth has made this project possible.

I would like to extend my gratitude to Ms. Rachna Parwani and Dr Alexander Kao for their assistance in providing very high quality micro CT scans through University of Portsmouth's Zeiss Global Centre. Your contribution has facilitated me with dataset that formed an essential component of this thesis.

My sincere thanks to Dr Julie Dee Bell for her support and supervision from 2011 to 2013. Your time, efforts and guidance was invaluable during my time at the LSBU. Your enthusiasm and focus on this subject allowed us to acquire samples from University of Alberta and outcrop samples from Canada. Furthermore, I would like to thank Dr Helen Turnell, Dr John Orin and Dr David Roberts for their guidance and support during my time at LSBU. Dr David Roberts your emotional support and guidance during my 2011 to 2014 has been invaluable and has allowed me to stay focused on this Ph.D. I would like to thank Mr. Lam Chung for your support and training on SEM laboratories to acquire SEM images for analysis within this project.

Special thanks to SkyScan for providing initial 8μm scan of all three core samples for 2D analysis of data. Furthermore, I wish to extend my gratitude to National Research

Council in Italy for helping us develop this section for such a complex unconsolidated sample.

I would like to take this opportunity to thank all students (Anane Boateng, Gabriel Okoloh , Mario Kazniakowski , Ovie Eruteya, Linda Morris, Adebimpe Momoh, Victoria Umejuru , Nasir Shah, Johan Fianu, Nikolas Pachipis, Luke Day, Helen Nodland, Sunny Mann, Boluwatife Olofun ) that have worked with me on peripherals projects related to this project in London South Bank University and University of Portsmouth. Your contribution has been extremely valuable and has contributed to some parts of this Ph.D.

I would like to thank my employer University of Portsmouth for funding my research since 2014 and facilitating me time to perform this research during my time at the University.

I would like to begin by remembering my late grandfather who believed in me and enthused me to apply for this Ph.D. your advice of persuasion has been my source of determination through difficult times during this Ph.D. My utmost gratitude to my parents and sister for their moral and financial support during this Ph.D. Your blessing and well wishes have always been source of power and determination to complete this project. My special thanks to my Wife for being my better half and supporting me all through this Ph.D. you care and support has facilitated me to undertake this project and complete my Ph.D. The blessing and well wishes bestowed upon me by my in laws have helped me achieve this success.

# Abstract

Canadian Oil Sands covering an area of 142,000KM$^2$ boasts one of the largest heavy oil proven reserves standing at 166 Bbbl. This volume makes it a promising prospect for the future of the oil and gas industry. Though, having large reserves it is not the easiest to produce from. The oil in this region is categorized as heavy, extra heavy to bituminous which means that it is highly viscous and incapable of flowing without reducing viscosity. Furthermore, the Geology for this reservoir is heterogeneous with bioturbated sections which adds to the complexity. Additionally, lack of cementing matrix within formation makes this reservoir an unconsolidated reservoir. The unconsolidated nature introduces challenges during routine core analysis leading to the inaccurate results and in certain cases questions reliability of the methodology followed to assess this reservoir. The lack of any reliable work flow with methodologies act as a primary research gas for this thesis.

Owing to aforementioned reasons, this study aims to establish a new workflow to determine properties from unconsolidated reservoirs, that includes use of Thin section analysis, Scanning Electron Microscopy (SEM), micro-CT techniques followed by image analysis to determine morphological and reservoir properties to simulate the reservoir to test applicability of the said workflow.

To achieve set aims this research has made good use of thin sections that were prepared from outcrop samples and has followed further with detailed studies on core samples. Analysis of the thin sections has demonstrated arrangements. SEM and micro CT are able to provide properties more reliably than RCAL analysis. The simulations developed to test applicability of the properties followed has demonstrated variations to the recovery that can be observed by applying variety of porosity and permeability determined following the workflow of this thesis. Furthermore, the effect of bioturbation can also be observed with variation to the production volume observed as part of the simulation results.

# Publications Through this research

1. Fianu J, Hassan M,Kulkarni K, Pachipis N,Turnell H (2016) Bioturbation in Athabasca oil sands: Property modelling and simulation. (Submitted)
2. Aminu MD, Kulkarni KS (2015) The Influence of Grain Morphology on Reservoir Quality of Some Athabasca Oil Sands Samples. 2015 Journal of Geology & Geoscience.
3. Julie D. Bell; Kanad Kulkarni; Linda Morris and Adebimpe Momoh. Oil Sands Fabric: The Grain Component and Influences on Reservoir Properties. 3rd June 2015 AAPG Annual Convention and Exhibition, Denver, Colorado
4. Bell, Julie; Kulkarni Kanad; and Maraj Marsha. Novel Approach to Determining Unconsolidated Reservoir Properties: Fabric and Flow in Oil Sands. 2013 Unconventional Resource Technology Conference (URTeC) Denver, Colorado.
5. Bell, Julie; Eruteya, Ovie; and Kulkarni, Kanad. Effect of Bioturbation on Oil Sand Fabrics and Implication for Reservoir Quality. 2012 GSA Annual Meeting, Charlotte

# Table of Contents

# List of Figures

# List of Tables

# List of Equations

# 1 Introduction

## 1.1 Introduction

Over the years due to the lack of new discoveries of large conventional resources. Unconventional forms of oil and gas have acquired significant importance. Heavy oil can be found in nearly seventy different countries around the world including Venezuela, USA, Russia and Canada. Canadian Oil Sands being one of the biggest resource of unconventional reservoir as they hold significant importance to the future development of the Oil and Gas industry.

Alberta's proven oil sands reserves were found to be around 166 billion barrels (Bbbl) in 2014 (Government of Alberta - Energy, 2014). As seen in Figure 1-1The majority of the oil reserves can be found across 142,200 $KM^2$ across three Alberta deposits namely: the Athabasca, Peace River and Cold Lake (Whalley & Krinsley, 1974).

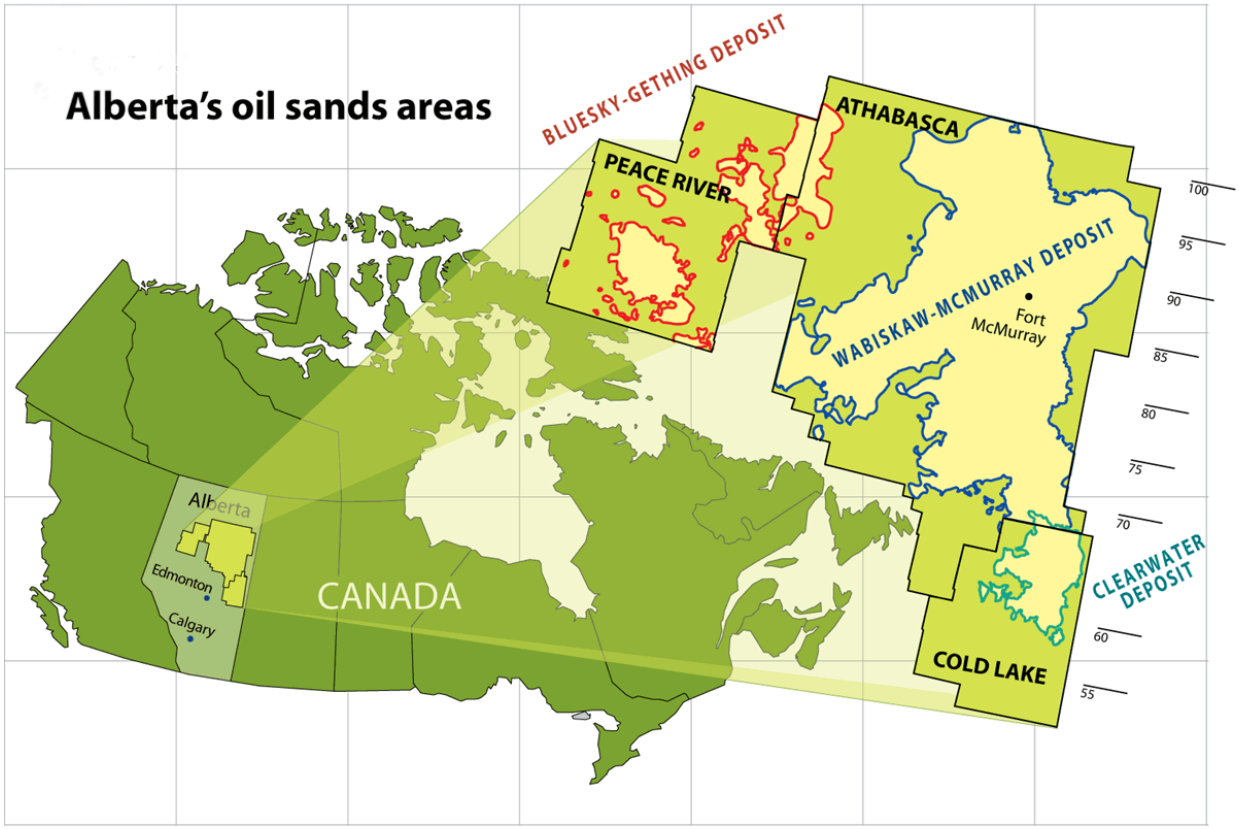


*Figure 1-1 Location Map of McMurray formation (Gulfport Energy, 2013)*

Unconventional oil and gas typically have reservoirs that vary from the conventional petroleum system models. For oil sands, the reservoir is not a consolidated rock, instead it is composed of unconsolidated to moderately consolidated sands. The petroleum product in oil sands is bitumen or ultra-heavy oil, being less than 10° API (Dusseault, 2001). Bitumen is a naturally occurring product of petroleum that can be described as a "black or dark-coloured (solid, semi-solid, viscous, amorphous, cementitious material" The viscosity of the oil in the Canadian Oil Sands varies depending on the area of interest. It has been found to vary between <1000 cP > 15°API oil such as in Pelican Lake and Amber Lake to values greater than 1 million cP found on the surface of the Athabasca deposit. (Oil Sands Fact Check, 2014).

Though being a large deposit only 3% or 1,850 square miles can be recovered through mining operations. The rest of the 97% can only be recovered by in-situ recovery techniques such as Steam Assisted Gravity Drainage (SAGD) or Cyclic Steam Simulation (CSS) due to its high viscosity values (Whalley & Krinsley, 1974).

Even though there are several recovery techniques available, effective and economical implementation of these techniques is challenging due to unreliable reservoir quality data that is obtained through routine core analysis.

## 1.2 Problem identification

As stated above, challenges associated with oil sands range from technical to environmental. The environmental concerns include land use and waste management especially in the case of surface mining which disturbs the Boreal Forest water management as vast amounts of water resources are used during separation of oil and sand, causing air pollution amongst other challenges. These challenges are of serious concern to environmental groups and have had an economic impact on the Canadian economy.

Technical challenges stem from accuracy of porosity and permeability data obtained through routine core analysis technique which is used in the determination of properties that are input to the simulation setup to study the reservoir under consideration. The primary source of this challenge is a result of the unconsolidated nature within the Canadian Oil Sands more specifically McMurray formation which is the principal unit hosting the bitumen.

As discussed by (Carrigy, 1967) and (Czarnecki, B., L., & R., 2005), the principle components of the oil sands are quartz grains which form the bulk of the oil sand material with bitumen and water. As stated by (Bell J. B., 2011) (Bell, Eruteya, & Oono, 2012) the Middle McMurray Formation is made up of mixed wet oil sands 70% sand and clay, 10% water and 0-18% bitumen wherein the reservoir quality is strongly dependent upon the fabric attributes.

As observed from the preliminary study and thin section images in Figure 1-2 the reservoir is predominantly made up of quartz grains, matrix, voids and bitumen. The study published by (Bell, Eruteya, & Oono, 2012) was also able to demonstrate evidence of bioturbation in the region. Bioturbation which creates heterogeneities that alter the host material reservoir qualities including porosity and permeability.

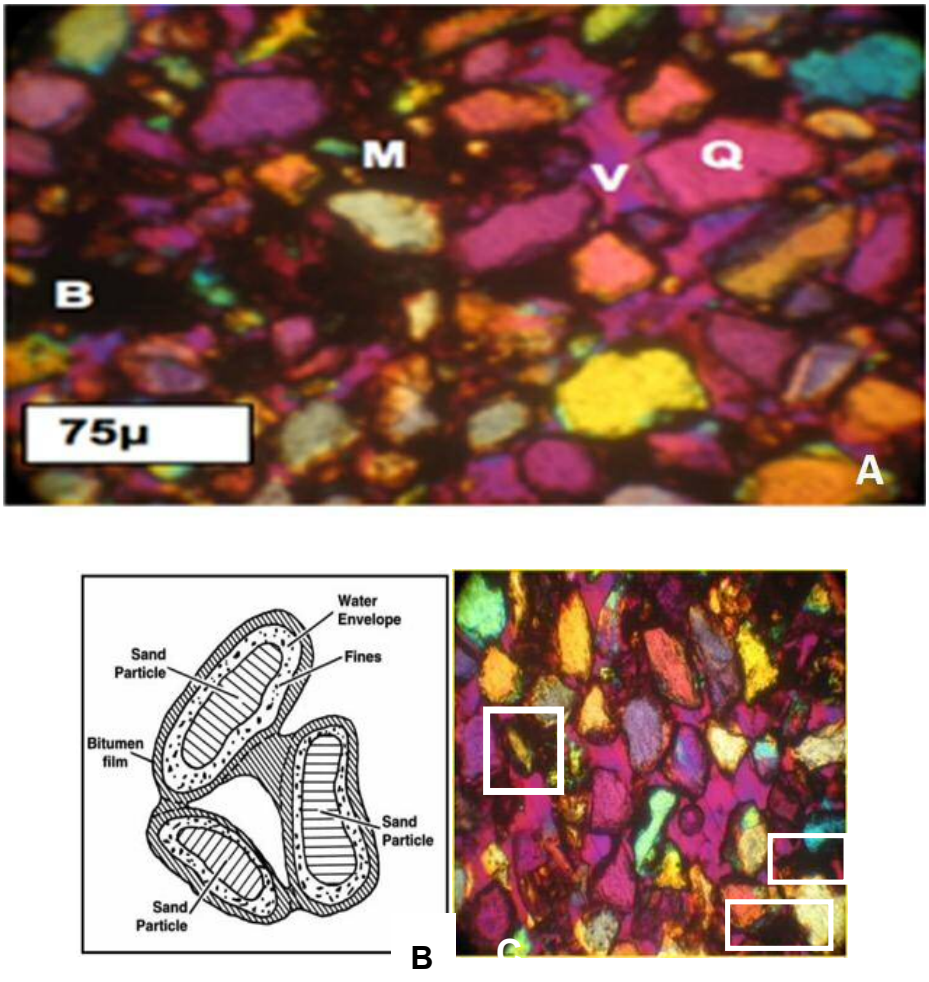


*Figure 1-2 A) Photomicrograph of host material with the components. B) Idealized diagram of Athabasca Oil Sands. C) Photomicrograph showing clay bridges between the quartz grains (Bell, Eruteya, & Oono, 2012)*

Core analysis requires samples to be cleaned prior to tests, furthermore Routine core analysis techniques requires samples to be held in sleeve and maintain its integrity to

predict properties accurately as the samples are subjected to high pressures during the tests. This is not achievable with the reservoir under consideration due to its unconsolidated nature and lack of cementing matrix as observed from preliminary studies. As soon as samples are subjected to soxhlet cleaning they lose integrity and become loose sand becoming unsuitable to perform any tests.

There are generally five in-situ methods for bitumen extraction namely, Steam Assisted Gravity Drainage (SAGD), Cyclic Steam Stimulation (CSS), Vapour Extraction Process (VAPEX), Toe to Heel Air Injection (THAI) and Cold Heavy Oil Production and Stimulation (CHOPS). SAGD is a widely implemented method that will be further elaborated upon – SAGD utilizes two horizontal wells drilled into the target formation with one of the wells at the bottom of the formation and the other about 5 metres above it; the upper well is a steam injection well and the lower well a producer well which produces oil, steam and condensates (McCormack, 2001). The success of this operation is based theoretically on two principal governing factors; thermal conductivity of the oil sands which affects the heat transfer between the reservoir and the injected steam and the flow of molten bitumen and condensates under gravity to the producing wells from where it is pumped out. (McCormack, 2001) This flow under gravity is a function of several factors ranging from viscosity of the oil to the properties of the reservoir material in the oil sands reservoir.

To overcome some of the aforementioned challenges, a detailed study on morphological and reservoir properties was carried out on oil sands samples from the estuarine environment of the McMurray Formation from the Athabasca region in Canada. The study investigates preliminary fabric characteristics of components of estuarine depositional environments – from both outcrop and core samples and attempts to identify variations observed in modelling through a series simulation studies.

The concept of soil fabric is followed which was first introduced by Kubiena (1938) as “the arrangement of constituents of the soil in relation to each other”. Brewer and Sleeman (1960) furthered this concept referring to fabric as the relative distribution of ‘skeleton grains’ and ‘plasma’. Later Stoops (2003) further defined the elements of fabric as ‘spatial distribution, orientation, size, sorting and shape of the material under consideration.

In this study, a 2D fabric analysis is carried out from a thin section. Further to studying morphological properties and determining porosity and permeability, SEM and micro-CT analysis techniques have been followed.

Since SEM analysis studies sample on 2D surface properties, all samples were cleaned and analysed for morphological properties. A selective set of samples were also analysed for transportation and weathering characteristics. Micro CT being a non-invasive method, this method was able to provide 2D and 3D images of the integrated samples to determine porosity and permeability that could be applied in simulation models.

To test the applicability of the results obtained through this study a representative simulation model has been developed and studied in comparison with published work of (Shin & Polikar, 2005).

To undertake this study several outcrop samples and few core samples were obtained from Canada. The outcrop samples were collected from Hangingstone River outcrop location and the core samples were collected around 350 km away from the Peace river location where the samples are deposited at the depth of around 80 - 100 m.

## 1.3 Aims and Objectives of this project

To overcome problems identified in section 1.2 the following aims and objectives were set for this PhD.

### 1.3.1 Aims

The aims of this study are set to test and develop a new workflow that can obtain morphological and reservoir properties from an unconsolidated reservoir following Thin Section Analysis, SEM analysis and micro CT analysis techniques, and to further test the results obtained through a representative simulation case study.

### 1.3.2 Objectives

- Perform literature review on Canadian Oil Sands, property determination through unconsolidated reservoirs and simulation case studies from the Canadian Oil Sands
- Perform morphological studies on outcrop and core samples following a) thin-section analysis, b) SEM, c) micro-CT (image analysis).
- Determine Porosity and Permeability of all three core samples through the use of 3D micro CT
- Test applicability of morphological properties and porosity, permeability obtained through this study by developing a representative geo model.
- Perform simulation study using CMG STAR simulator.

## 1.4 Thesis Outline

This thesis is divided into the following six chapters that include:

1. Chapter 1: Introduction
2. Chapter 2: Literature review
3. Chapter 3: Methodology
4. Chapter 4: Results /Findings
5. Chapter 5: Discussion/ Evaluation of Results
6. Chapter 6: Conclusion

The details of what each chapter contains can be found on the following pages:

Chapter 1: Introduces the thesis and provides problem statement and sets out the aims and Objectives for this PhD.

Chapter 2: Provides literature review conducted on reservoir, methods, simulation studies studied during this research.

Chapter 3: Provides details of sample collection and methodology followed through this research in order to obtain presented results.

Chapter 4: This chapter provides results from Thin Section analysis, SEM analysis, micro CT analysis and simulation studies.

Chapter 5: This chapter discusses the new framework setup and results from all the three methods in context one another. Further this chapter discusses simulation outcomes in context of the method being followed as part of this PhD.

Chapter 6: Provides conclusions drawn through this PhD along with future recommendations.

# 2 Literature Review

## 2.1 Oil Sands

### 2.1.1 Heavy Oil generation

Most of the heavy oil in the world is generated by aerobic bacteria or biodegradation. This process takes place at shallow depths of 5,000 ft. or less and temperatures below $176^0$F. The three main steps in this process include water washing, bacterial degradation, and evaporation. The process begins by the expulsion of light crude oil from the source rock and the subsequent migration to a trap. If the trap lies in an elevated oxidizing zone with an active water supply, the water carries bacteria, inorganic nutrients and oxygen to the trapped oil or the reservoir. This active water then removes low molecular weight hydrocarbon components and hydrogen sulfide which is a toxic by product (Baker, 1976)

According to Larter *et al* (2006), the third process is also biodegradation and identical to the previous process. The main differences are that this process is anaerobic and hence does not need fresh water and occurs in deeper or subsurface reservoirs. The main conditions for this degradation to take place are that the reservoir must have a water leg and that the temperature should not exceed $176^0$F.

### 2.1.2 Chemical and Physical Properties

The main differences that exist between light and heavy crude oils are the volatilities of the hydrocarbon fractions such as the paraffinic, naphthenic and aromatic constituents.

During biodegradation, light hydrocarbon fractions are lost; converting it to heavy oil containing significant proportions of asphaltic molecules. This is due to the substitution of nitrogen, sulphur and oxygen into the carbon network. These asphaltic molecules are characteristically heavy and consist of resins, asphaltenes and preasphaltenes (carbine-carboids) (Yen, 1984). The final form of the naphtheno-aromatic molecules are these resins and asphaltenes that are important contributors during processes of accumulation, recovery, processing and utilization of hydrocarbons. Heavy oil contains up to 50 weight percentage of asphaltenes.

The increase or decrease in density or viscosity of oil is controlled by the presence and amount of these large asphaltic molecules. In other words, the rheological properties of given oil and its aromacity is affected by the reduction of asphaltenes and preasphaltenes. In actual fact, all heavy oils contain asphaltenes. Asphaltenes are hereby defined as the crude oil fraction that precipitates upon addition of an n-alkane which may be n-pentane or n-heptane, meanwhile remains soluble in toluene or benzene. According to the Tissot and Welte (1978) crude oil classification scheme, aromatic-naphthenics and aromatic-asphaltic are the main characteristics of the heavy oil deposits of Canada and Venezuela which are the two largest heavy oil deposits in the world. The changes in physical and chemical properties of heavy oil are significantly reflected in the capital and operating expenses needed for the recovery, transportation, processing and environmental issues.

### 2.1.3 Geological setting of Heavy oil from around the world

One important way of describing heavy oils, is to relate its occurrence to the type of geological environment in which they are found. This is accomplished by describing the distribution and accumulation of heavy oil in the various geological basins scattered around the world. In principle, the amount of total known heavy oil is 8,900 billion barrels of original oil in place. In addition, there is probably a further 1,023 billion barrels of prospective resource (amount of unmeasured resource). On a regional scale, Middle East, North and South America have the largest heavy oil in place. However, the western hemisphere accounts for about 68.5 percent of the world's heavy oil. It is believed that there is a very large heavy oil resource deposit in Siberia, Russia but there are insufficient data to prove it. The global heavy oil resource is dispersed in 281 basins located all around the world. These basins are however grouped into seven basic major basins. The seven major basins were classified using the Klemme Basin Classification. According to Klemme (1980b, 1983, and 1984), the basin type, heavy oil accumulation and area of occurrence are as follows:

1. Type I- Interior Craton Basins contains 63 billion barrels with 95 percent occurring in Illinois, USA and Tunguska, Eastern Siberia basins
2. Type II- Continental Multi cyclic Basins
    a. Craton Margin (Composite) contains 158 billion barrels of the lighter type of heavy oil with 78 percent accumulated in West Canada Sedimentary

(North America), Putumayo (Columbia/Ecuador) and Volga-Ural (Russia) basins. This basin type contains 48 percent of world bitumen (heavier type of heavy oil) which is 2,623 billion barrels. However, 89 percent (2,334 billion barrels) of this amount occur in Athabasca, Cold Lake and Peace River deposits in Alberta, Canada.

b. Craton Accreted Margin (Complex) contains 215 billion of heavy oil located in West Siberia and Timan-Pechora basins in Russia.

c. Craton Collision Zone (Convergent Plate Margin) contains half of the world's total oil and gas. This type contains 1,610 billion barrels of lighter heavy oil with 95 percent located in Arabia, Eastern Venezuela and Zagros (Iran/Iraq) basin. The same type contains *2,507 billion barrels of which 83 percent is located in the Orinoco Oil Belt in Eastern Venezuela*

**3.** Type III- Continental Rifted Basins

a. Craton and Accreted Zone (Rift) contains 222 billion barrels of lighter heavy oil with the Bohai Gulf accounting for 63 percent, Gulf of Suez 11 percent and Northern North Sea 10 percent. They also contain 22 billion barrels of bitumen with half of it located in Northern North Sea basin.

b. Rifted Convergent Margin (Oceanic consumption) contain 534 billion barrels of lighter heavy oil with 323 billion barrels (60 percent) located in the Maracaibo basin (Venezuela/Columbia), 129 billion barrels (24 percent) in California (USA) and41 billion barrels (8 percent) in Central Sumatra (Indonesia). They also contain 231 billion barrels of which 178 billion barrels (77 percent) is located in the Maracaibo basin.

c. Rifted Passive Margin (Divergent) contains 158 billion barrels of lighter heavy oil with the Campos Basin in Brazil accounting for 66 percent. The bitumen accumulation is 47 billion barrels, out of which 38.3 billion barrels (80 percent) is located in the Ghana Basin (Ghana/Nigeria)

**4.** Type IV- Delta (Tertiary to Recent) contains 37 billion barrels of lighter heavy oil and no bitumen accumulation

**5.** Fore-Arc Basins contains no heavy oil.

### 2.1.4 Western Canada Basin

The Western Canada Basin as a whole covers an area of 142,000 $Km^2$ in the western part of North America. Figure 1-1, Figure 2-1 It comprises mainly of sediments ranging from Early Paleozoic to Early Tertiary age. The development of this basin in the Early Paleozoic took place in two main tectonic phases;

First Phase: This phase comprises Paleozoic to Jurassic platformal succession, which was laid down on the stable craton adjacent to the dominantly passive margin of North America and is characterised by carbonate rocks.

Second Phase: This comprises the overlying mid-Jurassic to Paleocene foreland basin succession which was laid down on active margin during the active margin orogenic evolution (Laramide Orogeny) of the Canadian Cordillera which is comprised mainly of clastic rocks,

"The Laramide Orogeny brought about the uplift of the Rocky Mountains" (Wright, McMechan, & Porter, 1994) at same time, tilting the basin to the west thus giving rise to the present asymmetrical geometry of the foreland basin, associated with an eastern margin that is gently dipping and a western margin that is thrust-bounded. The wedge of the foreland basin is characterized by upward-coarsening progradational cycles capped by extensive non-marine deposits. In the Early Cretaceous time, a major drop in sea level brought about significant erosion over the entire foreland trough resulting in the formation of the pre-Mannville unconformity followed by the deposition of the alluvial fan and braided stream deposits of the Cadomin Formation and the fluvial deposits of the Lower Mannville Group. The Mannville deposition took place across a prominent unconformity surface that truncated strata ranging from lowermost Cretaceous in the foothills to lower Paleozoic on the eastern margin of the basin.

On a Regional scale, the Devonian Prairie Evaporite contains a wedge-shaped cross-section that tapers to the northeast, while to the eastern side, over the edge of the salt collapse zone resulting from dissolution, anticlinal traps are develop within the Cretaceous section and this anticlinal structure form the structural component of the trapping mechanism that keeps the oil in the McMurray Formation. Though, the trapping mechanism here is not entirely understood but the oil sand is believed to be trapped both stratigraphically and structurally. The above mentioned westward regional deep in combination with the eastward salt collapse results in some degree

of structural closure (Vigrass, 1968) (Jardine, 1974) where a significant amount of the oil sand is found lying to the East of the anticlinal features, thus structure is only just a partial control on Bitumen Trapping. (Wightman, MacGillivray, McPhee, & Berezniuk, 1991) (Flach, 1984)

Identification of the source rocks of the Western Canadian Sedimentary Basin oil sands has remained a controversial subject. Although the Bitumen and oil have been found to have a biomarker characteristic that is almost identical to that of the Devonian- Mississippian Exshaw Formation (Fowler, Stasiuk, & Hearn, 1999). This marine source rock which is 10m thick is found to be quite thin, but highly organic-rich with TOC of about 20% and is mainly made up of the oil-prone type 1 kerogen with hydrocarbon indices of about 600. “As illustrated by the burial history models, the time of hydrocarbon formation from the Exshaw Formation ranges between 110 and 80 Ma in the region of the Alberta-British Columbia border and between 60-56 Ma in the Peace River area” (Reidiger, Fowler, & Snowdon, 1999) it is believed that the uplift that took place during the early tertiary (after the Laramide Orogeny) in the WCSB, brought a stop to hydrocarbon production and caused the reservoir to be up thrown closer to the surface. Light oil migrated eastward to the updip areas of Northeast Alberta (Masters, 1984) (Moshier & Waples, 1985) and finally stopped migrating when the liquid became immobile due to biodegradation (Mossop, 1980) and is hosted in this form in the Athabasca oil sand which is capped by the Clearwater formation shales. The migration path for the Athabasca deposit is believed to be atleast 360 and that for the Peace Rive deposit at least 80 kilometres (Anfort, Bachu, & Bentley, 2001) (Adams, Rostron, & Mendoza, 2004) The lighter oil that migrated was then subjected to the biodegradation transforming them into heavy oil.

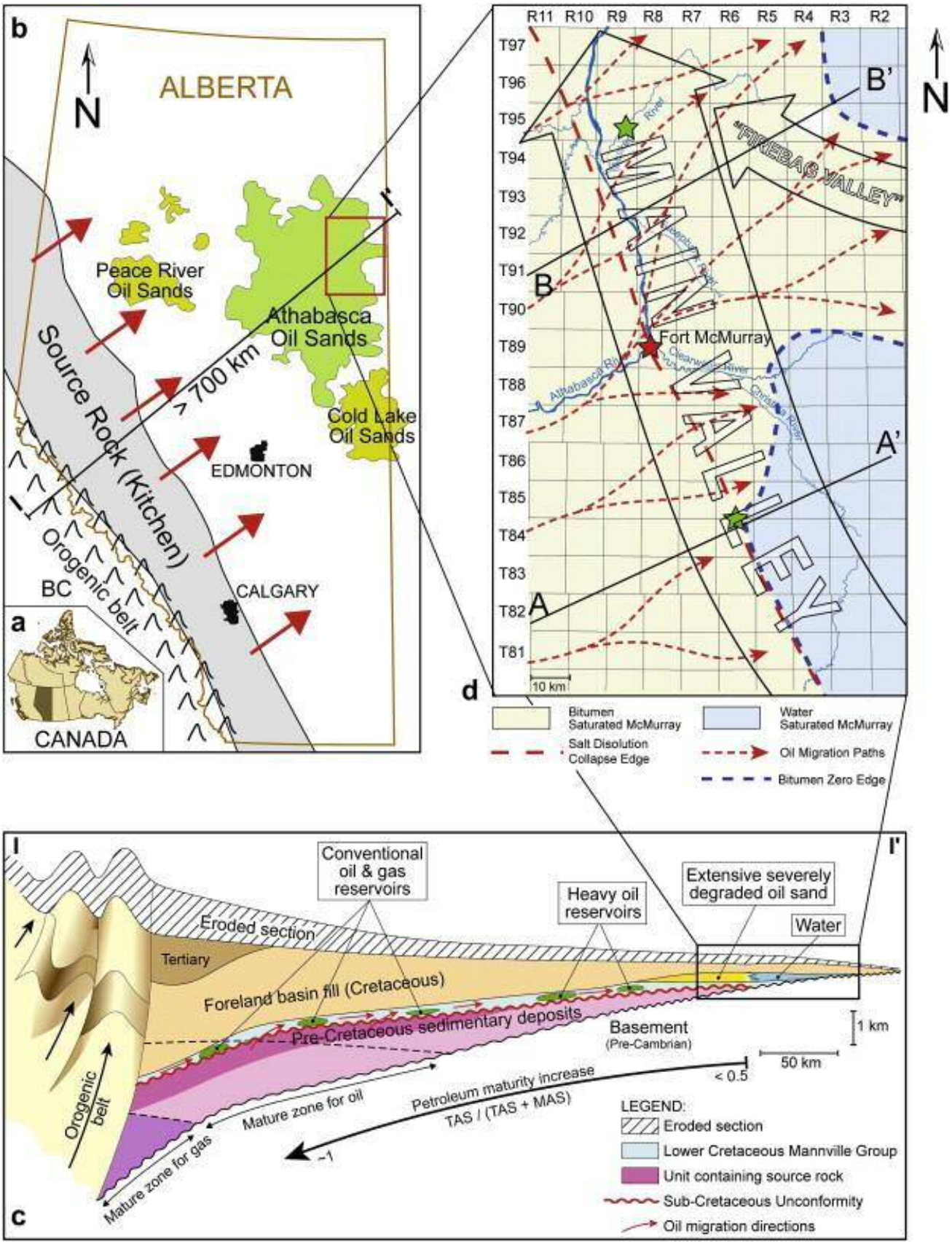


*Figure 2-1 Location map and petroleum system (sketch) of the Western Canadian Basin (modified after Wallace-Dudley, 1981)*

## 2.2 McMurray Formation

The area under consideration is geologically part of the McMurray formation. The McMurray formation ranges from 130m in thickness in the East and towards Grossmont high in the West less than 10m with an average reservoir pay thickness of 35m (Stanton.M.S, 2004). The McMurray Formation according to (Carrigy, 1959) can be divided into three informal units namely Lower, Middle, and Upper McMurray Formation. Authors (Wightman & Pemberton, 1997); (Flach, 1984); (Hein.F, Langberg.W, & Kidston, 2001) suggested that the middle and upper McMurray Formation due to absence of a regional chrono-stratigraphic surface separating simply represents auto-cyclic changes occurring in coexisting sub-environments.

Stratigraphic section in Figure 2-2 as per the preserved outcrop showcases the Fort McMurray area which includes the uppermost portions of the Devonian Christina and Moberly Members of the Waterways Formation (Beaverhill Lake Group) and the overlying Lower Cretaceous McMurray Formation and Wabiskaw Member of the Clearwater Formation (Mannville Group). The highly variable structural and erosional relief on the sub-Cretaceous unconformity greatly influenced sediment dispersal patterns and facies architecture of the overlying McMurray Formation and the Wabiskaw Member of the Clearwater Format (Hein.F, Langberg.W, & Kidston, 2001)

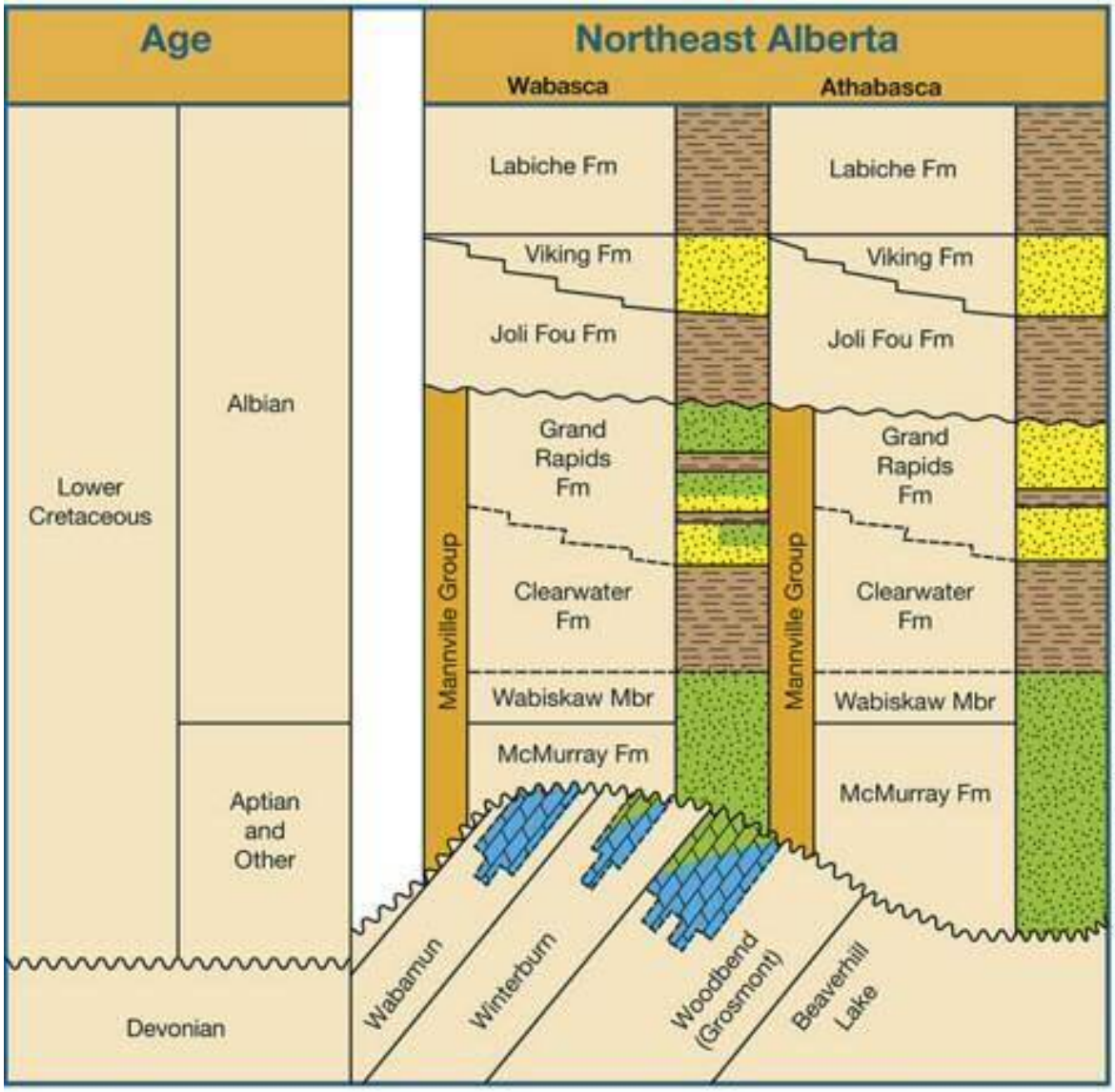


*Figure 2-2 Schematic cross section , Fort McMurray area ( modified from Wightman,et.al. 1995 and 1997) (Hein.F, Langberg.W, & Kidston, 2001)*

### 2.2.1 Lower McMurray formation

The Lower McMurray formation consists of coarse pebbly-sand that is massive and cross-stratified. Regional studies have interpreted the Lower McMurray formation as a coarse grained formation/ fluvial/conglomeratic unit (Pemberton, Mossop, & Flach, 1982) (Carrigy M. , 1959) (Flach & Mossop, 1985)(Biological evidences (Ichnofossils) such as trace fossil assemblage are essentially absent. Depositional environment for the Lower McMurray formation is fluvial with some braided channel systems.

#### *2.2.1.1 Middle McMurray formation*

The Middle McMurray formation is characterized by shallow dipping intercalations of

fine sands and mud (dipping 10° to 12°). Interpretation of the Middle McMurray formation has changed over time from a delta foreset (Carrigy M. , 1959) (Carrigy & Kramers, 1973)to an accreting fluvial deposit (Mossop, 1980) (Flach & Mossop, 1985) generally the Middle McMurray Formation is now accepted to be deposited in tidally influenced marginal marine channels (Wightman & Pemberton, 1997). The Middle McMurray Formation is the principal unit hosting the bitumen in the Athabasca oil sands. There is the presence of trace fossils interpreted to typical of the brackish water trace fossil assemblage in the Middle McMurray Formation.

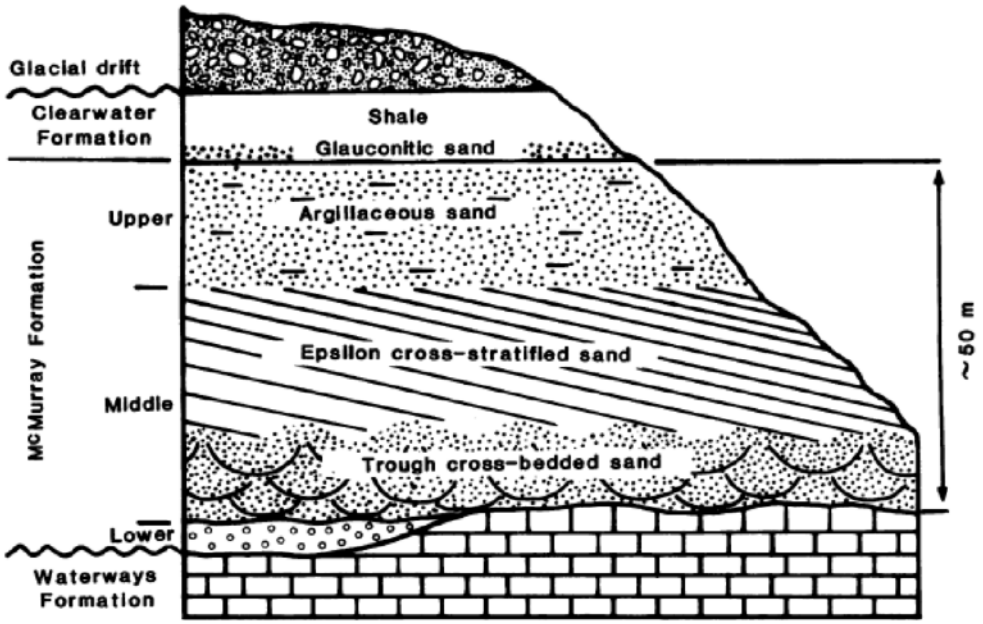


*Figure 2-3 schematic representations of the three facies that characteristically make up the McMurray formation sequence at the outcrop (Pemberton, Mossop, & Flach, 1982)*

### 2.2.2 Upper McMurray formation

The Upper McMurray Formation is characterized by tidally influenced / marine bar sands (Flach & Mossop, 1985) with thickening increasing towards the North. The Upper McMurray is highly variable and generally shallow unit deposited in a low energy and interpreted to be a Marine shore face deposit characterized by small deltaic complexes.

## 2.3 Depositional environment

Deposition of McMurray formation can be schematically observed in Figure 2-4 Figure 2-5,and Figure 2-6 the three models progressive development of current facies based on estuarine, marine and deep marine deposition process.

The succession is bounded unconformably at the base and the top, and has internal disconformities, locally disrupting the McMurray succession. The basal sub-Cretaceous unconformity, as previously mentioned, has significant relief, and had a profound effect on sediment distribution and depositional facies patterns within the McMurray Formation. As a result, study of localized depositional environment would play an important role in the process of modelling and field development.

The McMurray Formation was deposited on an exposed karstic landscape of ridges and valleys and varies in thickness from being absent over Devonian highs to over 130m thick in the Bitumont Basin. There is an increase in complexity of facies associations as assigned to the Lower and Upper McMurray Formation, concomitant with an increase in facies heterogeneity and interpreted lack of stability in the location of facies tracts. Bitumen-sand reservoirs accumulated as incised paleovalley-fills cut within the karstic pre-Cretaceous landscape and are within the Lower McMurray fluvial-dominated lowsand deposits Figure 2-6. Reservoirs occur mainly within braided channel-and-bar sands. Local water sands occur in paleolows along the basal sub-Cretaceous unconformity, and may pose problems for in situ thermal production of the oil sands (The most common, at present, being used in pilot schemes is Steam-Assisted Gravity Drainage, or ‘SAGD.’). (Hein.F, Langberg.W, & Kidston, 2001)

Bitumen-rich reservoirs formed within estuarine valleys stacked above the Lower McMurray channel sands are assigned to the Upper McMurray Formation. These bitumen-sand reservoirs occur mainly within stacked estuarine-tidal channel-and-point bar complexes. Local water-sands occur in the lower parts of the Upper McMurray, whereas in the upper parts somewhat more continuous gas and water reservoirs are relatively common. Bitumen, water and gas reservoirs formed within an estuarine complex and associated prograding coastal plain Figure 2-4 Figure 2-5 Sediments of the coastal plain proper in off-channel sites generally do not form thick enough accumulation of porous sands for significant hydrocarbon reservoirs; however, in off-

channel sites such as splays, thicker and more porous sands may serve as local gas reservoirs.

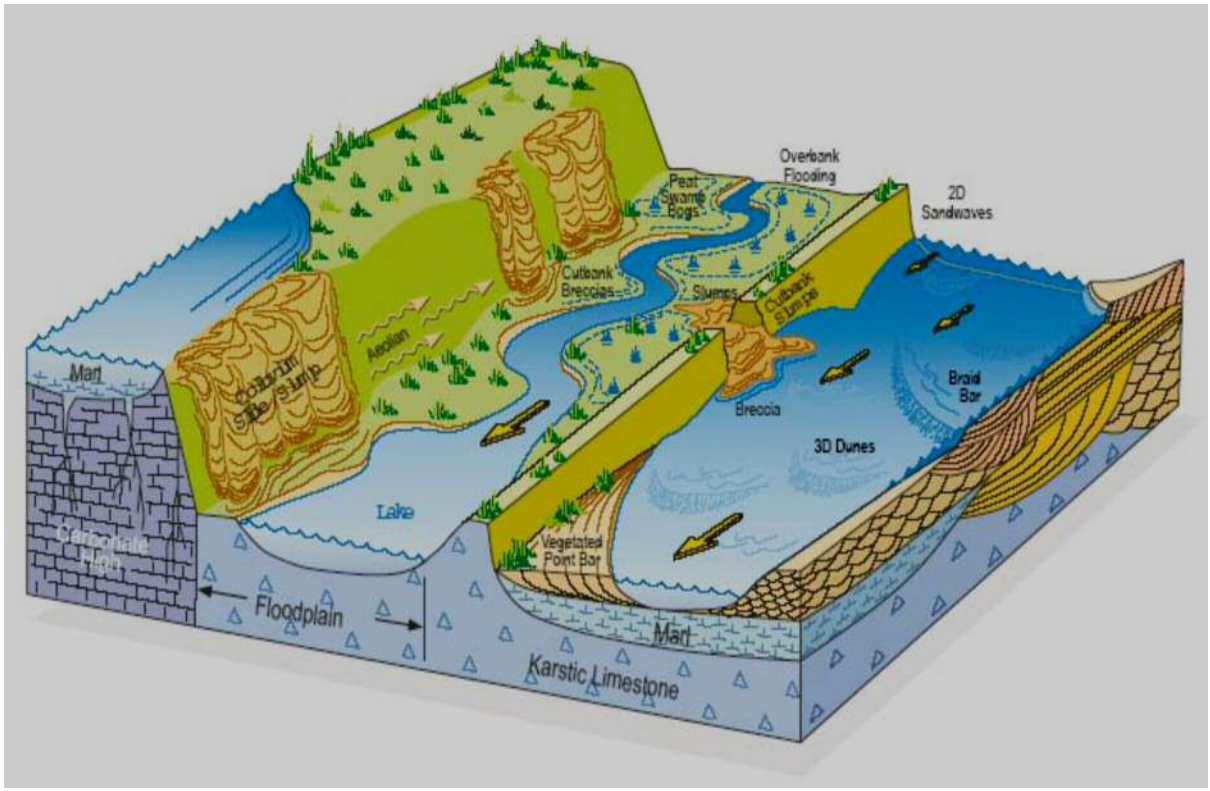


*Figure 2-4 Schematic facies model for the Lower McMurray Formation, Athabasca deposit, northeast Alberta (Hein.F, Langberg.W, & Kidston, 2001)*

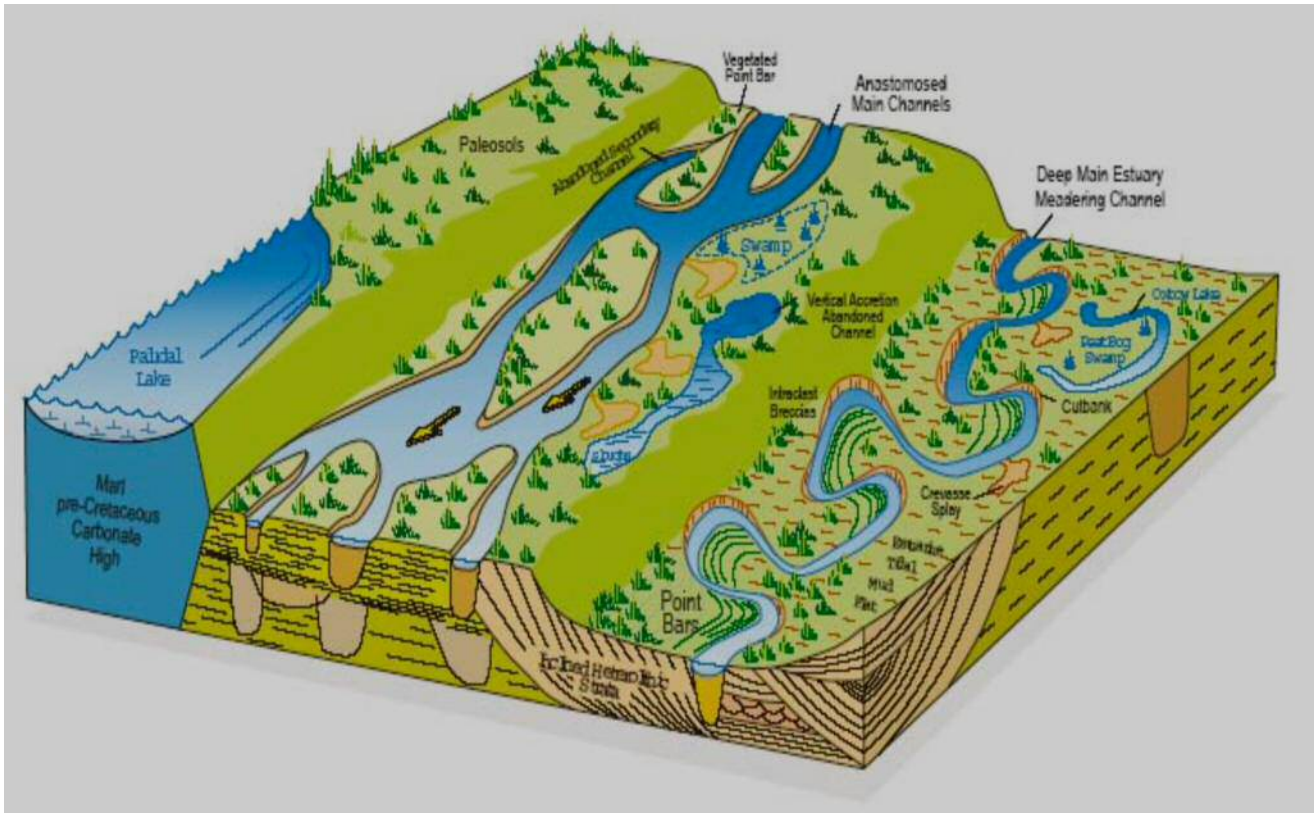


*Figure 2-5 Schematic facies model for the lower part of the Upper McMurray Formation, Athabasca deposit, northeast Alberta (Hein.F, Langberg.W, & Kidston, 2001)*

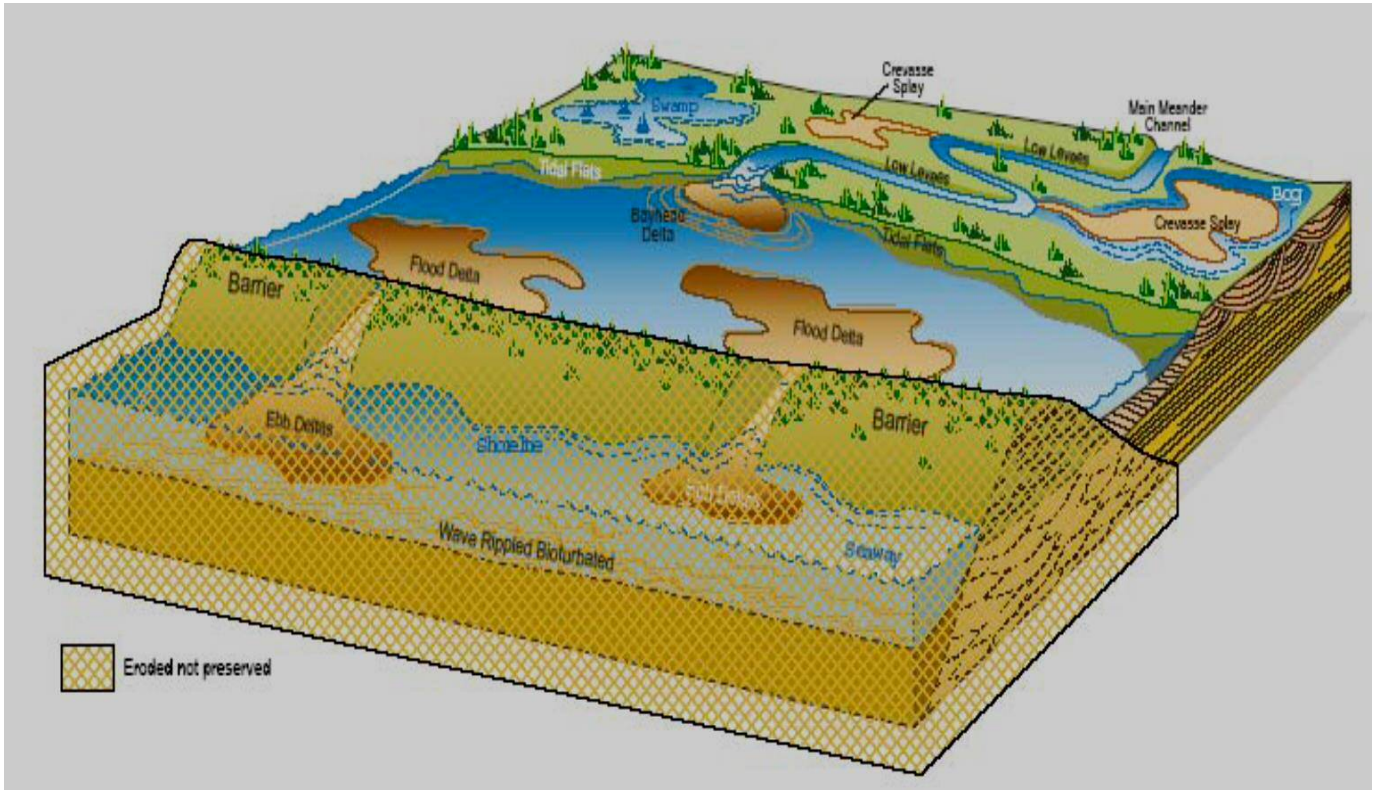


*Figure 2-6 Schematic facies model for the lower part of the Upper McMurray Formation, Athabasca deposit, northeast Alberta (Hein.F, Langberg.W, & Kidston, 2001)*

## 2.4 Reservoir Heterogeneity and Bioturbation

As can be seen from Figure 2-7 movement of plant roots and organisms through sediments produce several structures. These structures in certain cases stay as they are in host rocks and in other cases form pipes that increase permeability for different formations. Mcmurray formation being made up of sediments deposited in estuarine, fluvial, tidal environment has presence of micro fossils and fossil induced bioturbation.

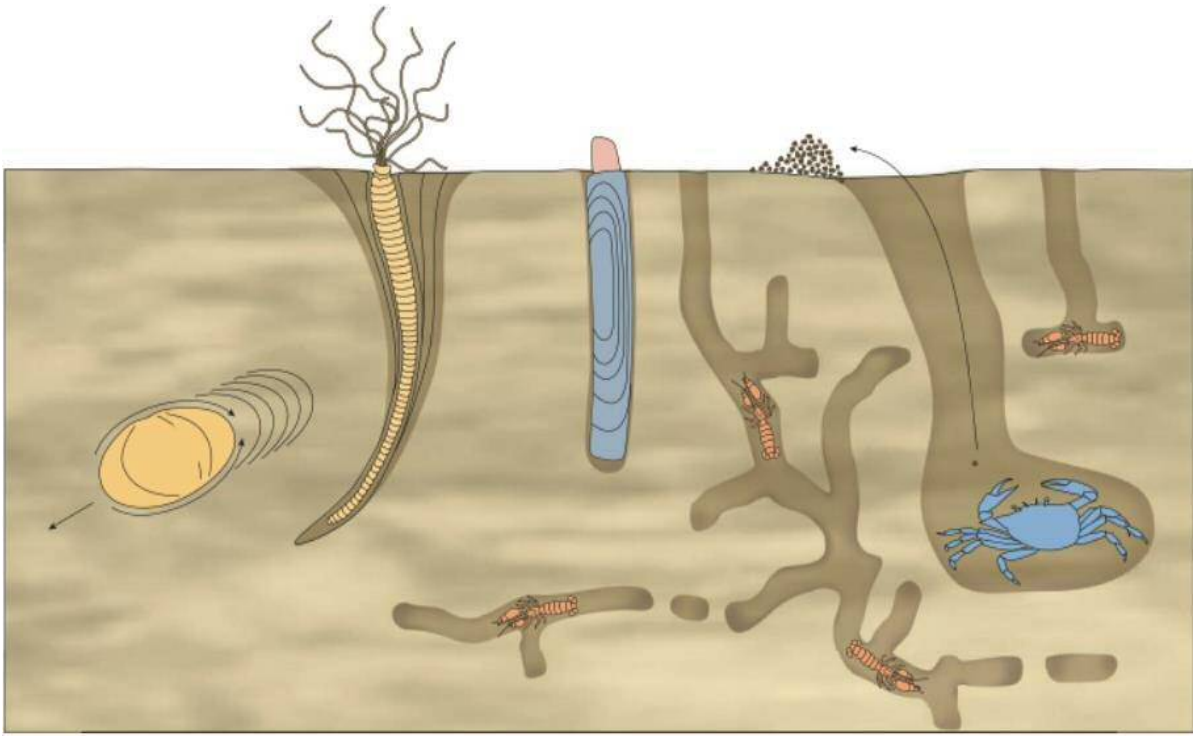

*Figure 2-7 Marine animals that live at or near the sediments/water interface leave traces of various shapes, sizes and complexity*

### 2.4.1 Sources of Bioturbation in the McMurray formation

The source of Bioturbation within McMurray formation can be associated to depositional environment of deep marine, Brackish water and fresh water trace fossils as discussed by (Gingras, Maceachern, Dashtgard, Pemberton, & Rangers, 2016) in their paper discussed the source of fossils.

The trace fossils are normally found in association with root traces and pedogenically altered sediments situated near the top of the lower McMurray. These assemblages confirm that during McMurray time, freshwater and brackish-water ichnocoenoses were present and yielded discrete and readily discernible trace fossil suites. Brackish-water thalweg, bar, and bar-top units, which are consistently devoid of pedogenic

alteration and root traces, are explained by: 1) the presence of brackish-water in the depositional setting; and 2) the presence of tides to facilitate the landward transport of marine-derived larvae and the establishment of a bar-top tidal zone. As such, contrary to some

(Pemberton, Mossop, & Flach, 1982)delineated the McMurray formation into three schematic facies as shown in: (i) a massive cross stratified thick-bedded sand at the base (ii) a middle sequence consisting of a large-scale of strata inclined and up to 25m thick generally referred to as epsilon cross-stratification in non-generic terms (iii) an upper most argillaceous unit consisting of horizontal beds of sands and silts which lie below the weathered strata of the Clearwater Formation.

Trace fossil studies by Pemberton *et al.,* (1982) revealed ten ichnogenera comprising *Rosselia, Monocraterion, Cylindrichnus, Dolopich-nus, Lockeia, Planolites, Bergaueria, Skolithos, Teichichnus, Palaeo-phycus* species. Some vertical escape structures left by burrowing organisms and numerous structures, which are not distinguishable resulting from bioturbation (disruption by the activity of organisms) in the Athabasca oil sands were also recorded as part of this study (Pemberton *et al.,* 1982).

Mossop and Flach (1977) and Pemberton *et al.,* (1982) studied the distribution of the trace fossils in Athabasca oil sands and found out that the distribution of trace fossils is consistent in epsilon cross-stratified sands and trace assemblages include abundant numbers of inclined to arcuate pipe typically up to 20cm in length and representing distinct morphotypes of *skolithos*, concentrically lined burrows of *Cylindrichus* appearing abundantly as sub-conically materials; common- rare escape structures ranging between 25cm in length, bioturbated features difficult to identify and horizontal branching features which are characteristics of *Planonites* and *Palaeophycus*.

### 2.4.2 Study Related to Effects of Bioturbation on Reservoir Qualities

According to Cannon & Gowland (1996) and Tokin *et al.,* (2010) the petrophysical characteristics of reservoirs intervals can be linked to the trace fossil morphology, the occurrence or non-existence of burrow fills and nature of burrow fills. Tonkin *et al.,* (2010) studied the effect of bioturbation on the reservoir qualities of pay zone from the

Ben Nevis Formation dominated by *Ophiomorpha* dominated ichnofabric. Corelogging, ichofabric assignment, visual estimation of bioturbation intensity and thin section petrography were applied in studying the effects of the animal sediment activities on the reservoir facie. The study revealed that animal sediment interaction can be classified into four groups based on the study area; sediment cleaning, sediment mixing, pipe working building strategy and sediment packing. The result obtained show that bioturbation has a dual implication on reservoir properties in that it is capable of reducing and enhancing porosity and permeability by as much as 33% to 600% respectively. This can be achieved by movement of animals through sediments wherein, their interaction either increases uniformity of grain size distribution through the destruction of sedimentary laminae via burrow homogenization or reduce grain size distribution uniformity through selective sorting of grains into the burrow lining resulting into a variance in the grain size distribution of the host sediment (Tokin *et al.,* 2010). This can lead to the development of channels and/or change in sorting resulting in reduction in porosity due to the changes brought to the formation.

Dabek and Knepp (2011) worked on the impact of biogenic structures on permeability in Upper Cretaceous Blackhawk Formation characterized by a wave dominated facie. The study involved examining the heterolithic shoreface facies consisting of abundant tracefossil assemblage of *Ophiomorpha* Figure 2-8*, Chondrites and Asterosoma* using a 3D object based model which involves varying orientations and dimensions, and subsequently superimposing the model on a process oriented stochastic model. The effect of varying the modelling parameters like diversity of the trace fossil assemblage, orientation, abundance and permeability in burrows were treated to flow-based upscaling to generate the effective permeabilities for each realization.

*Figure 2-8 Ophiomorpha in the Sowerby parasequence (Dabek and Knepp, 2011)*

The increase in the presence of burrowing structures in the model significantly affected the permeability anisotropy (Kx, Ky and Kz) and the porosity, this was particularly evident in models that hosted biogenic structures with low permeability fill. Using biogenic structures with a high permeability fill in the controlled model resulted in porosity and permeability being elevated.

Strobl, (2011) reported from the analysis of core samples from the UTF phase B oil sand pilot project (underground testing facility) that permeability in the bioturbated reservoir facie with values ranging from 150-700md was significantly higher than the permeability of the non-bioturbated facie having permeability value of between 0.04md to 50md. Breke and Couch (2011) while attempting to apply an image log as seen in Figure 2-9 to discriminate between tidal bar and point bar deposit in the Leismer Area, Athabasca discovered beds with bioturbation features consisting of *Skolithos*, *Planolites*, *Gyrolithes* and *Teichichnus* emphasized the presence of this bioturbation features in relation to the oil sand reservoir quality.

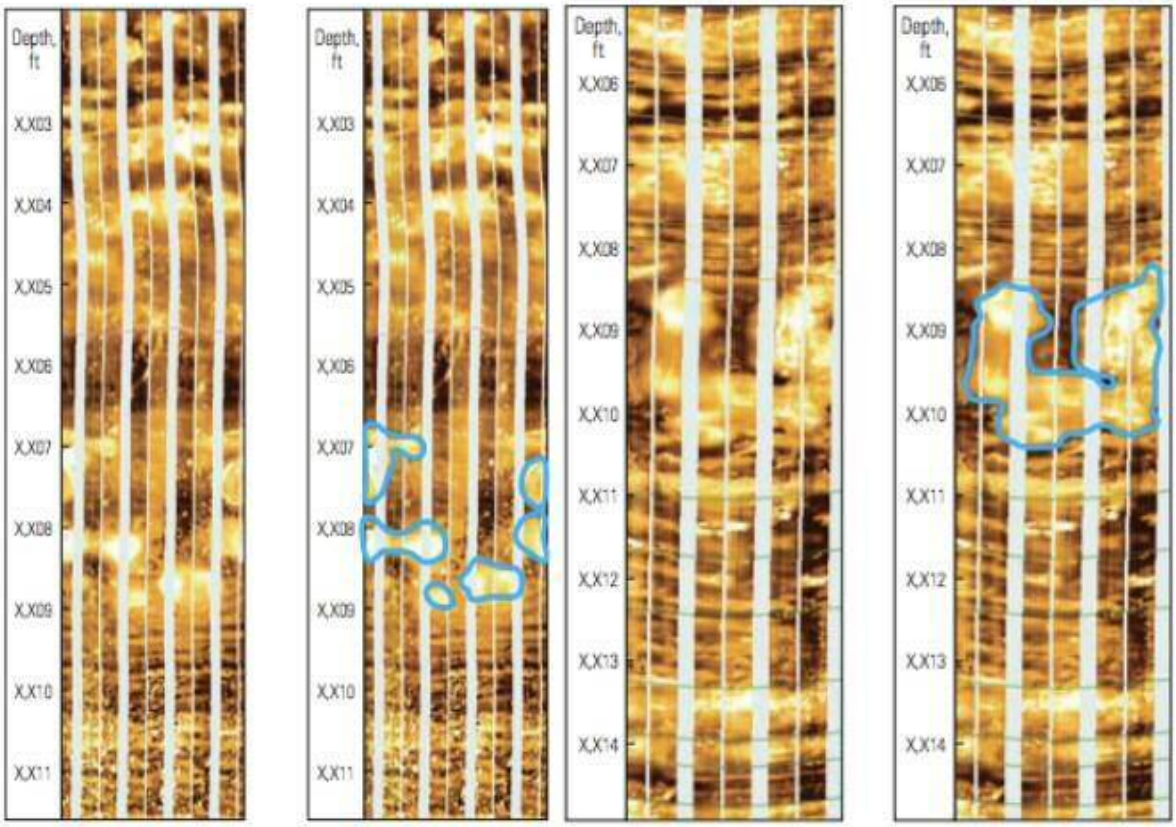


*Figure 2-9 Images of well log section showing bioturbation (Pemberton, 2014)*

### 2.4.3 Thin Section analysis

Thin section analysis is one of the oldest and most common method to perform petrographical analysis from samples. The process of thin section preparation is difficult as the total thickness of sample needs be less than 30μm to provide necessary transparency. Though several studies have been performed to prepare desired quality thin sections, there is no single method/ raw material that can provide the same quality each time due to the variety of samples.

(Richa, Mukerji, & Keehm, 2006) In their study to understand the accuracy of automated point count analysis for porosity determination prepared blue dye impregnated thin sections. To understand its efficiency, they studied patterns for recognition of typical properties through the use of thin section. As image analysis method requires images to be binarised, colour images are generally converted to black and white spectrum removing a primary deterministic element of colour. While studying pattern they analysed both RGB (Red Green, Blue) and HSV (Hue, Saturation, Value) colour space. This study concluded that HSV colour- space provides better results compared to RGB colour space for all approaches studied except for unsupervised classification techniques.

(Felipussi & Roque, 2002) In their studies attempted to identify 3D pores from 2D thin section digital images of petroleum rock sample. Several methods were tested to identify which works best for the material. (Hossain, 2011) Study focused at defining physical basis approach to calculate relative permeability of reservoir rocks from image analysis of thin sections. He studied application of Lattice-Boltzmann to network modelling and Kozeny's equation for numerical work. Results between Lattice –Boltzmann, Kozeny's equation and lab were compared and a good match was agreed between the three methods.

### 2.4.4 Thin section preparation

Large size (7X12cm) as shown in Figure 2-10 were prepared from the oil sands outcrop samples. The routine method for producing thin sections from unconsolidated or loosely consolidated material was employed following (FitzPatrick, 1984) (Jongerius, 1963).The steps followed involve dehydration, impregnation, sawing,

levelling, lapping and polishing. The care was taken to produce minimum disturbances in the samples while preparing these thin sections.

(Dress & Ulery, 2008) and (Pasu & Gautheyrou, 2006) while performing mineralogical analysis have provided detailed versions of thin section preparation procedure. Their study involves a variety of samples containing clays, wet sands, loose soil etc. As a result, they further provide details of variety of hardeners which is considered and experimented with while preparing thin sections for this study.

To successfully prepare thin section to perform analysis as part of this study, aforementioned steps were followed. Though primarily three hardeners were tried to understand applicability with unconsolidated sample that is filled with bitumen. This step was necessary as most of the steps involved generate heat and some of the hardeners used react exothermically while hardening the samples.

1. Polyester with Acetone Catalyst 0.2%
2. Epoxy
3. Epoxy with hardener.

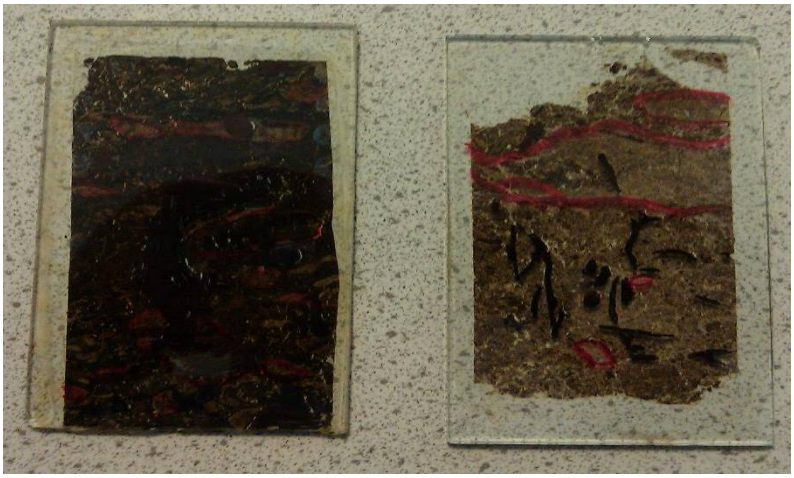

*Figure 2-10 Thin sections prepared for this study*

#### *2.4.4.1 Sectioning*

Sectioning is a first step where the sample is cut into usable sub sample and is further grinded down to the size that is suitable to prepare thin sections. As detailed by (Dress & Ulery, 2008) and (Pasu & Gautheyrou, 2006) This step may cause high disturbance to the sample if not performed carefully. Utmost care needs to be followed

while working with unconsolidated materials as there are higher changes of disturbing the samples. One way to avoid any issue is to use an appropriate blade that is suitable for sample, size, cutting speed etc.

#### *2.4.4.2 Impregnation*

After sectioning the sample, it is good practice to clean and dry it. When working with very porous material or unconsolidated material like in this study the use of a vacuum chamber is recommended to assure good impregnation. There are several resins in the market to be used, being the most common epoxy resin or polyester resin. It is a good practice to first impregnate the sample and then trim it. This process is often done for small or unconsolidated samples like those practiced by (Pasu & Gautheyrou, 2006).

#### *2.4.4.3 Trimming*

Once impregnated and polymerised the samples can be cut to desired thickness safely by avoiding any disturbance to the sample. This is usually performed with the help of an automated linear feed motor or with the use of a geological rock cutter. (Pasu & Gautheyrou, 2006) suggests use of cup grinder circular grinder until it reaches the desired thickness.

#### *2.4.4.4 Bonding*

Binding involves trimmed sample to be bonded to the glass piece. Utmost care needs to be taken to avoid formation of any air gap/ bubbles between the two surfaces. According to (Dress & Ulery, 2008) epoxy resin can be used for proper bonding. The bonding material needs to polymerise and then be grinded and polished.

#### *2.4.4.5 Grinding & Polishing*

Grinding is used to further reduce the sample's thickness and eliminate any irregularities from the surface. Grinding can be performed by disc grinders with coarse to fine roughness or by the process of lapping. The Lapping machine has two surfaces rubbed together with an abrasive sandwiched between. Some of the commonly used abrasive materials are aluminium oxide, silicon carbide, diamond amongst many others. (Dress & Ulery, 2008) observed few streaks produced during this process

which can be observed under microscope, Though this can be reduced by polishing on an appropriate horizontal polishing disc.

## 2.5 SEM Analysis

The scanning electron microscope (SEM) uses a high energy electron beam to scan the surface of a specimen, and uses temporal variations in the electron reflection intensities to assemble an image of the specimen (Bozzola & Russell, 1998). The electrons interact with the atom from the sample producing signals that corresponds to the sample's surface and provide properties e.g. compositions, surface topography etc. Unlike Transmission electron microscope (TEM), SEM analyses a 3-dimensional specimen while, TEM project electrons creates a 2-dimensional images.

According to (Nanoscience Technology, 2018) SEM works by scattering a focused beam of electrons on a sample of interest. The SEM components include:

- Electron Source
- Column down with electromagnetic lenses
- Electron detector
- Sample Chamber
- Computer and display to view images

Electrons are produced by the source at the top and are accelerated down passing through a combination of lenses and apertures set and adjusted by an operator. The arrangement is set in such a way that a focused beam can be created to the sample. The sample is mounted on the stage at the bottom of the chamber. Unless specifically designed, an entire setup is maintained in a vacuum to avoid any scattering or distortion of the beam.

According to the sample and nature of electron conductivity of the sample source electron charge is altered to generate an

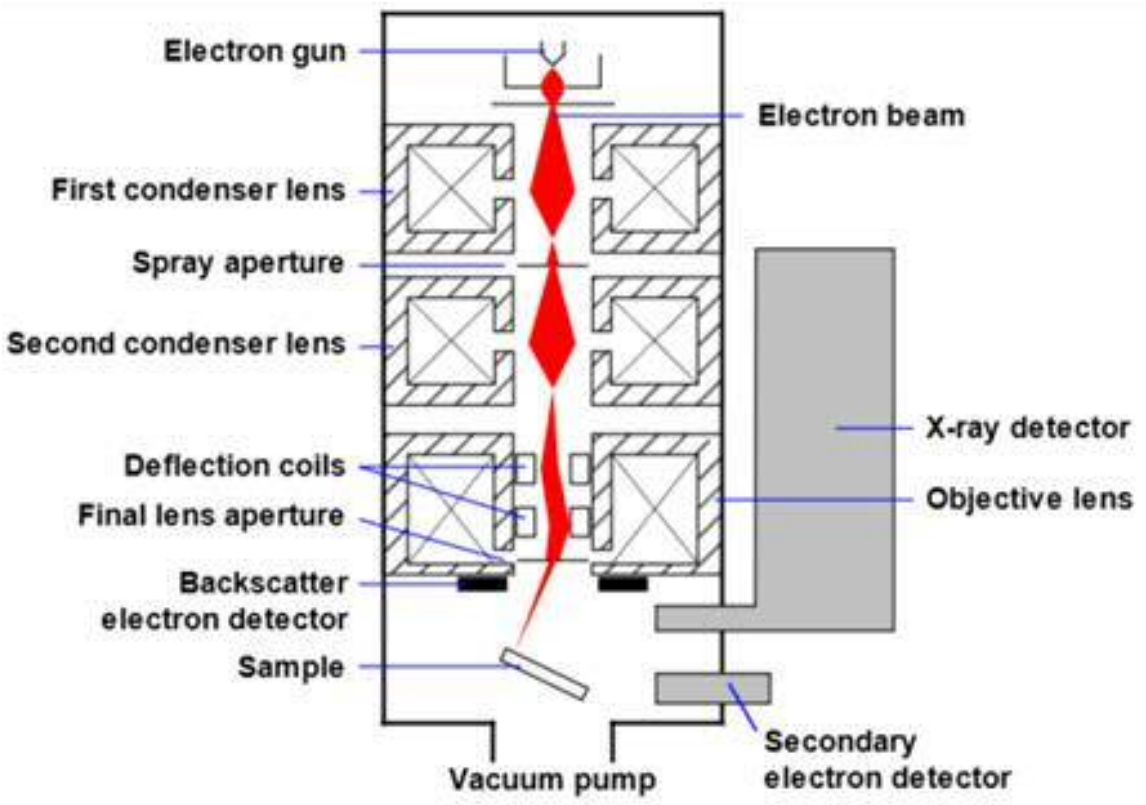


*Figure 2-11 Schematic of a Scanning Electron Microscope. (Nanoscience Technology, 2018)*

The position of the electron beam on the sample is controlled by scan coils situated just above the objective lens. These coils allow for the specific area to be rastered/ scanned. The raster of an image can be adjusted to produce multiple signals by adjusting source electron energy which produces desired electron sample interactions. The resulting beams are detected by an appropriate detector that are part of the SEM machines.

## 2.6 micro-CT

### 2.6.1 micro-CT Background

Computerized tomography (CT) was originated in 1972 (Sarker & Siddiqui, 2009) and is a non-harmful medical image system, which uses X-ray and calculations to analyse a portion of an object or particle. Besides, it has been helpful in other areas rather than only the medical perspective, including civil engineering, petroleum engineering, groundwater hydrology, mechanical engineering, material inspection, development and others.

Properties like bulk density, porosity, grain distribution, mineralogy, saturation and others are regularly used in the petroleum science. They can be obtained with the help of CT and all those properties are relatively important towards the calculation of multiphase flow properties namely capillary pressure and relative permeability.

With this in mind, a scanner, part of the CT group was created around the 80s, micro-CT. Introduced for scanning micro objects, for instance micro-devices, microfossils, small animals, diamonds, reservoir rocks such as sandstones and carbonates, wood, among others. In addition, micro-CT is the most reliable scanner in the market and this conclusion was based on direct observation and analysis from rock samples.

Furthermore, according to (Sarker & Siddiqui, 2009) there are two sets of rock properties, which can be obtained through micro-CT analysis:

Static properties: Reservoir properties for this research's reference. This entails determination of rock properties such as porosity, absolute permeability, electrical resistivity and formation factor.

Dynamic properties: those properties that rely on fluid flow through the core e.g. relative permeability, residual saturations, resistivity index and capillary pressure.

The first application of micro CT in petroleum engineering was by using cone-shaped beams, a work from Jasti et al. (1993). They wanted to identify 3D microstructures in reservoir rocks and describe the flow of multiphase fluids within porous spaces. A few years later when seemed trustworthy for the oil industry, one more application was created, Pore Network Modeling (PNM) with the purpose of predict petrophysical properties of a reservoir from drilled cuttings.

### 2.6.2 Digital Core Analysis (DCA)

In recent years there have been several attempts to determine porosity and permeability based properties through the use of Digital Core analysis (DCA). This technique principally focuses on obtaining high resolution 2D images and 3D scans to determine internal porous and permeable structure of rock. DCA techniques are significant to this study as the core samples under investigation are unconsolidated in nature.

According to Shandrygin (2014) a key DCA element is computed tomography which is generated using high resolution images. This is subsequently studied following various approaches to determine fluid flow modelling and absolute and relative (Demianov, Dinariev., & Evseev., 2014)permeability. Some of the prominent work consist of Navier-Stokes equation by finite difference methods (Hilfer.R, 1991) or finite element method (X.Garcia, et al., 2009); Pore network technique (Oren, Bakke, & Arntzen, 1998) as well as density functional method by (Demianov, Dinariev., & Evseev., 2014; Government of Canada, 2015)

(Zainudin, S., Md Zain, & Riepe, 2014) Performed detailed micro-CT and SCAL comparison on Malaysian field with Friable sandstone as a reservoir rock which faces similar problem due to the nature of the rock. The results from this study were able to demonstrate that good quality and replicative reservoir properties such as porosity and permeability can be obtained through the use of DCA techniques once careful collection of core samples is performed. Their study focused on using 3D grain and fluid partitioning and performing standard volumetric calculation to determine necessary petrophysical properties. Additionally, there are several studies that have used micro-CT, DCA techniques to determine petrophysical properties for difficult reservoir rocks such as Shale as well.

## 2.7 Image Acquisition

X-Ray is obtained from a two-dimensional (2D) projection from a three-dimensional (3D) object. In Figure 2-12 below can be seen how the X-Ray works. X-Ray is emitted from the source going through the 3D object then through the filters when applicable and then to the camera. (Micro Photonics Inc., 2015)

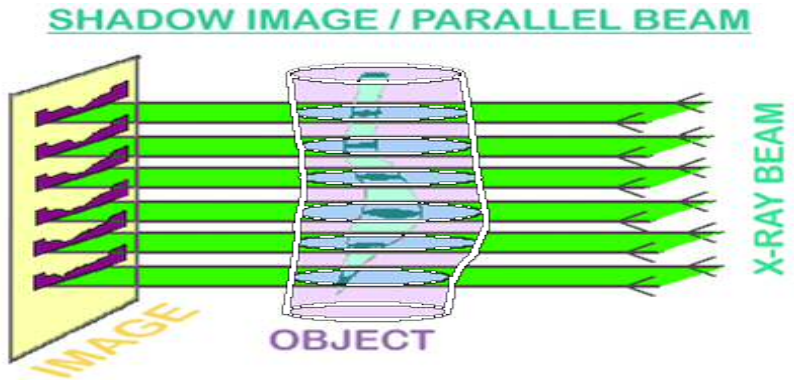


*Figure 2-12 Parallel Beam Geometry (Micro Photonics Inc. (2010)).*

The process shown above is then repeated in different angles/positions as shown in Figure 2-13 that will in each position add a new line to the possible reconstruction area called “back-projection”. After numerous rotations, the absorption point is determined inside of the object that will allow its reconstruction that is done by Feldkamp algorithm. As the number of projections obtained increases, the localisation of the point for reconstruction becomes more distinct as shown in Figure 2-14.

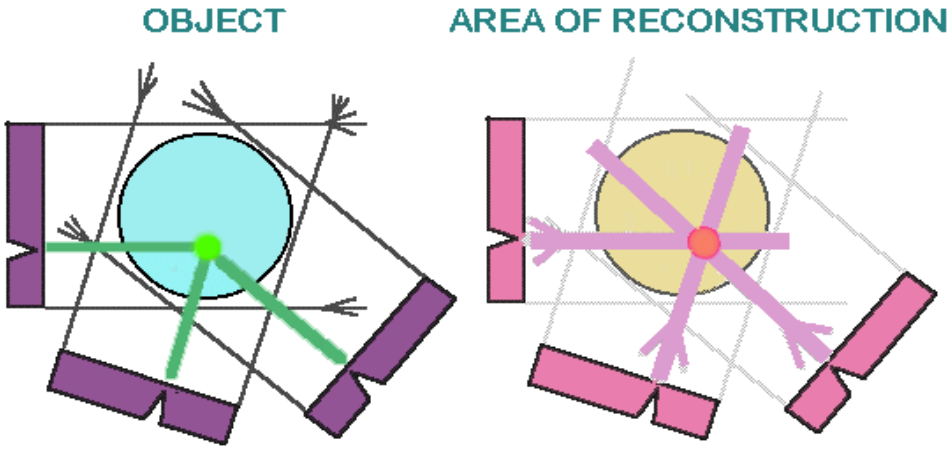


*Figure 2-13 Illustration of 3 different angles of an object and its respective reconstruction (Micro Photonics Inc. (2010)).*

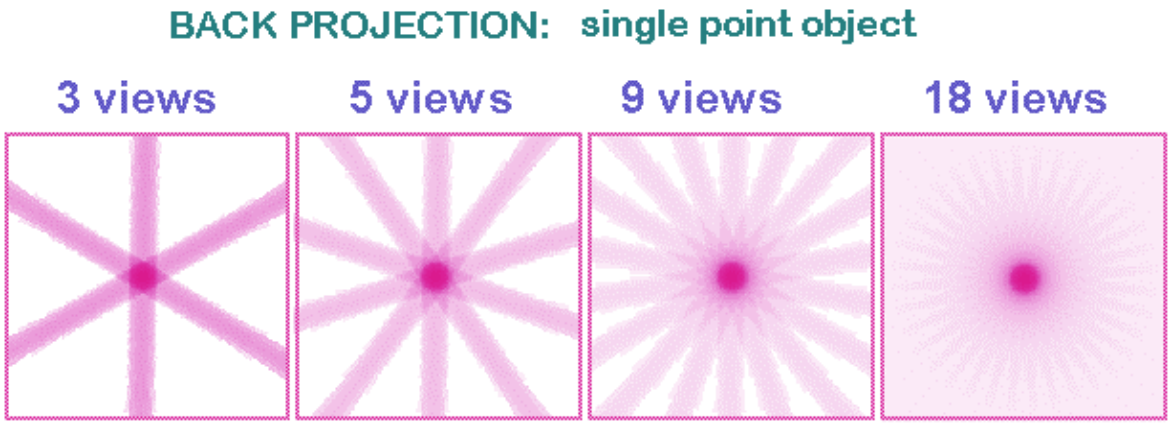


*Figure 2-14 Illustration of a single point object for reconstruction increasing the amount of rotations (Micro Photonics Inc. (2010)).*

Once projections start to be obtained one can have infinite number of projections from one object that will thus create some blurring of the image, and that is because one line will be on top of each other i.e. coincide with previous projections. To correct the blur, effect some negative absorption is added outside the point where the shadow of the object is as illustrate in Figure 2-15.

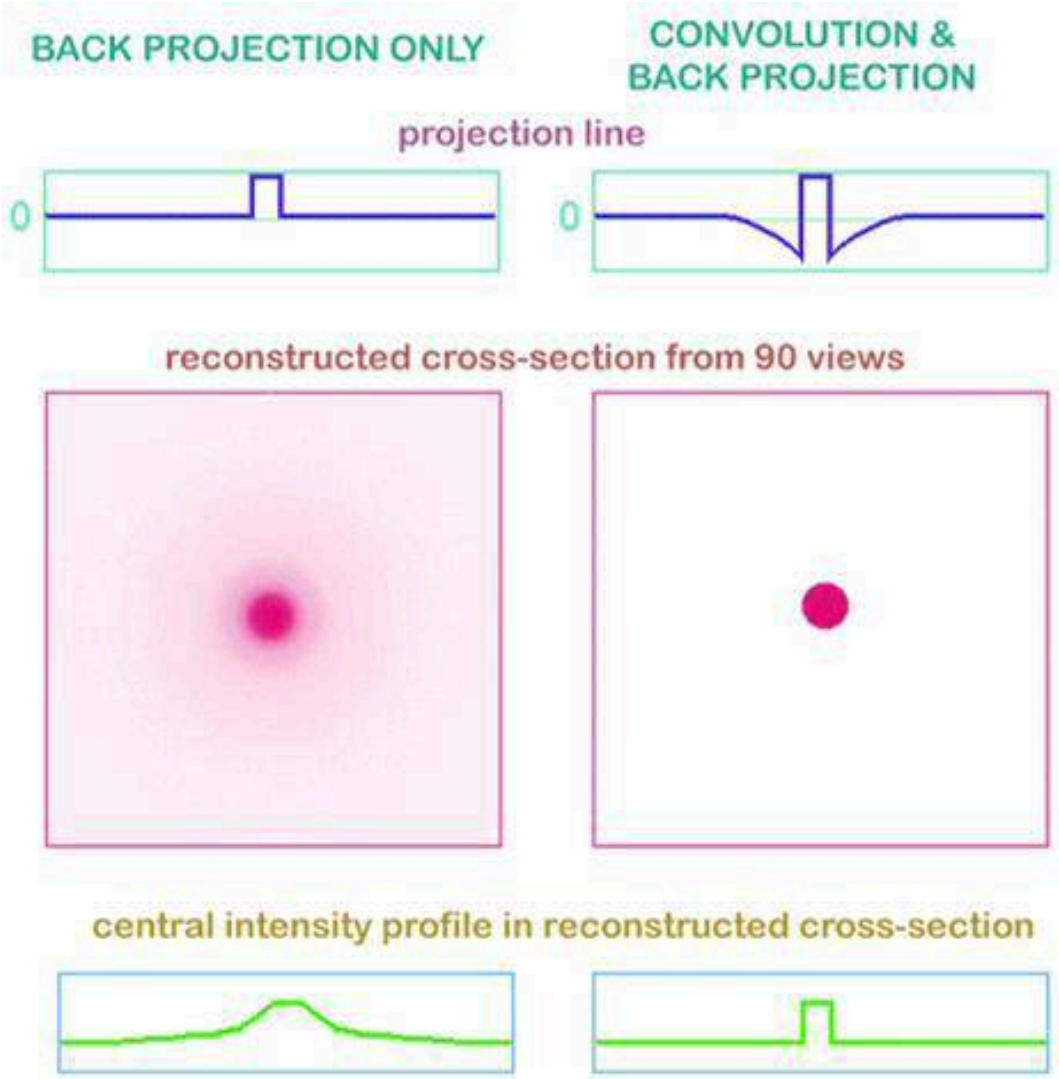


*Figure 2-15 Illustration of the effect of the filtered projection (Micro Photonics Inc. (2010)).*

### 2.7.1 Requirements to Perform a Tomography

To perform a successful scan the object needs to be in the focus range of the camera and must accept energy imparted by X- Ray during scan process until it reaches camera at all angles of scan. There must exist enough absorption of contrast to be detect by the use of the detector. Hence, high density material such as metals are avoided while working with micro-CT scanners.

### **2.7.2** Micro-CT Constraints

The resolution of an x-ray tomography depends on the type of material analysed which is directly related to the diameter and how much x-rays the material can absorb. This is the constraint related to the material, and the constraint related to the machine would be in terms of the power of the scanner, which is limited to 100 KV (for Skyscan). The

constraints in terms of resolution and size are limited to 0.9μm and 4000 pixels for each reconstructed cross section, respectively.

### 2.7.3 Geometry Analysis

Once the sample is placed into the machine, the degree of magnification can be modified by adjusting the distance of the sample in between the x-ray source and the camera. Figure 2-16 illustrates the sample placed in the middle, which can be moved. closer or further away from the detector which in turn will increase or decrease the magnification. (Micro Photonics Inc., 2015)

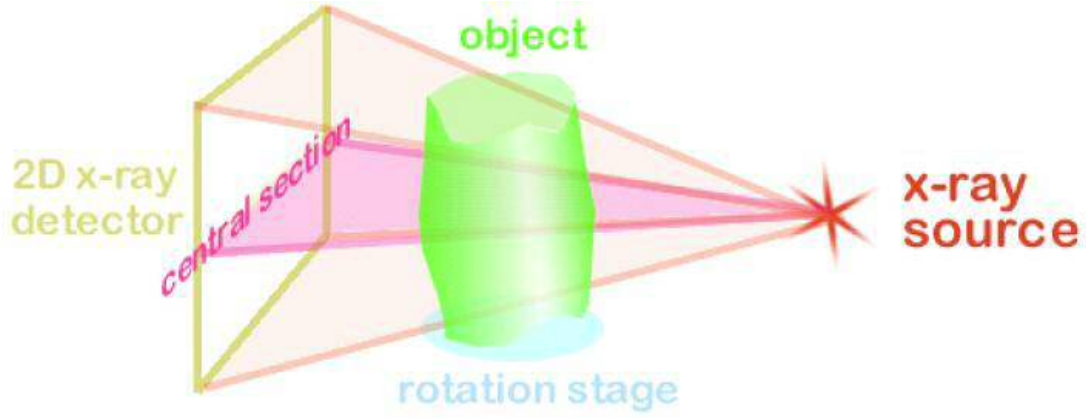


*Figure 2-16 Fan Beam Geometry (Micro Photonics Inc. (2010)).*

If the object is placed closer to the x-ray source, the magnification will be higher and if placed closer to the detector the magnification will be lower. It is also important to stress at this point that time taken to perform scans depend on the distance within the source and detector along with the resolution. So, if the distance between the detector and the source is decreased then the time required will also decrease.

### 2.7.4 Scanning Optimisation

To optimise the resulting scans several filters are fitted to the scanners. E.g. aluminium, copper and amorphous lead doped glass fragments. Aluminium will filter lower energy rays whereas copper will filter high power. Application of such filters allows optimum rays to be detected and noise generated due to the absorption of the rays by material is reduced. This further allows various degrees of grey scale to be produced rather than black and white image. The applied voltage should also be

optimized to avoid over powering of the scan and loosing important data from the resulting scans.

Scanning can be optimised through the camera exposure time. If the object is exposed to various shots, it will create more lines, which are better to reconstruct the material, although if the exposure time is too long it can create artefacts due to the superposition of the lines. Another way of optimising is the rotation step i.e. how many degrees the object will rotate for each shot.

### 2.7.5 Software and Hardware Corrections

Due to the usage, they might be out of alignment in which case depending on the resolution and magnification it may create some artefacts i.e. some white long line though the image, in this case, an alignment is needed.

#### *2.7.5.1 Ring artefacts*

Ring artefacts are another problem when scanning. They are complete or incomplete circles that appears after the image has been constructed and that happens due to the sensitivity of the camera. (Bell & Dawes, 2018)

#### *2.7.5.2 Beam hardening:*

Beam hardening is another problem that is present in micro-ct scan for some time. This is mainly caused by the polychromatic source. An example is an object that may have an outer layer with high density and its inner part with lower density. In such cases, the source will emit high voltage rays to pass through high-density region and thereby passing through lower density with the same energy. In these circumstances a hollow image will be generated due to the loss of internal material. To avoid this beam hardening correction needs to be applied. Where beam correction required is more than 50% filters can be used to help reduce this effect. Figure 2-17 and Figure 2-18 show beam hardening and ring effects respectively. (Weerakkody & Murphy, 2018)

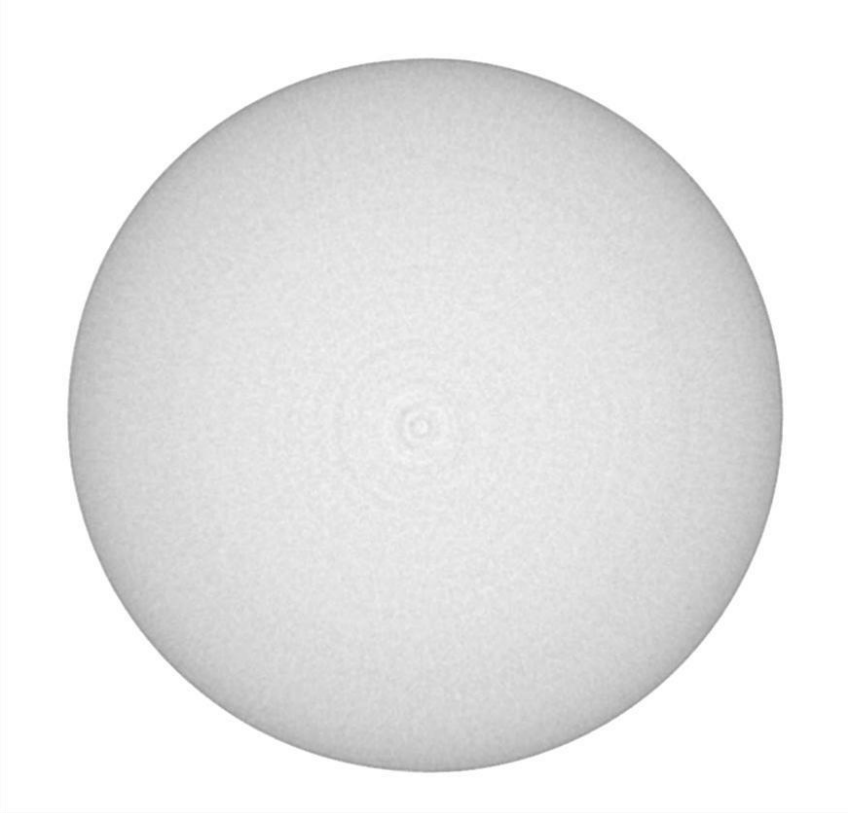

*Figure 2-17 Object without beam hardening correction (Micro Photonics Inc. (2010).*

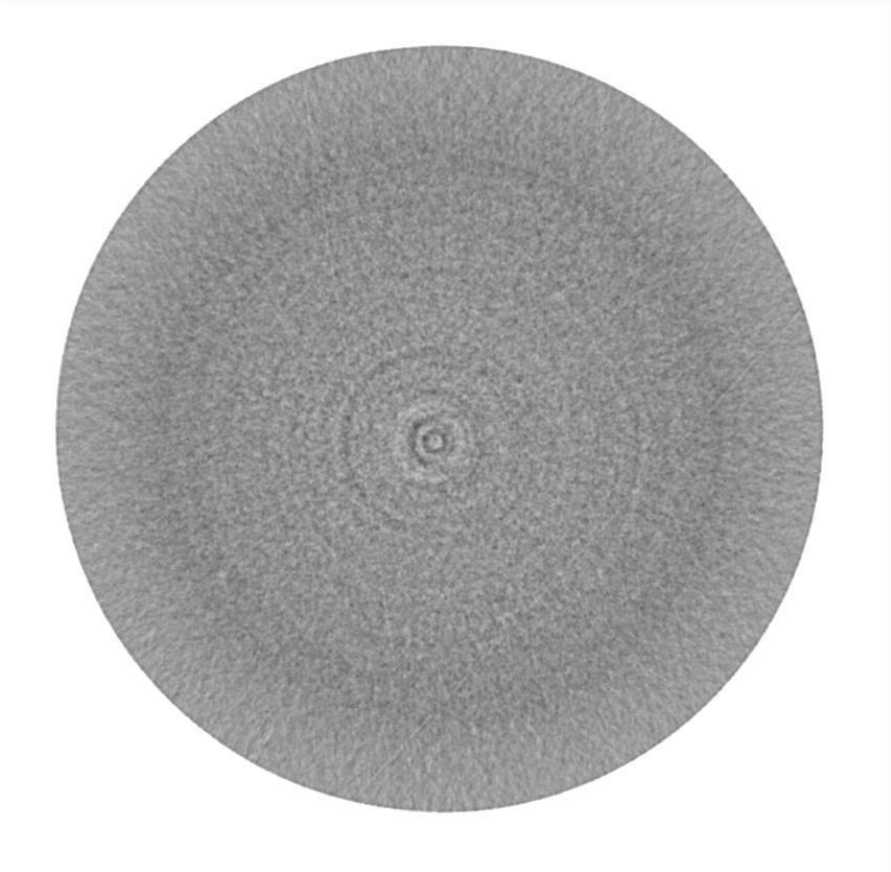

*Figure 2-18 Object with beam hardening correction ( Micro Photonics Inc. (2010).*

## 2.8 Image analysis

Image analysis of rock samples enable rapid estimation and characterisation of reservoir properties such as permeability, porosity, sorting, grain size and shape etc. (Coskun, 1996). The preparation of these samples is the most important step for successful image analysis in the sense that preserved core samples should be used with suitable thickness for transparent view when images are taken under light (Krinsley & Doornkamp, 1973). Although it is possible to achieve this on thin sections of consolidated samples it is difficult to do so while working on unconsolidated grains.

Typically, a digital camera is used via a high resolution microscope to capture images. (Al-Bazzaz & Al-Mehanna, 2007) Properties of the rock are characterised, assuming sufficient magnification to observe individual grains and pores (Solymar & Fabricius.M, 1999). The estimation of the permeability and porosity of the North Sea was performed with image analysis using an image magnification of 300x (Mortensen, Engstrøm.F, & Lind.I, 1998) Sandstone could be analysed under an image resolution of 5 μm/pixel but the magnification and resolution used for image analysis is dependent on the type of sample and the reservoir properties being investigated. Images acquired from SEM, TEM and optical microscopy give information about pore size and shape distribution. According to Andreola, et al. (2000), image analysis software converts the data gathered in a binary signal as a greyscale. Moreover, to, obtain a good image it is necessary to carefully choose the contrast because this has a significant impact when selecting the area of study from the matrix to be interpreted.

Likewise, an image with a good resolution must be obtained, using high-voltage filament, high collection time and a back-scattered detector (Andreola et al, 2000). The software can then calculate the chosen parameters from the pores of the object or sample.

This study uses image analysis as one of its principle methods to determine morphological properties followed by porosity and permeability through the use images that are sourced through Thin Sections images, 30 X- 300X magnification SEM images and 5μm to 8μm micro-CT images.

## 2.9 Morphological properties

This chapter primarily focuses on the literature review related to grain morphological properties and reservoir properties such as Porosity and permeability.

### 2.9.1 Grain Size

A grade scale is normally used to classify different sizes of In millimetre scale, each size grade differs from its predecessor by the constant ratio of 1:2 each size class has a specific class name used to refer to the particles included within it. This Udden-Wentworth scale is a geometric grain-size scale since there is a constant ratio between class limits. Figure 2-19 (Folk R. , 1951) (Blott & Pye, 2008). Krumbein (1934), as cited by Blott & Pye (2001), introduced the logarithmic transformation of Wentworth's millimetre grade scale into phi (ø) values, where, d is given as the grain diameter in millimetres as it can be observed from Figure 2-19. Determination of the grain size parameters can either be determined via mathematical or graphical measures. Although, many formulae have been proposed to determine the grain size parameters as summarized in Table 2-1, Mathematical method (method of moments) provides best calculated results , though due to the range with which it works from the data obtained, it also considers erroneous readings as part of the complete dataset introducing inaccuracies to the results obtained. On the other hand since logarithmic graphical method avoids errors it provides much better accuracy and hence is considered more applicable for this study. Only the logarithmic graphical method is explained, the remaining grain size formulae are summarized in Table 2-1.

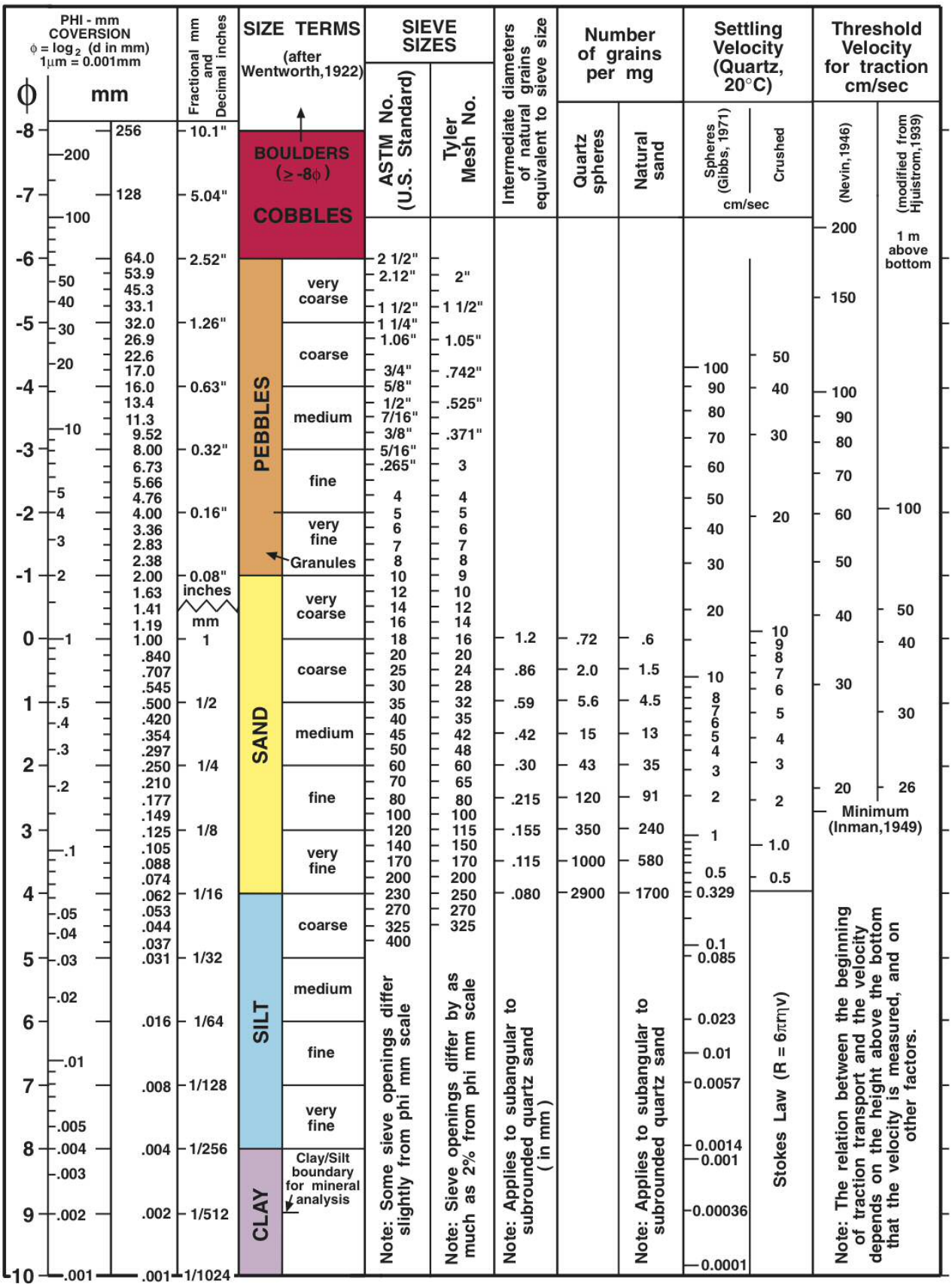


*Figure 2-19Udden-Wentworth grain size scale*

*Table 2-1 Formulae to determine grain size parameters*

| **Arithmetic Method of Moments** | | | |
|---|---|---|---|
| **Mean** | Standard Deviation | Skewness | Kurtosis |
| ____ | _____ _____ | S _____ | _____ |
| **Geometric Method of Moments** | | | |
| **Mean** | Standard Deviation | Skewness | Kurtosis |
| _____ | _____ _____ | S _____ | _____ |

| **Sorting (** | | Skewness (S ) | Kurtosis ( |
|---|---|---|---|
| **Very Well Sorted** | **<1.27** | Very fine skewed < -1.30 | |
| **Well Sorted** | **1.27-1.47** | Fine skewed -1.30 to -1.43 | Very Playtikurtik <1.70 |
| **Moderately Well sorted** | **1.47- 1.62** | Symmetrical -1.43 to +0.43 | Platykurtik 1.70 -2.55 |
| **Moderately sorted** | **1.62 - 2.00** | Coarse Skewed +0.43 to +1.30 | Mesokurtik 2.55- 3.70 |
| **Poorly sorted** | **2.00 - 4.00** | Very Coarse Skewed >+1.30 | Leptokurtik 3.70 – 7.40 |
| **Very Poorly Sorted** | **4.00 – 16.00** | | Very Leptokurtik >7.40 |
| **Extremely Poorly Sorted** | **>16.00** | | |

| **Logarithmic Method of Moments** | | | |
|---|---|---|---|
| **Mean** | Standard Deviation | Skewness | Kurtosis |
| ____ | _____ _____ | S _____ | _____ |

| **Sorting (** | **Skewness (S )** | **Kurtosis (** |
|---|---|---|

| | | |
|---|---|---|
| **Very Well Sorted <0.35** | Very fine skewed < -1.30 | Very Playtikurtik <1.70 |
| **Well Sorted 0.35 – 0.50** | Fine skewed -1.30 to -1.43 | Platykurtik 1.70 -2.55 |
| **Moderately Well sorted 0.50 -0.70** | Symmetrical -1.43 to +0.43 | Mesokurtik 2.55- 3.70 |
| **Moderately sorted 0.70 - 1.00** | Coarse Skewed +0.43 to +1.30 | Leptokurtik 3.70 – 7.40 |
| **Poorly sorted 1.00 - 2.00** | Very Coarse Skewed >+1.30 | Very Leptokurtik >7.40 |
| **Very Poorly Sorted 2.00 – 4.00** | | |
| **Extremely Poorly Sorted >4.00** | | |

## Geometric (modified) Folk and Ward (1957) graphical measures

| **Mean** | Standard Deviation |
|---|---|
| _____ | _____ _____ |

| **Skewness** | Kurtosis |
|---|---|
| _____ _____ | _____ |

| **Sorting (** | Skewness (S ) | Kurtosis ( |
|---|---|---|
| **Very Well Sorted <1.27** | Very fine skewed -0.3 to -1 | Very Playtikurtik <0.67 |
| **Well Sorted 1.27-1.47** | Fine skewed -1.0 to - 0.1 | Platykurtik 0.67-0.90 |
| **Moderately Well sorted 1.47- 1.62** | Symmetrical -0.1 to +0.1 | Mesokurtik 0.90 -1.11 |
| **Moderately sorted 1.62 - 2.00** | Coarse Skewed +0.1 to +0.3 | Leptokurtik 1.11 -1.50 |
| **Poorly sorted 2.00 - 4.00** | Very Coarse Skewed+0.3 to+1.0 | Very Leptokurtik 1.50 -3.00 |
| **Very Poorly Sorted 4.00 – 16.00** | | Extremely leptokurtic >3.00 |
| **Extremely Poorly Sorted >16.00** | | |

( f= frequency %, m= midpoint of each class interval in metric ($m_m$ ) or phi ($\phi$) units, P and $\phi$, grain diameter in metric ($m_m$) or phi ($\phi$) units respectively, at the cumulative percentile value of (x)

#### *2.9.1.1 Logarithmic Graphical Measures*

As suggested by (Blott & Pye, 2008) measurements derived from image analysis can be divided into four principal categories providing : average size, sorting, skewness and kurtosis. The selective columns from derived dataset can then be used to plot cumulative frequency curves. Which, primarily provides grain size distribution (average size, mode, median and mean) and the curve further provides prescribed values to substitute appropriate formulae to determine sorting, skewness and kurtosis.

Use of properties determined through image analysis of grains will provide means to determine morphology and further calculate porosity and permeability of respective samples by acting as an input values in necessary equations.

#### *2.9.1.2 Average Size*

The average particle size is defined by a variety of statically parameters. Mode corresponds to the highest point on the cumulative curve which represents the abundant or the most frequently occurring particle size. Median is the middle point on the cumulative curve, i.e. the 50% mark where sizes are divided equally in half (50% fines and 50% coarse) (MIT OCW, 2007). And Mean is the point on the cumulative curve where the areas below and above are exactly equal. The arithmetic mean is calculated using the method of moments, where the midpoint of each grade is the arithmetic midpoint between the grade-size limits in millimetres This is determined using the expression:

*Equation 2-1 Average size determination (Folk R. , 1966)*

Where corresponds to the grain size at 16, 50 and 84 % by weight (Folk, 1974).

### 2.9.2 Sorting

Sorting and packing is grain distribution property in relation to each other and grain sizes. Figure 2-20 developed by (Folk R. , 1966), provides means of inclusive graphic standard deviation for estimation of sorting.

*Equation 2-2 Sorting determination formula (Folk R. , 1966)*

$$\overline{\qquad} \quad \overline{\qquad},$$

where represent phi values at the same percentiles (Folk R. , 1966)

According to the range of readings sorting can be divided from very well sorted to very poorly sorted as seen in Figure 2-20, To determine properties, values are obtained through cumulative curve and substituted in equation. Sorting not only allows to assess type of sample and distribution of grains but it also assists in calculation of porosity , tortuosity and permeability and provides visual means for visualization, where in combination with grain mode factor and cementation index provides visual aspect for calculation.

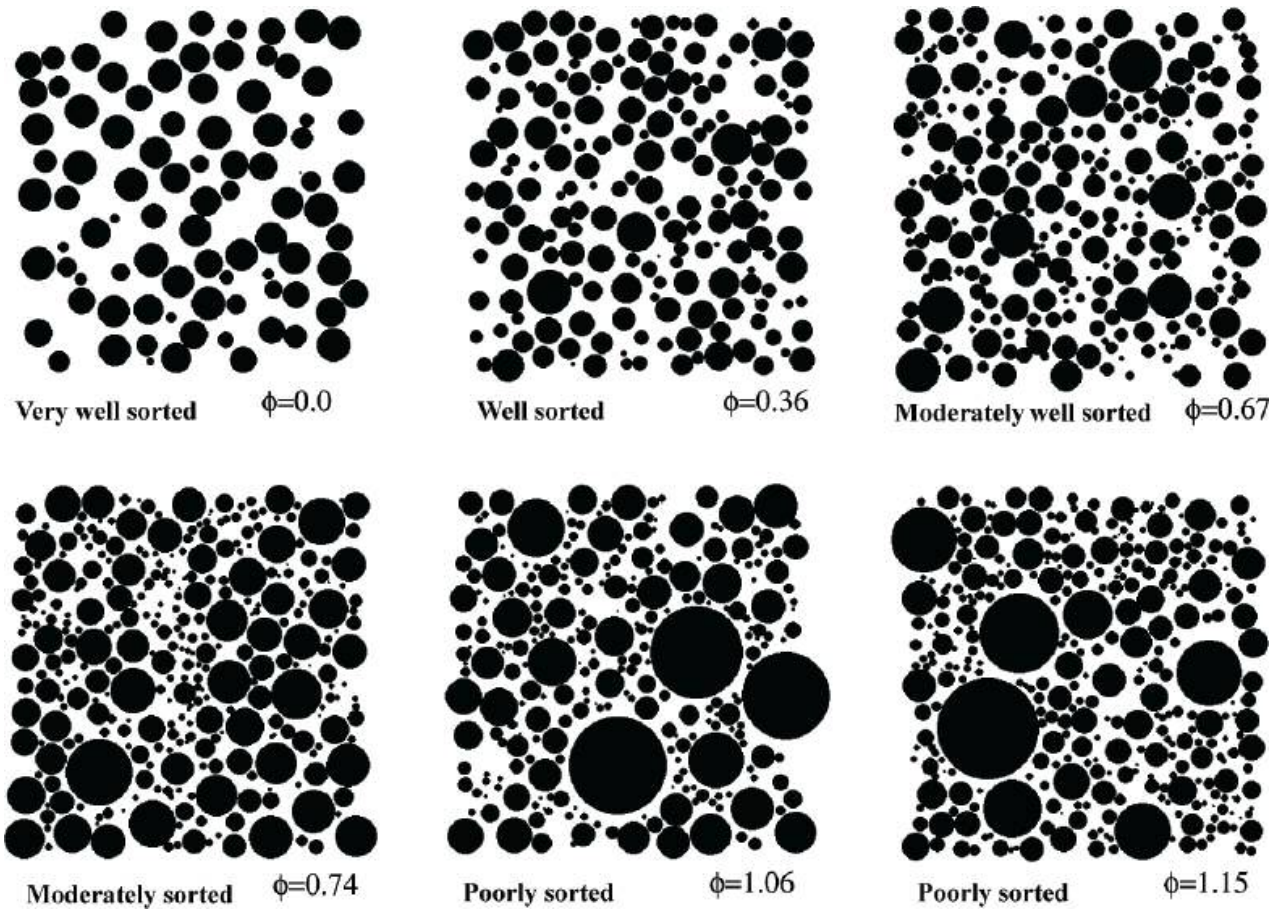


*Figure 2-20 Diagram explaining verbal Folks verbal classification (Folk R. , 1951)*

### 2.9.3 Skewness

Skewness measures the degree of symmetry of a cumulative curve. Different samples of similar sorting and average size may have different degree of symmetry, with one curve being symmetrical and the other curve may be asymmetrical (Folk, 1974). Inclusive graphic skewness is given by the following formula

*Equation 2-3 Skewness Calculation formula based on (Folk R. , 1966)*

$$\frac{\qquad\qquad}{\qquad\qquad}$$

where represent phi values at the same percentiles (Folk R. , 1966). Table 2-2 shows the summary of classification of skewness parameters and their interpretation. Skewness provides an estimate as to what kind of grain assemblage is present in grains. This assemblage provides further means of co relating grain properties to porosity and permeability.

*Table 2-2 Skewness classification and interpretation parameters*

| Values from | To | Mathematically | Graphically skewed to the |
|---|---|---|---|
| **+1.00** | +0.30 | Strongly positive skewed | Very Negative phi values , coarse |
| **+0.30** | +0.10 | Positive Skewed | Negative phi values |
| **+0.10** | -0.10 | Near Symmetrical | Symmetrical |
| **-0.10** | -0.30 | Negative Skewed | Positive phi values |
| **-0.30** | -1.00 | Strongly negative skewed | Very Positive phi values, fine |

### 2.9.4 Kurtosis

Kurtosis is defined as the measure of the “peakness” of a normal probability curve (Folk, 1974). The graphic kurtosis is defined by the formula

*Equation 2-4 Kurtosis calculation equation based on (Folk R. , 1966)*

$$\frac{\qquad\qquad}{\qquad\qquad},$$

where represent phi values at the same percentiles.

As seen from the graph of size vs abundance in Figure 2-21 it is a relative relation between the sorting observed within the central portion to the tail portion of the graph. A better sorting in the central portion of curve is described as been leptokurtic while a better sorting in the tails portion of the curve is described as platykurtic if the normal curve is followed, then it is considered to have normal kurtosis with the value 1.00. Figure 2-21 (East Carolina University, 2007; Folk, 1974). Table 2-3 shows the summary of classification of kurtosis and its interpretation derived by Folk and followed by East Carolina University as part of their studies.

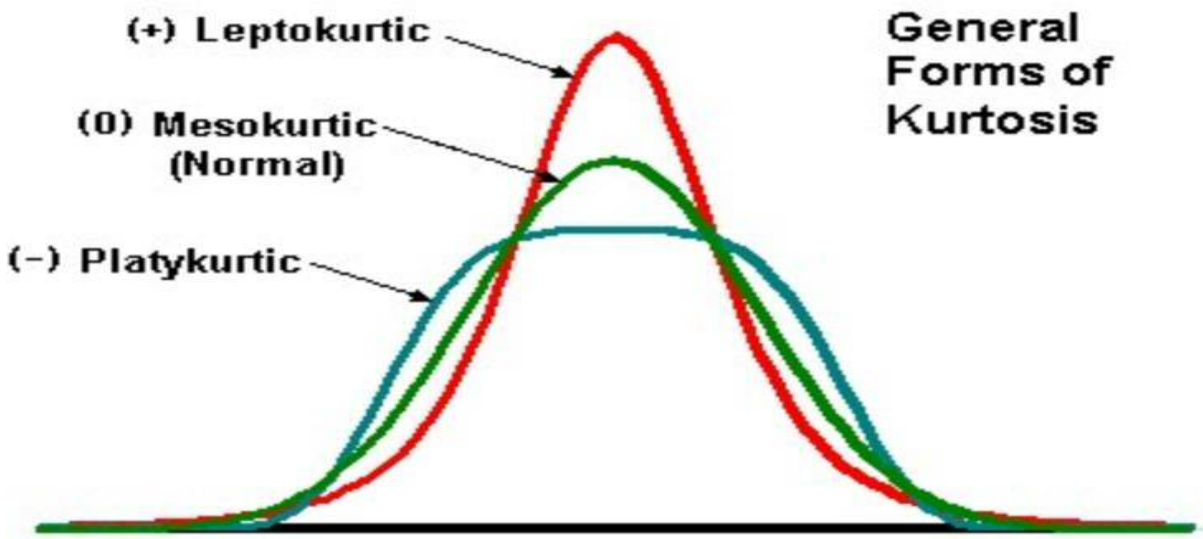


*Figure 2-21 Types of Kurtosis as described by (East Carolina University, 2007; Folk, 1974)*

*Table 2-3 Kurtosis Classification and determination parameters (Folk, 1974)*

| Values from | To | Equal |
|---|---|---|
| **0.41** | 0.67 | Very platykurtic |
| **0.67** | 0.90 | Platykurtic |
| **0.90** | 1.11 | Mesokurtic |
| **1.10** | 1.50 | Leptokurtic |
| **1.50** | 3.00 | Very leptokurtic |
| **3.00** | | Extremely leptokurtic |

## 2.10 Grain Shape

Shape of a grain sample can be defined in various ways by considering variety of approached shown in

Table 2-4 (Diepenbroek et al., 1992). It is more complex as a result of the consideration of 3 dimensional elements that are generated due to the weathering and transportation process that each grain passes through. Independent scientists and institutions have classified it through different definitions as it can be read ahead. The Oxford dictionary defines *"the shape of an object as an outline or its external form*"; Barrett (1980) defined shape as *"the external morphology of a particle which basically includes the form, roundness and the surface texture*"; while Winkelmolen (1982) defined shape as "*an exclusive parameter which is used to determine the amount of surface area of a given volume*'.

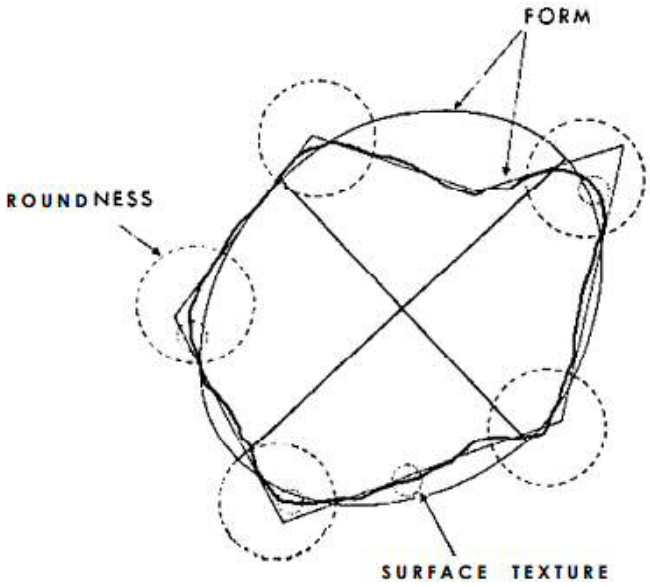


*Figure 2-22 Grain shape analysis guidance image(Diepenbroek et al., 1992)*

These variations in shape definition have always presented a challenge in the quantification of shape, especially since it is difficult to find a particular shape parameter that can accurately determine major characteristics of a grain or show the differences between various grain types (Cox & Budhu, 2008).

Table 2-4 shows a summary of parameters and methods that have been used for grain shape characterization

*Table 2-4 Methods and parameters used for characterization of grain shape*

| Property | Parameters, Features or Definitions | Authors |
|---|---|---|
| **Form** | Elongation and flatness | Wentworth,1992; Zugg,1935; Luttig in Sames ,1966; Calleux 1947 |
| | Angularity | Less 1964 |
| | Sphericity | Wadell,1932; Krumbein 1941; Aschembermer,1956; Sneed & Folk,1958 |
| | Factor 'F' | Aschembermer,1956;; Shape factor of Williams. 1965 |
| | Use of unmarked shape classes | Holmes ,1960 |
| **Roundness** | Roundness of sharpest corner | Wentworth 1919,1922; calleux,1947;Kuenen,1956; Dobkins & Folk, 1970 |
| | Average Roundness Corners | Wadell 1932; Russle & Taylor ,1937; Krumbein , 1941 ; Pettijohn 1949; Powers ,1953 |
| | Average Roundness from Convexity of outline | Krumbein & Pettijohn 1938 |
| **Surface texture** | Pebble features | Conybare & Crook ,1968 |
| | Quartz grain features | Krinsley & Doomkamp 1973 |
| | Surface texture resulting from internal texture | |
| **Fouriers Series** | Shape (wave of profile ) estimated by expansion of periphery radius as function | Ehrlich and Weinberg 1970 |

| | | |
|---|---|---|
| | of angle of grain's centre of gravity Fourier series | |
| **Fourier descriptors** | Calculation of shape descriptors from Fourier series coefficients | Beddow and Vetter 1977 |
| **Fractal dimension** | 2-D value ranging from 0 -1: describes the ability of a rugged boundary to occupy void space | Kaye 1982 |

### 2.10.1 Form

Sneed & Folk (1958) identified the concept of form as being the overall shape of a particle, which is also independent of roundness and surface texture (cited by Barrett, 1980). Form is usually quantified on the basis of its three main axes i.e long, short and intermediate axes. Table 2-5 shows a summary of some parameters which has been suggested historically for estimating form (Barrett, 1980).

*Table 2-5 Form estimation parameters*

| Author | Formula | Name or Description |
|---|---|---|
| **Indices of Flatness** | | |
| **Wentworth, 1922** | ____ | Flatness Indes |
| **Calleux, 1945**<br><br>**Zingg, 1935** | _ _ | Ordinate and adscissa for plot to characterize shape |
| **Luttig (In Sames,1966)** | ____ | Elongation |
| | ____ | Flatness |
| **Sneed & Folk, 1958** | _ | Flatness |

| | | |
|---|---|---|
| |  | Flatness I to the long axis |
| **Indices of Sphericity** | | |
| **Wadell 1932** | 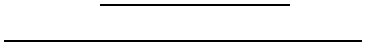 | |
| **Krumbein, 1941** |  | Intercept sphericity |
| **Sneed &Folk, 1958** |  | Maximum projection sphericity |
| **Aschenbremer, 1956** | 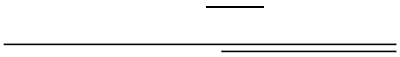 | Woking sphericity |
| **Other shape factors** | | |
| **Dobkins & Folk, 1970** | 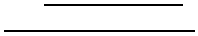 | Oblate-prolate index (OP index0 |
| **Aschenbremner,1956** |  | Shape factor F |
| **Williams,1965** |  | Williams shape factor |

### 2.10.2 Sphericity

Sphericity is one of the most important parameters when determining the form of a particle because it is a quantification parameter which is used to present the relationship between the three orthogonal axes. A particle has a higher sphericity if the three axes are closer in length and lower sphericity when there is a large difference in axes length (Alexzohrab, 2012). Wadell (1932) pioneered the estimation of sphericity of particles by comparing their surface area to the surface area of a sphere of the same volume (cited by Miller & Henderson, 2010) and various improvements have been made to this correlation as shown in Table 2-5.

### 2.10.3 Roundness

Roundness, which is another measure of grain shape characterization, describes the absence of angularity or a type of smoothness of the grain (Barrett, 1980). It is related to a particles curvature around its edges or corner (Cox & Budhu, 2008). Researchers have tried to develop a way to measure and visually describe the roundness of a grain from Wadell‟s (1932) roundness definition, Russell and Taylor‟s (1937) shape descriptors (angular to well rounded) to Powers‟ (1953) additional sixth class to the qualitative shape descriptor, with one major challenge: subjective to operators error, which is due to the fact that various users view the visual charts differently, thereby, giving different results (Miller & Henderson, 2010). The current practice for determination of a grain shape still involves using same visual charts in combination with other qualitative methods that are listed in Table 2-6 with their known challenges.

*Table 2-6 Methods for roundness characterization and their known challenges.*

| **Authors** | **Method** | **Characteristics** | **Problems** |
|---|---|---|---|
| **Wentworth 1919** |  | Regards position of measured corner on the particle , definite ultimate shape ( Sphere) | Only one corner, influence of sphericity extremely laborious |
| **Wentworth 1922** |  | Reduction to maximum projection plane measurement | Only one corner, influence of spericity laborious |
| **Wadell 1932** |  | Curvatures of all corners averaged, influence of sphericity reduced | Only convex parts, no definite ultimate shape, laborious |
| **Szadeczky-Kardoss 1933** | Relation : %C, $\%C_v$,% $C_c$ | Curvatures of the complete outline are evaluated | Semi- quantitative, no single roundness value, very laborious |
| **Russell & Taylor 1937** | Visual chart, five classes | [Wadell]. Quick procedure | Subjective (operator error), no discrimination |

| | | | |
|---|---|---|---|
| | | | of higher roundness grades |
| **Krumbein** | Visula chart, nince classes at equal steps | [Wadell], quick procedure, closely spaced discrimination | Subjective (operator error ) , difficult assignment of deviating forms |
| **Cailleux 1947** | — | [Wentworth] | Strong influence of sphericity, only one corner, laborious |
| **Pettijohn 1949** | Visual chart, five classes, geometrical scale | [Wadell], quick procedure | Subjective ( Operator error) , no discrimination of higher roundness grades |
| **Powers 1953** | Visula chart, six classes, geometrical scale | [Wadell], quick procedure, sensitive to lower roundness grades | Subjective ( Operator error) , no discrimination of higher roundness grades |
| **Kuenen 1956** | — | [Wentworth], Influence of sphericity reduced | Only one corner, laborious |
| **Schwarchz & Shane 1969** | Fourier analysis : ‘ roughness’ – rrot mean square difference (RMS) between calculated and observed radii on outline | Rapid procedure, objective, influence of sphericity is compensated, regards position of curvatures | No definite ultimate shape, insufficient discrimination of higher roundness grades |
| **Enrlich & Weinberg 1970** | Fourier analysis : ‘roughness’ | Rapid procedure, objective | No definitive ultimate shape, insufficient discrimination of higher roundness grades, influence of sphericity |

| | | | |
|---|---|---|---|
| **Dobkins & Folk 1970** | — | [Wentworth] & [Wadell], influence of sphericity reduced | Only one corner, laborious |
| **Swan 1974** | ——— — | [Wentworth] & [Wadell], influence of sphericity reduced | Only two corners, laborious |
| **Mazzullo & Haines 1988** | Fourier analysis | Rapid procedure | No definite ultimate shape, high mean errors, no discrimination of higher roundness grades, influence of sphericity |

### 2.10.4 Fourier Analysis

Fourier series has been applied in the quantification of grain shape through the application of a mathematical relationship to the grain shape. A polar signature technique is used whereby the Fourier series is represented using the periodic function (R) as shown in Figure 2-23 (Miller & Henderson, 2010; Cox & Budhu, 2008). The description of the grain profile is carried out by measuring the radii (R) at equally distributed angles, and also determining the value of after every radii measurement. A waveform is obtained by unrolling the particle profile Figure 2-23. The measured parameters are presented in an equation (Fourier series) which is used to describe the particle's shape.

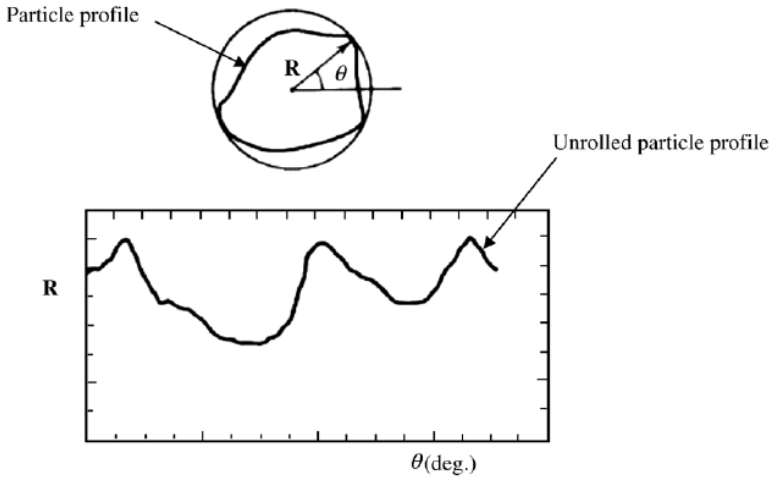


*Figure 2-23 Fourier series using polar signature function (Miller & Henderson, 2010; Cox & Budhu, 2008)*

Re-entrant angle is the major challenge associated with this technique resulting in various radii values for one angle. Another approach to the grain analysis using Fourier shape descriptor solved the re-entrant problem (Miller & Henderson, 2010; Bowman et al., 2001). The grain boundaries are analysed using Fourier shape descriptors which were determined using a set of complex Fourier analyses which yielded the descriptors. Bowman et al. (2001) concluded that the lower order descriptors provide information about the grain morphology signatures (grain shape) such as Asymmetry, Elongation, Triangularity and Squareness while the higher order descriptors correspond to information about the grain's texture.

## 2.11 Athabasca Oil Sands Properties

### 2.11.1 Grain size Distribution

Carrigy (1976) noted that Athabasca oil sands displays only a limited grain size distribution pattern and classified the grain size distribution into three self-defined classes which are a function of stratigraphic position and physico-chemical properties of oil sands as shown in Table 2-7.

The classes are listed as:

**Class I** defines oil sands that are coarse grained poorly sorted sandstone with conglomerates representing an ancient river channel deposit.

**Class II** are the richest oil sands typified by the middle McMurray formation with thicknesses of the order 100 feet or more having well sorted grains.

**Class III** consists of sands and silt particles that are generally less porous and thus contain less bitumen.

*Table 2-7 Classification of the McMurray Oil sands (Carrigy, 1976)*

| **Outcrop description** | **Characteristics of Particle size Distribution** | **Stratigraphic Occurrence** | **Depositional Environment** | **Oil Impregnation** |
|---|---|---|---|---|
| **Massive cross-bedded, coarse- grained sands and conglomerate** | Class I Maximum size greater than 1mm, median diamater not less than 0.13mm, percentage weight greater than 0.074mm is more than 80mm | Lower/Basal McMurray | Fluviated | Variable: may be very rich or leached of all oil |
| **Massive sand with some cross-bedding** | Class II maximum size less than 0.3 mm, median diameter not less than 0.074 mm | Middle McMurray | Lacustrine | Good |
| **Horizontally-laminated: silty and clayey micaceous sands** | Class III Maximum size less than 0.3mm, median diameter less than 0.12mm. Percentage by weight greater than 0.074 mm is less than 80 percent | Middle and Upper McMurray | Lacustrine or lagoonal: calm shallow fresh to brackish water | Variable: depends on sedimentary structure, interbedded sands and silts are richer than silty-sands |

## 2.12 Fabric studies

As detailed (Brewer & Sleeman, 1960) Fabric is the simplest concept of describing the physical characteristics of soil materials and rock. Wherein for soil fabric is the physical constitution of a soil material as expressed by the spatial arrangement of the solid particles and associated voids. In section 2.9.1 several methods of determination

of the size and shape are discussed. Though another important parameter that needs to be considered when working with sediments are that of the transportation. As transportation governs the final shape and size of the particle which is a direct result of undergoing destructive forces during this process.

(Mazzullo and Magenheimer, 1987) while determining the effect of weathering on grain size, shape and sphericity to ascertain their origin in Gulf coastal plain, Llano Uplift performed shape analysis, studied quartz grains of average size 120- 180 microns under the scanning electron microscope by selecting twenty grains from each slide by line method to conduct shape analysis. This study proposes to establish a connection between the grain, its origin and further assist in the determination of weathering processes it has undergone during transportation. (Marceline and Stoops,1996) developed a semi quantitative method to assess relative weathering of tropical sandy soil, where grains are classified on the basis of frequency and the size of etch pits on the basis of surfaces, using Scanning Electron Microscope. These studies have defined five grain classes based on etching size, further on the basis of which frequency of abundance is determined for all soil samples. Having frequency allows establishing a weathering score and comparing horizons.

(Baba and Komaros, 1981) studied quartz grains to measure and analyse the settling velocity of natural quartz grains by conducting sieve analysis method and considering the longest axial diameter intermediate diameter with settling time for grains. This analysis provides a mean settling velocity that takes into account average degree of grain irregularities found in natural sands. The results demonstrated that the settling velocity is not a function of roundness, but it is a function of sphericity of the grain. This is either expressed as a “Correy shape factor or E shape factor”.

### 2.12.1 Microstructural studies

According to the reservoir heterogeneity classifications by Krause et al. (1987) (cited by Slatt, 2006), microscopic (microstructural) heterogeneities are associated with pore morphology and grain morphology, grain size and grain arrangement. Therefore, microstructural study of the Athabasca oil sands is crucial to estimate their porosity and permeability. Further, it also helps in determining the nature of the grains" depositional environment. There are twelve possible microstructural studies but this study will only examine the grain shape, grain size, texture, image acquisition and

image analysis as these parameters primarily influence grain arrangement and reservoir properties.

### 2.12.2 Textural Maturity

This entails a combination of results obtained from the grain size and morphological analysis of grains to determine the degree of maturity of the sediments and consequently, infer the environment of deposition. The degree of maturity could either be immature, sub mature, mature or super mature. (Plumely, 1948) Defined a mature gravel or sand as one consisting of well sorted, mineralogically mature framework of grains. While (Folk R. , 1951) defined it as the degree to which sand is free of interstitial clay and it is well sorted and well rounded. Folks work reflects 3 stages involved in maturity of sediments; the first has to do with the removal of clay, followed by sorting of grain framework and finally the rounding of grain and its believed that the final depositional environment controls textural maturity.

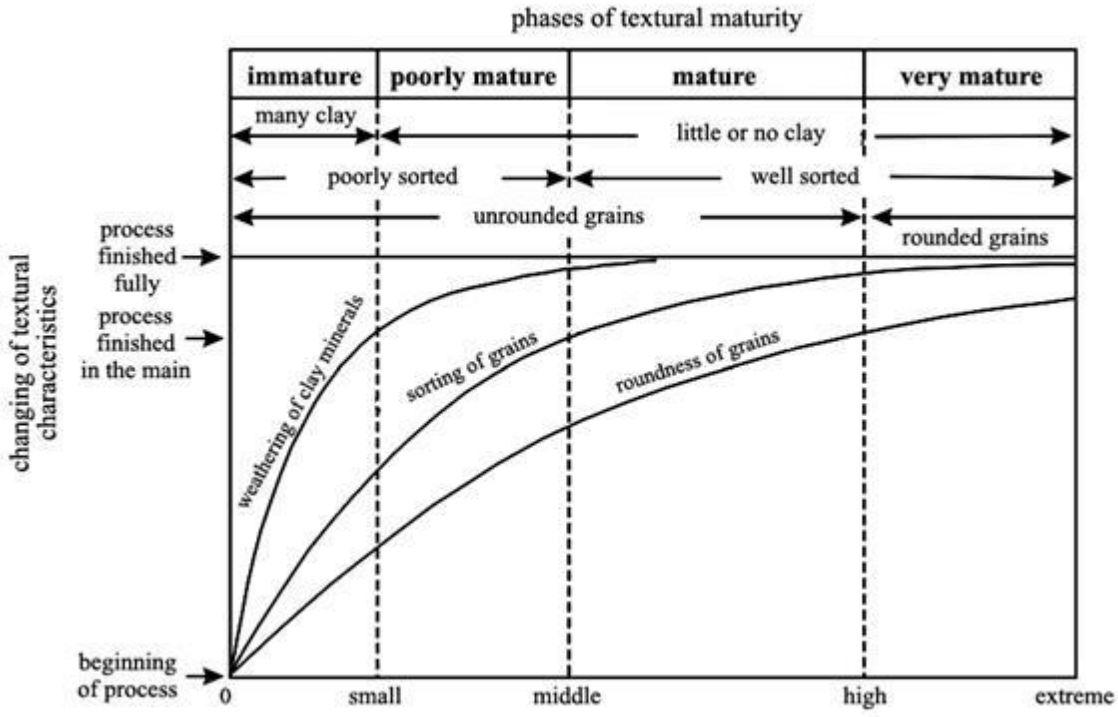


*Figure 2-24 Stages of textural maturity (Folk R. , 1951)*

Studies overtime have shown that the best sorting is achieved when sands/sediments are subjected repeatedly to reworking by a current of moderate intensity while the worse sorting is associated with sands/sediments that have undergone only one brief episode of mass transport. It is believed that sediments or rock which contain well

sorted & well rounded grains are texturally mature and these features imply large transport distance (with low mud content). Sediment maturity is a measure of the distance or length of time from the source area to the depositional location of the sediment as well as the kinetic energy during transport and reworking. As an effect of this transportation activity grains become well-rounded and well-sorted. Implying that maturity of resulting sediment is dependent on the transport distance, period in transportation medium, and the energy of that medium  Figure 2-24 (Folk R. , 1951). Some of the other features affecting sediment maturities are transport history and dispersion pattern.  Finally, the different level of sediment maturity is then used together with results from microtextural analysis to interpret the different depositional environments for the sediments.

Table 2-8 Grain Maturity and  Depositional environments (Folk R. , 1951)

| | **Immature** | **Submature** | **Mature** | **Supermature** |
|---|---|---|---|---|
| **Sorting** | Extremely poorly sorted to very poorly sorted | poorly sorted to moderately sorted | moderately well sorted to well sorted | very well sorted |
| **Grains Size** | very coarse or bigger | Coarse | Medium | Medium |
| **Roundness** | Angular | Sub angular | Rounded | well rounded |
| **Quartz composition** | Sparse | Common | Abundant | Very abundant |
| **Depositional environment** | Glacier Ice, mudflow, debris flow, alluvial fan | River, tidal current, surf, deltaic | Marine | Aeolian, beach |

### 2.12.3 SEM based Micro textural analysis

Studies have shown that the physical features contained within sediments as well as their Morphology (Roundness & grain Size and Sphericity) can provide important information on the origin/provenance of sedimentary deposit as well as the behaviour of sand grains within the medium in which they are being transported. The SEM (Scanning Electron Microscope) analysis of the surface features and shape of quartz grains has been used by many to explain the mechanical and chemical processes to which the grains were exposed to and their relationship with the different environment of depositional (Mazzullo & Magenheimer, 1987; Mazzulo, Sims, & Cunningham., 1986; Pye & Mazullo, 1994; Okhravi & Amini, 2001; Kasper-Zubillaga & Faustinos-Morales, 2007) SEM allows for in-depth examination of sand grains surface morphology. A large number of quartz grain surface textures have been qualitatively identified (Margolis and Kennett, 1971; Krinsley & Doornkamp, 1973;Higgs, 1979), and nominal and ordinal scale measurements of these textures have been used to infer environmental conditions (Margolis and Kennett, 1971; Bull, 1978; Flageollet and Vaskou, 1979). Some surface Identified include upturned cleavage plate, isolated depressions, chatter marks, conchoidal fractures, globules, pellicles of quartz etc. some of which could either be weathered, polished or fresh. It is also essential to identify the location of the microstructure, whether it is found in the depression or at the summit. Analysis carried out on grain surface makes it easy to differentiate quartz grains that have been wind transported (Mazzullo et al. 1986), as well as differentiation between glacial (Mahaney & Kalm, 2000; Pandey, et al., 2002), dune and beach sediments (Mazzullo et al. 1986; Kasper-Zubillaga, 2005). The Roundness of grains as well as their surface textures constitutes some of the important features used in studying fluvial environments ((Oakey, et al., 2005; Shine, 2006). In essence, the surface texture (microtextures) of quartz provide essential information about the various processes that grains were exposed to during their transportation as well as post deposition (Krinsley & Funnell, 1965; Doornkamp & Krinsley, 1971 (Moral-Cardona, et al., 1996, 1997; Mahaney, 1998; Newsome & Ladd, 1999). The method employed to identify mechanical and chemical features on grain surface and their significance to the different environments have been well established by several researchers (Krinsley & Donahue, 1968; Brown, 1973; Whalley & Krinsley, 1974; Baker, 1976; Al-Salech & Khalaf, 1982; Rahman & Ahmed, 1996). Hence, the

microtextural analysis of quartz grains is considered a powerful tool in the identification of provenance, processes of transport and diagenetic history of the detrital sediments (Krinsley, et al., 1976; Madhavaraju and Ramasamy, 1999; Madhavaraju et al., 2004, 2006; Armstrong-Altrin, et al., 2005; Kasper-Zubillaga & Faustinos-Morales, 2007). Various impact features as well as abrasion marks that are observed on surfaces are actually a result of dynamic transportation medium that a grain was subjected to. Being permanent changes these transportation effects are retained by grains even post deposition unless otherwise eroded by post depositional chemical reactivity. The features resulting from chemical reactions consists of various types of etching and overgrowth, the quartz grains from marine environment generally exhibit V-shaped patterns (V's), straight and curved scratches, with several protrusions (Krinsley and Doornkamp, 1973; Higgs, 1979; Madhavaraju and Ramasamy, 1999; Madhavaraju et al., 2004, 2006). The presence of subrounded features, bulbous edges along with a certain amount of V-shaped pits indicate fluvial origin (Linde, 1987; Mahaney, 1998). According to Margolish and Kenett (1971), V's generally occur on less than 50% of the grains from the fluvial origin and on more than 50% of those from high energy beaches. Those quartz grains of Aeolian origin exhibit well rounded shape, pattern of meandering ridges that resulted from the intersection of slightly curved conchoidal breakage patterns and upturned plates on their surfaces (Krinsley & Takahashi, 1962; Krinsley and Doornkamp, 1973; Mazullo and Ehrlich, 1983; Mazullo et al., 1986). Quartz grains from glacial origin display parallel striations, chatter marks and imbricated grinding features (Margolis, 1968; Higgs, 1979; Mahaney, 1995a, 1995b; Mahaney et al., 1996). On the basis of the different types of microtextures observed on the quartz grains, it is possible to distinguish the particular depositional environments such as marine, fluvial, aeolian and glacial. According to Ribault and Kristley, a very essential tool in studying successive depositional environment is the availability of similar work done on modern grains with widely varying provenance and great contrast in method of inheritance Figure 2-25

According to Margolish and Kenett (1971), V's generally occur on less than 50% of the grains from the fluvial origin and on more than 50% of those from high energy beaches. Those quartz grains of Aeolian origin exhibit well rounded shape, pattern of meandering ridges that resulted from the intersection of slightly curved conchoidal breakage patterns and upturned plates on their surfaces (Krinsley & Takahashi, 1962;

Krinsley and Doornkamp, 1973; Mazullo and Ehrlich, 1983; Mazullo et al., 1986). Quartz grains from glacial origin display parallel striations, chatter marks and imbricated grinding features (Margolis, 1968; Higgs, 1979; Mahaney, 1995a, 1995b; Mahaney et al., 1996). On the basis of the different types of microtextures observed on the quartz grains, it is possible to distinguish the particular depositional environments such as marine, fluvial, aeolian and glacial. According to Ribault and Kristley, a very essential tool in studying successive depositional environment is the availability of similar work done on modern grains with widely varying provenance and great contrast in method of inheritance Figure 2-25

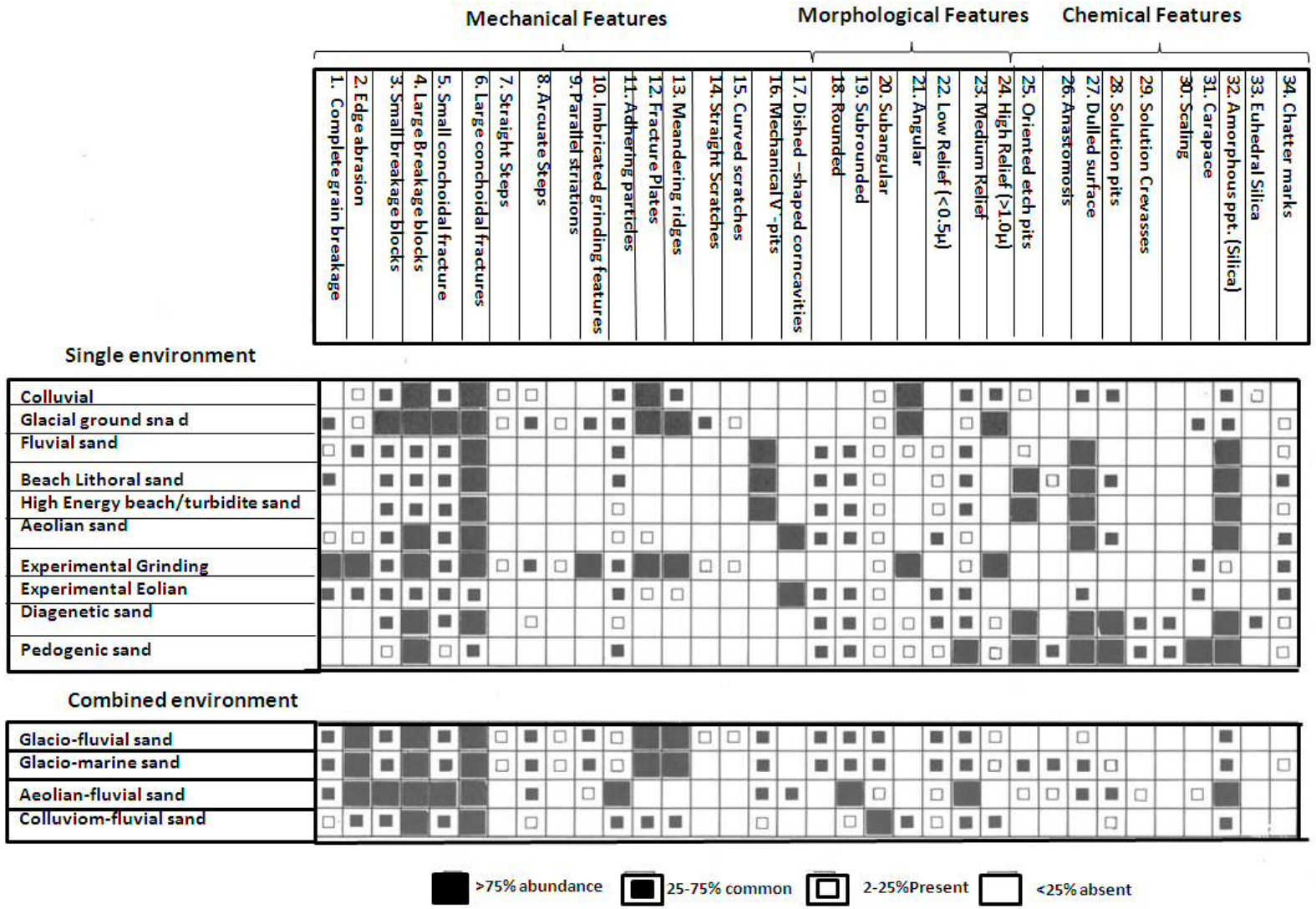


*Figure 2-25 Microstructures possible in variety of depositional environments based on (Bull, 1978)*

## 2.13 Reservoir Properties

### 2.13.1 SCAL analysis

To determine primary reservoir properties such as porosity grain density, horizontal permeability, saturation parameters and lithological description core plugs/ whole cores are subjected to the routine core analysis. Details of these techniques are described by (American Petroleum Institute, 1998) These techniques use 1 o r1.5-inch diameter core plugs to determine properties such as porosity, permeability, fluid saturation. (Mattax, McKinley, & Clothier, 1975) RCAL testing mainly implements three techniques: mercury injection method, porous plate method and the centrifuge method. The results of these tests are typically presented graphically as a capillary pressure vs. saturation curves. The implementation of these tests on the cemented samples is very well established, though the results may be affected when applied to non-cemented samples. Core testing on unconsolidated samples are typically extensions of the techniques for consolidated core plugs. However, there is often debate regarding the reliability and accuracy of these tests on unconsolidated core samples as demonstrated and studied by (Mattax, McKinley, & Clothier, 1975; Mele.G, 2011). (Shafer.J, et al., 2013) while reviewing advanced Petrophysical techniques describes all issues right from the stage of collection, that includes freezing, Epoxy based consolidation to performing experiments. One of the issue's with freezing being fracture formation due to rapid solidification and further author stresses upon requirement of minimum 50% water saturation in core for it to be solidified properly. The Epoxy method can also be debated based on the effects observed during thin section preparation as part of this study. Where an exothermic reaction of epoxy and polymer reduced viscosity of oil and resulted in loss of integrity of the core samples. (Shafer.J, et al., 2013) paper further states several issues with conventional core analysis being implemented to study unconsolidated sands and proposes use of digital core analysis which is a non-destructive method of analysis.

### 2.13.2 Porosity

Porosity can be defined as the percentage of pore volume or void space, or that volume within rock that can contain fluids and is measured in ( 1PU=1%) (Aminu.M.D. & Kulkarni.K., 2015)

Porosity can be generated during deposition of rock (Primary) or can be developed due to alteration of rock under physical conditions and/ or bioturbation (Secondary). It may also be generated due to the development of fractures during tectonic events. Total Porosity is the total void space in the rock whether or not it contributes to the flow. Thus, effective porosity is less than total porosity as it only consists of inter connected pores. As may be seen from Figure 2-26 the area denoted by V stands for Vugs ( large pores) which along with all other smaller intergranular spaces contributes towards total porosity of a sample.

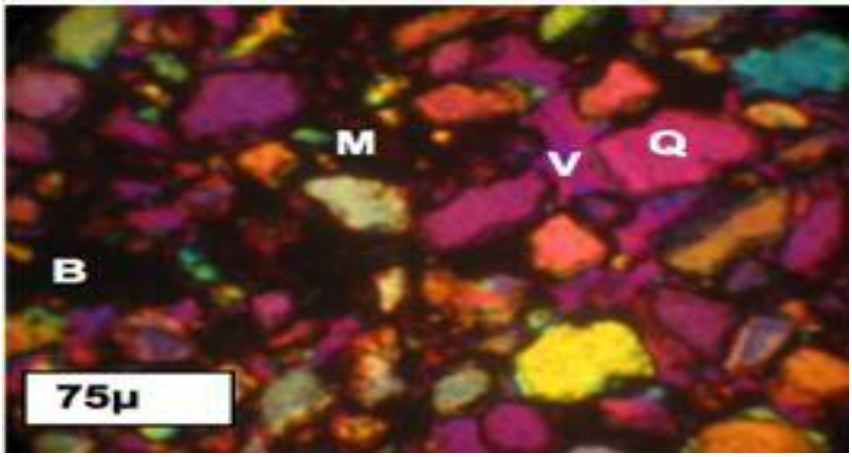


*Figure 2-26 Thin section image showing components of the outcrop samples (B: Bitumen,M: Matrx,V: Vugs, Q: Quartz). (Aminu & Kulkarni, 2015)*

Porosity can be measured with the help of core samples, Petrographic Image Analysis (PIA) or even with logs (NMR, density, neutron and sonic). It is calculated by obtaining the ratio between the pore and bulk volume:

*Equation 2-5 Porosity equation*

$$\phi = \frac{V_{pore}}{V_{bulk}}$$

Where:

$V_{pore}$ = pore volume

$V_{bulk}$ = bulk rock volume

### *2.13.2.1 Helium Porisimetry*

This technique is used to determine the effective porosity of a material using helium gas expansion. Notably, helium is a small molecule, so it can easily occupy smaller

spaces (pores) of a rock. This method uses two chambers to examine change in pressure to calculate the volume of sample (Andreola et al., 2000). However, this method presents a slightly higher porosity value on any selection of rock sample.

On completion of the process porosity is calculated by using

*Equation 2-6 Helium Porosity equation*

$$\frac{V_{matrix}}{V_{Bulk}}$$

Where:

$V_{matrix}$ = volume of solid particles that are part of the rock matrix

$V_{Bulk}$= Total Volume of the rock sample.

#### *2.13.2.2 Mercury Porosimetry*

In the view of Giesche (2006), this is a unique method that can provide data related to the pore size distribution, porosity, the specific surface area of a sample and apparent density. The only drawback is that it can take up to 30 minutes to complete the analysis and it does not measure the inner size of a pore, just the largest entry moving to the pore. This occurs because of the high interfacial tension of mercury, in other words, mercury does not wet every surface.

If the external pressure were increased, the rate of liquid penetrating small pore spaces would be higher. In order to do that, the Washburn equation, a commonly used mathematical correlation, can be manipulated to determine pore volume (Andreola et al, 2000).

Wherein, The coarsely granular sample of the thoroughly outgassed material is weighed and placed in a steel pressure bomb which is then evacuated until all absorbed gases are removed. Pure mercury is then admitted to fill the bomb and a series of pressure and volume measurements are made at various pressures up to the highest pressure it is desired to employ.

A force balance equation known as Washbunr's equation Equation 2-7 for the core sample having pores can be given as

*Equation 2-7 Washburn's Mercury injection based porosity calculation equation*

$$\_\_\_\_\_$$

Where: = Pressure of liquid

= Pressure of Gas

= Surface-tension of liquid

= Contact Angle

=Pore Diameter

Since this is performed in vacuum the pressure is zero. The contact angle os mercury with most solids is between $135^0$ to $142^0$ The surface tension of mercury at $20^0$ C under vacuum is480 mN/m.

As pressure increases, so does the cumulative pore volume, From the cumulative pore volume determined porosity can be reported.

*2.13.2.3 porosity using Image Analysis System*

As it may be seen from previous sections there are well established methods to determine porosity following laboratory experiments. Though, both methods apply pressure on samples that are subjected to property determination. This may work properly in the case of consolidated samples, though it will not work in case of an unconsolidated sample where a lack of cementing matrix will impact accuracy of the readings. As a result, an alternate approach to determine porosity following use of image analysis is considered. The following section looks at some of the case studies related to the use of Image analysis in determination of Porosity.

Image based porosity as estimated by James, (1996) involves the digitization of *25 fields* of view for each of the examined thin sections using fourier analysis of the 2-D *binary image* of the digitized thin sections. A reliable correlation and results have been obntained 2-D images of thin-section to characterize pore spaces in reservoir rocks by several studies such as (Ehrlich *et al.,* 1991; James, 1996, Krause *et al.*, 2009).

Similarly, Coskun and Wardlaw (1995) applied image analysis to calculate porosity of the sandstone core sample. Thin section images were digitized using AREISS-II image analyser, using a resolution of 5µm/ per pixel. The PIA software was applied to aid image transformation into binary image which allowed discrimination between pores and non-pore based on the light intensity.

Solymar and Fabricius (1998) used microscopic images to estimate porosity in the poorly consolidated Arnager Greensands by classifying the rock components into three phases based on their grey value; macro-pores, clay and particles. Porosity was calculated by estimating the ratio (pixel ratio) of the macro pore phase to the clay phase and the particle phase.

Tomutsa et al (1989) correlated values of porosity determined by image analysis of thin sections to porosity derived from the use of core plugs. The study involved the correlation of porosity from the Muddy formation and the Shannon formation. A high positive correlation was obtained from the Image analysis porosity when compared with the porosity derived from the use of core plugs as seen from Figure 2-27. However, a lower positive correlation was obtained in the Shannon formation whose composition include higher concentration of clays and silt-sized materials Figure 2-28.

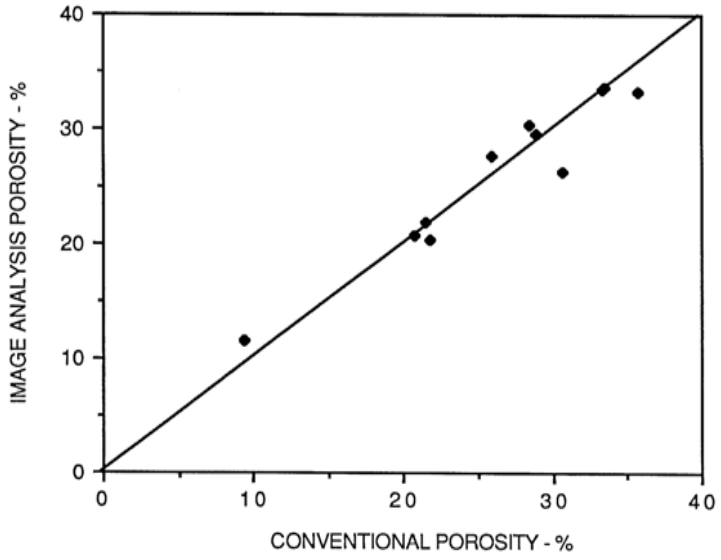


*Figure 2-27 Correlation of Porosity derived from Image Analysis to porosity derived from the used of core plug in a Muddy Formation (Tomutsa et al., 1989)*

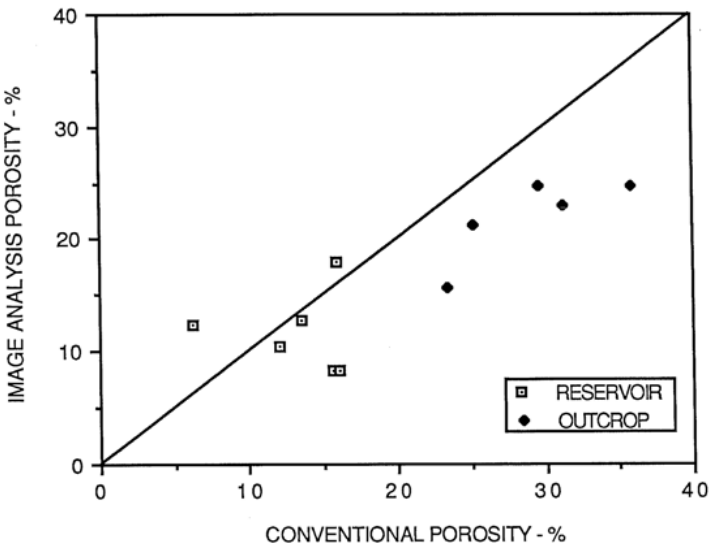


*Figure 2-28 Correlation of porosity values obtained from applying both Image Analysis and Core plug in determining porosity based on outcrop sample and reservoir samples of the Shannon Formation (Tomutsa et al., 1989).*

Al-Bazzaz *et al.,(*2007) and Krause *et al.,* (2009) similarly measured porosity in thin-sections prepared from core sample after the image of region of interest (ROI) have been converted using image analysis program from the thin sections into grey-scale images. A grey scale image consists of values from 0-255, wherein 0 represents black and 255 represents white spaces. Krause *et al*, (2009) noted that the grey scale image must further be converted into binary images (two-valued images 1 and 0) by the image analysis software selecting a threshold value between 1 and 255, where values above 255 are converted into black (rock) or the selected threshold colour and value below are converted into white representing pore spaces.

Image based porosity was calculated using the equation below:

*Equation 2-8 Image Analysis based Optical Porosity calculation equation*

$$\text{Total Optical Porosity (TOP)} = \frac{\qquad\qquad\qquad\qquad\qquad\qquad\qquad\qquad}{}$$

### 2.13.3 Permeability

Permeability can be defined as an ability of a rock to transmit fluid through. It is generally measured in decries and milidarcies (mD). Formations that readily transmit the fluids due to its interconnected nature are said to be permeable (e.g. sandstones) these rocks are expected to have well connected pore spaces that facilitate transmission of this fluid. These rocks can be classified as good quality reservoir rocks. On the other hand, rocks that do not readily transmit the fluid through are known

as impermeable (e.g. Shale) Even though shale has high porosity, those pores are not interconnected to allow passage of fluid through. Being impermeable these rocks tend to have poor reservoir quality.

#### *2.13.3.1 Permeameter*

In 1856, Darcy laid foundation to measuring permeability through his experiment. During this experiment he measured flow of fluid through a sandpack at a defined pressure using gravity. While the fluid was allowed pressures were measured at the top and bottom of his apparatus. The setup developed through this mechanism is called permeameter. The American Petroleum Institute (API) have published Darcy's complete technique (Hepler & Hsi, 1989, Glover, 2013). The Darcy equation is then presented as

*Equation 2-9 Darcy's Permeability Equation*

$$q = \frac{kA(P_i - P_o)}{\mu L}$$

Where:

q = the volumetric flow rate ($m^3/s$)

k = the permeability (darcy or md)

A = the cross sectional area of the sample ($m^2$)

$P_i$ = the inlet pressure (Pa)

$P_o$ = the outlet pressure (Pa)

$\mu$ The viscosity of the fluid (centipoise)

L = the length of the tube (m)

Darcy's experiment used different units for calculation, which later had to be determined considering their utility in different areas of work. In geological terms, darcy is a very large number so normally millidarcy (mD) replace it (1D = 1000mD = $0.9869 \times 10^{-12}$ $m^2$).

In the absence of Darcy's flow, other models such as Kozeny and Carman (1956) developed the following equation to determine permeability of a porous medium,

*Equation 2-10 Cozeny Karman Permeability equation*

$$\frac{\quad}{\quad}$$ ,

where:

c is a constant based on the porous medium as well as the tortuous channels (Di Giovanni et al., 2012).

As well as Kozeny and Carman, Happel (1965) announced a model that was a function of porosity only.

*Equation 2-11 Happel's Porosity based Permeability calculation equation*

Depending on applicability to the reservoir conditions a variety of models have been developed. There are many other equations that have been developed to adopt variety of reservoir conditions around the work but the most widely used are Kozeny-Carman and Van Baaren, Bergs Equation and Krumbien and Monk's equation.

### *2.13.3.2 Krumbein and Monk's equation*

Krumbein and Monk initiated determination for permeability using sand pack that had consistent porosity of 40%. This was achieved by sieving the samples and maintaining well sorted nature of the sample. Analysis of their data, coupled with dimensional analysis of the definition of permeability, led to

*Equation 2-12 Krumbien Monk's Permeability determination equation*

where:

- $k$ is given in darcies
- $d_g$ is the geometric mean grain diameter (in mm)
- $\sigma_D$ is the standard deviation of grain diameter in phi units, where phi=-$\log_2(d)$ and $d$ is expressed in millimeters

Since Krumbien and Monk did not use variation within porosity Beard and Weyl experimented using similar setup and Krumbien and Monk's equation but having variation within porosity of the sample ranging between 23% to 43%. Based on their tabulation they came up Figure 2-29. Where they observed rather than change in porosity primary control on the k is due to the changes in sorting.

(Morrow, Huppler, & and Simmons, 1969) using statistical techniques on gulf coast data observed that permeability correlated best with the logarithm of grain size times sorting if the fines fraction, taken to be <44 μm, was accounted for.

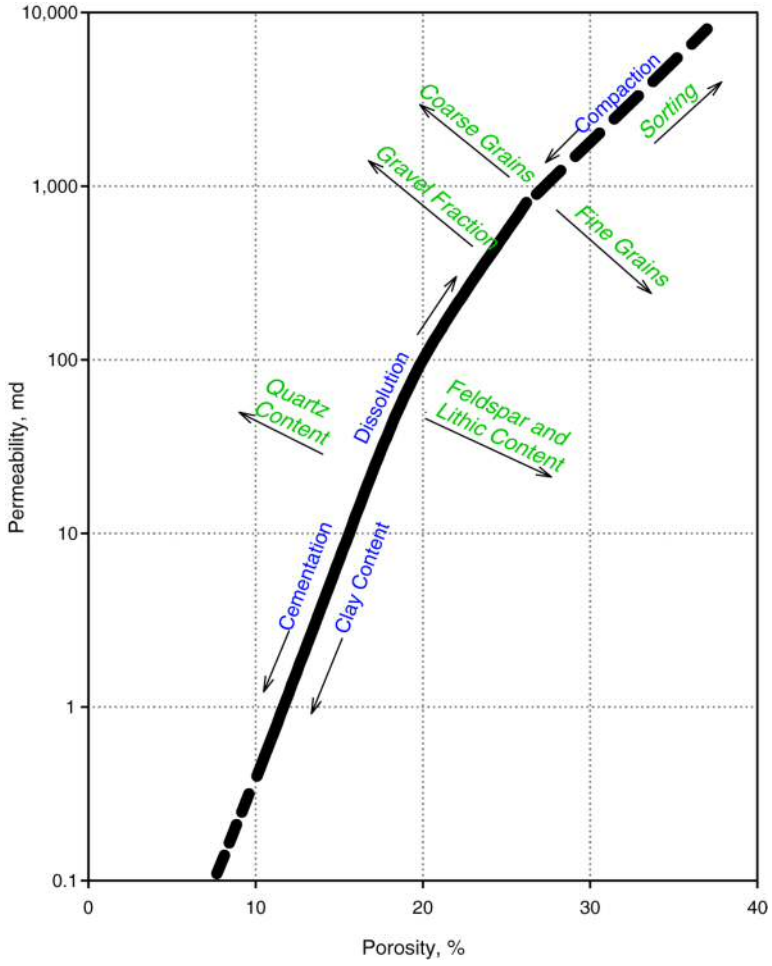


*Figure 2-29 Sketch of the impact of primary depositional features (such as quartz content and sorting, in italics) and diagenetic processes (such as compaction and cementation) on permeability/porosity trends in sandstones. (PetroWiki Porosity Vs Permeability for Morrow paper)*

### *2.13.3.3 Berg's model*

An interesting model linking petrological variables—grain size, shape, and sorting—to permeability is that of Berg. Berg considers "rectilinear pores," defined as those pores that penetrate the solid without change in shape or direction, in various packing's of

spheres. Simple expressions for *k* are derived from each packing, which form a linear trend when log(*k*) is plotted against log(*Φ*). From these geometrical considerations comes an expression relating *k* to *Φ* raised to a power and to the square of the grain diameter,

*Equation 2-13 Berg's Permeability equation*

where:

*k* is given in darcies *d* (in mm) is the median grain diameter *Φ* is porosity in percent *p*, a sorting term

If permeability is expressed in millidarcies, *d* in micrometres, and *Φ* as fractional porosity, this expression becomes

*Equation 2-14 Berg's equation for k:millidarcies d: micrometres and fraction porosity*

To account for a range of grain sizes, Berg considered two mixtures of spheres and assumed that k will be controlled primarily by the smaller grains. This introduces a sorting term $p=P_{90}-P_{10}$, called the percentile deviation, to account for the spread in grain size. The *p* term is expressed in phi units, where (in mm). For a sample with a median grain diameter of 0.177 mm, a value of 1.0 for *p* implies that 10% of the grains are >0.25 mm and 10% are <0.125 mm.

As seen from Figure 2-30 that takes *p*=1 and varying *d*. Permeability increases with in proportion to the fifth power of while simultaneously migrating downwards and to the right with decreasing grain size. (Nelson, 1994) while studying Porosity-Permeability relationships in sedimentary rocks found remarkable similarities found that this is concordant to many other models available and is applicable to quartzose rocks. This model can also assist is study of porosity values <30%.

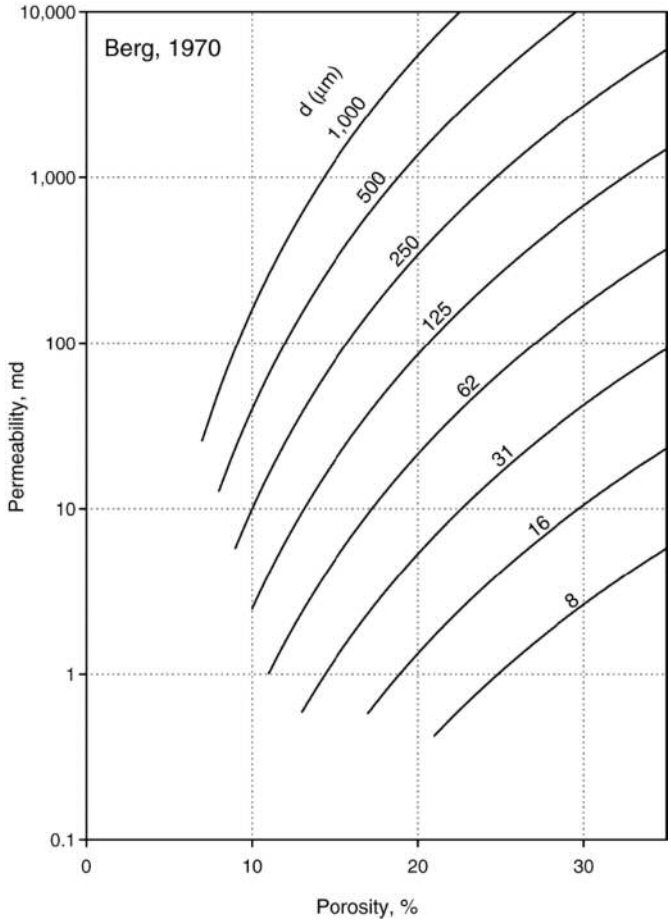


*Figure 2-30 Theoretical model by Berg relating permeability to porosity with varying median grain size (d).*

### *2.13.3.4 Van-Baaren method*

Van Baaren (1979) used a similar method to Berg (1970) in which Berg developed a model that incorporates porosity, grain size and sorting and so did Van Baaren.

*Equation 2-15 Van Barren's Permeability equation*

Where:

= modal grain size

m = Archie cementation exponent

C = sorting index

Depending on depositional conditions different rocks have distinct permeability values. Table 2-9 below summarizes how permeability can be classified. Taking into

consideration that permeability is dependant on Porosity, the following assumptions are made in constant conditions.

1. The higher the porosity, the higher permeability it will have depending on turtosity.
2. Small grains mean smaller pores. Therefore, the permeability is reduced and there will be high friction between the fluid and the rock.

*Table 2-9. Classification of reservoir permeability (Glover, 2013)*

| Permeability (mD) | Classification |
|---|---|
| **<10** | Fair |
| **10 – 100** | High |
| **100 – 1000** | Very High |
| **>1000** | Excellent (rare) |

#### *2.13.3.5 Estimation of Permeability based on Grain size Distribution*

The Athabasca oil sands have been described as unconsolidated sandstone reservoir with a very high permeability value in the McMurray Formation (Mossop, 1980). The oil sands have been described as parallel to a cohensionless formation in soil and rock mechanics, this term is used to describe formation with no significant grain to grain cementation (Dusseault, 2001).

Grain size has been identified as a fundamental independent variable controlling Permeability in unconsolidated sediments and rocks (Graton and Fraser, 1935; Reyes, 1966; Morrow et al., 1969; Shepherd, 1989). Several empirical relationships have been developed to estimate permeability based on the measured grain size distribution in the sample under investigation most popular is the intrinsic permeability equation:

*Equation 2-16 Intrinsic Permeability equation*

Where:

K= Permeability

C= is a dimensionless constant (C usually includes properties such as path turtuosity, particle shape, sediment sorting)

D = representative grain diameter

The works of Carman and Kozeny in estimating permeability has been applied by Wyllie and Gardner (1958) to petroleum engineering in estimating permeability based on the use of empirical relationships using grain size distribution, sorting and the permeability for sand particles and sandstone (Beard and Weyl, 1958).

Carman-Kozeny equation version based on grain diameter has also been developed to predict permeability as shown below for uniform spherical grains:

*Equation 2-17 Carman- Kozeny equation for spherical grains*

Where:

K = permeability = Tortuosity

= Porosity

= Particle diameter

Mortensen et al., (1998) presented a version of Kozeny's equation (Kozeny 1927) based on the theoretical relationship for a laminar flow through a porous medium. The equation relates permeability to the physical properties of rocks as shown below:

*Equation 2-18 Carman-Kozeny equation modified by Mortensen et.al. 1998*

Where k= permeability of the fluid

S = grain surface per bulk volume

= specific surface (grain surface area per grain volume)

d = equivalent spherical diameter

c = Kozeny's constant (found to be between 0.22 and 0.24 for natural materials).

Semi-empirical equations relating permeability to the textural property of a rock such as grain size distribution, porosity and sorting was derived by Van Baaren (1979) as shown below:

*Equation 2-19 Semi Emperical Permeability equation by Van Baaren*

Where:

= grain diameter in $\mu m^2$, derived microscopic inspection

= porosity

m= Archie cementation factor

c= a constant derived from the sorting when rock is observed under microscope

Van Baaren ,(1979) presented a range of values (Table 3 ) for the constant "c" to ranging from a value of 0.70 for extremely well to very well sorted.

*Table 2-10Relationship between the constant c and Degree of sorting (Van Baaren, 1979)*

| **Degree of Sorting** | **C** |
|---|---|
| Extremely well to very well sorted | 0.70 |
| Very well to well sorted | 0.77 |
| Well sorted | 0.84 |
| Well to moderately sorted | 0.87 |

| | |
|---|---|
| Moderately sorted | 0.91 |
| Moderately to poorly sorted | 0.95 |
| Poorly sorted | 1.00 |

Similar for the cementation factor Van Baaren (1979) derived factors comparing the degree of consolidation to the cementation factor for atmospheric sample (exposed samples) and for in-situ samples as outlined in Table 2-11Relationship between cementation factor and degree of sorting (Van Baaren, 1979)..

*Table 2-11Relationship between cementation factor and degree of sorting (Van Baaren, 1979).*

| **Degree of Consolidation** | **Cementation Factor (Atmospheric)** | **Cementation factor (in-situ)** |
|---|---|---|
| Shallow , very consolidated sands | 1.2 | 1.2 |
| Unconsolidated sands | 1.4 | 1.6 |
| Unconsolidated to friable sands | 1.5 | 1.7 |
| Friable sands | 1.6 | 1.8 |
| Hard to friable sands | 1.7 | 1.9 |
| Hard sandstone | 1.8 | 2.0 |
| Very hard sandstone | 2.0 | 2.2 |

### 2.13.4 Relative Permeability

A dimensionless term devised to adapt the Darcy's equation to multiphase flow conditions. Relative permeability is the ratio of effective permeability of a particular fluid at a particular situation to absolute permeability of that fluid at total saturation. As

relative permeability takes into account relative movement of fluids in presence of one another, it is extremely important to consider it oil production. This is primarily due to the presence or addition of fluids to produce hydrocarbons. The composition of material produces an additional challenge in this case as the matrix phase of the samples is not cemented.

This being one of the most important properties, several studies have been conducted to understand how relative permeability behaves for unconsolidated samples with variety of viscosity.

One of the early attempts at studying permeability through experimental means was performed by Polikar(1980). This study was followed by Polikar et.al (1990) study that took into consideration the effect of temperature range from $100^0$ C to $250^0$ C with water and oil being the principle fluids to move through the reservoir at an unsteady state . They observed that oil relative permeability curve was convex and concluded that temperature has little or no effect on relative permeability of water oil systems. Additionally, it was reported that there was no significant difference between steady and unsteady state methods. Relative permeability in Canadian Oil Sands is quite difficult to predict though several researchers have conducted detailed studies. One of the major study's conducted by Romanova et.al. 2015 talks about working with laboratory-based core analysis from twenty years of data for Cretaceous formation in Western Canada. While consolidating his work team has studied core samples under thin sections, micro CT and SEM analysis. Their observations have revealed that samples from Mcmurray formation has 90% quartz with 5% of fines with 1 % of kaolinite and trace amounts of other clay elements. Further their study reveals that open pores within Mcmurray formation may allow kaolinite to migrate through the reservoir causing some plugging effect within reservoirs depending on flow rates and placement of clays. In certain conditions due to high temperatures and chemical reactions taking place within reservoir the clays have altered from Kaolinite to Smectite. This may definitely lead to the plugging of reservoir due to inherent properties of smectite to swell while in affinity of water causing significant reduction in porosity and permeability of reservoir.

The data of low and high temperature water-oil relative permeability and steamflood data for sand suggests the following observations

1. Water Oil relative permeability curves are very supressed an end point relative permeability to water is typically in the 0.01-0.1 range.
2. Residual oil saturation decreases in hot water/steam flooding with an increase in temperature
3. A general increasing trend of the brine permeability with increasing temperature is observed with the largest increase in brine permeability being noted at temperature <100$^0$ C
4. Data from high temperature oil floods conducted after water flooding to examine hysterisis effects show that temperature increased with trapped water saturation increases.

The relative permeability curves for good quality reservoir with 10D air permeability with 38% porosity and 90% PV initial Oil saturation gives high recovery factor of 94%. The data set shows that as temperature increases, end point brine permeability increases i.e. no formation takes place in this case.

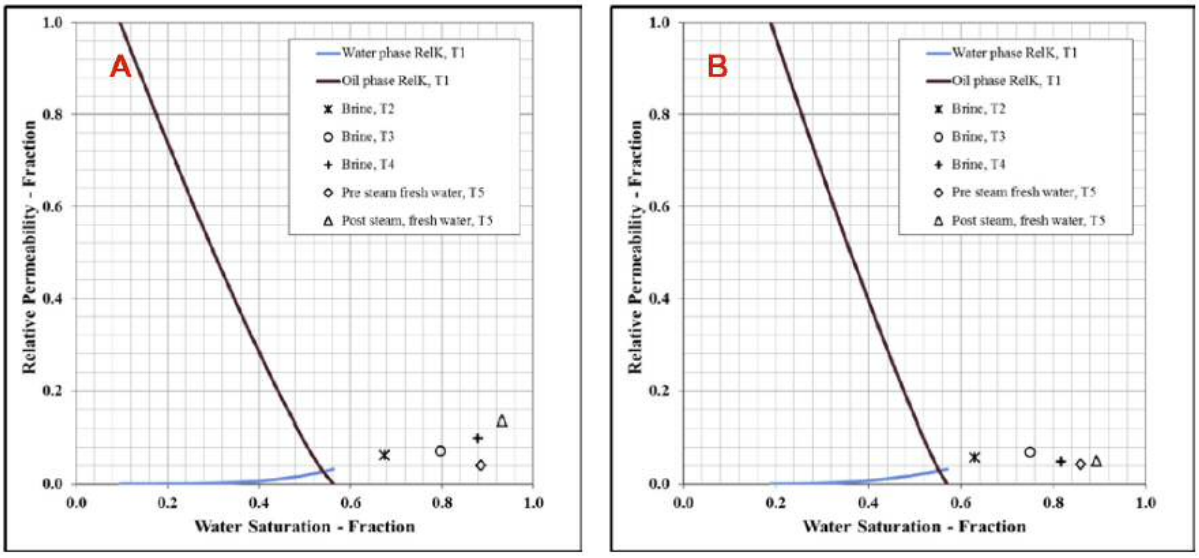


*Figure 2-31 Examples of high temperature -high pressure water-oil relative permeability and steam flood test results for typical McMurray sands (Romanova.U.G, Ma.T, Piwowar.M, Storm.R, & J., 2018)*

## 2.14 Oil properties for this region

Oil can be characterized in numerous ways, but some of its characteristics can play a huge role when determining the type of oil being investigated. Some of these characteristics might be porosity, permeability, viscosity, specific gravity and others as shown in Table 2-12.

Viscosity measures the resistance of a fluid to flow, measured in centipoise (cp). It helps determining the quality of the oil. In most cases, for heavy oil the viscosity is always above 100 cp. Most of the recovery methods in the oil industry tend to reduce the viscosity so oil can pass through the pipes.

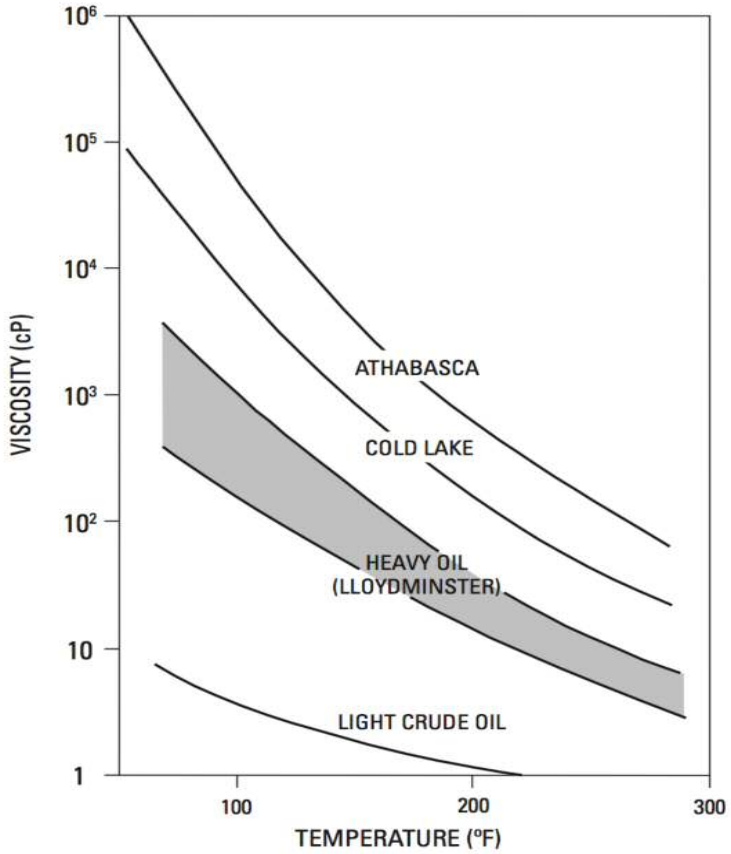


*Figure 2-32 Variation of heavy oil viscosity in some Athabasca oil (Laricina Energy, )*

Specific gravity is the correlation between the density of any material to the density of water. American Petroleum Institute (API) is the scale chosen to measure gravity (Raymond & Leffler, 2006).

Its relation is represented by the formula API

*Equation 2-20 Specific Gravity Equation by API*

---

*Table 2-12.Properties of oil sands in Athabasca, Canada (Hepler & Hsi, 1989)*

| API Gravity | 7.7 to 9.0 | | Oil Saturation (%) | 13.6 to 15.3 |
|---|---|---|---|---|
| **Density at 25° C** | 1.0077 | | Water Saturation% | 1.75 |
| **Viscosity (cp) at 15° C** | $1.8x10^4$ to $1x10^6$ | | Porosity (cp) | 34 |
| **Sara composition (%)** | | | Sulphur (%) | 4.41 to 5.44 |
| | | | Elements (%) | |
| **Saturates** | 14.5 | | C | 81 to 84 |
| **Aromatics** | 34.8 | | H | 10 to 11 |
| **Resins** | 38 | | N | 0.3 to 0.6 |
| **Asphaltenes** | 12.7 | | S | 4.6 to 5.6 |

## 2.15 Oil Sands Recovery Techniques

Heavy oil is viscous hence does not flow readily which makes its production difficult and different from that of conventional oil. There are two main ways of production of heavy oil which are namely open-cast surface mining and well production. The mining deals with production at the surface and the well technique deals with subsurface production. The well production technique is similar to the conventional oil recovery type but in this case, heavy oil recovery has to be enhanced since this type of oil does flow readily to well bore. There are several methods developed over the years for insitu production. Some of these techniques include: cyclic steam simulation (CSS), steam flooding and steam assisted gravity drainage (SAGD).

In view of this, there is an extensive research taking place to improve the old and develop new in-situ production methods but these are not commercially viable yet. The most notable ones include the use of solvents, hybrid methods (mixed steam and solvents), *in-situ* combustion using vertical and horizontal wells, electric resistance, supercritical fluids, induction and radiofrequency heating, downhole steam generation. There is also research into alternative fuels other than natural gas used for steam generation and *in-situ* upgrading.

### 2.15.1 Steam Assisted Gravity Drainage (SAGD)

SAGD is a more recent technology compared to Steam flood which is used to produce heavy oil from reservoirs that are too shallow (100 m to a few hundred) for steam injection methods. In this method two horizontal wells are drilled with 5 to 7 m spacing depending on oil viscosity. Typically, the horizontal sections are between 500 and 1500m and are fitted with slot liners to reduce sand production. During injection stage of the project, steam is injected through both wells for optimised time. Following which the upper well is maintained as an injector and the lower well is turned into a producer to collect drained oil.

As steam reduces viscosity of oil gravity acts as a driving mechanism to produce reservoir fluids compared to steam flood where steam is essentially used as a drive mechanism. Artificial lift (ESP and PCP) is then used to lift reservoir fluids to the surface. The recover factor for this technique is 50 to 70 percent and the extraction cost is between $16 and $18 a barrel. An example of a successful SAGD project is the Firebag SAGD project in Athabasca, Canada which produces 42,000 bpd. (DeepwellOil, 2018)

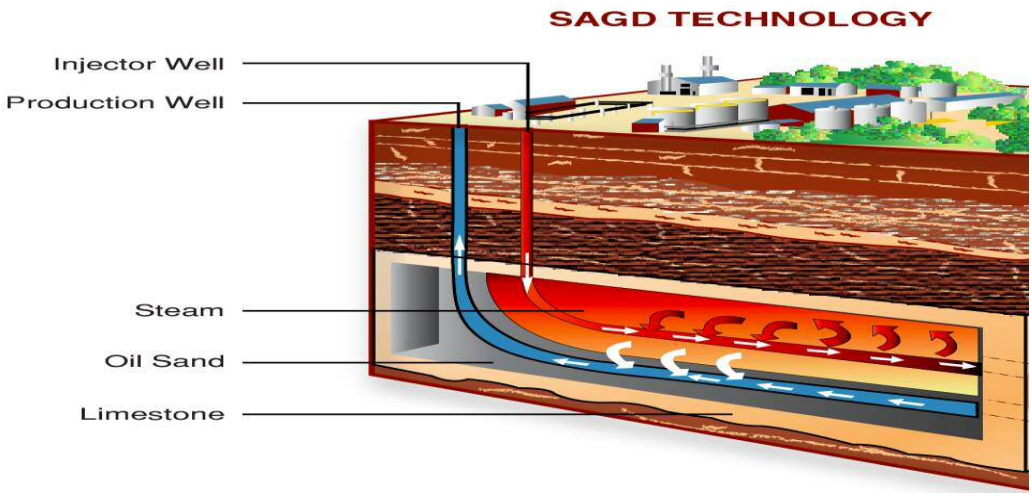


*Figure 2-33 SAGD technology representative diagram (Antonio & Palacios Chun, 2014)*

According to R.M Butler (1994) who developed the concept of two horizontal well pair and injection of steam to develop the bitumen deposits, this process has several features among which are

1. The displacement or the oil is systematic and high recoveries can be obtained.
2. Oil to steam ratio is higher than those found for conventional steam flooding where it is suitably applied
3. The process can be used in the heaviest of bitumen reservoirs without extensive preheating.

The major advantage of using SAGD are numerous among which are that it allows steam flooding at economic rates without the bypass of steam ensuring high recoveries in both bitumen and heavy oil reservoirs. Also, there have been observed reduction in green house effects as compared with steam flooding and cyclic steam flooding.

## 2.16 Simulation optimization

Canadian Oil Sands being primarily made up of heterogeneous geological deposition has significant variations throughout Western Canada Basin. To achieve optimum production with minimum input an optimisation study was necessary to perform. As it can be visualised from the work conducted all simulation models were tested using necessary parameters. Though primary focus was provided on operating pressure, well spacing, steam injection pressure , steam injection rate, Preheating period and steam quality.

### 2.16.1 Operating Pressure

A low operating pressure means a lower operating temperature in the reservoir so that the steam has more latent heat, making it more energy efficient. The advantage of using a higher pressure is that a higher pressure meaning that higher temperatures are retained for longer, thereby facilitating further reduction of viscosity resulting in a higher rate of production. Though aforementioned statement needs to consider reservoir quality and type of formation. According to (Butler, 1997) production rate is proportional to the square root of the mobility of oil:

*Equation 2-21 Butler's Mobility to flow relation equation (Butler, 1997)*

$$\frac{}{}$$

Where q = production rate (m/s), k = permeability ($m^2$), v = velocity (m/s) (Butler, 1997).

In case of the MacKay River reservoir which is 125m deep has an operating pressure of 1750 kPa which considering standard operating pressures is lower though when you determine operating pressure gradient it operates at 14 kPa/m, that lies above the hydrostatic pressure gradient of 10 kPa/m. Foster Creek is 380 m deep and operates at 2800 kPa, which gives a pressure gradient of 7.4 kPa/m. This value lies below the hydrostatic pressure gradient, meaning that the system relies solely on conduction in terms of heat transfer and reservoir quality has a significant role to play in overall operating pressures.

It was also found that the performance of the SAGD operations in MacKay River depend more on the geology of the reservoir than the pressure. No clear trends between either injection pressures or pressure gradients were found as both high and low-pressure pads had both excellent and poor performers. Therefore, high pressure gradient operations are not necessarily better than low pressure operations.

### 2.16.2 Well Spacing and Length

A well spacing of 100 m is the average spacing used by operators between each well pair (Cheung, 2013). A well spacing greater than 100 m usually leads to a poorer SAGD performance. However, the well length and spacing changes for different reservoirs. It is also important to consider the supply of steam as longer wells would be useless if there is insufficient availability of steam. SAGD projects are initially designed and simulated using appropriate simulation software in order to give an estimate of how much steam will be required to operate in the early stages of SAGD. After the early stages, lower temperatures and pressures can be implemented in order to cut operating costs as it no longer is necessary to work with high pressures and temperatures.

### 2.16.3 Steam Injection Pressure:

Generally, as stated by Li, Chan, & Froehlich (2009) higher steam injection pressures, aid in the lift of fluid downhole towards the surface. An increase in the production rate of oil, a reduction in the wells lifespan and an overall increase in the recovery factor, are all a result of an increased steam injection pressure. These effects are not solely caused by increased steam injection pressure, but also the geo-mechanical effects induced by the high steam chamber pressure. In unconsolidated oil sands, higher

steam injection pressures can cause larger volumetric strain, which is commonly associated with shear dilation and thermal expansion. This process can improve reservoir permeability and accelerate oil recovery (Li, Chan, & Froehlich, 2009).

On the other hand, an increased steam injection pressure can cause very undesirable effects. One such effect could be the breaching of the cap rock, which would in turn, then produce a very high steam oil ratio. Due to this, the time to implement the higher steam injection pressures need to be optimised for the maximum benefits of increased production, without the risk of losing large quantities of steam. The best time for higher pressure steam injection to be safely applied is when the partially drained zone approaches the cap rock. Following this rationale, the oil production rate will be accelerated and peak oil production during SAGD processes will be attained earlier than otherwise possible (Li, Chan, & Froehlich, 2009).

### 2.16.4 Steam Injection Rate:

As stated by Diwan & Kovscek (1999) when the steam injection rate increases, the production of oil and water also increases. This is partly due to the better steam contact within reservoir facilitating better productivity of oil as seen from Figure 2-34 and Figure 2-35 (Diwan & Kovscek, 1999).

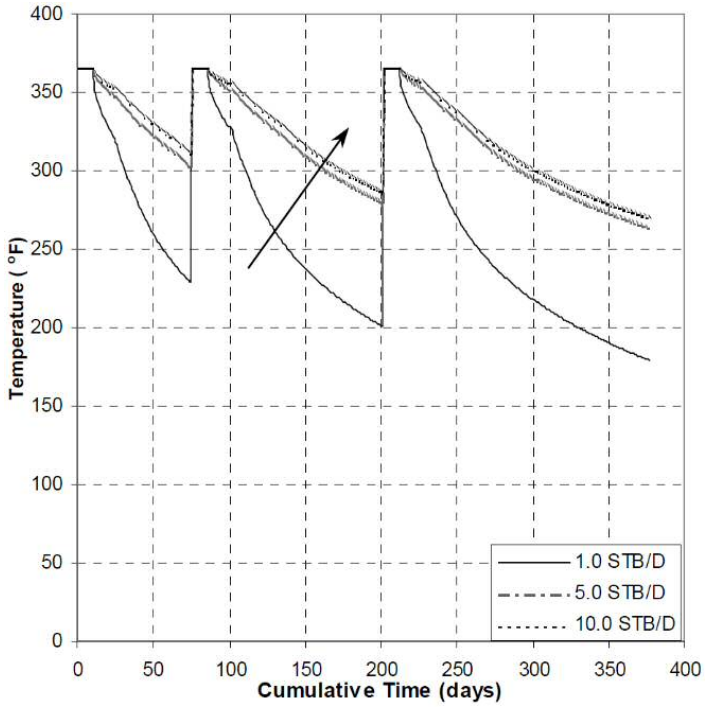


*Figure 2-34 Graph to show reservoir temperature when varying quantities of steam is injected over a period of time by (Diwan & Kovscek, 1999)*

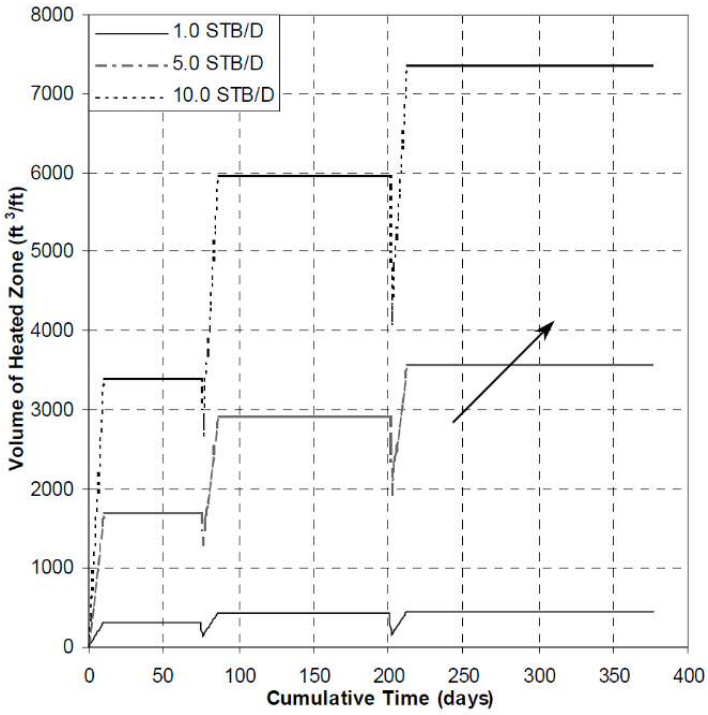


*Figure 2-35 Graph to show volume of reservoir heated when varying quantities of steam is injected over a period of time by (Diwan & Kovscek, 1999)*

As seen in Figure 25, when steam injection rates are increased, the decrease in the net temperature over a cycle is considerably less, meaning the reservoir holds greater thermal energy and this energy is slower to dissipate. In Figure 2-35 it can be seen that with higher steam injection rates the heated zones are correspondingly larger. The surface area of these larger zones do not transfer heat as rapidly, this also leads to greater volume of heat retention in the reservoir (Diwan & Kovscek, 1999).

### 2.16.5 Pre-Heating Period:

The pre-heating period involves the circulation of steam downhole, in both the production and injection wells. Whenever a pre-heating period is carried out it will positively affect the production, with longer heating periods proving most effective; however this is only apparent up to a specified period of time where there is no significant improvement in extended heating periods (Kiasari, Sola, & Naderif, 2010).

A study by Kiasari, Sola, & Naderif (2010) investigated the effect of pre-heating on SAGD performance in three cases, with no pre-heating, two months of pre-heating and 4 months of pre-heating (called ‘base case’ in Figure 2-36). The investigation found, that when the pre-heating period was increased, the initial communication

between the pairs of wells improved significantly, and the injection rate reached its desired production rate a lot quicker. The oil production rate also increases with the length of the pre-heating period, however after the early stages of production there is no difference in oil produced regardless of pre-heating period, this trend can be seen in Figure 2-36 below.

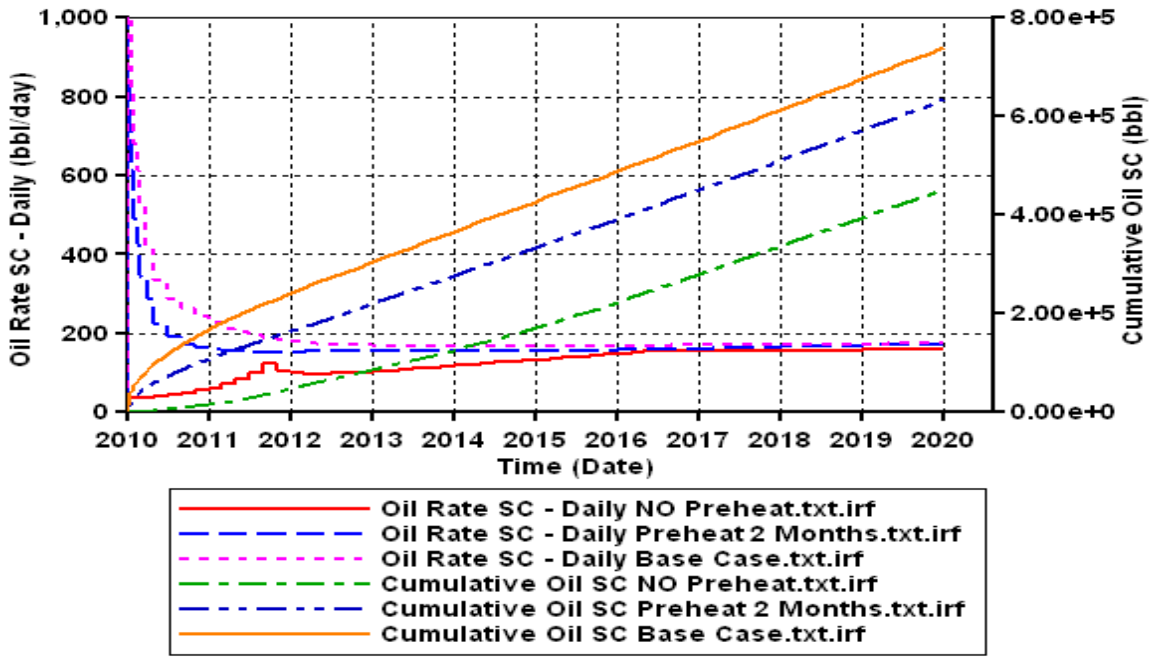


*Figure 2-36 Pre-heating period effect on the oil rate and cumulative oil production by (Kiasari, Sola, & Naderif, 2010)*

### 2.16.6 Steam Quality

A study carried out by Kiasari, Sola, & Naderif (2010) investigated the effects that the quality of steam had on SAGD performance. Three cases were used with different steam qualities of 0.5, 0.7 and 0.95 (called the 'base case') (Kiasari, Sola, & Naderif, 2010). A higher steam quality exhibits a higher latent heat, meaning it is capable of mobilising more of the heavy oil. If the steam used in a SAGD operation was of low quality, it would lack the ability to rise up into the further reaches of the reservoir; this is because of its larger water content. This would mean the steam chamber wouldn't be as large when compared to a high steam quality operation. As the steam quality is increased, the oil rate also increases. In later production the use of higher steam quality would result in greater consistent oil production (Kiasari, Sola, & Naderif, 2010)

# 3 Materials and Methods

## 3.1 Materials and Methods

As stated in problem identification section 1.2 this study is carried out in two stages using several outcrop samples and three core samples representing McMurray formation. Field study was conducted by my supervisor Dr. Julie Bell along with Dr. Fran Hein from The Energy Resource Conservation board, Alberta. In July 2010. The outcrop locations were selected in consultation with Dr. Fran Hein on the basis of her reports and previous work in this region (Hein.F, Langberg.W, & Kidston, 2001) (Hein, Cotterill, & Rice, 2006).

### 3.1.1 Outcrop Samples

Samples from the Upper McMurray Formation were collected from the Hangingstone# 2 Section near Fort McMurray, Canada, which is a well-documented estuarine tidal depositional environment (Hein F. J., 2001). The stratigraphy of the study area *is* summarised as being part of the Wabiskaw Member, overlying the Upper McMurray Formation, which in turn overlies the Middle McMurray Formation as shown in the Figure 2-2 and Figure 2-3 For the purpose of the study sampling focused on two categories of samples from the Upper McMurray Formation, one from the Argillaceous Sands *[argillaceous – contains clays]* and the other from the bioturbated areas. Individual outcrop samples were collected in Teflon tubes d=81 mm and h=150 mm to ensure sample integrity i.e. to maintain an undisturbed nature.

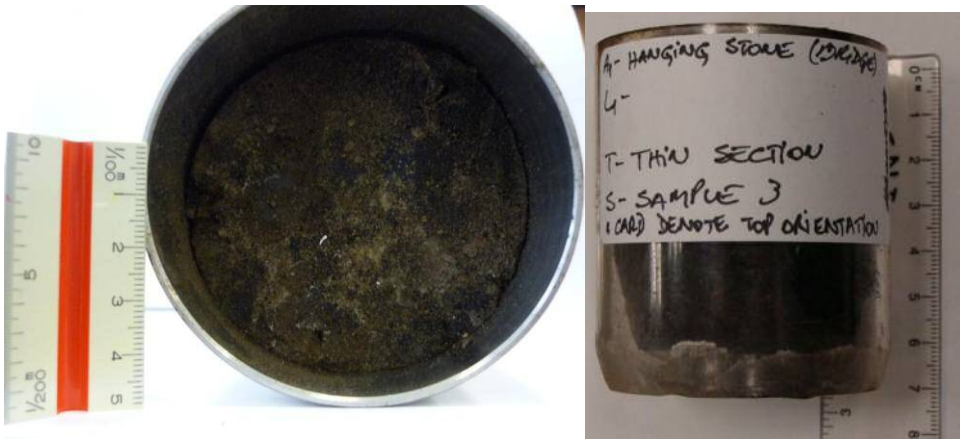


*Figure 3-1 Outcrop sample collection in steel and plastic sleeves.*

*Figure 3-2 Outcrop photographs captured at Hangingstone #2 (Bridge section) while collecting the outcrop samples in 2010*

Error! Reference source not found.Figure 3-1 and Figure 3-2 represents an outcrop s tratigraphical representation wherein Hangingstone #2 location contains 50 high outcrop which starts with fine grained mud stone which is overlain by sediment with abundant cross bedding including trough high angle planer tubular, planar tangential m and low- angle sandy or muddy incline units. According to (Hein.F, Langberg.W, & Kidston, 2001) this unit also represents substantial amount of bioturbation and is persistent locally.

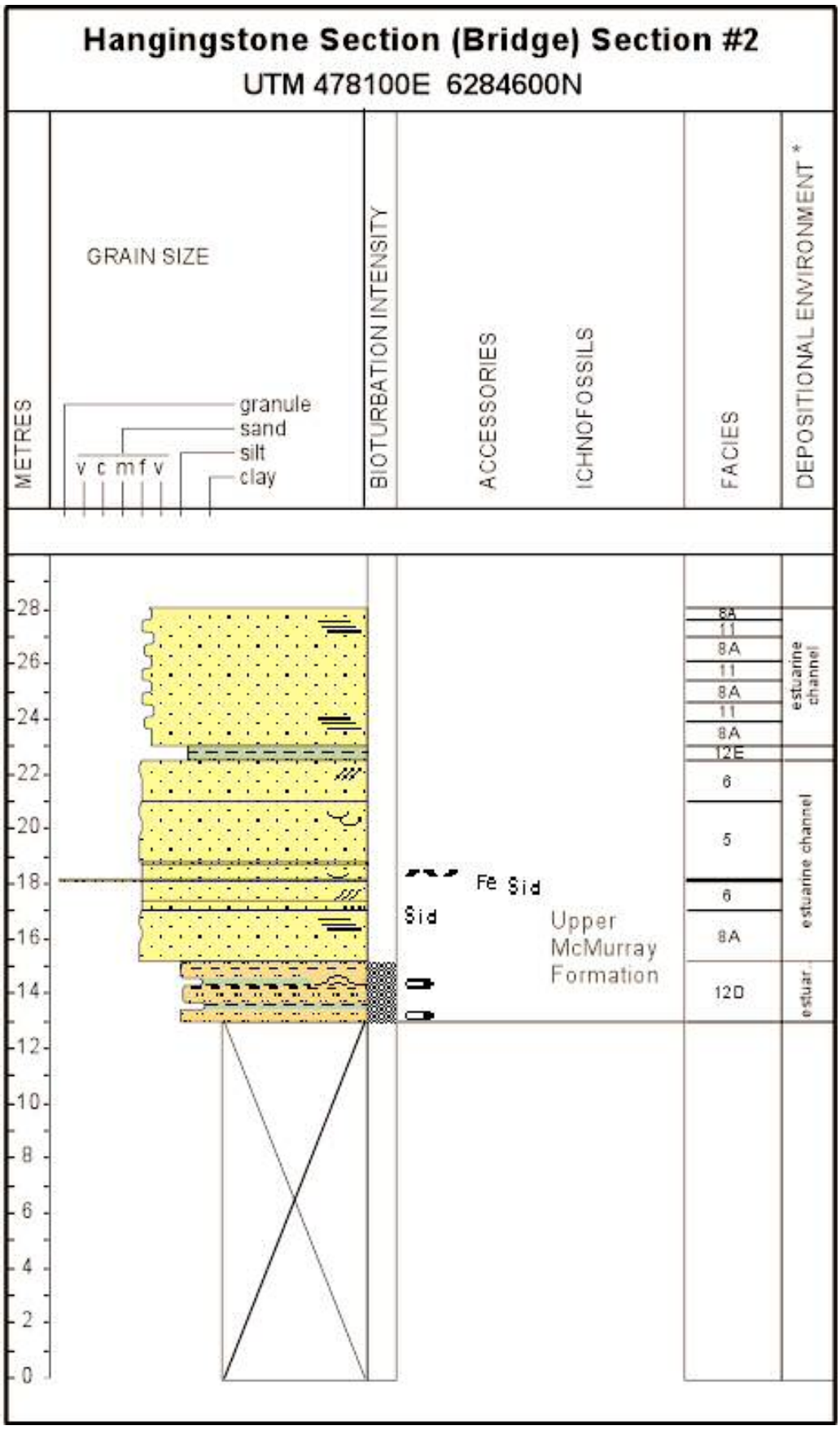


*Figure 3-3 Schematic representation of the measured hangingstone river ( Bridge section ) Vertical scale 1 M height (Hein.F, Langberg.W, & Kidston, 2001)*

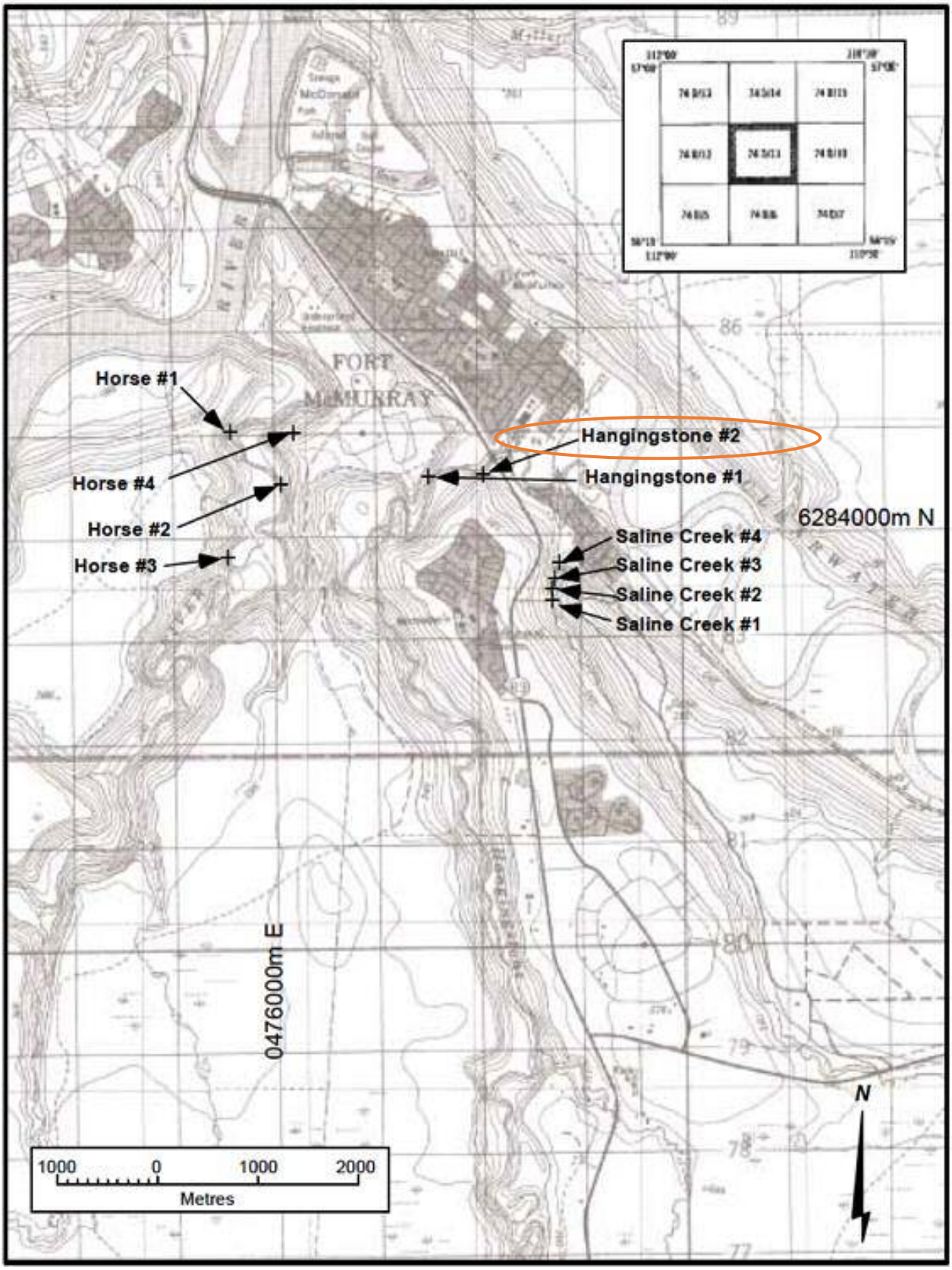


*Figure 3-4 Location Hangingstone#2 river (Bridge) on the map showing the outcrop sampling area. (Hein.F, Langberg.W, & Kidston, 2001)*

### 3.1.2 Core samples

The limited amount of core samples used in this study were obtained from a location to the west of the outcrop samples. The unavailability of more core samples from the same reservoir has introduced limitation to the study. As seen from Figure 3-5 well AA/14-20-094-08W4/0 is located approximately 350 km away and the outcropping McMurray formation is encountered at the depth of 80m to 90m. The core samples were from three depositional settings including a transition depositional setting, estuary reservoir and the main estuarine reservoir from the Upper McMurray formation. As described in section 2.3

**Sample A** - collected from the depth of 81.4m and taken immediately below a depositional environment transition. On preliminary examination coarse-grained sands are saturated with bitumen and some fine lamina.

**Sample B** - collected from the depth of 85.0m in the estuarine depositional reservoir. On preliminary examination are medium to fine grained sands, consolidated with bitumen, and some very fine grained lamina.

**Sample C** - collected from the depth of 89.2m in the main estuarine reservoir and on preliminary examinations are fine to very fine-grained sands, consolidated with bitumen


*Figure 3-5 Location map showing Outcrop and core sample well location*

## 3.2 Laboratory Procedure

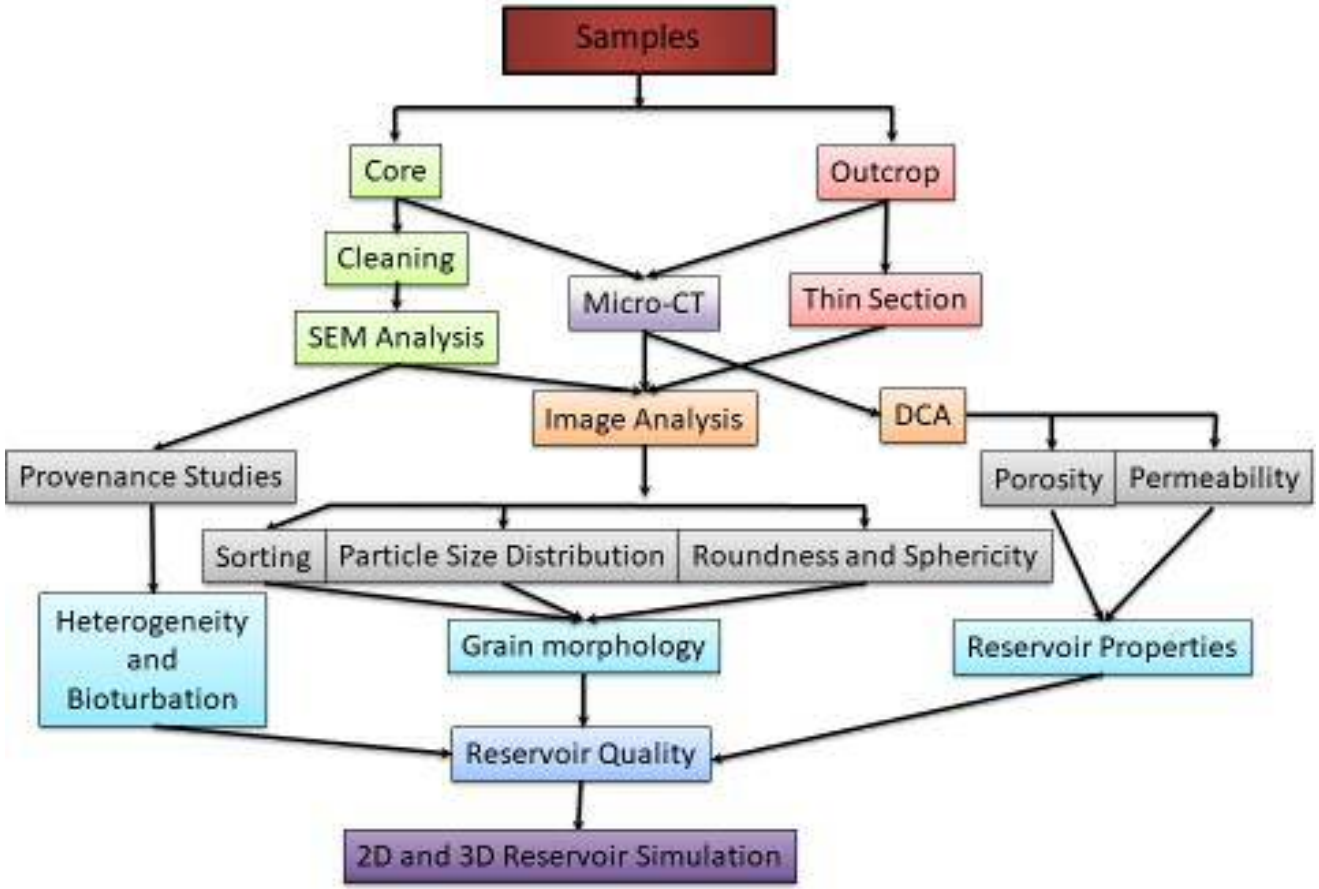


*Figure 3-6 Outline of methods followed in this research*

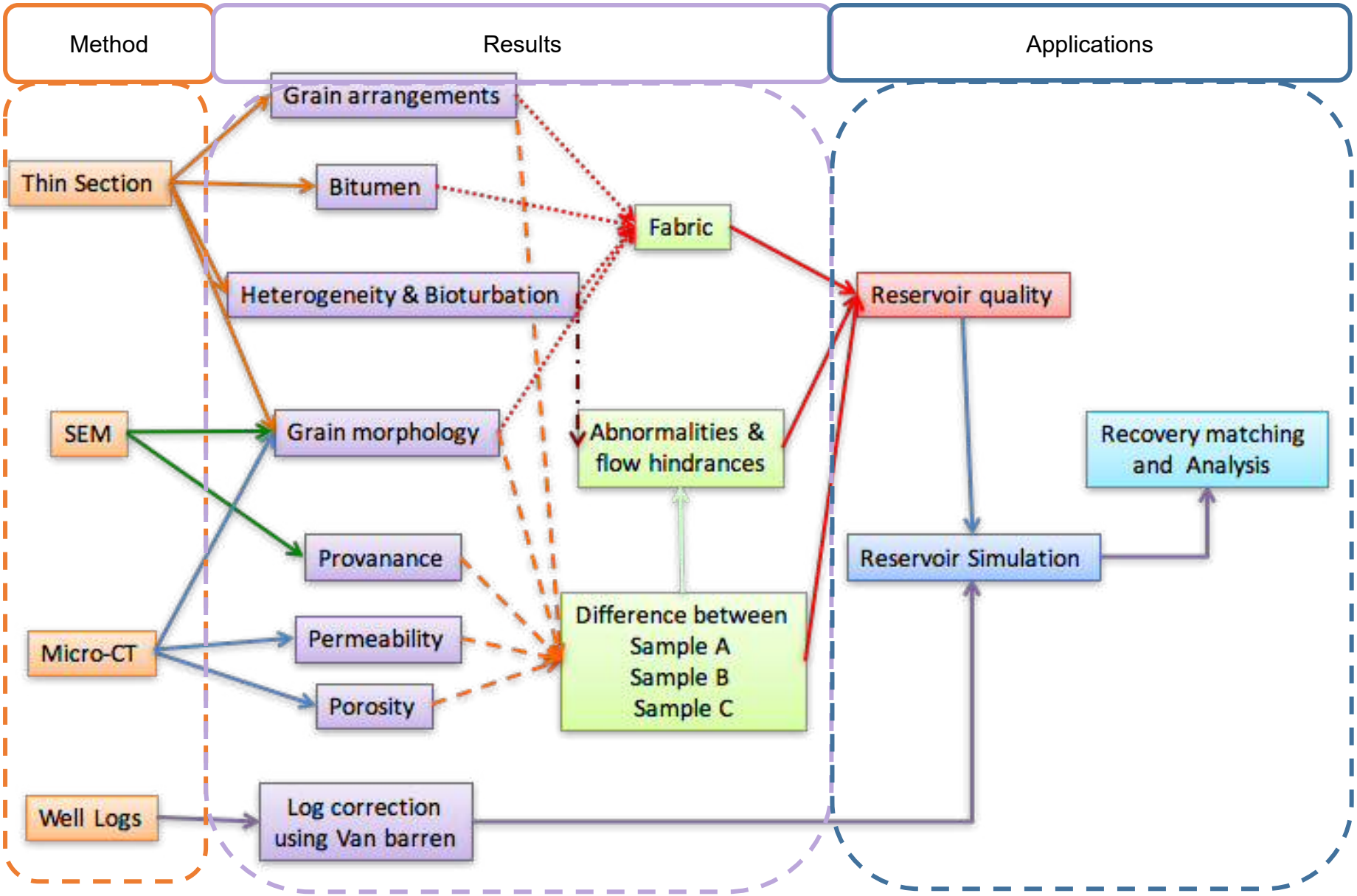


*Figure 3-7 Work flow of Methods, Results and their application*

The Figure 3-6 shows a sequence of laboratory procedure followed through this thesis and provides expected results and what their interpretation means as part of this thesis.

### 3.2.1 Thin section preparation

National Research Council in Italy's laboratory infrastructure was used to prepare thin section for this study. As the samples were unconsolidated some modifications and trial and errors had to be conducted in order to obtain desired thin sections.

Table 3-1 shows the division of available two outcrop samples to develop desired thin sections.

*Table 3-1 Sample Thins selection and resin used*

| Outcrop Sample | Slices | Resin | Coolant |
|---|---|---|---|
| **Sample 1** | 1 | Epoxy Bond Mix | ISOPAR |
| | 1 | Epoxy Bond Mix | Water |
| | 1 | Epoxy Bond Mix | ISOPAR |
| | 1 | Epoxy | Water |
| | 1 | Epoxy | |
| **Sample 2** | 1 | Polyester | |
| | 1 | Epoxy | |

#### *3.2.1.1 Resin Preparation*

To prepare thin sections three different types of resins were prepared namely polyester, epoxy and ERMS

### Polyester resin

Acetone was chosen as preferred resin to prepare this polyester, the same acetone was used to submerge the sample prior to impregnation as well.

to prepare resin

- 300 ml of polyester resin  same as amount of acetone
- 150 ml of acetone
- 0.3 gm pigment
- 0.6 ml catalyst

This mixture takes around a month to polymerise if correctly prepared. This can be adapted by changing the quantity of catalyst used. Polyester resin offers superior optical performance when observed under the microscope compared to epoxy resin.

### Epoxy Resin

Epoxy resin is preferred in dry samples compared to wet samples.  This resin is also very good at impregnation as it can access many pores within inaccessible pore volume of the sample.

To prepare this resin

- 162 ml epoxy resin;
- 42ml diluent;
- 0.3gr pigment;
- 96ml hardening agent.

Polymerisation can be achieved within 6 hours and solid state in 12 hours' time depending on the  size of the sample.

### ERMS

For this method, only hardening agent and epoxy resin were used.  They were mixed and were ready to use immediately.

### *3.2.1.2 Methods for Polyester Resin*

Primarily to understand interaction between an unconsolidated sample and acetone. To initiate the process sample was placed in aluminium tray and Acetone was poured in to set the sample. As expected highly viscous oil holding the grains together started to lose its integrity and was found to be dissolved in acetone. Figure 3-8

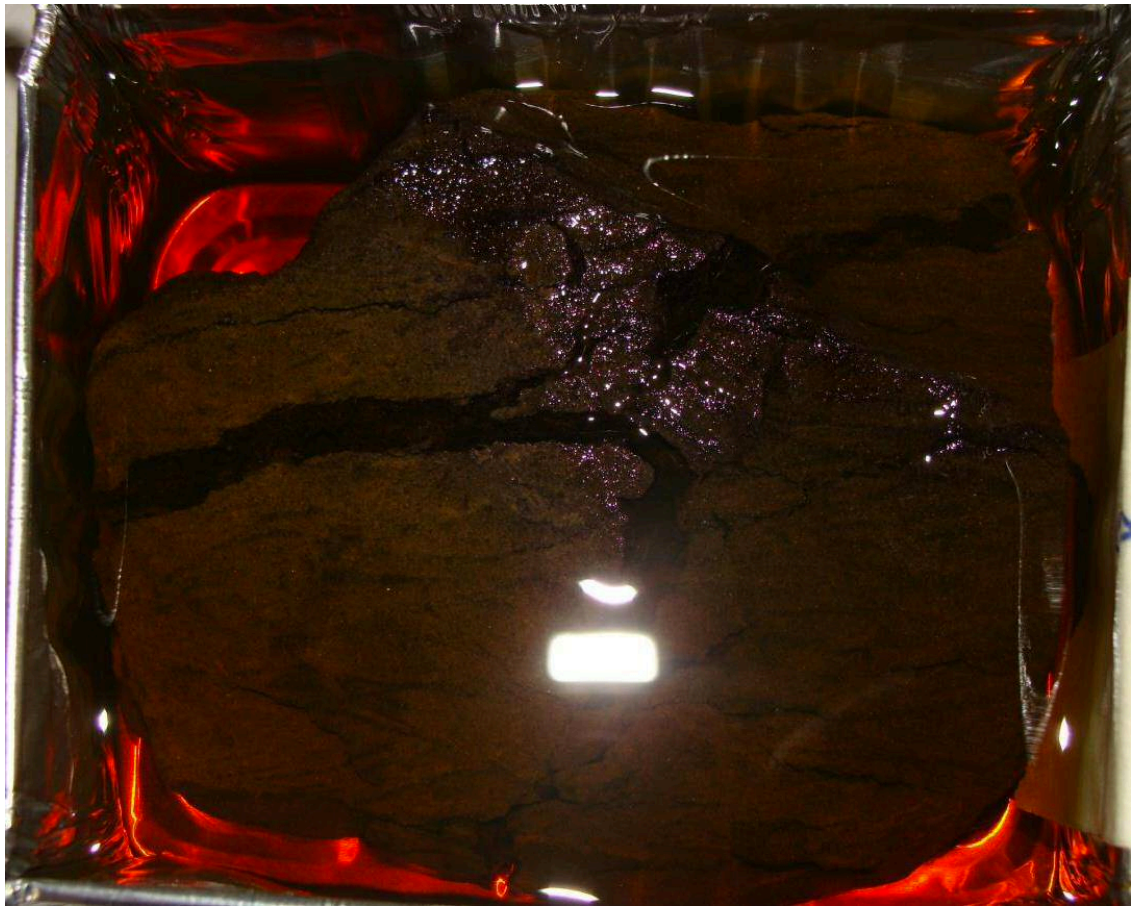

*Figure 3-8 Outcrop sample immersed in acetone showing loss of integrity and dissolved oil in Acetone based resin.*

Following initial tests, the sample was submerged in 4 cm deep container to provide sufficient time to occupy all the pores. Upon completion it was subjected to vacuum chamber for up 75 cm/hg to extract all trapped air and air bubbles.

On completion the resin was continuously topped up until the material stopped absorbing resin. Following this the material was rested to consolidate and form a block to work further.

### *3.2.1.3 Method for Epoxy Resin*

A similar setup as in Figure 3-8 was used in which the sample was placed in an aluminium tray and then submerged in epoxy resin. Due care was taken to suspend the sample with a non-reactive element to allow even submergence of sample under epoxy.

Once satisfied with the level of epoxy in the tray, the sample was placed in a vacuum chamber to allow passage of epoxy through the sample and sucking out all the possible air from the container. The sample was subjected to Vacuum chamber Figure 3-9 until it reached 45cm/Hg. Special care was taken with this sample, as epoxy polymerisation is an exothermic reaction which is further invigorated by the presence of organic matter and vacuum chamber. The sample was also continuously monitored to make sure that resin does not reach boiling point and cause forth and destabilization. To achieve a perfect result, this step was repeated three times following which the samples were left to harden and checked every 48 hours


*Figure 3-9 Vacuum chamber used for this experiment to reduce amount of air*

*Figure 3-10 Vacuum process working as air bubbles can be seen leaving the resin dipped sample.*

On completion of sufficient polymerisation, the sample is cut longitudinally to check the state of polymerisation. If not sufficient, the sample is further subjected to UV light to accelerate process of polymerisation. This also helps understand internal structure of the sample as the internal pigment within the sample will show up under UV light Figure 3-11

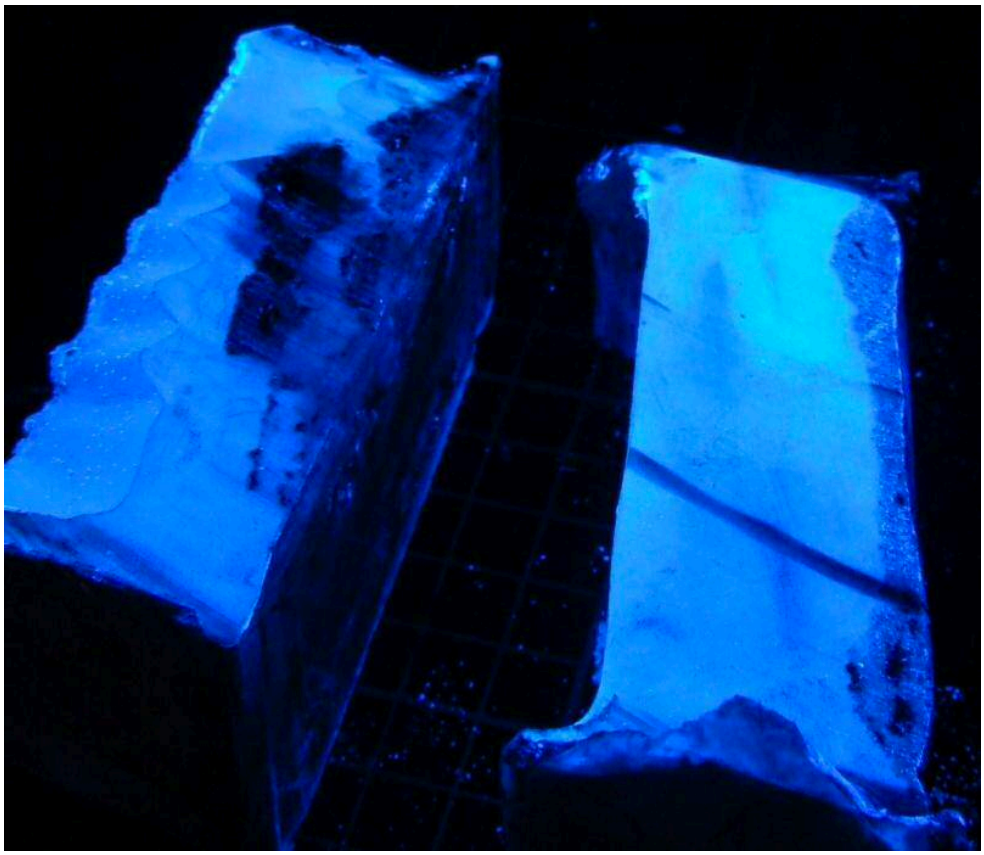

*Figure 3-11 Sample being subjected to UV light to accelerate polymerisation process.*

It was also noted the sample had not achieved complete impregnation of epoxy due to the presence of heavy oil, though the area of interest within the sample was showing promising results.

Further the sample was held in a metallic jug that was mounted on a surface grinder and was withheld by the electromagnetic forces provided by the stage. Surface grinding thickness was set for 6mm to obtain a good quality sample. Though as seen from Figure 3-12 after initial 2.5 mm grinding the bottom support could be seen protruding out of the sample.

*Figure 3-12 Surface grinder with rectangular support and sample*

*Figure 3-13 Sample post completion of 2.5 mm grinding*

On closely observing the sample it was noticed that the actual sample did not get impregnated due to the presence of hydrocarbons all internal features could easily be seen. As the slab was grinded down the ISOPAR was used as a cooling agent which melted the outer section of the thin section. Figure 3-13

Post this initial grinding phase, the sample was subjected to second impregnation and allowed to set for 12 hours. This impregnation assured that the initial 3 mm thickened was properly impregnated and was then ready to be trimmed and thinned down to prepare thin section. Though in second grinding stage water was used instead of ISOPAR to stop melting the oil. This was followed by the thin grinded sample to be bonded on to the glass phase Figure 3-14 Figure 3-15

*Figure 3-14 State of impregnation after post polymerisation*

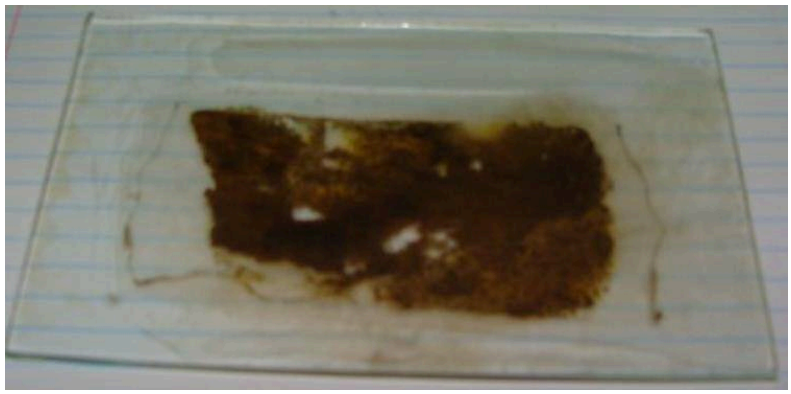

*Figure 3-15 Resulting thin section from epoxy resin method*

#### *3.2.1.4 ERMS Thin section preparation method*

To form thin sections using ERMS the sample was initially divided into three sections with the use of a knife Figure 3-16 as diamond cutter blades heat started to melt the oil from sample. Once the desired thickness of 2.5 to 3 mm was achieved for the sample, The sample was then adhered to thin section with the help of resin and was then covered with thin plastic piece and glass thin section to clamp and apply pressure for the sample to adhere to the glass surface Figure 3-17. Upon completion, the sample top glass covered was removed and resin was poured over the sample to cover the entire thickness and cover the surrounding area of the sample.

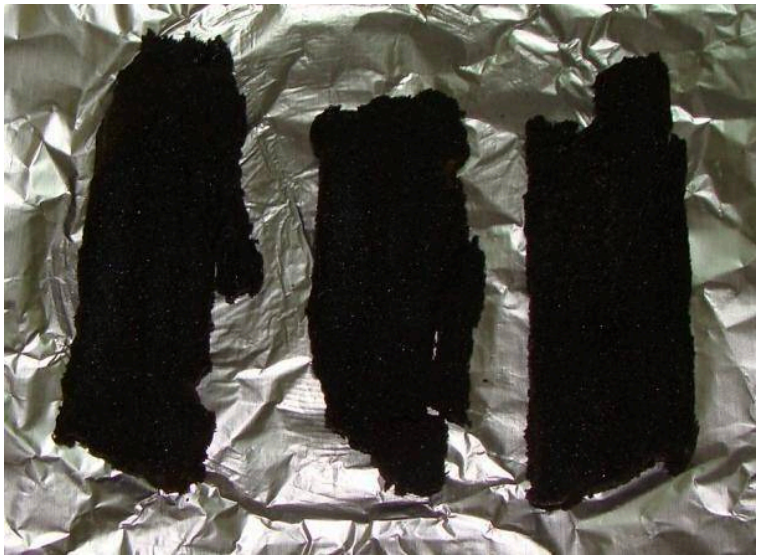

*Figure 3-16 Sample cut to the desired 3mm thickness*

*Figure 3-17 Sample being bonded to the glass piece for preparation of thin section*

Post bonding sample was covered with resin to allow sufficient impregnation and solidification of the resin being used. This process was given 12 hours followed by additional 12 hours to stick the sample completely. The resulting slide can be observed in Figure 3-18,

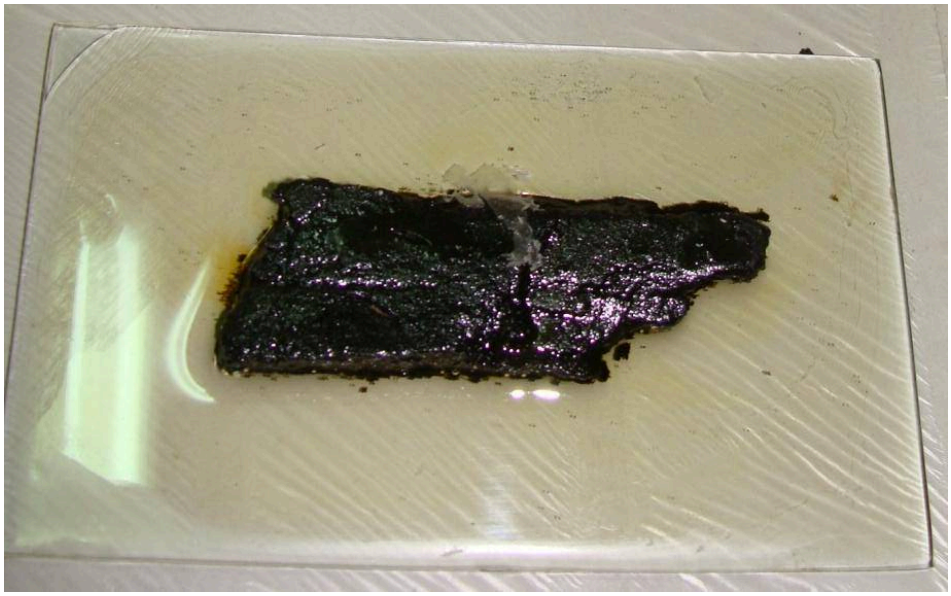

*Figure 3-18 Impregnated sample for further process of thins section preparation*

This sample was then held on a grinding table by applying suction from bottom. The sample was then subjected to a grinding process to achieve the desired 30 micron thickness of the sample. Grinding was performed using water based cooling liquid, utmost care was observed by following stages of 3 mm pass , 1 mm pass to 0.5 mm pass to allow better quality control over the thin section being prepared. The grinding process was stopped at 137 microns to observe internal impregnation of this sample, which revealed that sample was not completely internally impregnated. At this point initial sample was observed under microscope to check for the quality of thin section. Though due to the thickness desired results were not obtained. To further reduce the thickness of this sample, it was sanded down manually with small sand paper. The manual sanding paper allowed the avoiding of heat of the grinding process and thereby reducing the chances of impregnated oil being mobilised. Figure 3-19 and Figure 3-20

*Figure 3-19 Sample grinded with ISOPAR cooling liquid*

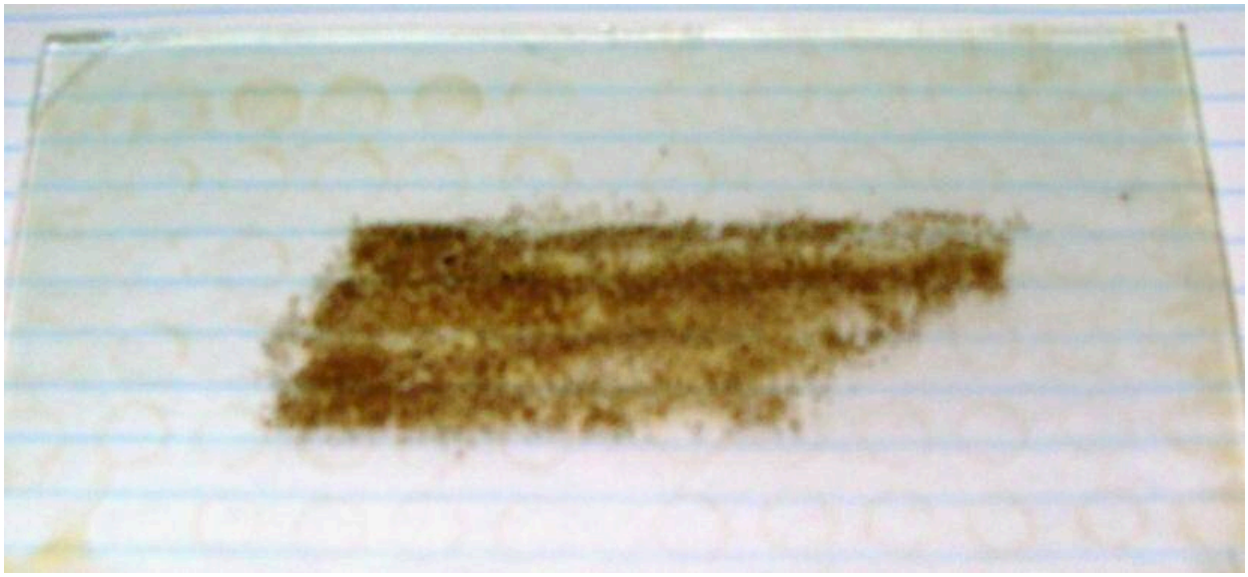

*Figure 3-20 Sample grinded using water cooling*

### *3.2.1.5 Thin Section Image Capturing*

To acquire quality images from petrographic microscope Olympus petrographic microscope BH -2 equipped with light source and an ultraviolet light option was used. This microscope was attached with Canon A 640 Power shot Camera with resolution of 3648pixel by 2736 pixel and optical zoom ratio of 4 and an effective picture element of 10 megapixel was used. The images were calibrated for scale with 2.76 pixel/μm using slide in Figure 3-22.

*Figure 3-21 Microscope and camera setup with an attachment to capture thin section Images*


*Figure 3-22 Motic calibrating slide used to calibrate the image analysis system. The black dot above the blue dot is 1500µm while the little black dot above the red dot is 600µm.*

To ensure accurate measurement of features from the thin section using the petrographic microscope, the intensity of the light source in the petrographic microscope was adequately adjusted to reveal the oil sand component present in the thin section images, likewise, the coarse adjuster and the fine adjuster were adequately adjusted in the microscope to reveal a non-blurry image in the digital camera. All images for this study were taken using the same microscope objective and zoom ratio in the digital photography.

### 3.2.2 SEM

#### *3.2.2.1 Pre-Analysis Treatment*

SEM analysis chambers required the sample that was devoid of any oil (i.e. grains). To achieve this samples were cleaned following API standard Soxhlet cleaning methodology. Toluene solution was used for distillation process as it was able to extract and separate grains from bitumen.

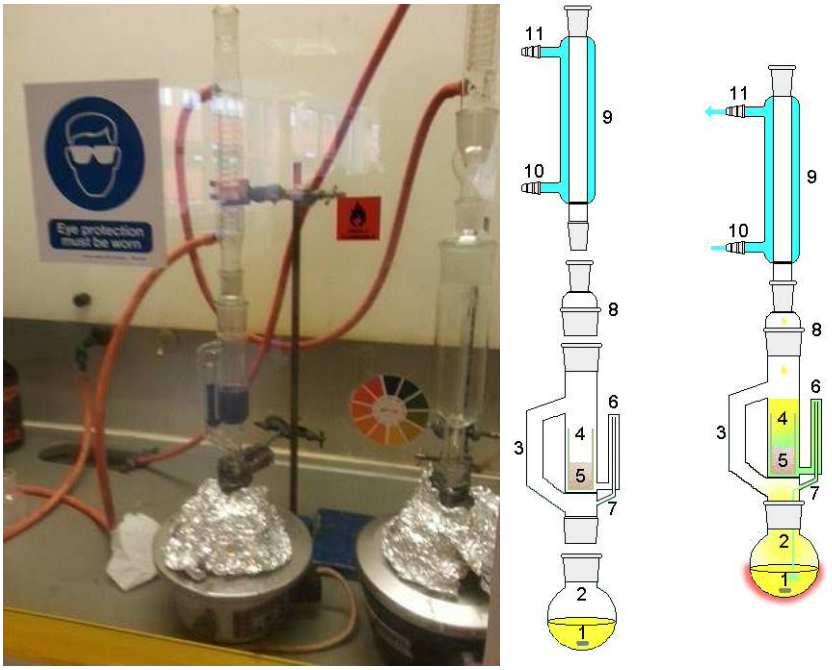


*Figure 3-23 Sohxlet Separation apparatus with schematic diagram 1.Stirrer 2.Stillpot 3.Distillation path 4.Soxhlet Thimble 5.Extraction Solid 6.Syphon arm inlet 7.Syphon arm outlet 8.Expansion adapter 9 Condenser 10.Cooling water In 11.Cooling water out.*

As can be seen from Figure 3-23 Soxhlet apparatus utilizes heated jacket system to achieve best distillation. Initially an outcrop sample was tested following this method, on observing successful results all three samples were independently cleaned. Care was taken to observe quality of toluene when it was in the cleaning chamber as the objective was to achieve an absolutely colourless toluene.

#### *3.2.2.2 Sample Mounting*

The cleaned samples were mounted on aluminium stubs using carbon tabs. As can be seen in Figure 3-24 the sample was further divided in four quadrants.

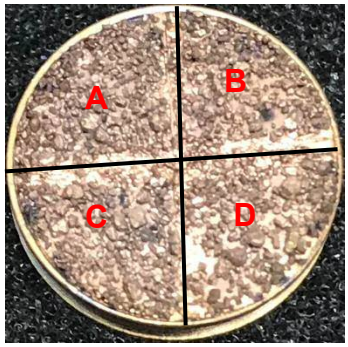


*Figure 3-24 Stub prepared for SEM Analysis showing quadrants for scanning.*

### *3.2.2.3 Sample Coating*

Since, quartz grains inherently cannot conduct electivity, it was necessary for the prepared stub to be coated with gold to provide conductive surface. To achieve an even and uniform coating aluminium stubs were placed in *E500 Series II Sputter Coater* and then pressured to 0.2 Torr (26.66 Pascals) at 20mA of current for a period of 120 seconds. The process and resulting coated stubs can be observed in Figure 3-24 Figure 3-25 and Figure 3-26.

*Figure 3-25 Gold coating machine at London South Bank University SEM laboratory*

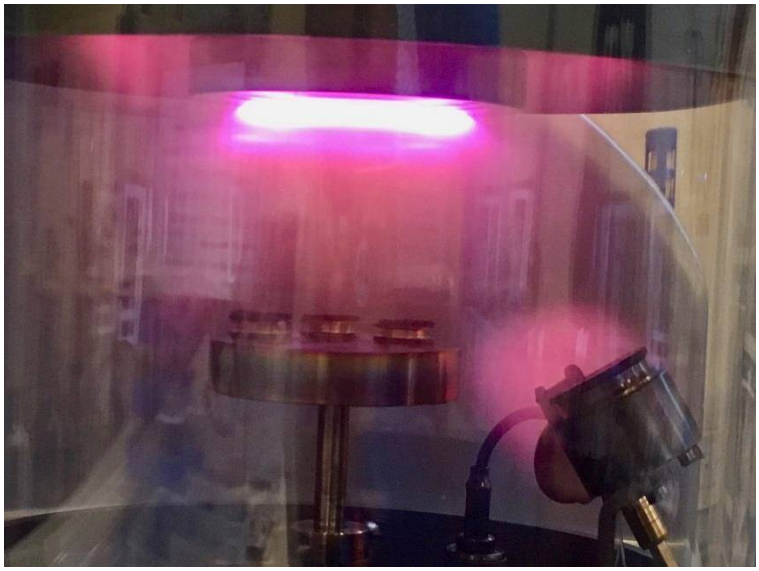

*Figure 3-26 Samples being coated at University of Portsmouth for additional bioturbation studies.*

#### *3.2.2.4 SEM Image Acquisition*

This study being carried out at two Universities both SEM setups have been demonstrated in following Figure 3-27 and Figure 3-28.

The London South Bank Setup consisted of four basic components: Figure 3-27

- Scanning Electron Microscope (Hitachi S2500) consisting of Energy Disperse X-Ray, and Back-Scattered Electron for sample composition, and digital imaging, respectively.
- TV Screen for observing SEM chamber through the help of inbuilt cameras in the chamber.
- SEM monitor for observing scanned samples.
- A desktop computer connected to the SEM machine, installed with *Rontec Quantax* software for scanning and saving images to a computer.


*Figure 3-27 The Scanning Electron Microscope and its constituent components*

Whilst at the University of Portsmouth, Carl Zeiss EVO MA 10 SEM machine was used. Being modern machine, it is directly connected to a computer with an acquisition software of smart SEM. This machine is capable of scanning 100 mm sample at 2 to 10 nm resolution with magnification that ranges from 7 up to 1 million times. (London-nano.com, 2017).


*Figure 3-28 Scanning electron microscope device*

#### *3.2.2.5 Scanning Procedure*

To achieve a good scan and images from SEM, sample chambers were subjected to vaccum which removed any disturbance for the beam. Following this the beams were accelerated at respective 20kv and the scanned images were allowed to settle and then the area of interest was focused using software utility. This allowed detailed capture of images at 30X onwards magnification depending on the purpose of images being acquired.

Both machines were equipped with multi stub stages which allowed a number of different samples being placed in the chamber at a single time. Hitachi machine at LSBU being an older variant had to be adjusted manually as compared to the Carl Zeiss machine which was modern and could be operated easily.

#### *3.2.2.6 High magnification scanning*

To observe and identify the effect of weathering and transportation images with higher magnification than 30X was required. To achieve this depending on the sample, images were scanned from 50X to 2000X. e.g. The grains of sample were quite coarse and needed magnification between 40X & 110X except in regions where conscious effort was made to capture the finer grains amongst the coarser grains that in sample B with finer grains, magnification went as high as 300+X. Sample C which represents smallest particles were scanned as high as 2000X.

On completion of image acquisition of all three samples for image analysis and high magnification, images were studied for properties and transportation interpretation.

### 3.2.3 Surface Features analysis

The micro textural analysis is based on the studies conducted by (Mahaney, 2002 )and (Krinsley & Doornkamp, 1973) who completed a detailed analysis on quartz sand and developed an Atlas quartz sand surface textures. This was used in tandem with the (Bull, 1978 ) work on surface feature abundance plot (SFAP) (containing 34 surface features) as well as that redrawn from (Higgs, 1979) (containing 30 features). The SFAP technique as detailed in Figure 3-29 and Figure 3-29 utilized the recognition of the presence or absence of a list of surface features identified on a quartz grain. This has allowed the understanding of transportation and weathering effect of samples.

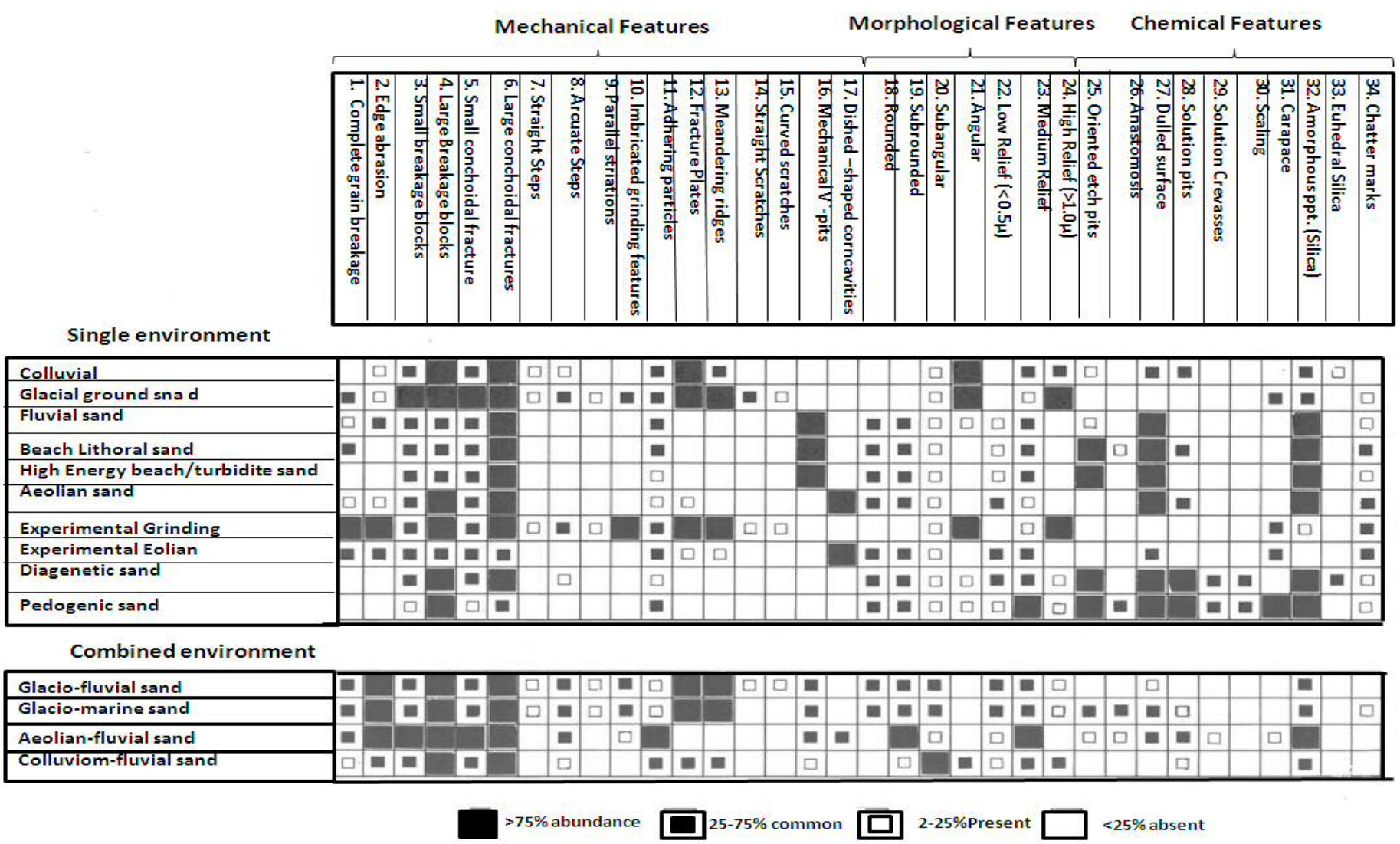


*Figure 3-29 wide variety of microstructures by SEM on modern sand and possible environmental significance (Bull, 1978)*

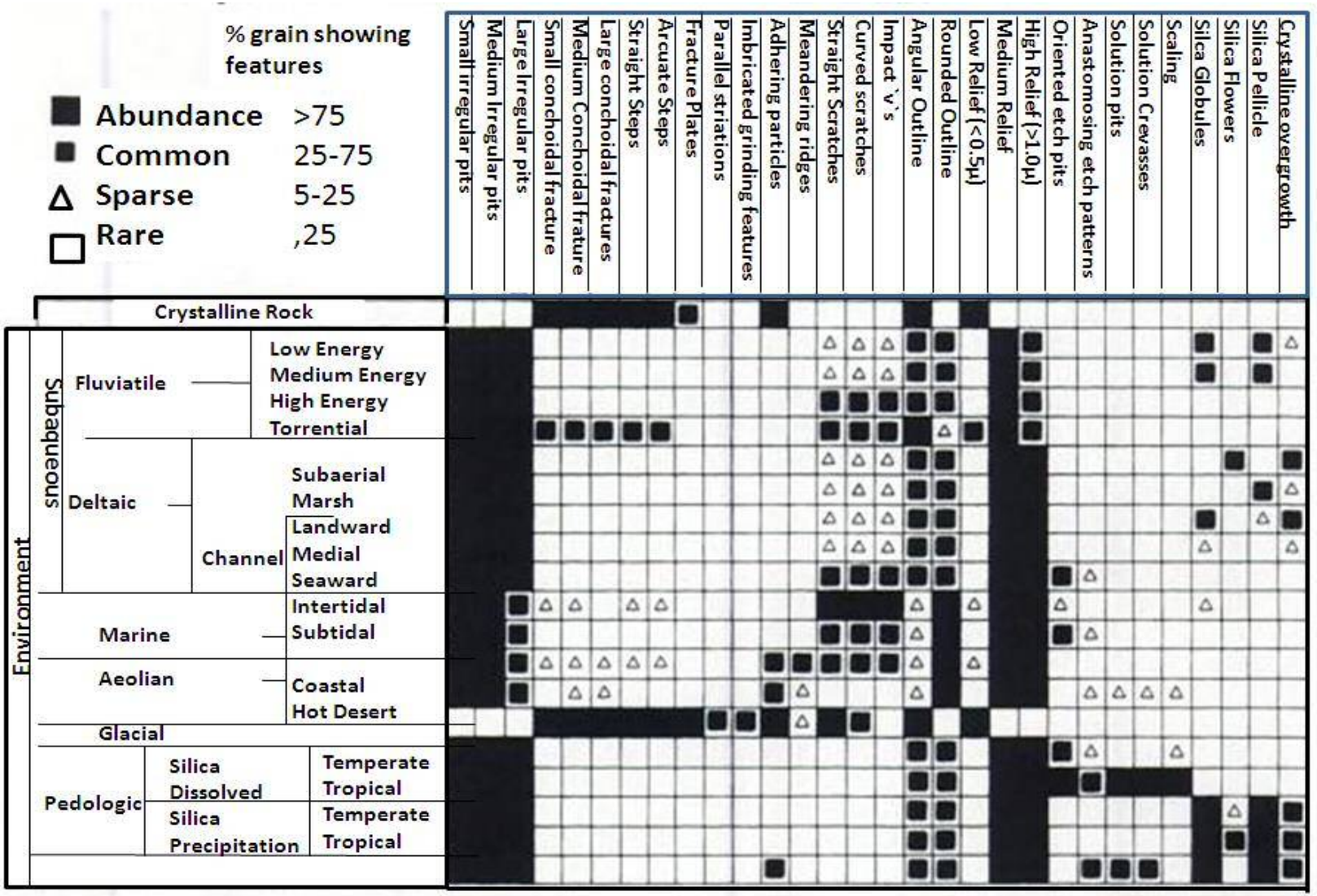


*Figure 3-30 A wide variety of microstructures by SEM on modern sand and possible environmental significance (redrawn from higgs 1979)*

All samples were analysed and data was recorded using excel sheets. This was followed by cumulative frequency plots to ascertain abundance of features in each sample.

According to (Bull & Morgan, 2006)in current practice, 30-60 grains are believed to be sufficient, for such an analysis and 100 grain per sample believed to be a bit on the extreme. Although a few researchers use 100 or more grains per sample, it is believed that there is no statistical rationale behind this reasoning. As such 60 grains per sample has been chosen for the purpose of this work.

## 3.3 Micro-CT

This section will describe methods followed to obtain micro-CT data. This work being focused at two elements was conducted at two instances and using two different scanning machines. Primarily the samples were scanned using Skyscan-112 to determine grain morphological properties at 8 µm. This was followed by recent work being conducted at the University of Portsmouth, where samples were scanned at 5 µm and 20 µm respectively to determine grain morphology as well as porosity and permeability from the core samples.

### 3.3.1 Preparing Sample for X-Ray

As shown in Figure 3-34 in case of Sky Scan sample was placed on mounting table and was secured with masking tape to avoid crack, shatter or split. Whereas for Zeiss scan sample sections of core samples from all the three A, B and C samples were planted on stage and were wrapped in cellophane tape as shown in Figure 3-35.

### 3.3.2 Equipment Used

#### *3.3.2.1 Skyscan -1172*

A 70 mm cylindrical sample was subjected to scan in SKyScan-1172 equipment. The resolution of 5 µm was adapted to achieve sufficient resolution for reconstruction of images into the stack. This resolution provided approximate voxel size of $10^{-7}$ $mm^{3.}$ The function built into the scanner allows for the camera to move as needed there by providing high quality image resolution.

The apparatus presents an X-ray micro focus tube with high-voltage power supply, a sample point with precision adjustment, a two-dimensional X-ray CCD-camera attached to the frame-grabber and a Dual Intel Xeon computer with LCD monitor as described by Micro Photonics Inc. (2010).

*Figure 3-31 Sky Scan -1172 desktop micro-CT scanner.*

This equipment uses a charge coupled device (CCD) with C4742-55-12HRF camera. This compact, and high-performance machine that provides a 12-bit digital output. The camera can produce images with high resolution presenting an effective pixel number of 4000x2624 (horizontal x vertical) pixels. This camera is a Fibre Optic Plate X-Ray Scintillator (FOS) coupled X-Ray camera.

#### *3.3.2.2 Image Acquisition*

The sample was x-rayed in 180º although 360º could have been used as well. At each angle, a shadow image or projection image is acquired. As the acquisition took place through the cone beam all images in 16-bit TIFF file were saved. The table below shows the settings used when acquiring the images.

#### *3.3.2.3 Zeiss Xradia 510 Versa*

The same samples were then used in the micro-CT scanner ZEISS Xradia 510 Versa X-ray Microscope from Carl Zeiss, being one of the most recent developments in the 3D X-ray microscopy (XRM) industry.


*Figure 3-32 ZEISS Xradia 510 Versa X-ray Microscope (Zeiss.com, 2017)*

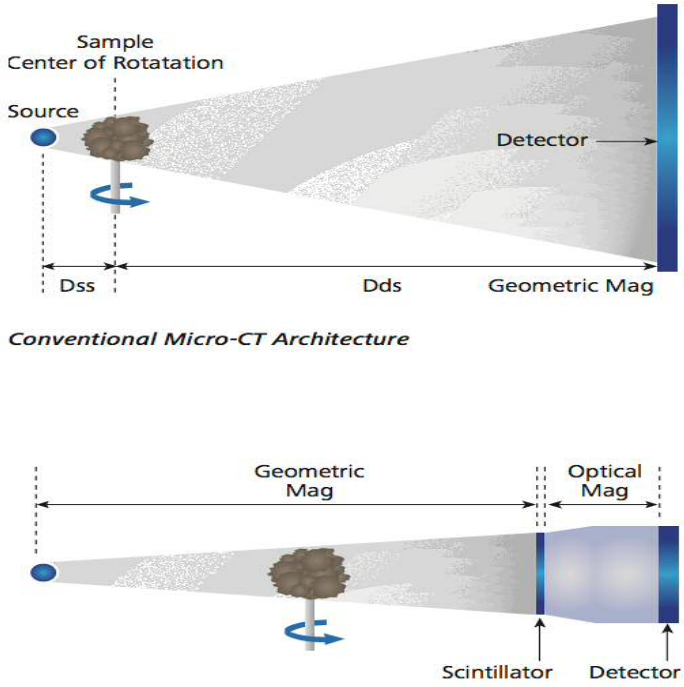


*Figure 3-33 Comparison between common and RaaD technique (zeiss.com 2017)*

The Zeiss equipment uses two stage magnification method allowing acquisition of resolution at distance (RaaD). This assists in achieving much finer and better images as it maintains resolution. At first instance, this machine works as a conventional - CTs. After that, X-rays are converted to visible light by using a scintillator that can be optically amplified.

### 3.3.3 Resolution

For 8 µm resolution, the sample has been trimmed to fit a polystyrene base created to fit the size of the sample that would allow the aimed resolution. A polystyrene mould with a hollow of around 2 cm height by 1.5 in diameter was used to place the sample. The total size of the sample is approximately 3.5cm height and approximately 1.5cm in diameter. Figure 3-34

*Figure 3-34 Part of the sample mounted on polystyrene holder and is ready to be scanned in micro -CT equipment.*

To achieve best resolution from all the three samples and study reservoir properties in detail all the three samples were scanned at 5µm and 20 µm respectively. This allowed 3D reconstruction of samples.

*Figure 3-35 Part of sample held on stage and wrapped in Cellophane tape while scanning in Zeiss equipment.*

## 3.4 Image Analysis

Image analysis technique is followed to analyse images obtained through all three data acquisition methods, which is expected to provide meaningful morphological, weathering and reservoir properties from the samples.

To achieve this Fiji a version of ImageJ software was utilised. This selection of the software package is on the basis of funding and facility availability in the organisation. Fiji is developed by contributors around the world, and funded from various sources. It is maintained by Curtis Rueden and the ImageJ development team at the Laboratory for Optical and Computational Instrumentation (LOCI) at the University of Wisconsin-Madison. Furthermore, elements of civil Engineering specifically plugins (Xlib and Geodesics) were used. A sample 3 D reconstruction was also performed using Fiji and Drishti packages.

The following sections provide the steps followed during image analysis and its rationale.

#### *3.4.1.1 Size Calibration for Petrographic Image Analysis System*

To acquire accurate measurements from image analysis all the sources of data was initially calibrated using appropriate scales. For thin section Motic scale Figure 3-22 was used whereas that for SEM and micro CT analysis resolution of scanning provided an appropriate scale to calibrate images. This allowed for accurate measurements.

#### *3.4.1.2 Region of Interest selection*

While working with images captured through three sources a region of interests was selected for each of the sample. This allowed for reduction in errors due to deselection of an unwanted region from images. Figure 3-36

#### *3.4.1.3 Image editing*

To achieve best results image contrast and brightness were adjusted to provide accurate readings during analysis.

#### *3.4.1.4 Image Bionarisation*

All images being used were either converted or saved in black and white format to allow allocation of 0-255 range of greyscale to images. Wherein an image value of 0 represents black and an image value of 255 represents white. The images were then applied with thresholding to enhance the image contrast to allow separation between the grains and the pores and converted to binary image in 8bit –image (0-255). This image represents the pore spaces as white and the black spaces as the grains/rock part of the thin section.

#### *3.4.1.5 Parameter selection and analysis*

Parameters such as grain size, grain shape, Circularity, Kurtosis , skewness etc. were selected in this step in Fiji software to provide meaningful data.

### 3.4.2 Dataset quantities

According to the method implemented appropriate quantity of data is chosen based on the statistical requirement of this study.

For Thin Section, SEM and micro-CT 6000, 18000 and 20000 plus grains were analysed for and outcrop and core samples respectively.

For all samples region of interest was methodically chosen by avoiding corners/ edges/ disturbed section. In case of thin sections having disturbances due to preparation procedures were excluded for analysis. In case of SEM analysis quadrant formation and edge omission as shown in Figure 3-36 was performed while capturing and further analysing the images.

.

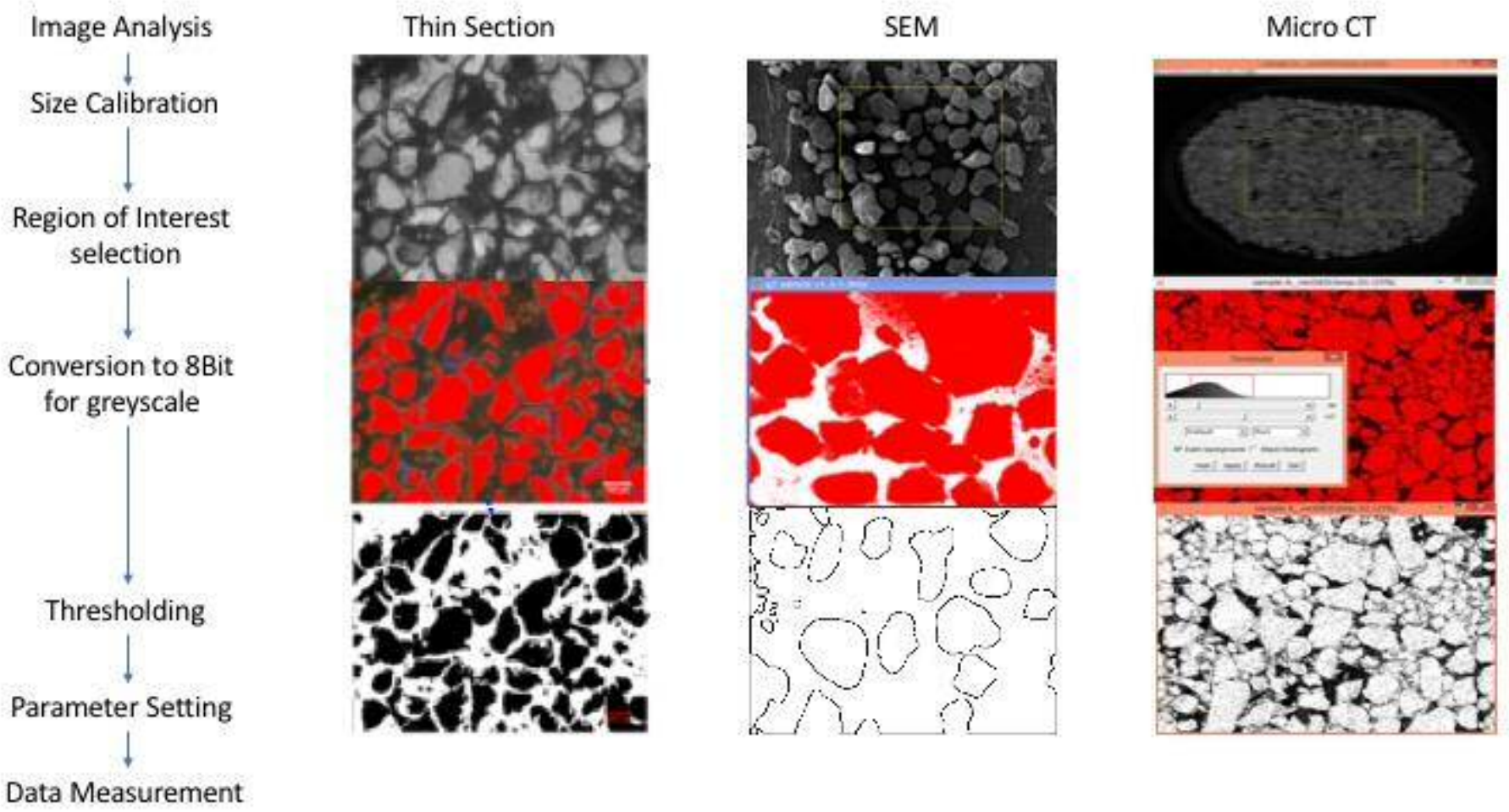


*Figure 3-36 Fiji workflow for all three sample types with  grey scale, thresholding and binaries images for measurement*

For micro CT analysis since the data obtained was in the range of 950 to 2250 2D images per sample the initial 10 % and last 10 % of the sample was neglected and from the central section of the sample every 50$^{th}$ image was scanned for 2D image analysis. This provided an equal distribution of core sample for property assimilation from 2 D image analysis.

On completion of analysis through ImageJ freeware resulting in an automatically generated excel sheet were saved. These excels include Area, Roundness, Circularity, skewness, kurtosis, standard deviation, solidity etc. which were further used for sorting calculations by plotting a cumulative frequency curve as seen in the results section.

## 3.5 Grain Morphology

To obtain parameters necessary to determine grain morphology following calculations and statistical measurements were performed.

#### *3.5.1.1 Grain size*

Folk and Ward (1968) inclusive graphiocal method was used to calculate grain size, Skewness within this sample and Kurtosis. To achieve this primarily feret diameter values generated by imageJ were converted to phi unit which is the transformation from logarithmic millimeters to whole integers. The values so obtained were then plotted on a cumulative frequency curve to obtain necessary data for statistical calculations of aforementioned properties.

Firstly, the feret diameter generated by imageJ was converted from microns to millimeters by dividing each value by 1000.

It was then converted from millimeter to phi (ϕ) unit using equation

*Equation 3-1 Grain size conversion equation from millimetre to Phi.*

Where,

ϕ = phi

d = diameter of the grain in millimeters

The resulting phi diameters were then plotted as cumulative frequency curve.

The standard deviation was calculated on obtaining necessary values from cumulative curve using the equation-- shown below

*Equation 3-2 Standard Deviation Equation (Folk, 1968)*

$$\text{Where,}$$

$б_1$ = standard deviation

$\phi 5$ = phi value of grain size at 5 percentile

$\phi 16$ = phi value of grain size at 16 percentile

$\phi 84$ = phi value of grain size at 84 percentile

$\phi 95$ = phi value of grain size at 95 percentile

The resulting values were compared to the values in Table 3-2.

*Table 3-2 Verbal classification for grain sorting (East Carolina University, 2007)*

| Values from | Values To | Sorting |
|---|---|---|
| 0.00 | 0.35ϕ | Very well sorted |
| 0.35 | 0.50ϕ | Well sorted |
| 0.50 | 0.71ϕ | Moderately well sorted |
| 0.71 | 1.00ϕ | Moderately sorted |
| 1.00 | 2.00ϕ | Poorly sorted |
| 2.00 | 4.00ϕ | Very poorly sorted |
| 4.00 | ϕ | Extremely poorly sorted |

### *3.5.1.2 Skewness*

Following Folks equation skewness was calculated

*Equation 3-3 Folk's Skewness Equation (Folk, 1968)*

$$\frac{\qquad\qquad}{\qquad\qquad}$$

Where

$SK_1$ stands for skewness

ϕ5 = phi value of grain size at 5 percentile

ϕ16 = phi value of grain size at 16 percentile

ϕ50 = phi value of grain size at 50 percentile

ϕ84= phi value of grain size at 50 percentile

ϕ95 = phi value of grain size at 50 percentile

### *3.5.1.3 Kurtossis*

Kurtosis of the grain size distribution is determined from the cumulative frequency curve using the Folk (1968) formula below;

*Equation 3-4 Kurtosis Equation based on (Folk,(1968)*

$$\frac{\qquad\qquad}{\qquad\qquad}$$

Where

$K_G$ represents kurtosis

ϕ95= phi value of grain size at 95 percentile

ϕ5 = phi value of grain size at 5 percentile

ϕ75 = phi value of grain size at 75 percentile

ϕ25 = phi value of grain size at 25 percentile

### *3.5.1.4 Grain Shape*

To determine shape descriptor following equations set in ImageJ were used.

*Equation 3-5 Image J Aspect ratio equation*

*Equation 3-6 ImageJ Circularity Equation*

*Equation 3-7 Image J Roundness Equation*

*Equation 3-8 Image J Solidity Equation*

To demonstrate results obtained through grain shape analysis a scale was set at an interval of 0.17 from 0-1 was selected to correctly represent six subsections of roundness from angularity to well rounded, accurately. The data obtained on angularity from ImageJ was then distributed using cummulative frequency curve and achieve the distribution of results.

### *3.5.1.5 Degree of sorting using visual comparators*

The use of visual comparators has become an established practise in the study of the distribution of grain sizes in plane and thin sections to estimate the degree of sorting in a grain population (Jeram, 2001; Harrell, 1984; Mansfield 1985 and Longiaru1987). The visual comparators are usually generated from 3-D sphere models with known sorting characteristics which are then sectioned to 2-D to serve as an analogue for comparison of real rock texture (Jeram, 2001). A Visual comparison chart Figure 2-20 was used for visual estimation of the degree of sorting. The sorting of grains from the thin section was expressed as PHI (Φ) and the standard deviation of grain sizes have been divided into standard classes by Friedman and Sanders (1978).

*Equation 3-9 Friedman and Sanders Phi ( ) grain size standard deviation equation 1978.*

Where D= Grain size diameter.

*Table 3-3 Classification of sorting based on the Standard deviation of grain sizes (Φ) (Friedman and Sanders, 1978).*

| Standard Deviation (Φ) | Sorting Class |
|---|---|
| **<0.35** | Very well sorted |
| **0.35-0.50** | Well sorted |
| **0.50-0.80** | Moderately-well sorted |
| **0.80-1.40** | Moderately sorted |
| **1.40-2.00** | Poorly sorted |
| **2.00-2.60** | Very poorly sorted |
| **>2.60** | Extremely poorly sorted |

### 3.5.2 Porosity determination

#### *3.5.2.1 Image Derived Porosity (Optical Porosity)*

Rocks are defined as composite materials consisting of essentially two-phase: solids and pores making up the rock Figure 3-37. The definition of a rock type is then governed by the amount and spatial distribution of each phase (Torabi *et al,* 2008).

According to the Delesse Principle (Ruzla, 1986) which states that "*the volume density of a rock components can be estimated by the measurement of the areal density of the components on random sections*"

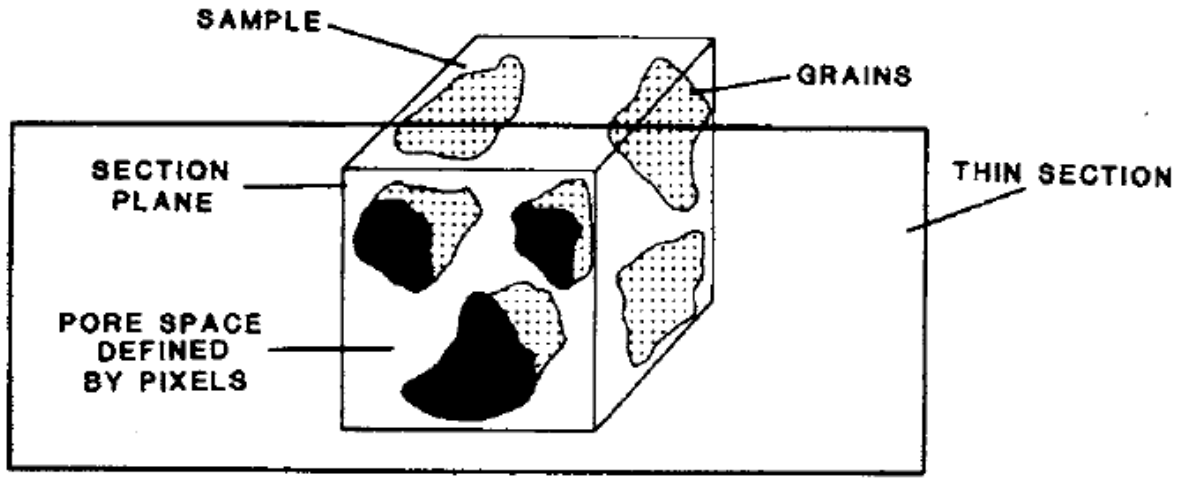


*Figure 3-37 Model for a rocks sample showing rock grains and pore spaces in a random-section plane of a sample (Ruzla, 1986)*

Then it follows that the total porosity for a typical thin section image can be calculated using the conventional porosity formula

*Equation 3-10 Total Porosity Equation*

—

Where volume of void and

= total volume

Now considering 2-D images in this case a thin section image the *optical porosity* (Ehrlich *et al.,* 1984; Layman and Wayne, 2001; Krause *et al.,* 2009) *is* defined as ratio of area occupied by void to the area occupied by void and non-void can be calculated using the following relationship derived from the equation above

*Equation 3-11 2D Image based Porosity determination equation*

———————————————————

=————————————=—

Optical porosity was determined using the image processing software Fiji stated in 3.4 and a work flow that is demonstrated in Figure 3-36. The software was used to convert the coloured thin section image to grey scale image (black and white image). The

pixels in the grey scale image has a value which ranges form 0-255, where an image value of 0 represents black and an image value of 255 represents white. The image was first threshold to enhance the image contrast to allow separation between the grains and the pores and converted to binary image in 8bit –image (0-255) the binary image represents the pore spaces as white and the black spaces as the grains/rock part of the thin section. The number of data point obtained from any thin section is then dependent on the number of ROI (region of interest) the thin section has been subdivided into.

In case of image stacks that represented 3D core sample above workflow of standard image binarisation and thresholding was followed. A stack of 993 images were further analysed using the Particle Size Distribution (PSD) and Pore Size Distribution, values for the total void and total grain area. Upon generation of these parameters the porosity was calculated using the formula:

*Equation 3-12 Total Optical Porosity*

---

To perform this operation Xlib plugin within Fiji was utilised. This plugin is developed by the Laboratory for Concrete and Construction Chemistry in Switzerland (ImageJ, 2017) for data regeneration, quantitative data, filtering and tools for segmentation, evaluation and control of image data.

### 3.5.3 Permeability determination

The permeability result was calculated based on image stacks for all the three samples. Van Barren's Equation 2-15 was used to perform necessary calculations. A grain based model that relates grain size distribution and porosity.

The sorting index used in this calculation is based on Table 3-2 providing the range for all the three samples. For samples under considerations Sample A is poorly sorted, Sample B and C are moderately sorted. There are two variables in Archie law, *m* and *n*. Archie cementation factor can be calculated by the expression

*Equation 3-13 Tortuosity determination equation based on Archie's Cementation factor*

,

where  is tortuosity. This value can also be found in Fiji using the plugin Geodesics.

By applying natural logs on both sides of the equation, using , we get:

The grain size was found by using the Feret Diameter, a morphometric feature that measure objects in a giving direction, mostly used in particles that are not entirely rounded (Legland and Beaugrand, 2013). Table 3-4 Provided collaboration between sorting , cementation and deposition condition.

*Table 3-4 Relationship between the constant c and Degree of sorting*

| **Degree of Sorting** | **c** | **Degree of Consolidation** | **Cementation Factor (Atmospheric)** | **Cementation Factor (in-situ)** |
|---|---|---|---|---|
| Extremely well to very well sorted | 0.70 | Shallow , very consolidated sands | 1.2 | 1.2 |
| Very well to well sorted | 0.77 | Unconsolidated sands | 1.4 | 1.6 |
| Well sorted | 0.84 | Unconsolidated to friable sands | 1.5 | 1.7 |
| Well to moderately sorted | 0.87 | Friable sands | 1.6 | 1.8 |
| Moderately sorted | 0.91 | Hard to friable sands | 1.7 | 1.9 |
| Moderately to poorly sorted | 0.95 | Hard sandstone | 1.8 | 2.0 |
| Poorly sorted | 1.00 | Very hard sandstone | 2.0 | 2.2 |

#### *3.5.3.1 3D Rendering*

To separate and visualise grain phase and pore phase from all the three core samples, 3D rendering was attempted. Fiji and Drishti software packages were both utilised to re construct representative core plug depicting each phase.

Dataset for each of the sample subset was around 1 – 2.5 Gigabyte ( at least). This provided significant challenges while reconstructing images from 2D slices to 3D representative model. Due to the machine capacity Fiji software was crashing continuously while working with the data. As a result Drishti software package was utilised for reconstruction. Drishti Paint element within software was further able to provide a histogram of image saturation which could be easily utilised in separating Grain and Pore phases of 3D scans. Though upon ROI application to the core data reliability of the Fiji software improved to a certain extent though it was still unable to provide clear and sharp phase separation between grains and pores.

## 3.6 Geomodelling and simulation

### 3.6.1 Geomodelling

To understand applicability of results obtained so far (e.g. Grain morphology, porosity, permeability, internal structure of grains bioturbation) number of reservoir models were simulated and results were analysed to understand effect of detailed modelling process. To benchmark and compare (Shin & Polikar, 2005) study was chosen as they have standardised properties for Canadian Oil sands and simulated a representative reservoir model and further calculated economical viability based on the thickness of the reservoir.

To appropriately replicate reservoir conditions and aforementioned results primarily, a three case approach was designed. The Three cases include

1. Shin and Polikar model

2. Property model

3. Bioturbation models

All of the above mentioned cases will have similar reservoir properties except for porosity , permeability and inclusion of bioturbation. The following sections will talk

in detail of the rationale behind this approach and will further provide a snapshot of the respective geomodel.

### *3.6.1.1 Shin and Polikar studies:*

According to Shin and Polikar (2005) economics of the Canadian Oil Sands are dependent on the thickness and permeability of the reservoir. Their paper correlates reservoir thickness, permeability and economics for the field. Though, their hypothesis does not take into consideration the effects of geology, depositional environment and the effect of bioturbation on the reservoir and overall simulation.

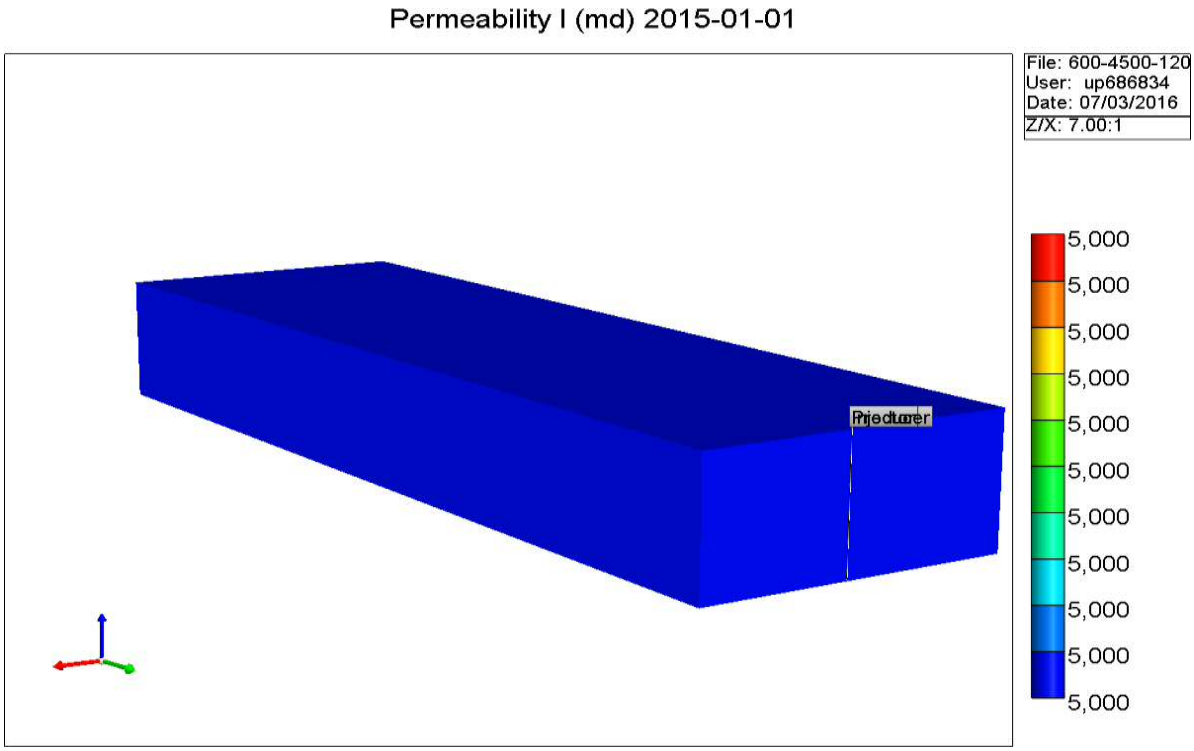


*Figure 3-38 Shin and Polikar based 3D model.*

As can be seen from Figure 3-38 this model consists of uniform reservoir properties as described in Table 3-5 where uniform porosity of 35 % and standard permeability of 5000md horizontally and 2500 md vertically is considered.

*Table 3-5 Values of Porosity and Permeability used in development of Case 1*

| Porosity | | 35 % |
|---|---|---|
| Permeability | **I – direction** | 5000 md |
| | **J – direction** | 5000 md |
| | K – direction | 2500 md |

### *3.6.1.2 Property model*

The aim behind developing this model was to modify the Shin and Polikar model and directly compare variation to the productivity under similar simulation conditions. This study will allow us to understand how porosity and permeability on its own will vary production in Canadian Oil Sands following SAGD recovery technique. To populate this model results obtained through initial 2D SEM analysis have been followed. Table 3-6 shows detailed porosity and permeability values used to develop simulation model that can be seen in Figure 3-39.

*Table 3-6 Values of Porosity and Permeability used in development of Case 2.*

| | | |
|---|---|---|
| | Layer1 | |
| Porosity | | 29 % |
| Permeability | **I-direction** | 2626 md |
| | **J- direction** | 2626 md |
| | **K-direction** | 1313 md |
| | Layer2 | |
| Porosity | | 23% |
| Permeability | **I-direction** | 840 md |
| | **J- direction** | 840 md |
| | **K-direction** | 420 md |
| | Layer3 | |
| Porosity | | 26% |
| Permeability | **I-direction** | 906 md |
| | **J- direction** | 906 md |
| | K- direction | 453 md |

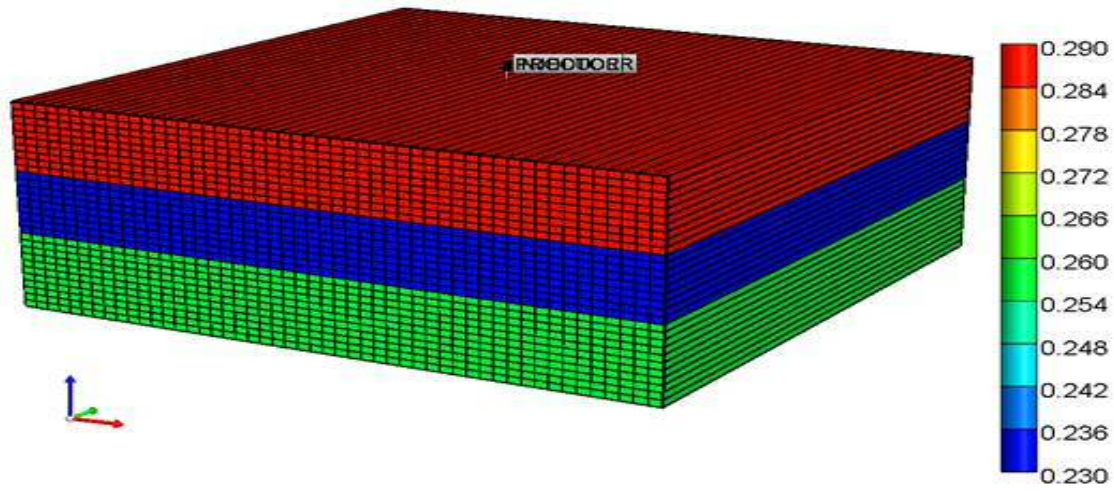


*Figure 3-39 Showing Porosity and permeability model developed through this study.*

### *3.6.1.3 Bioturbation model*

*To understand an effect of bioturbation on recovery a representative model has been developed. The section 2.4.2 on bioturbation in the Literature review was able to provide quantifiable variation to the properties. This can be*

*further visualised by looking at Figure 2-9. In addition, some of the bioturbated sections as seen from Figure 4-13 Which show presence of clays surrounding bioturbation forming isolated pore spaces.*

Both conditions explained above will have a certain effect on reservoir production due to use of steam/ hot water as part of SAGD process. Wherein, part of clays may swell due to its affinity with water thereby reducing permeability within the bioturbated section of the reservoir. Furthermore, absence of clays may provide conduit for steam to escape reservoir reducing its effectiveness on viscosity reduction.

Following Figure 3-40 shows the reservoir model developed to represent bioturbation through the entire reservoir and Table 3-7 shows properties with variation in non bioturbated and bioturbated sections of the reservoir.

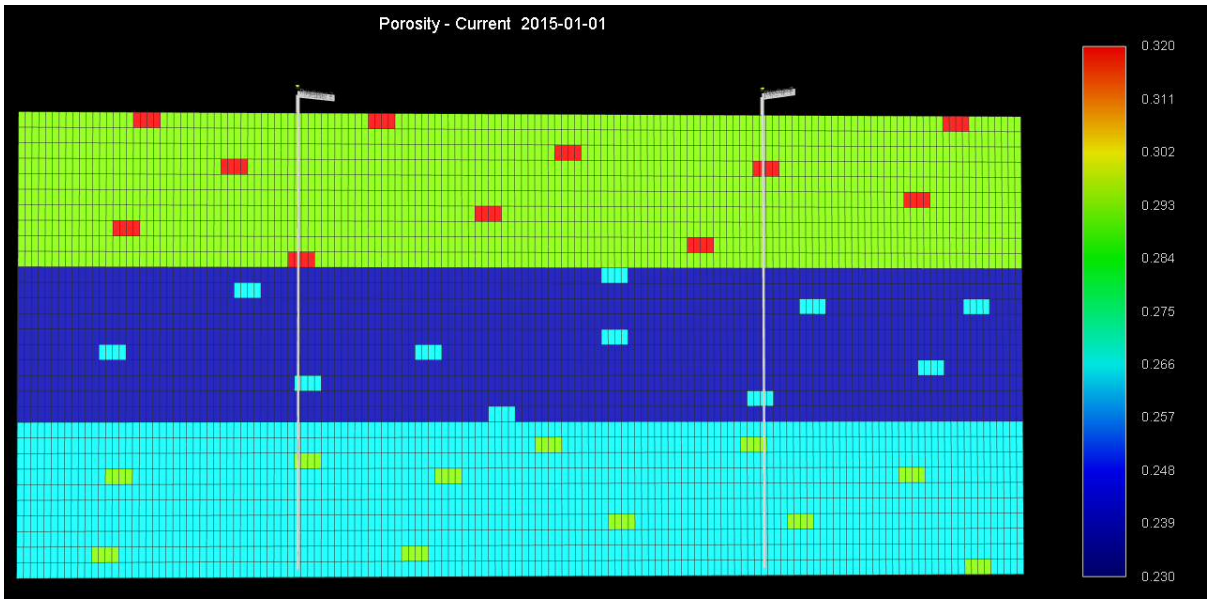


*Figure 3-40 Showing simulation model with uniform bioturbation distribution*

*Table 3-7 Comparative population of properties within non bioturbated and bioturbated sections of the reservoir.*

| | Layer 1 of Matrix | | Layer 1 Bioturbated Region |
|---|---|---|---|
| **Porosity** | 29% | | 32% |
| **Permeability** | I Direction | 2626 md | 2889 md |
| | J Direction | 2626 md | 2889 md |
| | K Direction | 1313 md | 1444 md |
| | Layer 2 | | Layer 2 Bioturbated Region |

| | | | |
|---|---|---|---|
| **Porosity** | 23% | | 26% |
| **Permeability** | I Direction | 840 md | 924 md |
| | J Direction | 840 md | 924 md |
| | K Direction | 420 md | 462 md |
| | Layer 3 | | Layer 3 Bioturbated Region |
| **Porosity** | 26% | | 29% |
| **Permeability** | I Direction | 906 md | 997 md |
| | J Direction | 906 md | 997 md |
| | K Direction | 453 md | 498 md |

### 3.6.2 Development Strategies

Aforementioned models were further developed and run for number of optimisation parameters. As can be seen from Figure 3-41, each type of model was studied for optimisation in the number of wells, spacing between wells for property determined models and that for bioturbated models the increase and reduction in porosity around bioturbated section. These optimisations have allowed for analysing the detailed effect of properties and bioturbation on reservoir and mobility within reservoir.

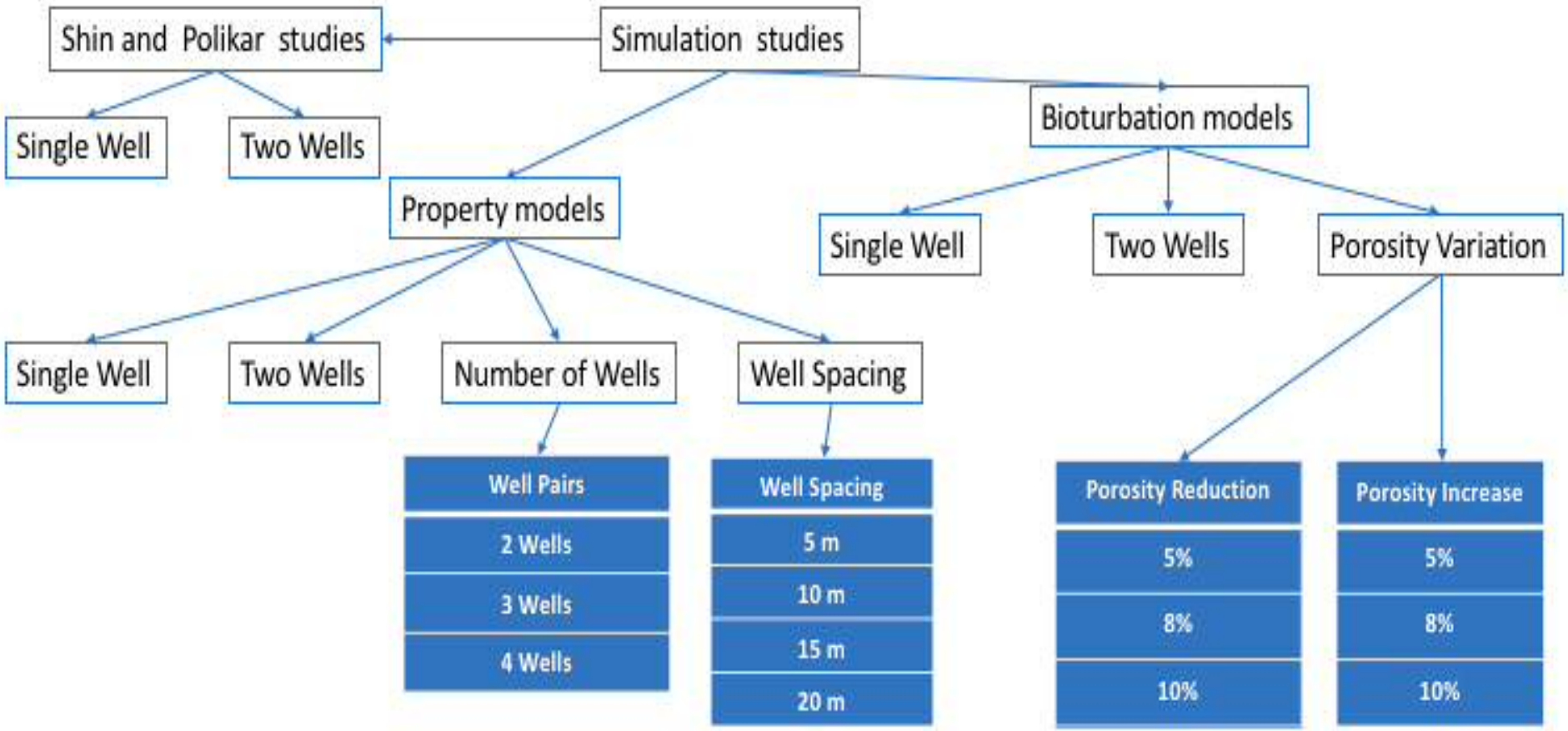


*Figure 3-41 Reservoir Simulation optimisation parameters followed as part of this study*

### 3.6.3 Reservoir properties

In absence of any real field data, it was a challenge to populate simulation models with required reservoir properties other than porosity and permeability. To overcome this challenge a number of different publications were studied and the closest matching reservoir location. The PVT fluid model was built in CMG Winprop using data from (Souraki, Ashrafi, Karimaie, & Torsaeter, 2012), which analysed the bitumen properties of the McMurray samples using gas chromatography. However, the relative permeability data for the model was taken from (Chen, 2009). Further optimisation work was conducted using a number of different parameters as it can be seen from above. In addition, the initial study primarily focused on following injection pressure and injector to producer well spacing.

- Injection Pressure (2000, 3000, 4000, and 6000 KPa)
- Injector to producer spacing (I/P spacing) (5m, 7m, 9m)

Other optimised reservoir parameters were chosen from (Souraki, Ashrafi, Karimaie, & Torsaeter, 2012) in which parameters such as injection rate, and pre-heating period were tested. In (Souraki, Ashrafi, Karimaie, & Torsaeter, 2012) it was found that an injection rate of 300 STB/day and a pre-heating period of between 60 and 100 days was optimal, thus 90 days was chosen to initiate the study. It was also seen that (Shin H. , 2012) found similar findings, in which it was found that 90 days gave the 2$^{nd}$ highest Calendar Day Oil Rate (CDOR) whilst also giving the highest Cumulative Steam Oil Ratio (CSOR).

Once reservoir optimisation was completed, the best cases from each were input into a new base model, from which other parameters could be optimised. These parameters were steam temperature and steam quality. However, there is a limitation to using these on CMG, for example, in a real-life situation as you continue to inject, the quality of the steam would decrease within the reservoir, affecting the steam pressure, the volume of steam, and thus the enthalpy of the steam chamber. However, CMG assumes the steam quality is consistent through-out, resulting in a less realistic result. Whilst for steam temperature, it also assumes no surface or wellbore heat loss, only formation heat loss, where realistically, heat will be lost at all of these stages to some extent.

### 3.6.4 Reservoir Data

Following this, Table 3-8 provides all the reservoir data that is gathered from several studies of (Souraki, Ashrafi, Karimaie, & Torsaeter, 2012).

*Table 3-8 The reservoir data taken to make the CMG simulation in Builder (Souraki, Ashrafi, Karimaie, & Torsaeter, 2012)*

| Properties | Data |
|---|---|
| Grid Top | 80m |
| Grid size | 0.33m |
| Grid dimensions (I, J, K) | 151 x 10 x 30 |
| I direction | 151 x 1 |
| J direction | 10 x 50 |
| Reservoir Thickness | 10m |
| Reservoir Temperature | 10 °c |
| Reference Pressure | 2068 kPa |
| Rock Thermal Heat Capacity | 2350 KJ/m³*°c |
| Formation Rock Compressibility | 9.6 x 1/Kpa |
| Overburden/Under burden Heat Capacity | 2600 KJ/m*day*°c |
| Reservoir Rock Thermal Conductivity | 6.6 x J/m*d*°c |
| Oil Thermal Conductivity | 1.15 x J/m*d*°c |
| Water Thermal Conductivity | 5.35 x J/m*d*°c |
| Gas Thermal Conductivity | 1.4 x J/m*d*°c |
| Initial Oil Saturation - Soi | 0.8 |

| | |
|---|---|
| Water Connate Saturation - Swc | 0.2 |
| Bitumen Density | 1013.3 kg/m³ Molecular |
| Bitumen Weight | 534 g/gmole Specific |
| Bitumen Gravity | 1.129 m³ |

### 3.6.5 Saturation & Relative Permeability data

Considering studies discussed in the literature review for relative permeability, we can observe that relative permeability curve used in this model shows a similar trend of reduction in oil saturation at high water saturation leaving behind lower quantities of irreducible oil saturation for Canadian oil sands.

Additionally, the effect of viscosity, and temperature on relative permeability in Canadian oil sands are discussed in section ----of this thesis.

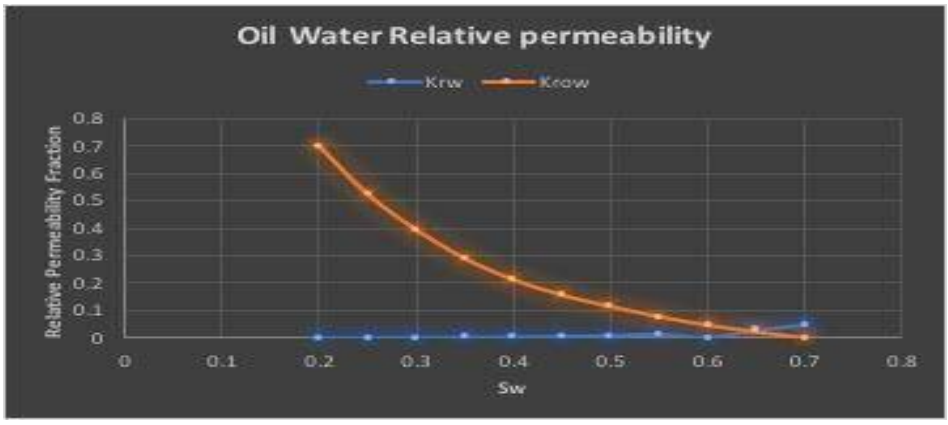


*Figure 3-42 Graph showing relative permeability against water saturation (Chen, 2009).*

## 3.7 Simulation

Advanced dynamic reservoir modelling is required for taking into account flow and rock properties challenges in the unconsolidated formations. The most widely used reservoir simulation software for thermal processes in Canadian oil sands is STARS, CMG package.

Reservoir simulation packages have the flexibility to add top or bottom water, mobile water, top gas and compositional dependency to the model. Top water can either be

detrimental or helpful to a SAGD process based on the continuity of the water zone. Water has a very high thermal conductivity and heat capacity and therefore can act as an enthalpy sink once the steam chamber encounters it.

### 3.7.1 CMG STARS - Simulator Workflow

The software had the following eight sections:

- I/O Control
- Reservoir
- Components
- Rock Fluid
- Initial Conditions
- Numerical
- Geomechanics
- Well and Recurrent

In this study, advanced geomechanics and well hydraulics data were not inputted due to the complexity and lack of data.

#### *3.7.1.1 Reservoir Section*

In the reservoir section you can build your grid followed by the setup of fundamental rock properties and fluid properties. All properties utilised in development and build-up of this model are represented in Table 3-8.

#### *3.7.1.2 Thermal Rock Types*

This section takes into account rock compressibility, thermal conductivity and heat loss element of the rock to passage the heat generated by steam injection. The properties utilized for this section are detailed in Table 3-8 .

#### *3.7.1.3 Reservoir Array Properties*

This was one of the most important sections within this study as it allowed for variation within several models to be introduced. The section allowed for properties such as porosity, permeability in I, J & K directions to be defined along with Oil Saturation, Temperature and Water Connate saturation etc.. The properties adapted for each model for Porosity and Permeability being different are provided in Table 3-5,Table 3-6 and Table 3-7.

### *3.7.1.4 Components Section*

A live oil case was considered where the bitumen was considered as a pseudo-component with defined properties. It was assumed that initially the composition in the reservoir is made up of both bitumen and a small fraction of gas. According to Ashrafi (2011), the composition of the bitumen was determined using Gas chromatography. The heavy composition made up of C10 to C30+ was considered to be the primary composition. This was called heavy, with a mole fraction of 0.91767 plus a mole fraction of 0.008233 of CH4 added.

The Pressure Volume temperature (PVT) properties of the Athabasca bitumen such as density, molecular weight and viscosity behaviour versus temperature, measured in the laboratory, were used in the fluid characterization model (Ashrafi et al., 2011).

*Table 3-9 Defined Pseudo- Components properties*

| **Pseudo-component** | **Amount (Weight %)** | **Amount (mol %)** | **Molar mass[a](g/mol)** | **Density[a] ($g/cm^3$)** |
|---|---|---|---|---|
| C10 | 0.21 | 0.842 | 134 | 0.7780 |
| C11+C12 | 0.948 | 3.286 | 154 | 0.7945 |
| C13+C14 | 1.976 | 5.782 | 182.5 | 0.8165 |
| C15+C16 | 3.006 | 7.501 | 214 | 0.8355 |
| C17+C18 | 3.731 | 8.166 | 244 | 0.8495 |
| C19+C20 | 4.068 | 8.075 | 269 | 0.8595 |
| C21+C22 | 3.959 | 7.094 | 298 | 0.8695 |
| C23+C24 | 3.759 | 6.186 | 324.5 | 0.8790 |
| C25+C26 | 3.594 | 5.453 | 352 | 0.8870 |
| C27+C28 | 3.602 | 5.048 | 381 | 0.8945 |

| | | | | |
|---|---|---|---|---|
| C29+C30 | 3.437 | 4.487 | 409 | 0.9005 |
| C31+C32 | 3.265 | 3.989 | 437 | 0.9075 |
| C33+C34 | 2.577 | 2.959 | 465 | 0.9130 |
| C35+C36 | 2.599 | 2.815 | 493 | 0.9180 |
| C37+C38 | 2.309 | 2.366 | 521 | 0.9230 |
| C39+ | 56.960 | 25.950 | 1172.1 | 1.1474 |
| Total/average | 100 | 100 | 534 | 1.0129 |

### 3.7.2 CMG WINPROP

The WinProp function of CMG was used in defining the fluid model by creating a PVT model that was imported into the component section of the builder. The experimental data for both density, viscosity and saturation pressure was taken from Ashrafi et al, 2011. In order to match these experimental data with the simulation results, a number of regression analysis was undertaken to match the results as close as possible.

```
************************************************
*                                              *
*               WINPROP  2012.11               *
*             2012-Dec-14   09:32:00           *
* Computer Modelling Group Ltd., Calgary, Canada *
*                       2                      *
************************************************
Summary of Regression Variables

  Variable              Lower Bound   Upper Bound  Initial Value    Final Value     % Change
  --------              -----------   -----------  -------------    -----------   ----------

  PC  Heavy               8.2033E+00    2.6902E+01     1.0254E+01     1.0230E+01       -0.24
  TC  Heavy               6.3401E+02    1.2445E+03     1.0371E+03     8.1062E+02      -21.84
  PVC3 1                  0.0000E+00    1.8000E+00     1.2000E+00     1.2000E+00        0.00

************************************************
*                                              *
*               WINPROP  2012.11               *
*             2012-Dec-14   09:32:00           *
* Computer Modelling Group Ltd., Calgary, Canada *
*                       3                      *
************************************************
Summary of Regression Results

       Calculation  Data    Pressure   Experimental   Before      After       ERROR        ERROR      Weight
         option     type   (MF-SWELL)     data      regression  regression   reduction     after      factor
       -----------  ----   ----------  ------------ ----------  ----------   ----------  ---------- ----------
        4 FLASH
                    DL                  1.0133E+03  8.0497E+02  1.0133E+03   2.0559E-01  5.5001E-06 1.0000E+00
        5 PRESSAT
                    PSAT                2.0680E+03  2.5469E+03  2.0680E+03   2.3159E-01  2.7729E-06 1.0000E+00

       ERROR Reduction = ERROR before regression - ERROR after regression
       ERROR = (experimental - calculated) / experimental

WinProp 2012.11
Total EOS calls without derivatives =       329
Total EOS calls with    derivatives =       312
Total calculations performed        =         9

Date and Time at End of Run : 2015 Sep 21,  11:10:50
CPU seconds used            :    0.02
```

*Figure 3-43 Results of regression analysis in WinProp*

Figure 3-43 shows that an exact match was achieved in matching the experimental density value to that of the simulation value. The saturation pressure of 2068 Kpa was also accurately matched to that of the simulation

### *3.7.2.1 Rock Fluid Section*

Since water is a standard component in Canadian Oil Sands, Stone's model was selected for oil relative permeability curves assuming the aqueous phase "water" is the wetting phase.

### *3.7.2.2 Numerical Section*

Numerous variations were applied and tested to come over some of the error messages. The errors were primarily related to convergence and extensive long simulation runs.

More specifically, the Maximum Number of Timesteps (MAXSTEPS) and the First Time Step Size After Well Change (DTWELL) were changed in various models to 90,000 steps and (0.1-0,5 days). This was mainly done in Live Oil cases where the

simulator required extensive simulation time to track complex reservoir and injection fluid flow across the reservoir.

#### *3.7.2.3 Wells & Recurrent Section*

The wells and recurrent section allows the user to define the number of wells and the configuration of the wells. In STARS, it allows for the option to use a heater well for the pre- heating stage of the SAGD. To implement the number of cases developed and detailed in Figure 3-41 numerous variations were performed using this section. A common model setup t used two horizontal wells with a spacing of 5 metres apart. The first well was called injector and was placed at an upper location (1:50 1 7) with the second well called producer placed below that of the injector in location (1:50 1 15). It has been suggested by various authors that for a successful SAGD, ideal injector- producer spacing is 5 meters. (shin & Polikar, 2005).

A range of 300, 400 and 500 $m^3$/day injection rate was used. Injection pressure was varied from the low case of 3000 Kpa to 6000 Kpa.

Steam quality will also have an overall effect on the production levels in a SAGD process. For a given injection rate, increasing the steam quality increases the volumetric flow rate, pressure drop and heat transfer. (Yuan & McFarlane, 2009). A high steam quality of 0.9 throughout all of the models have been used. A steam temperature of 250$^oC$ has been used throughout all the models.

For producer constraints, a bottom hole operating pressure of 2000 Kpa have been used and a maximum surface liquid rate of 500 m3/day.

The base case model was optimised for a SAGD process by changing the operating conditions. The three main operating conditions which were optimised throughout this project were pre-heating period, injection rate and also the injection pressure. The simulation results have been optimised to have the lowest Cumulative Steam to Oil Ratio (CSOR), high Recovery Factor (RF) and highest Cumulative Oil at standard condition (Cum Oil).

### 3.7.3 Pre- Heating Period

The key to a successful SAGD operation is for the viscosity of the bitumen to be reduced between the injector and producer. The process of establishing good heat

communication between the producer and injector occurs at the start-up period by injecting steam in both wells for a period of time. The wells act as hot fingers in the reservoir, and heating is by conduction (shin & Polikar, 2005)

In CMG STARS, this is made possible by the use of Heaters. There are three different strategies for mimicking this phenomenon in CMG, these are the HEATER option, which uses the heater keyword applied to the grid block of the injector and producer wells to help raise the temperature. The second option used is the HTWELL which offers more flexibility especially when a well undulates through layers following some real trajectories. (CMG, 2013). The final one is the use of FlexWell model.

However, in this study, all cases of preheating have been modelled by the use of HTWELL option.

According to Shin and Polikar (2005), it has been found that usually a period of 6 months or less is reasonable for a field SAGD project. Throughout this project, a pre-heating period of 60, 90 and 120 days have been used to observe the effect on CSOR, Cumulative oil produced and recovery factors (RF).

# 4 Results

## 4.1 The initial study

To establish work flow for this PhD an initial study was carried out on outcrop samples and thin sections. This involved studying sedimentary properties, morphological analysis, undertaking laser based particle size distribution. Results obtained were able to provide detailed information on reservoir, internal arrangements, applicability of thin section analysis and provide morphological properties as detailed below.

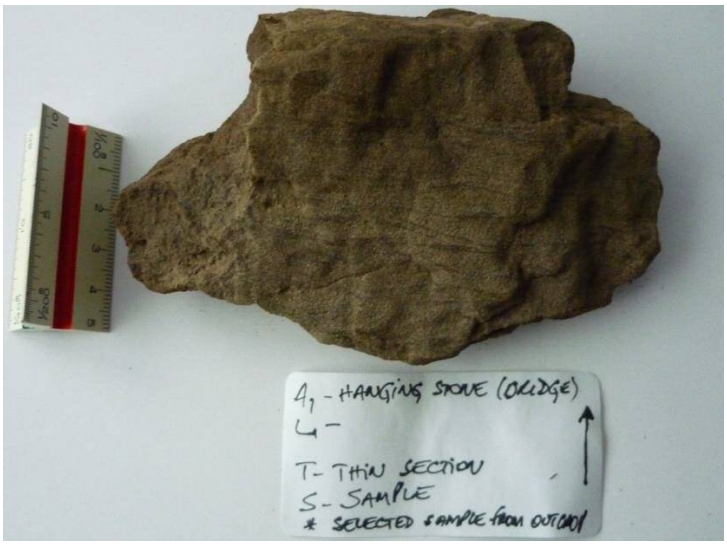


*Figure 4-1 Hand specimen from outcrop for initial observation studies*

### 4.1.1 Thin preparation.

Thin section preparation process for unconsolidated samples is quite a complex task as the material first needs to be impregnated and subsequently allowed to polymerise. Following this technique for consolidated, non-hydrocarbon bearing samples may be easier. Though, in this case as hydrocarbons are acting as a cementing elements due to the reservoirs nature and fluids viscosity it proves to be extremely difficult. The elements used in impregnation and polymerisation process e.g. Acetone and exothermic reactive epoxy starts to melt hydrocarbons thereby altering the integrity of the samples. Further process of cutting and thinning the samples use of diamond coated disc, grinding wheels and cooling agent ISOPAR all contributed to the heat generation and loss of integrity of the sample.

*Table 4-1 Results from resin reaction to bitumen*

| Resin | Effect observed |
|---|---|
| Polyester | Just contact with sample melts bitumen |
| Epoxy | Heat generated during polymerization melts bitumen |
| ERMS | Just contact with resin initiates the melting of bitumen |

#### *4.1.1.1 Polyester Method:*

To calculate the required quantity of polymer required acetone was used, that could also help resin travel through all the pores within the sample, though which as expected melts the bitumen sample and disturbed the integrity of the sample.

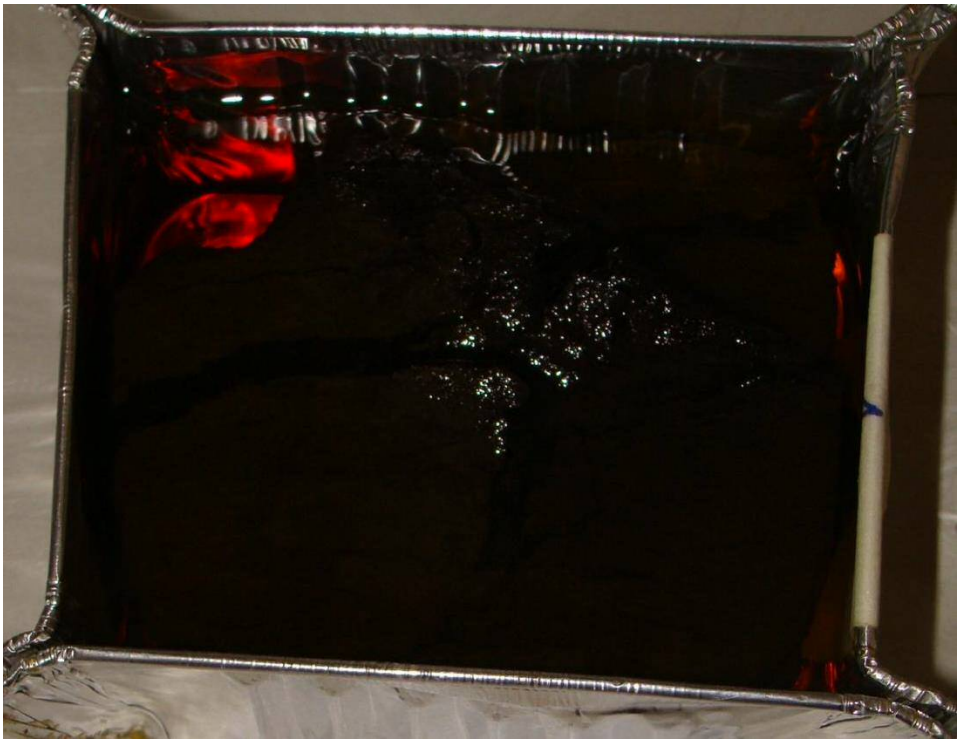

*Figure 4-2 Sample loosing bitumen when subjected to Acetone*

The sample was further polymerised and thin sections were prepared. The resulting thin sections were of no use to determine integrated properties of the sample though it helped to understand the grain characteristics and morphology.

*Figure 4-3 Sample undergoing Polymerisation using polyester resin.*

#### *4.1.1.2 Epoxy Resin Method*

The thin sections were attempted to prepare using standard process of trimming, grinding and ISOPAR based cooling, though it was observed that the sample did not achieve full impregnation. As a result, the sample was re-impregnated to achieve necessary sample impregnation thickness for thin section preparation. To overcome the melting of oil observed during ISOPAR cooling water based coolant was used this time. This method did provide some success to the preparation of thin sections that were useful for initial understanding of the samples.

*Figure 4-4 Thin section prepared using standard epoxy based polymer, re- impregnation and regrinding using water based coolant*

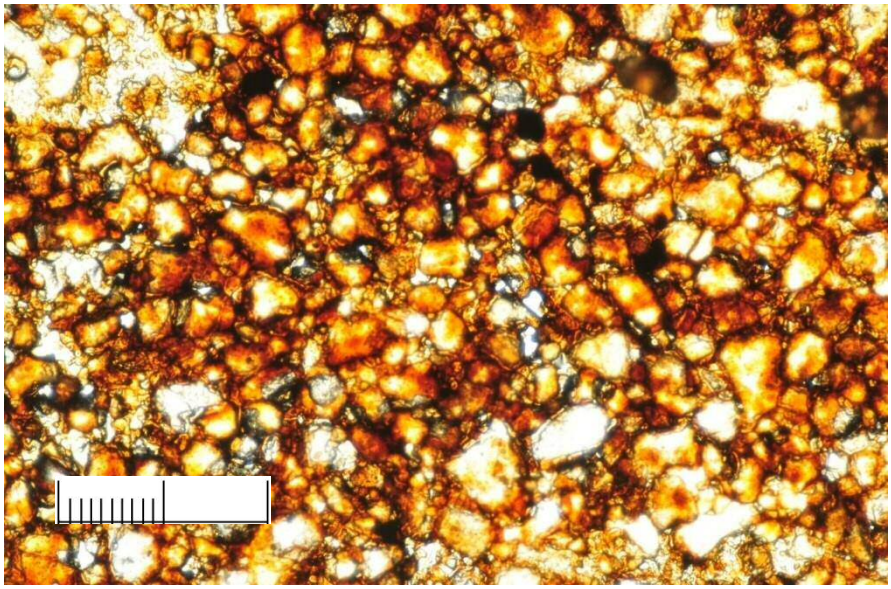

*Figure 4-5 One of the thin section where large amount of oil can be seen with partially melted state.*

As you may see from Figure 4-6 few air bubbles could be observed within thin section as well as having more oil compared to the previous thin section. Figure 4-7 shows that the pressure applied to bond the sample with thin section until it polymerised, as a result a stream of oil can be observed at the edge of thin section.

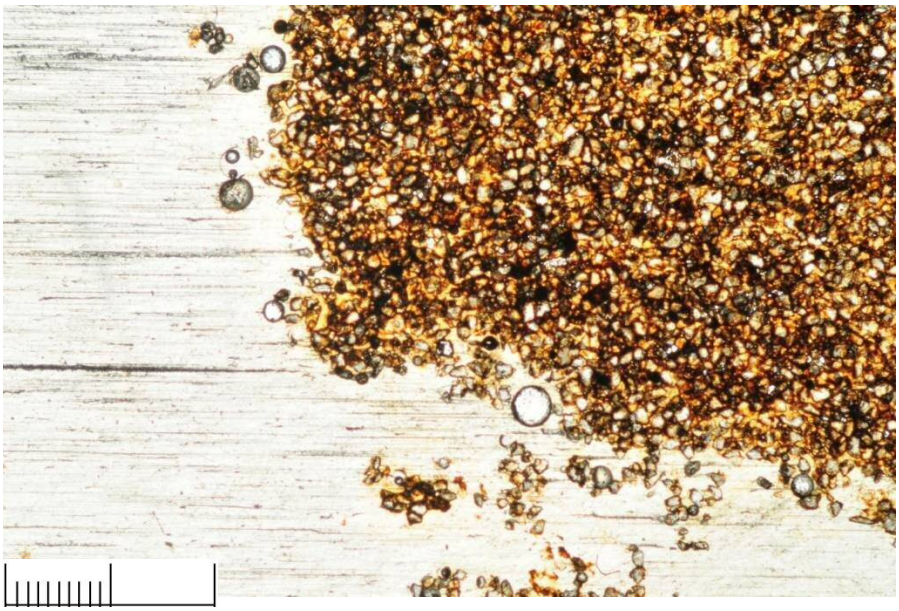

*Figure 4-6 Thin section with higher pressure and exothermic reaction of the epoxy resin*

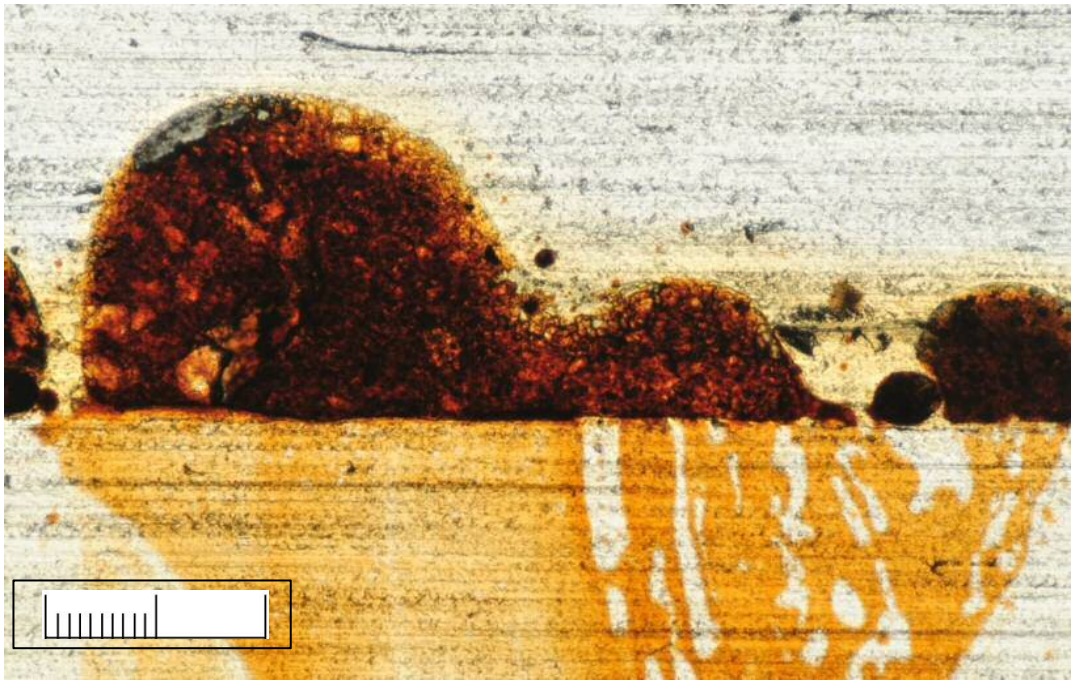

*Figure 4-7 Close up of the oil stains left after the grinding process.*

#### 4.1.1.3 EROMS Method

There were two different ways which were followed where in samples were pressurised at two different levels as a result of impregnation problems. One of the samples was hand grinded down to reach the desired thickness. Figure 4-8 and Figure 4-9 show the half impregnated samples to trapped air within the thin sections. Also it shows the grinded out area while manual grinding was applied.

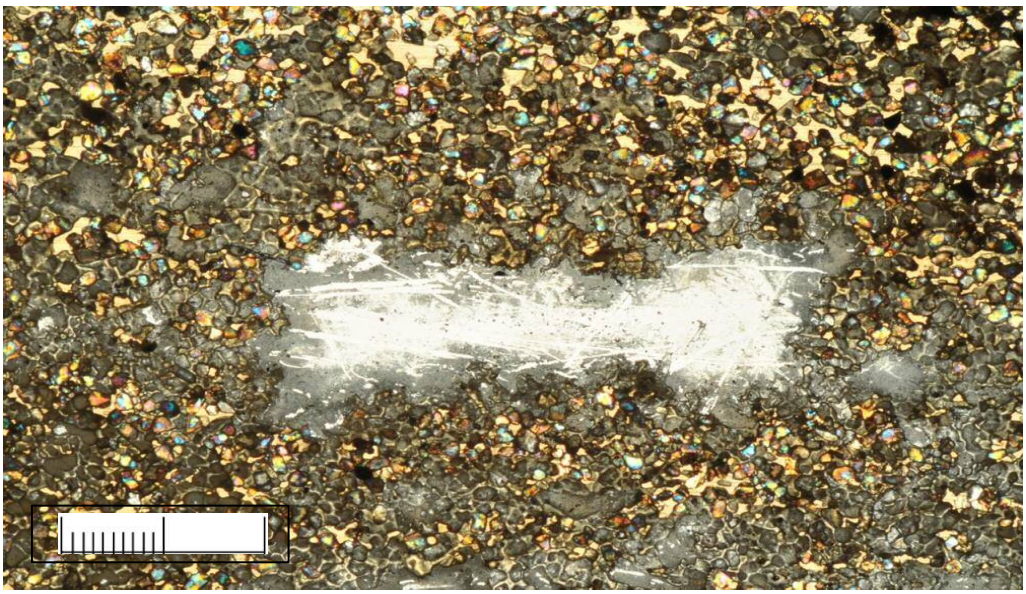

*Figure 4-8 Under polarised light showing lost part of the sample.*

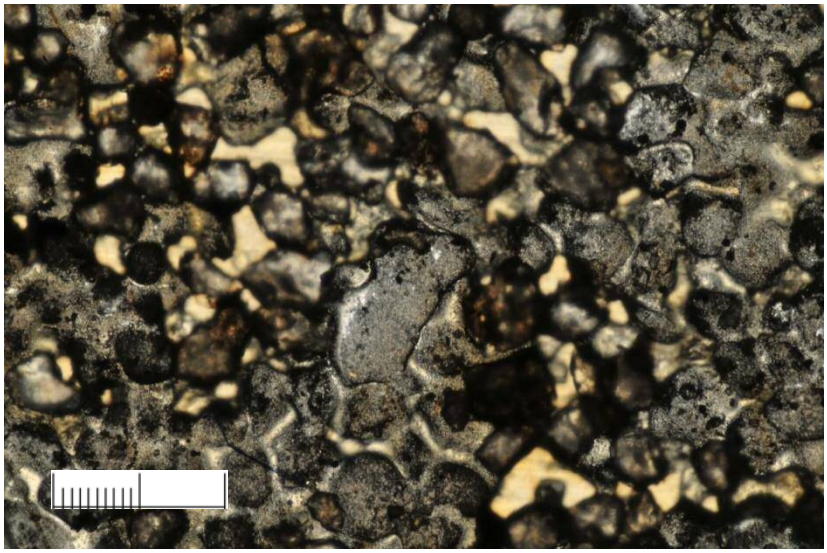

*Figure 4-9 microscopic picture showing the focus onto superficial layer.*

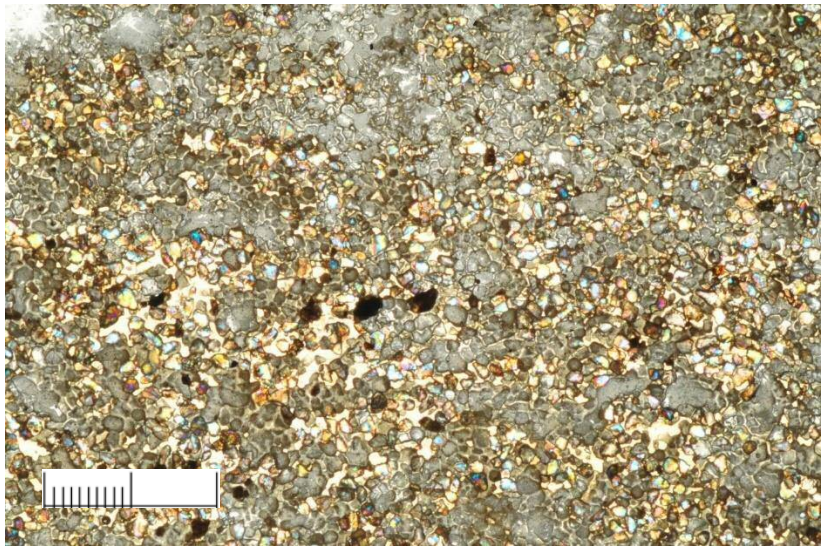

*Figure 4-10 Thin section grinded using ISOPAR showing an effect of lost oil while grinding*

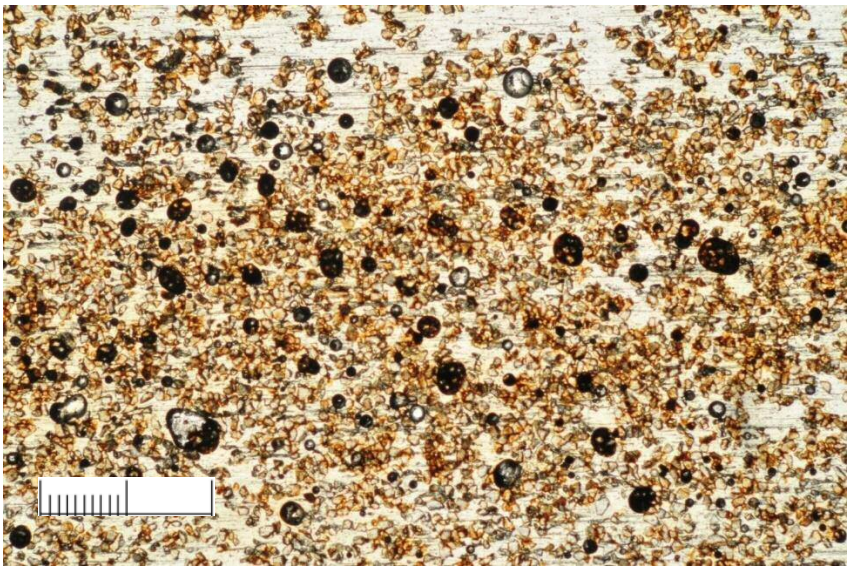

*Figure 4-11 Thin section grinded using water coolant compared to ISOPAR*

#### *4.1.1.4 Thin section observations*

Figure 4-12 shows the presence of quartz grains clay bridges, pores, oil coated grains and few vugs. Some of the quartz grains observed showed internal fractures leading to the conclusion that there has been post depositional activity leading to fractured grains. Presence of clay bridges also provided an early indication of being an element that would hinder flow through the reservoir on having contact with the water phase.

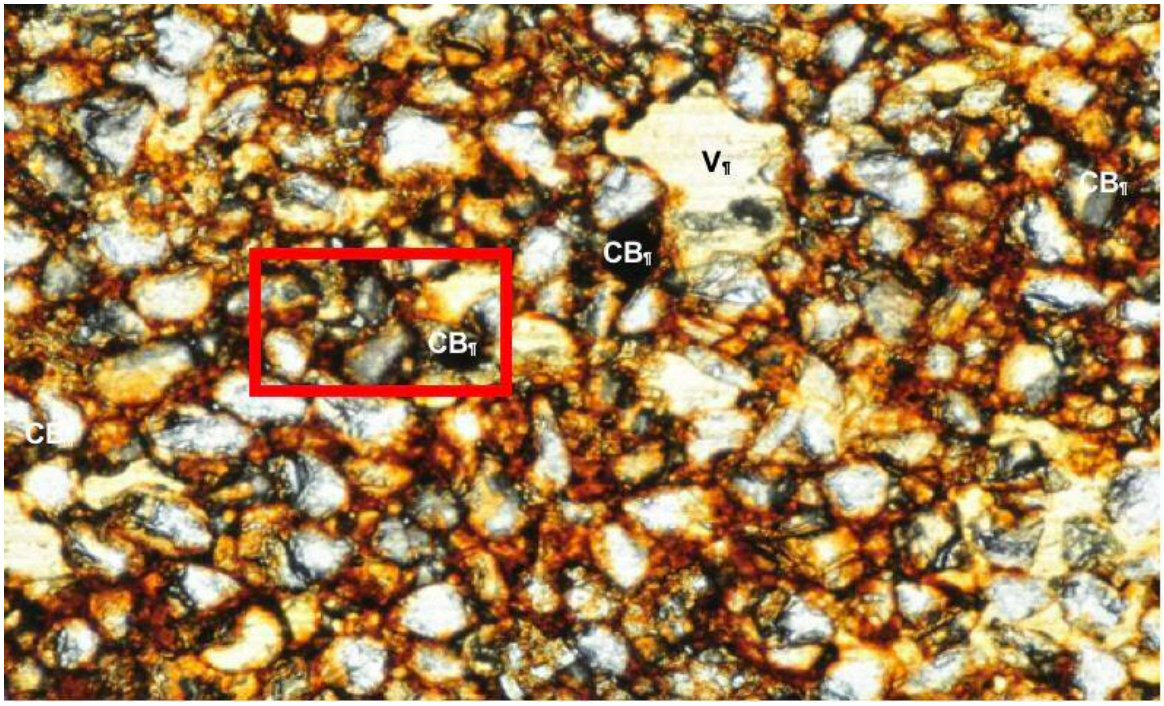


*Figure 4-12 Thin section image showing presence of Oil wet grains (V) Vugs (CB) Clay Bridges and presence of ground mass in the red box . The brown colour shows the presence of oil within the thin section.*

### 4.1.2 Outcrop Sample Analysis

Some of the outcrop samples of the thin sections demonstrated the presence of Bioturbated material as seen from Figure 4-13 .

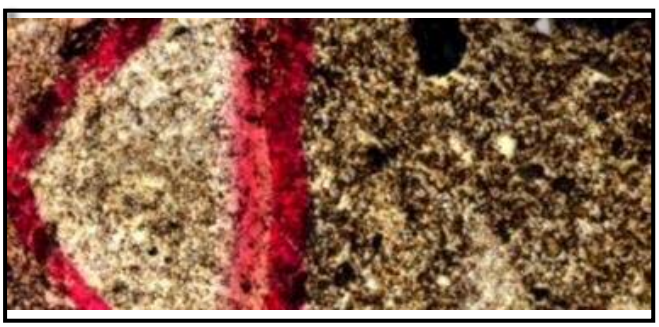

*Figure 4-13 Thin section Image under microscope demonstrating visual comparison between host and bioturbated section (in red circle).*

Detailed point count analysis of outcrop samples assisted initial understanding of the samples under consideration. The results from initial point count analysis was able to demonstrate that Canadian Oil Sands are made up of Grains (mainly Quartz), Bitumen and micro mass mixture (matrix) and pore (void and vughs). The distribution of these elements amongst host material and bioturbated section was found as shown in Figure 4-14 Figure 4-15.

The following charts show the difference between the Bioturbated and Host oil sands material in the various samples analysed. On average the bioturbated sample contained 5% - 10% less Quartz (principal component); 3% - 5% lesser bitumen; 2% - 5% higher percentage of micromass including clays and silts and significant increase of 8% - 18% in the voids observed in the bioturbated material.

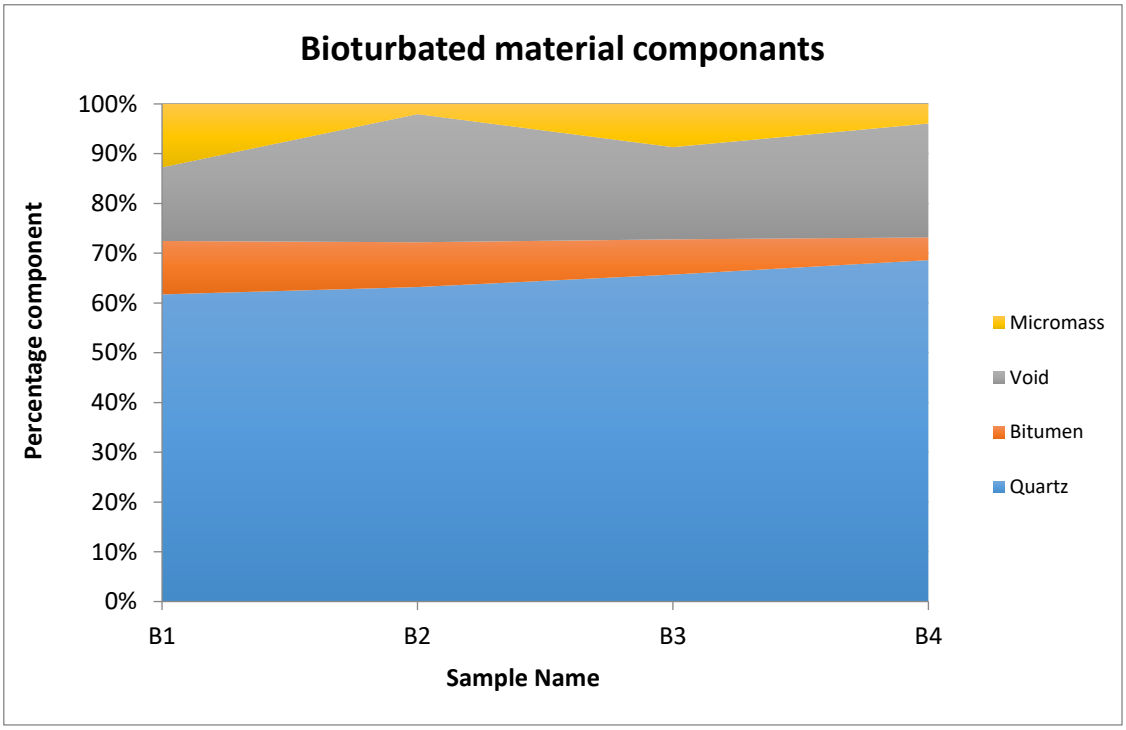


*Figure 4-14 Chart showing component abundance in bioturbated oil sands sample.*

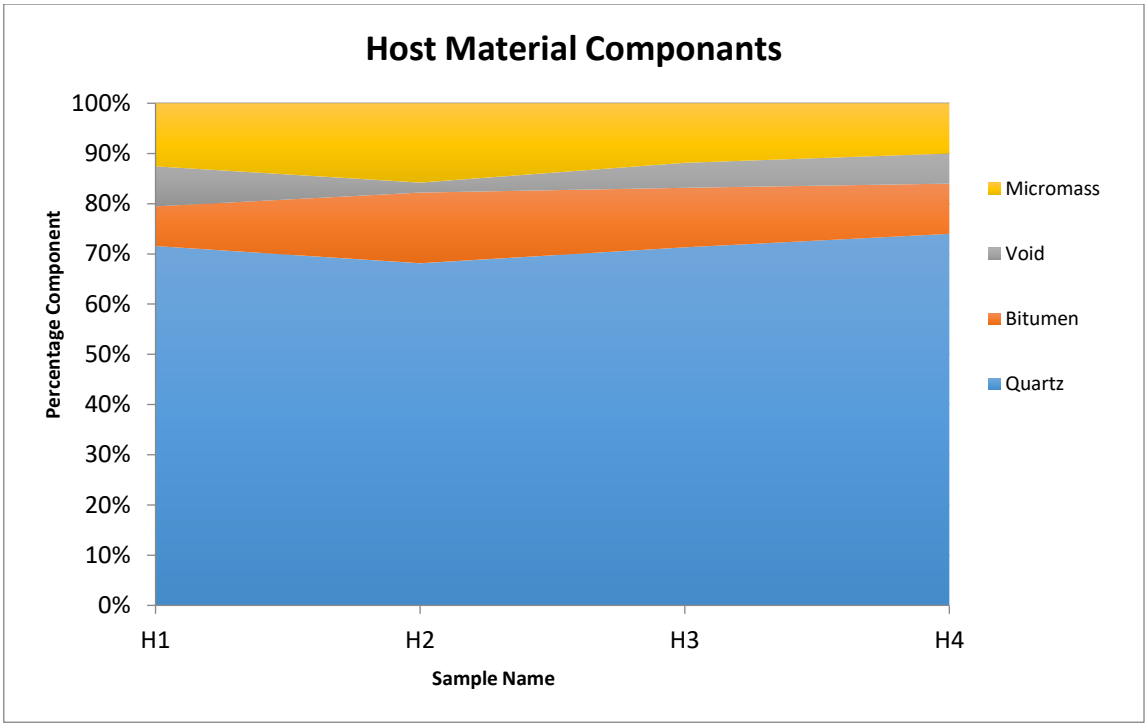


*Figure 4-15 Chart showing Component abundance in host oil sands sample.*

The increase in the amount of voids and fine material is important, as it will have an effect on the production following SAGD procedure. The increase in the voids can also be traced to the presence of organisms in the vicinity and the effect of their movement on the deposited material.

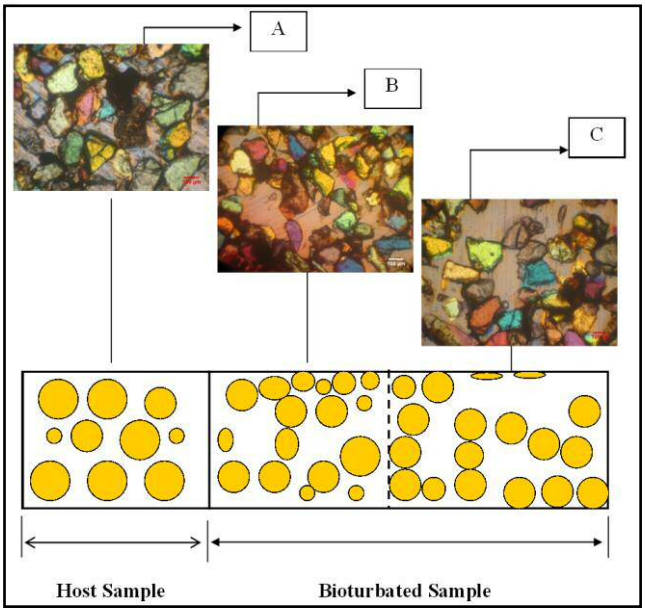


*Figure 4-16 Comparative model showing the textural variation between the host sample and the bioturbated sample. A: Host sample without disturbance, B& C: Showing effect of Bioturbation*

The above figure shows a match between ideal host and bioturbated material properties to the properties observed from thin section analysis.

#### *4.1.2.1 Grain Size Distribution*

Result from grain size distribution excluding clay elements show that the mean size of grains was around 180μm with range of 84μm to 369μm while bioturbated sample averaged at 152μm and ranged between 79μm to 276μm. as shown in Figure 4-17 and Figure 4-18.

The graphs are also able to demonstrate visible variation between the host sample and bioturbated oil sands sample. Wherein, the bioturbated samples are seem to have been made up of more fine grained material as compared to the host material. Estimate of sorting derived from use of visual comparator charts shows that the bioturbated oil sands samples are relatively more well sorted compared to the host oil sand sample but both fall under the sorting value of 0.77 using the VanBaaren (1979) scale for estimating consolidation.

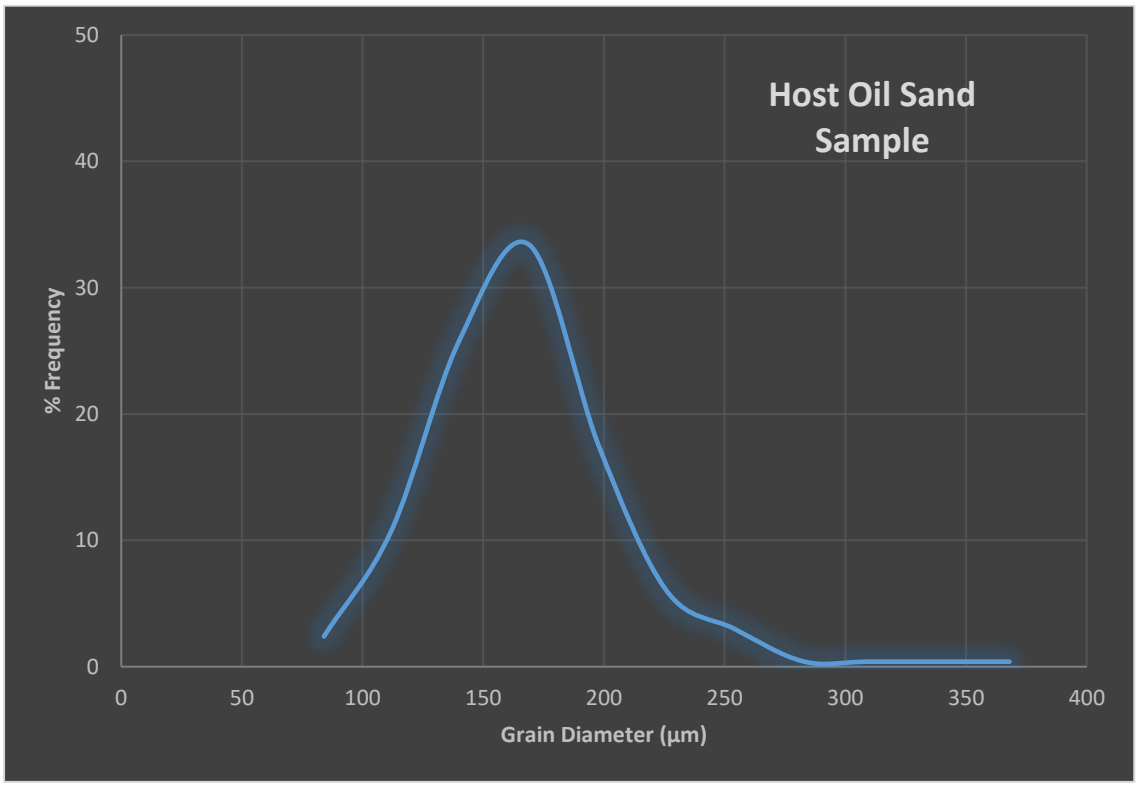


*Figure 4-17 Grain size distribution in Host oil sand sample*

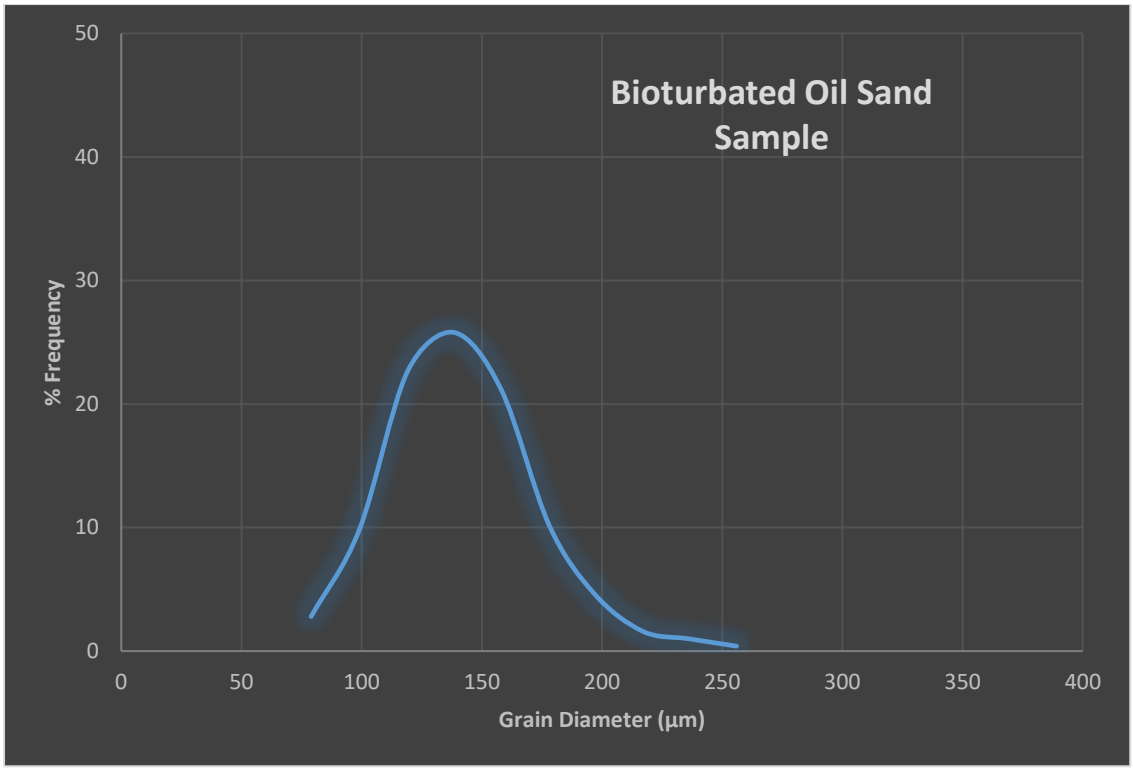


*Figure 4-18 Grain size distribution in bioturbated oil sand sample*

### *4.1.2.2 Grain Shape*

While determining the roundness host material demonstrated significant amounts of angular grains as compared to bioturbated samples. The roundness ranged between 0.35 to 0.99 as calculated by image analysis in the host oil and that for bioturbated samples roundness factor ranged between 0.51 to 0.97. This range implied that bioturbated sections show more rounded grains.

### *4.1.2.3 Nature of Matrix / micromass*

The result of the petrographic examination of micromass components in the host and bioturbated thin section using cross-nicols in the petrographic microscope shows that the host oil sand sample consists of more micromass compared to the bioturbated sample (This has been statistically validated from the earlier result of point counting). Occurrence of micromass in both samples is similar, with the micromass distributed between quartz grains and bitumen. From the petrographic examination of both samples groups, micromass component was not found to be isolated in occurrence and was likewise absent in micro-pore, and vughs in both oil sand sample

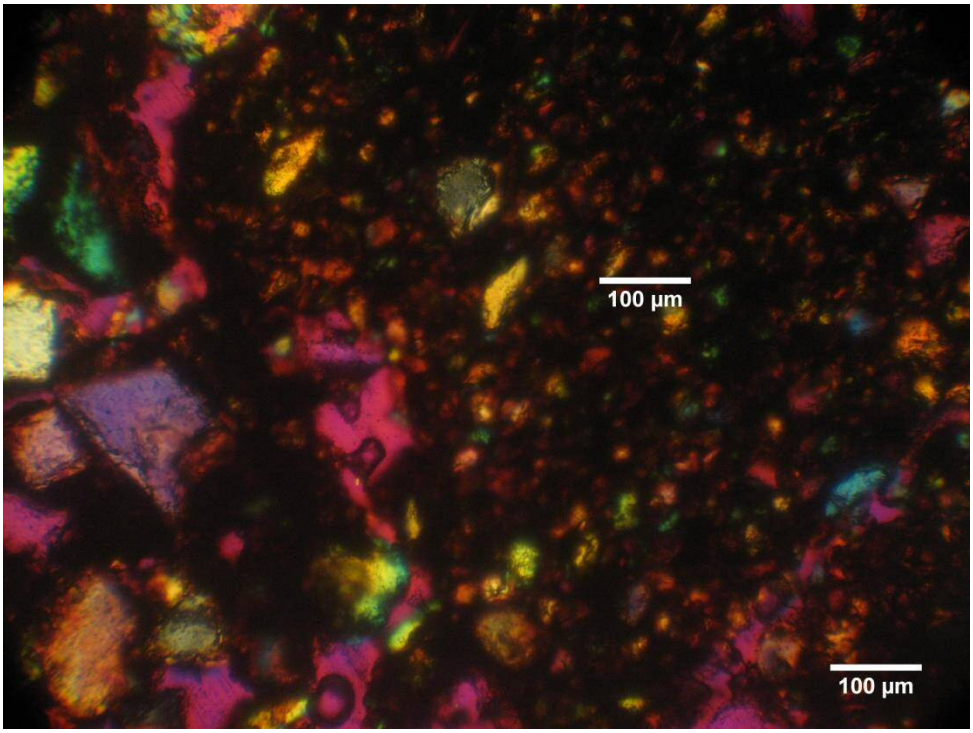


*Figure 4-19 Distribution of micromass in the host oil sand thin section*

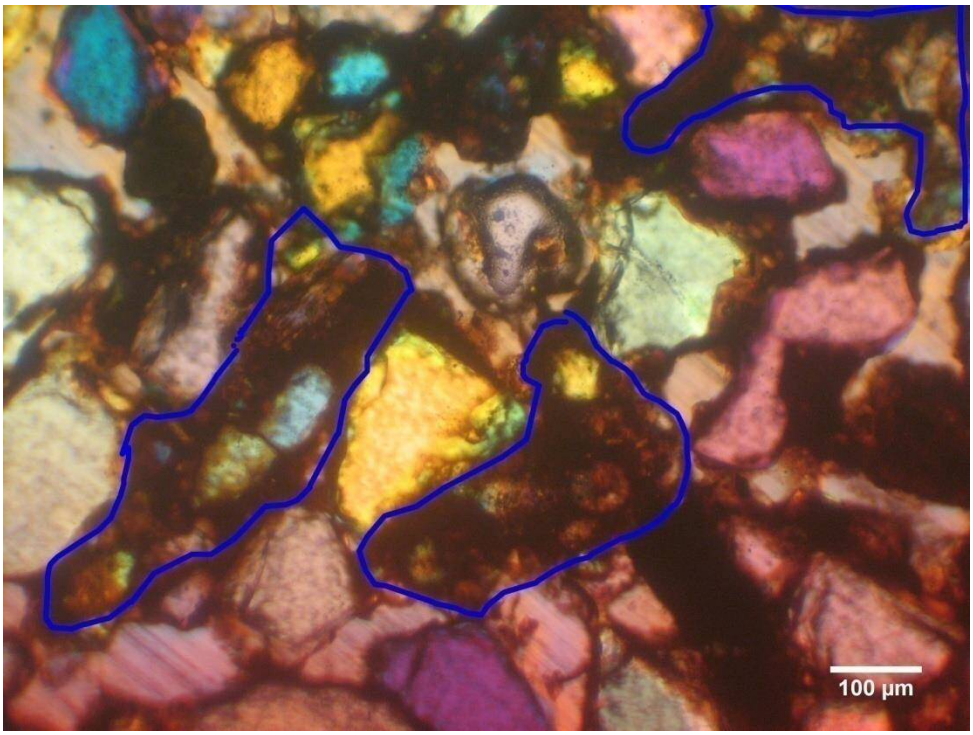


*Figure 4-20 Distribution of micromass in the bioturbated thin section*

#### 4.1.2.4 *State of bitumen in Host and Bioturbated samples*

Based on examination of thin sections under petrographic microscopes plane polarized light at low magnification revealed difference between the two samples. As it can be observed from Figure 4-21 A & B host material shows much darker hydrocarbon as compared to the bioturbated sample. This may be due to quantity of hydrocarbons that it contains or due to the viscosity variation observed within these two samples.

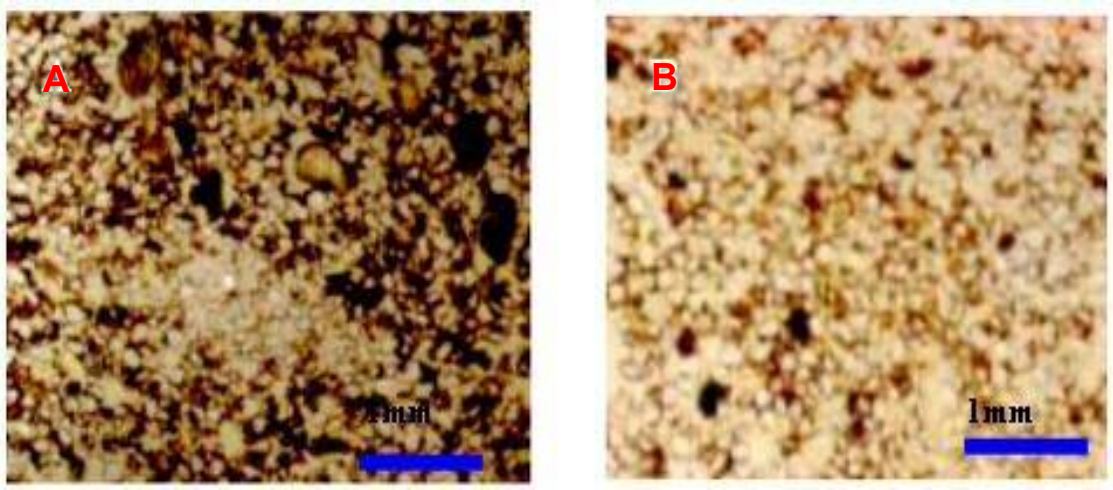


*Figure 4-21 Plane polarised low magnification observation of thin sections A= Host Sample B= Bioturbated sample.*

#### 4.1.2.5 *Pore Void structure in Host and Bioturbated section*

Four fundamental pore Morphometry variables were measured for each pores and vugs which includes pore area ($\mu m^2$), Pore Perimeter (µm), Pore Diameter (µm) and Roundness. Univariate summary for each of this pore geometry observed in the host and bioturbated samples are presented in the Table Below. The distribution of pore diameter in reveal that bioturbated sample shows a wide spectrum of pore diameter sample (40.78 µm -399.30 µm) compared to the host sample (50.05µm – 631.13 µm)

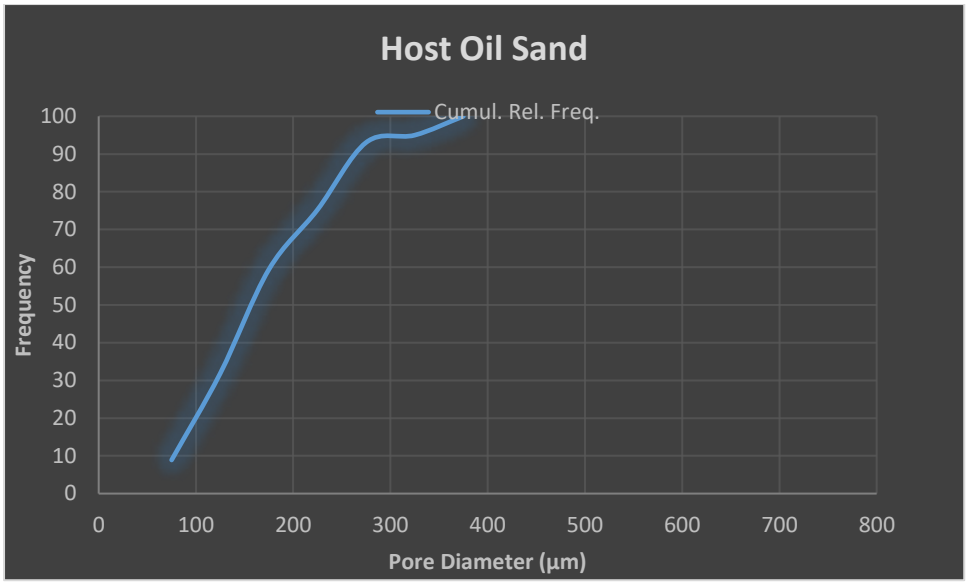


*Figure 4-22 cumulative frequency plot for pore distribution in the host oil sand sample.*

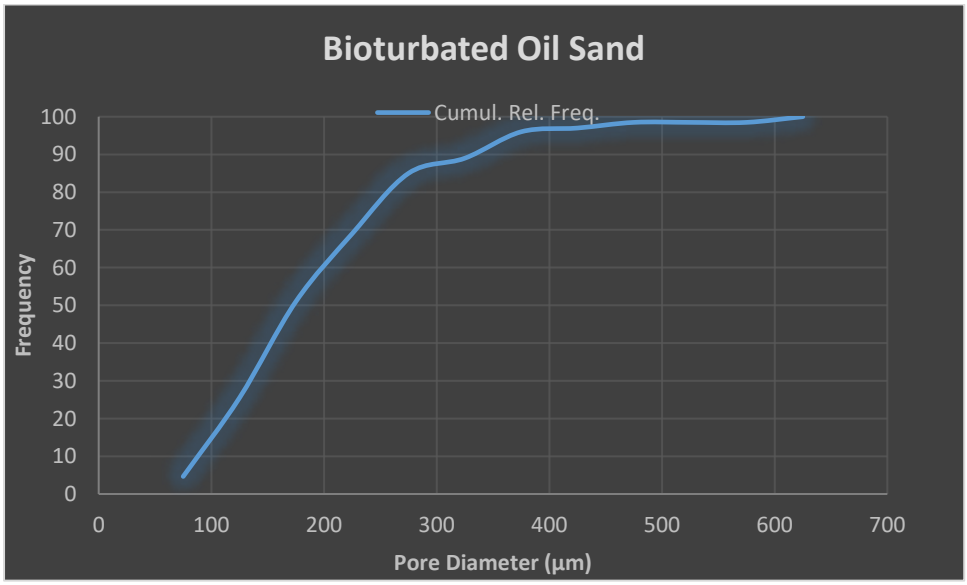


*Figure 4-23 cumulative frequency plot for pore distribution in the Bioturbated oil sand sample.*

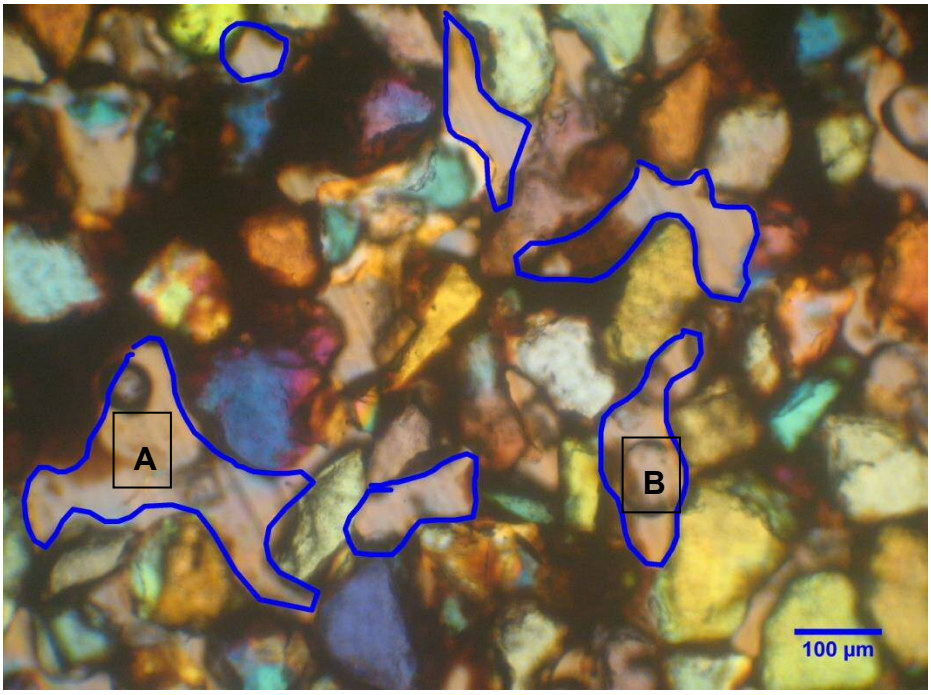


*Figure 4-24 Distribution of pore space in the bioturbated section photomicrograph (A=vuggy pores and B= interparticle pores).*

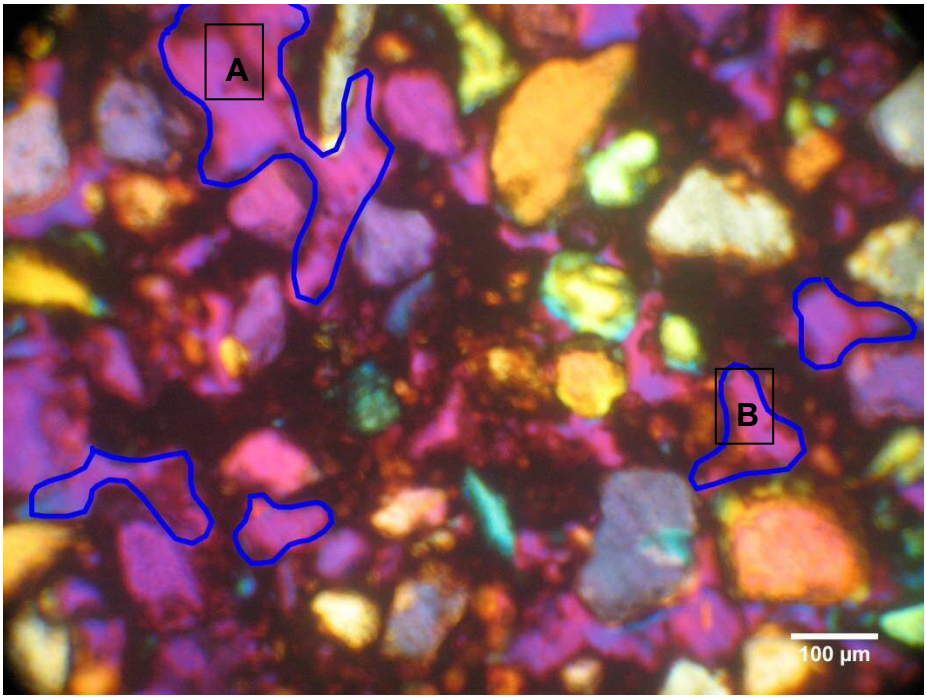


*Figure 4-25 Distribution of inter-particle pores in the host oil sand thin sections.(A=vuggy pores and B= interparticle pores).*

#### *4.1.2.6 Optical Porosity determination*

Porosity was determined using Equation 3-10, On calculation of ten thin sections prepared for host material provided an average porosity of 38% with range of 35% - 40% and bioturbated was calculated as 46% having range of 41% -53%. Considering this calculation bioturbation samples have accounted for 21% increase in porosity value compared to the host sample.

#### *4.1.2.7 Permeability determination*

Taking into account available statistical results permeability was estimated using Van Barren's Equation 2-15. that related permeability to grain size distribution and the image based porosity

Grain size distribution of the images used in the determination of the image based porosity based on grain area is presented in Appendix.

##### 4.1.2.7.1 Average Permeability in the Host oil sand sample.

= 180 μm

$= 0.38$

m = cementation factor = 1.3 for oil sands (Prison, 1958; Luo and Kantzas, 2008)

c = constant derived from microscopic examination of sorting **= 0.77** Table 2-10

##### 4.1.2.7.2 Permeability of the Bioturbated section

= 151 μm

$= 0.46$

m = cementation factor = 1.3 for oil sands (Prison, 1958; Luo and Kantzas, 2008)

c = constant derived from microscopic examination of sorting **= 0.77** Table 2-10

Permeability in the host oil sand sample is estimated at 7044mD Darcie compared to a value of 12739.45 mD in the bioturbated section (Bioturbation accounting for 80.85% increase in permeability).

### 4.1.3 Laboratory Analysis results

Statistical analysis shows that the grain size, the median and mean grain sizes were in the range of 2.6σ and 2.66σ respectively Table 4-2

Figure 4-26. This corresponds to 170 and 160 microns and is in agreement to values published in the literature (Carrigy, 1966). Further the grains in outcrop samples were evenly distributed with standard deviation of 0.5 indicating well sorted nature of the sample. The grain shapes were defined according to Petijohn *et al.* (1973) showing variation between very angular to well rounded with most abundance of subrounded and subangular grains Table 4-2.

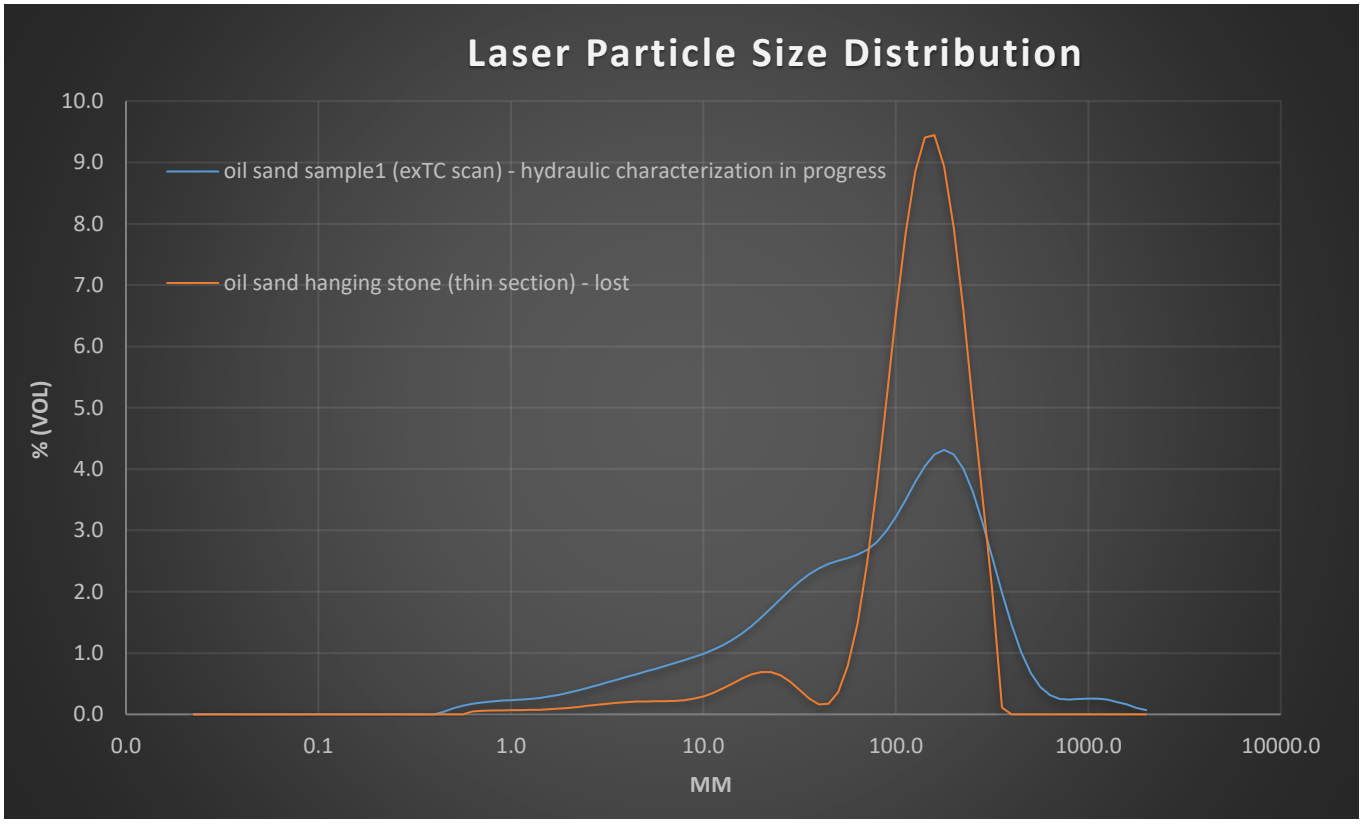


*Figure 4-26 Laser based particle size distribution of outcrop samples conducted as part of initial studies*

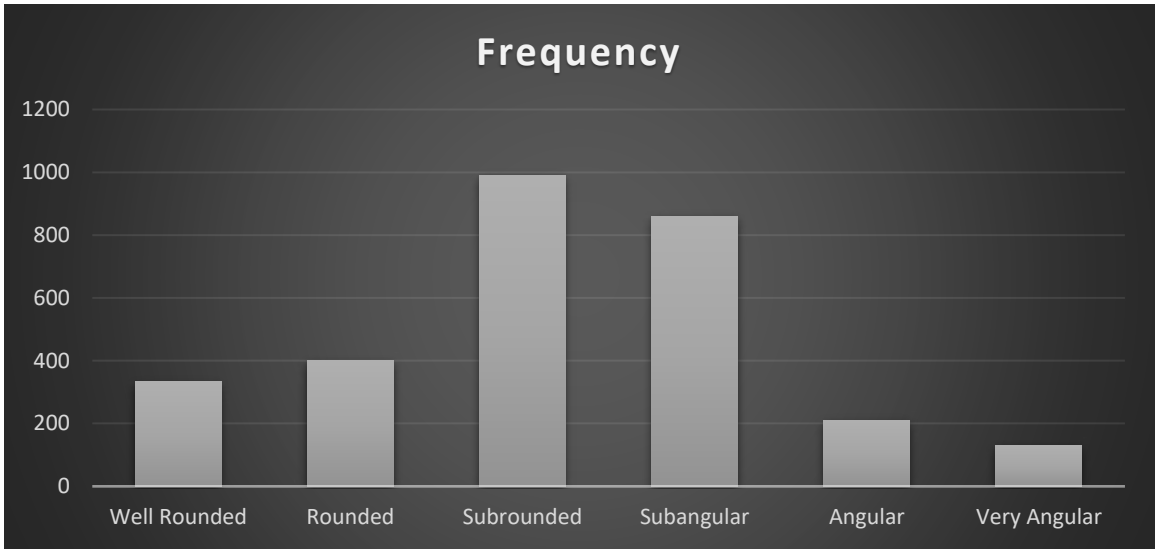


*Figure 4-27 Roundness from Outcrop Samples*

*Table 4-2 Outcrop sample characteristics*

| **Shape** | **Rounded to Sub rounded** |
|---|---|
| **Form** | Coeffecient of Sphericity 0.7-0.9 |
| **Grain Size** | Fine to Medium |
| **Sorting** | Well Sorted |
| **Skewness** | Fine Skewed |
| **Fines** | Fair amount of clays and  fines occurring as fine mass |
| **Flatness** | Flatness index 0.4-0.8 |
| **Size** | |
| **Median** | 2.6 |
| **Mean** | 2.66 |
| **Standard deviation** | 0.500152 |
| **Skewness** | 0.093233 |

*Table 4-3 Outcrop Sample Roundness analysis*

| Nature of Grain | Frequency |
|---|---|
| Well Rounded | 333 |
| Rounded | 400 |
| Sub rounded | 991 |
| Sub angular | 860 |
| Angular | 210 |
| Very Angular | 130 |

### 4.1.4 Confirming the depositional environment

To understand the depositional environment and reservoir arrangements grain morphology was studied using thin sections. This provided transportation and weathering characteristics through sedimetological form analysis along with quartz grain morphology. Furthermore when compared with Takamura's model quartz grains show little or no water presence whereas matrix elements show presence of oil amongst the particles that are observed in Figure 4-28. The abundance of Quartz, matrix / fines, oil and their internal relation through arrangements show presence of several clay bridges and empty grains. This is in contrast to the model prosed by Takamura et.al in 1984 shown in Figure 4-28. Further careful observation of grains revealed few grains having internal fractures though with intact nature. Based on its appearance it was concluded that prior to deposition the grains were transported for some distance evident through sub angular to sub rounded nature and post deposition grains were subjected to subsurface activities which along with transportation may have introduced internal fractures to the grains. (Bell, Boateng, Olawale, & Roberts.D, 2011) discusses the effect of grain morphology and depositional environment correlation of the samples followed by above explanation of comparison between takamura's model and observations from thin sections show wettability and relative wettability of the grains.

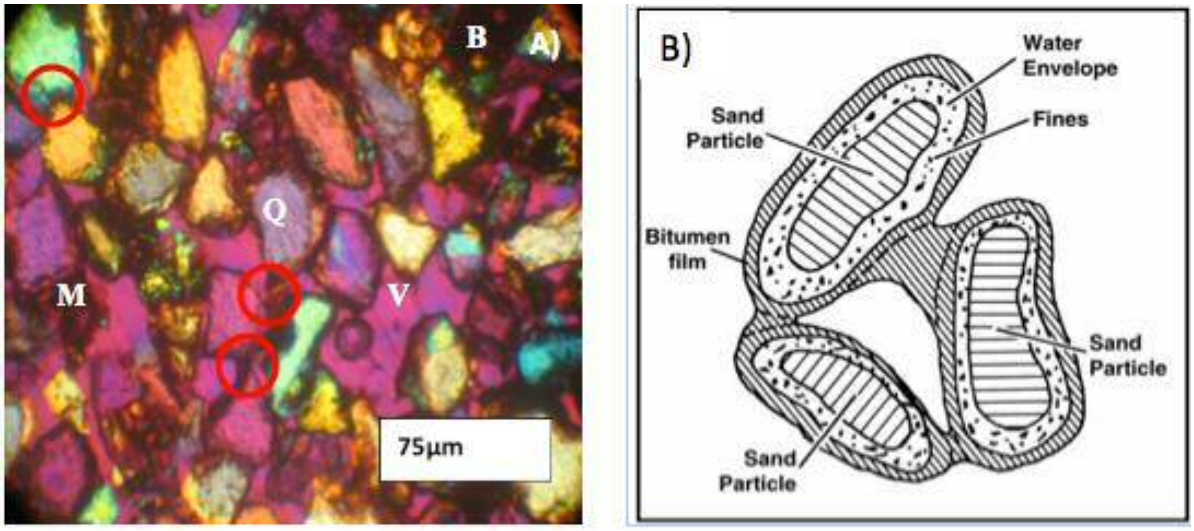


*Figure 4-28 Canadian Oil Sands Grain Diagram. Oil Sand Fabric and idealized diagram of Athabasca Oil Sands showing relationships of Components (Bell, et.al 2013)*

### 4.1.5 SEM analysis

To overcome the issues associated with the reliability of thin sections and obtain further properties at microscopic level use of SEM analysis was tried. A small piece from an outcrop sample was initially photographed with bitumen. The resulting stub in Figure 4-29 was able to reveal small bridges between the grains which may be formed due to the presence of clays. Though for further studies to obtain detailed grain morphology the samples were cleaned using Sohxlet technique as detailed in 3.2.2.1

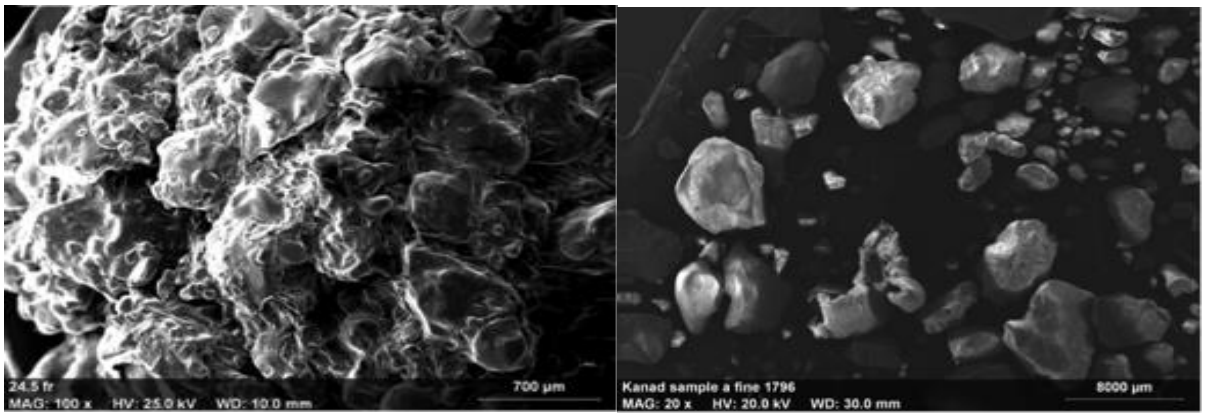


*Figure 4-29 Initial attempt at SEM analysis technique A) with oil in place B) cleaned sample with sohxlet technique.*

The SEM images and photomicrographs were analysed and studied to determine parameters such as grain size shape and weathering characteristics. Figure 4-30 Figure 4-32 Figure 4-34 shows the differences between the three samples.

#### *4.1.5.1 Grain size Analysis*

As seen from Figure 4-30 Figure 4-31 Figure 4-32 Figure 4-33 Figure 4-34 Figure 4-35 Figure 4-36 following detail grain size parameters were observed.

**Sample A:**

In all more than 6000 grains were analysed to determine the following results. The image from SEM analysis shows the variation in the grain size observed in the sample A. SEM analysis revealed that grain sizes vary from coarse sand to very fine sand according to the Udden-Wentworth grain scale. Though grains were predominantly medium to fine sand sized with graphic mean of 1.8

**Sample B:**

To obtain the results more than 6000 grains were analysed from SEM image analysis. The image in Figure 4-33 shows the grain sizes from the depth. As seen from the figure Sample B has mix of all the grains from coarse sand, coarse silt with medium sand to very fine sand being predominant with graphical mean of 1.6 .

**Sample C:**

In Sample C more than 6000 grains were analysed following SEM Image analysis. The grains from this section are much more finer in nature with an average value of 1.95 . Most of the grains based on the Udden Wentworth scale fall into the category of fine sand with traces of coarse, fine and very fine silt present on the graph.

#### 4.1.5.1.1 Sample A


*Figure 4-30 SEM image of Sample A showing the range of grains for the depth.*

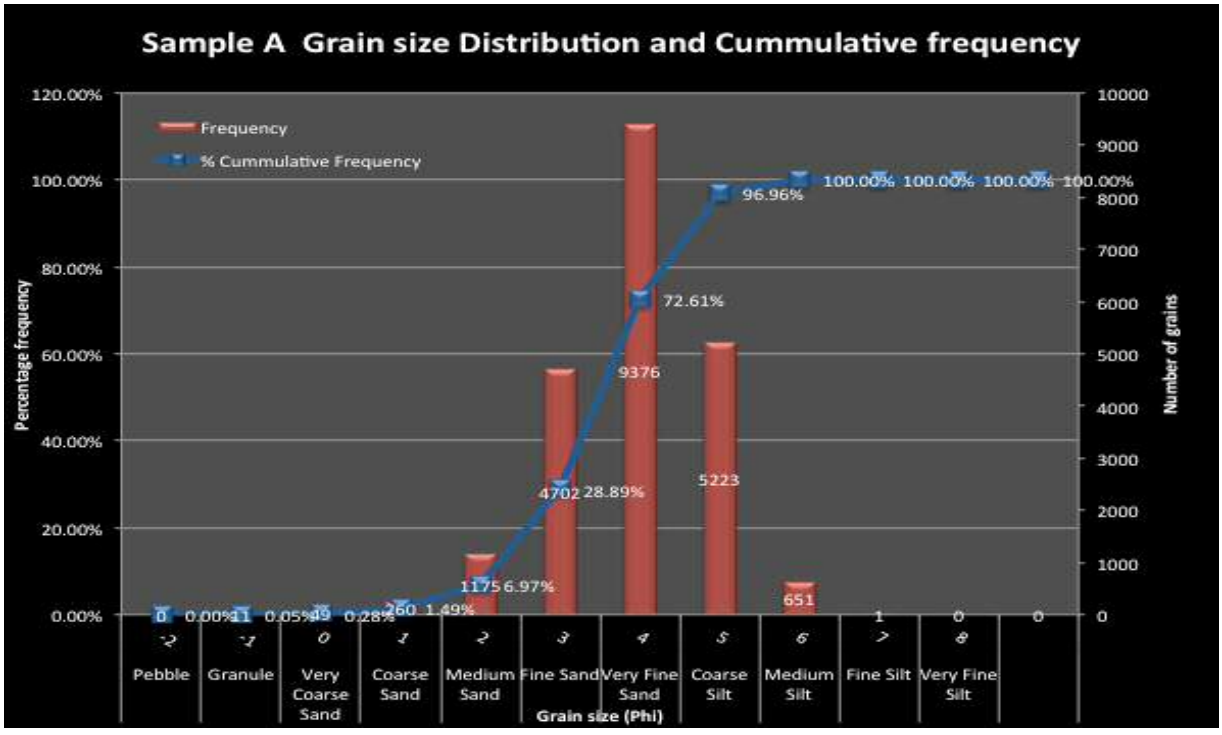


*Figure 4-31 Grain size distribution in Sample A following Udden-Wentworth scale.*

#### 4.1.5.1.2 Sample B

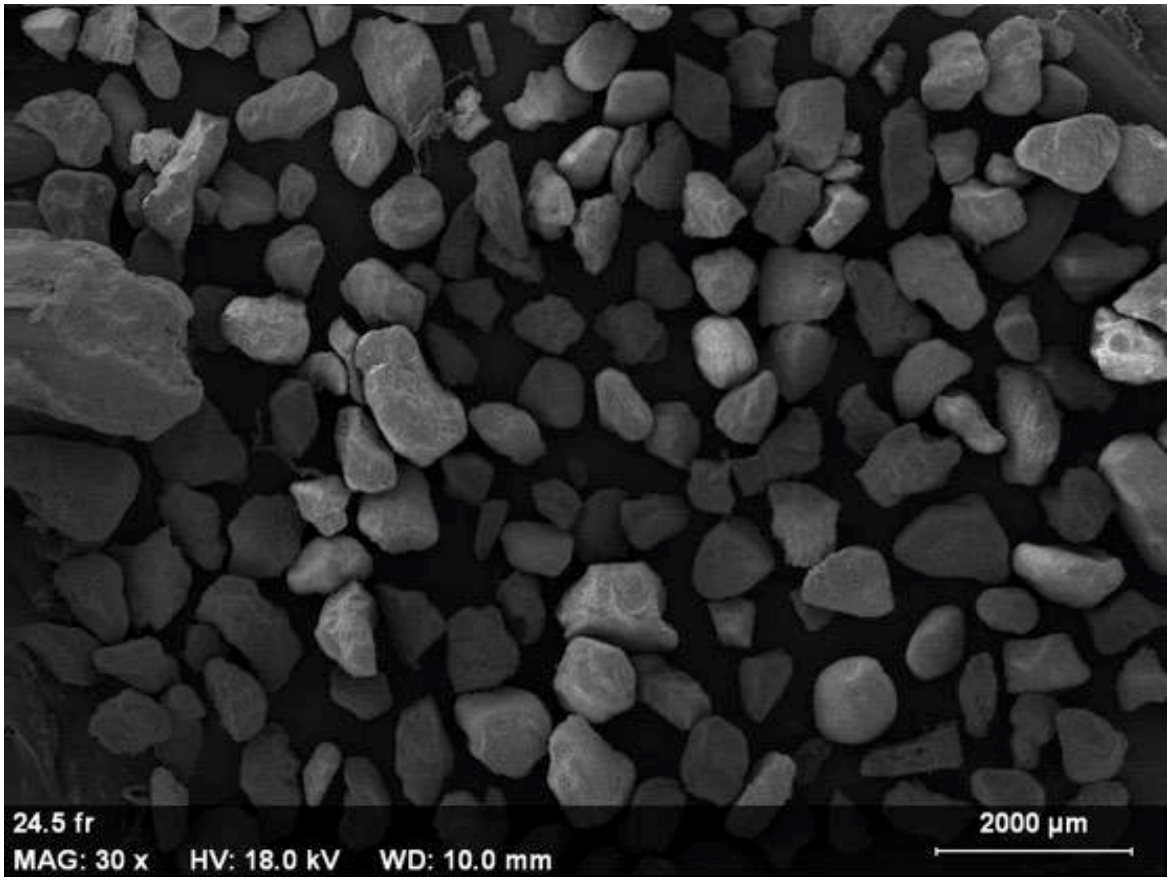


*Figure 4-32 SEM image from Sample B showing the variation in the grains at depth.*

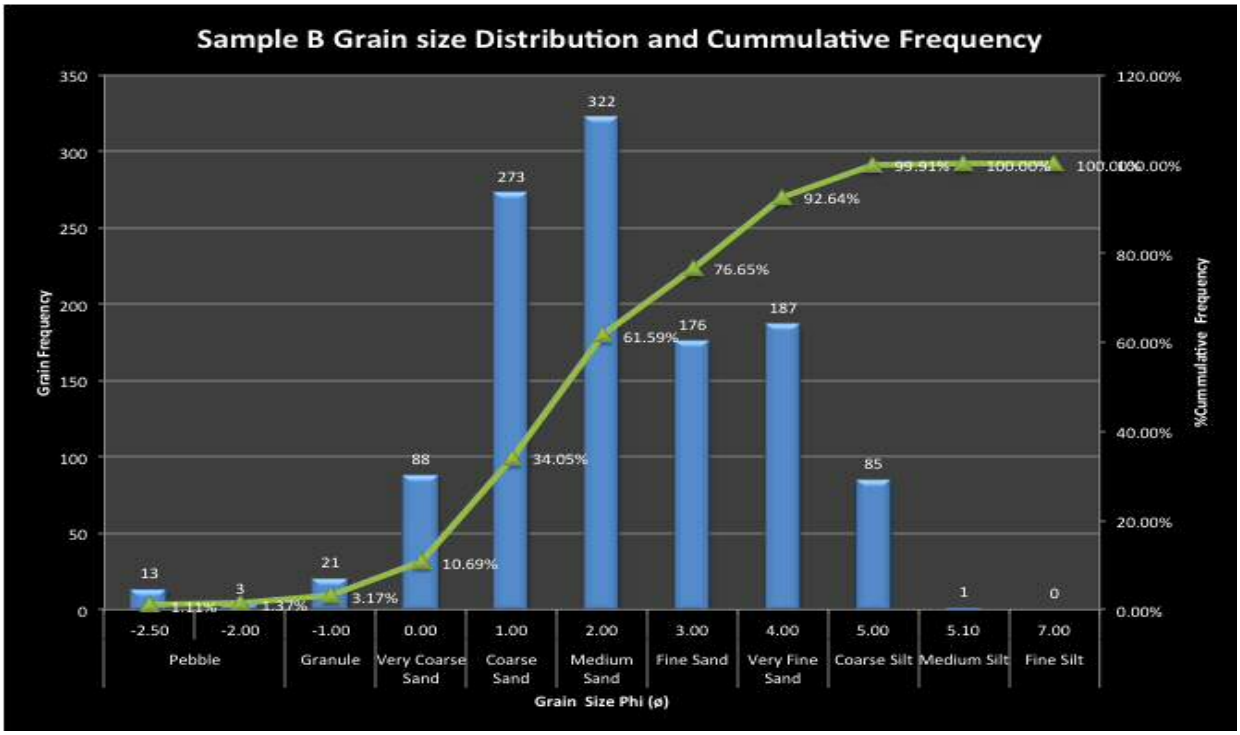


*Figure 4-33 Grain size distribution of SampleB based on Udden-Wentworth scale.*

#### 4.1.5.1.3 Sample C

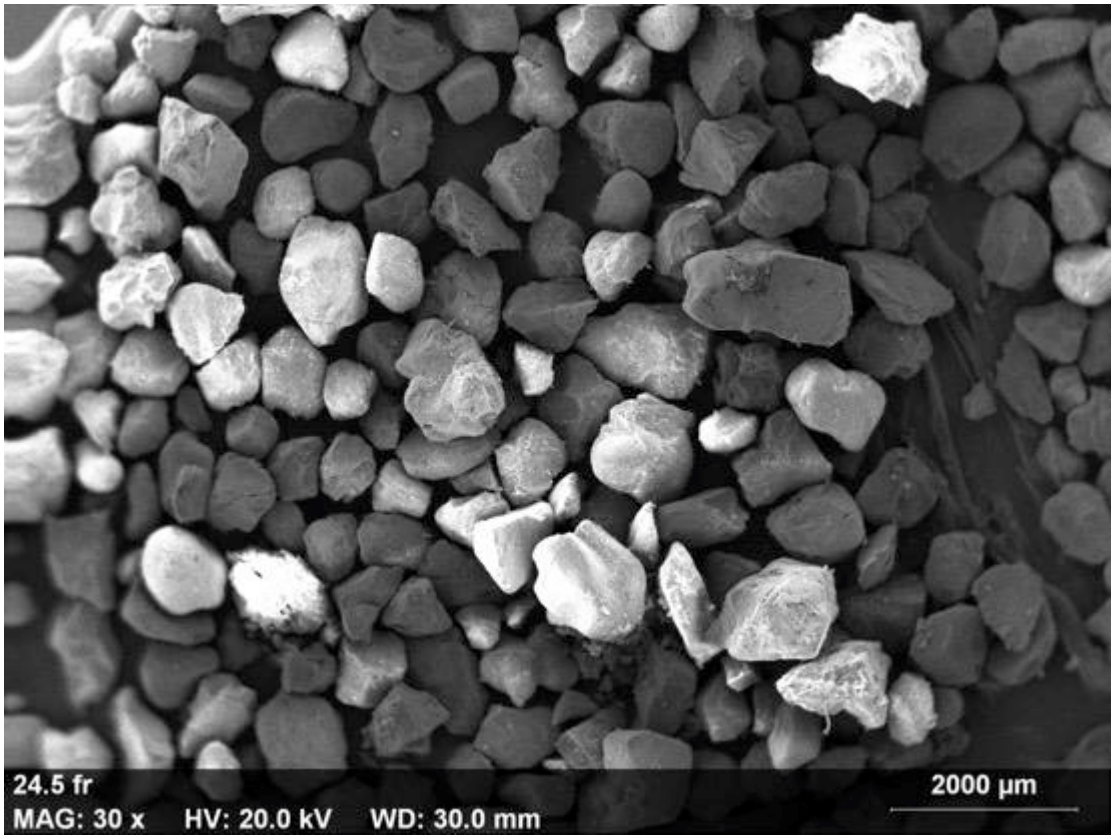


*Figure 4-34 SEM Image of Sample C showing the variation in the grains at the depth.*

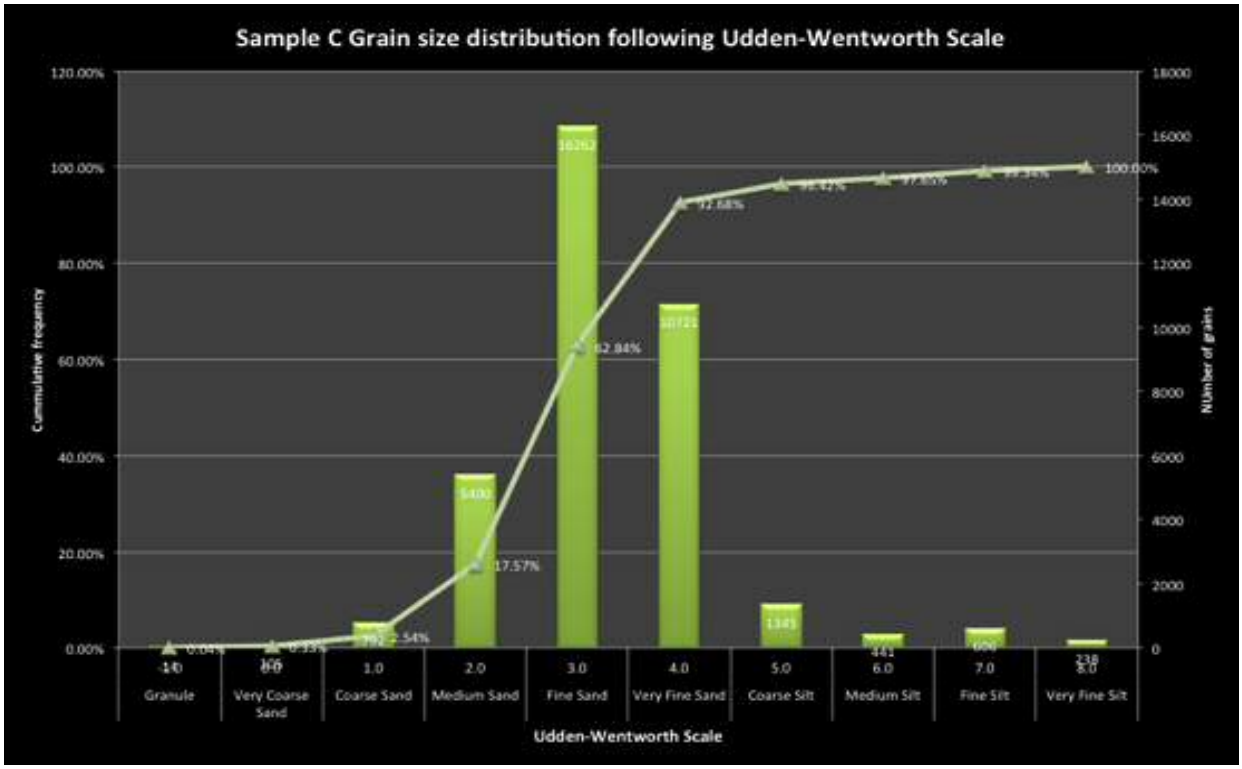


*Figure 4-35 Grain size distribution of Sample C based on Udden-Wentworth scale.*

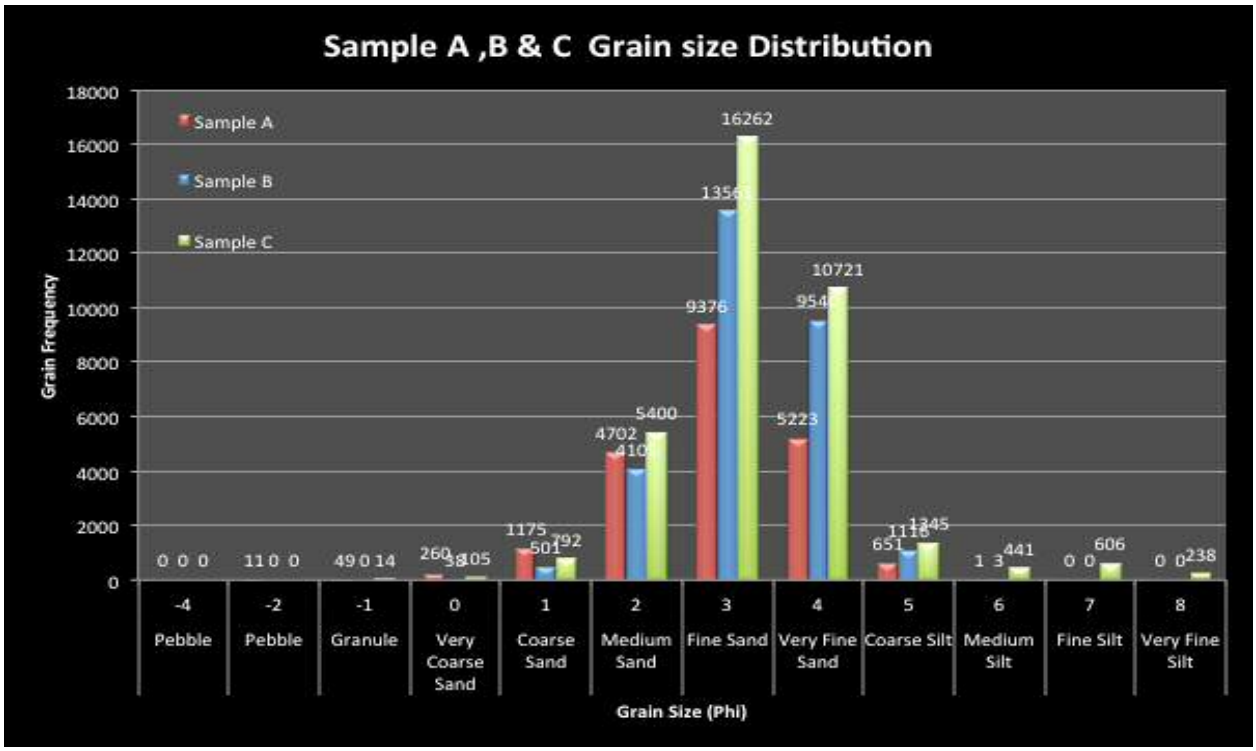


*Figure 4-36 Comparative grain size distribution graph comparing the size of the grains between t he samples A B and C. This graph also confirms the coarsening upwards sequence observed in the core samples.*

Figure 4-36 demonstrates comparative reduction in size from Smaple A to Sample C with increase in concentration of fines.

### *4.1.5.2 Roundness comparison between the grains*

As you may see from Figure 4-37

Figure 4-38 Figure 4-39 Figure 4-40 variation in the roundness of the grains is observed.

Sample A: This sample has significant amount of grains that fall into the sub angular to sub rounded category with little presence of grains from the Angular nature. This indicate the moderate nature of transportation until deposition of these grains.

Sample B: The grains in sample B have relatively large number of grains that fall into Sub Angular, Sub Rounded to Rounded. This demonstrates that these grains have been through significant amount of transportation until their deposition.

Sample C: The grains in this category shows an equal divide between the categories with dominance of Sub Angular to Sub Rounded nature being present. This indicate the moderate amount of transportation of these grains.

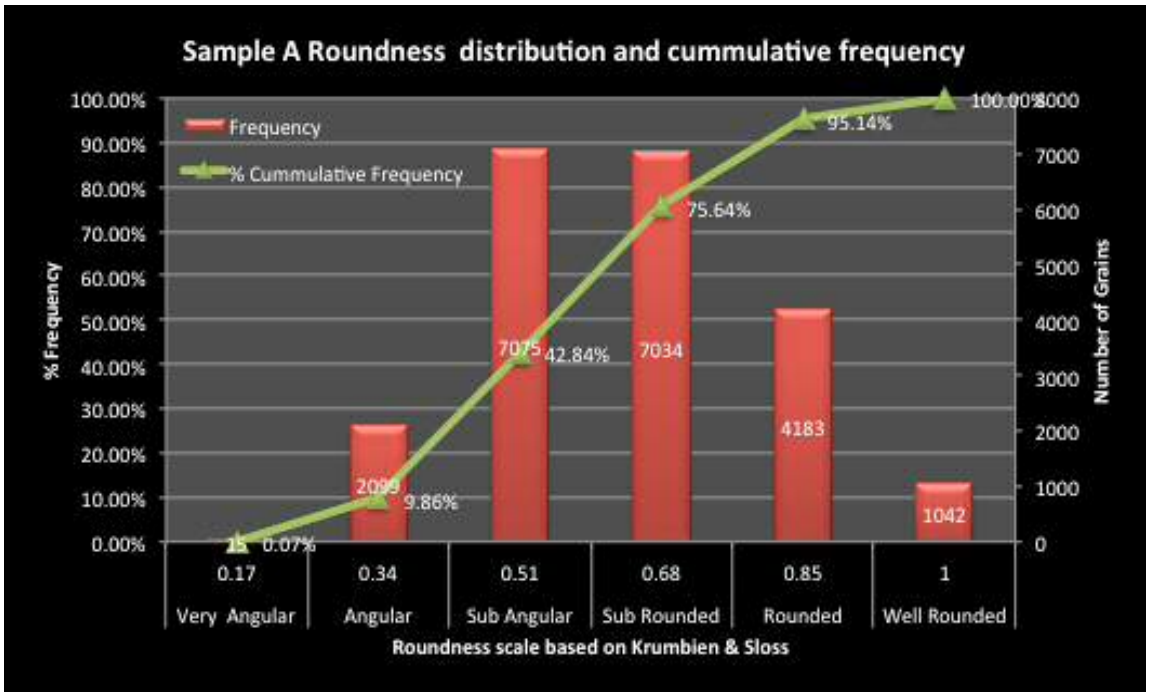


*Figure 4-37 Sample A Roundness graph based on Krumbien and sloss roundness scale*

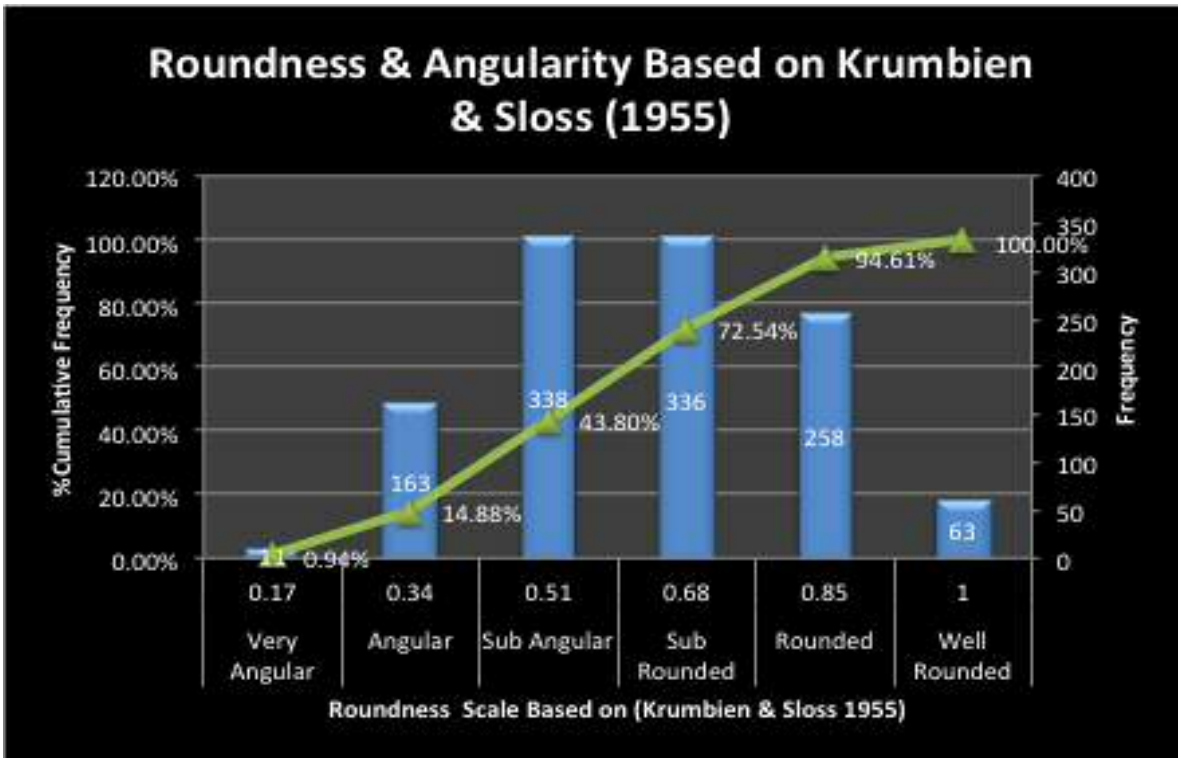


*Figure 4-38 Sample B Roundness gaph based on krumbien and sloss roundness scale*

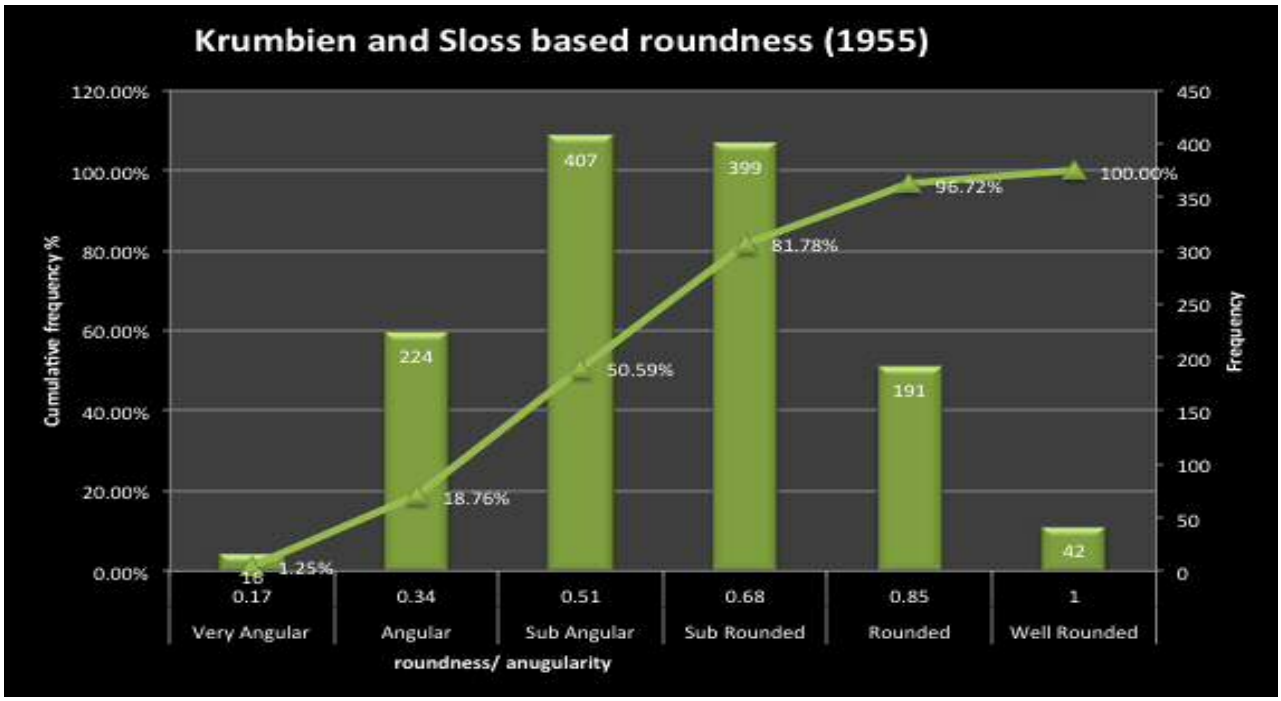


*Figure 4-39 Sample C Roundness graph based on Krumbien and sloss roundness scale*

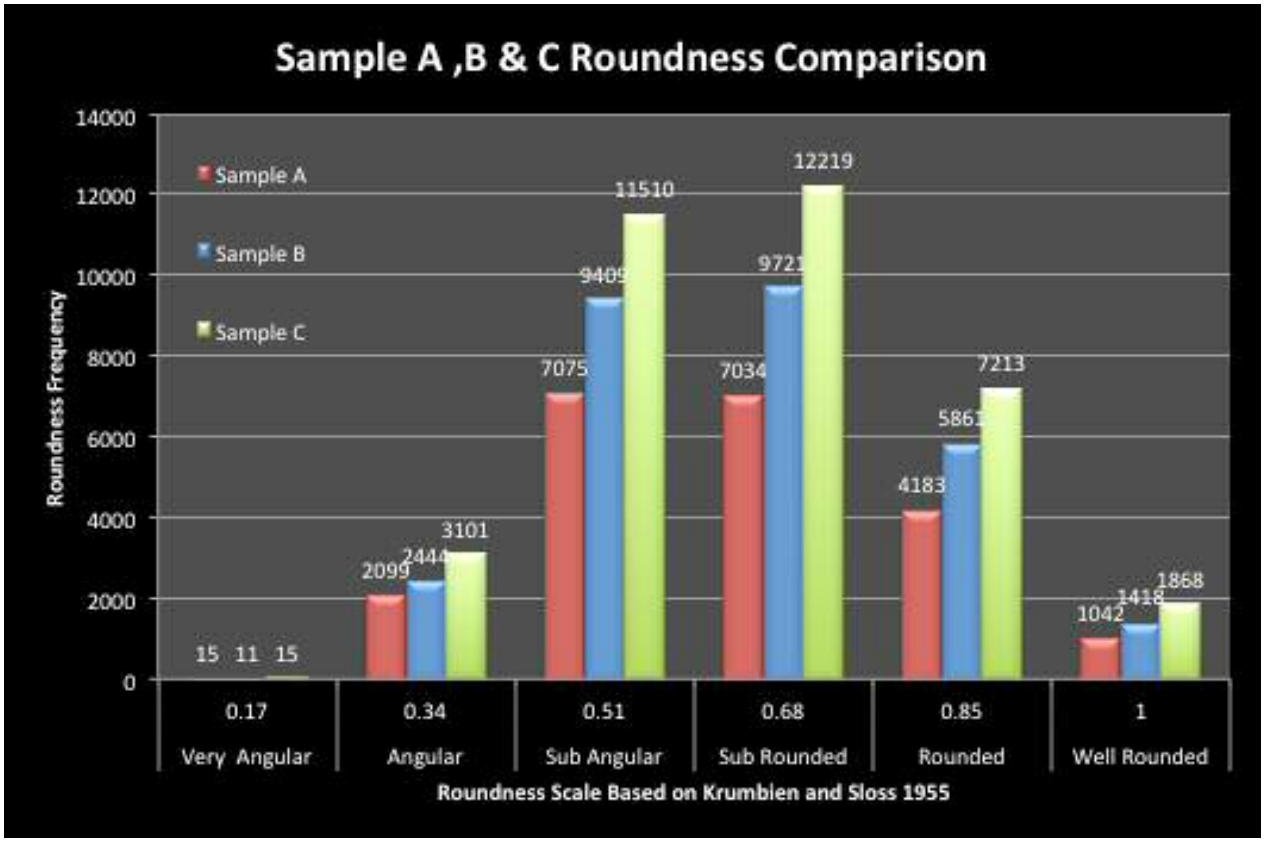


*Figure 4-40 Comparative Roundness comparison graph demonstrating the differences between the three samples.*

### *4.1.5.3 Weathering analysis*

#### 4.1.5.3.1 Sample A

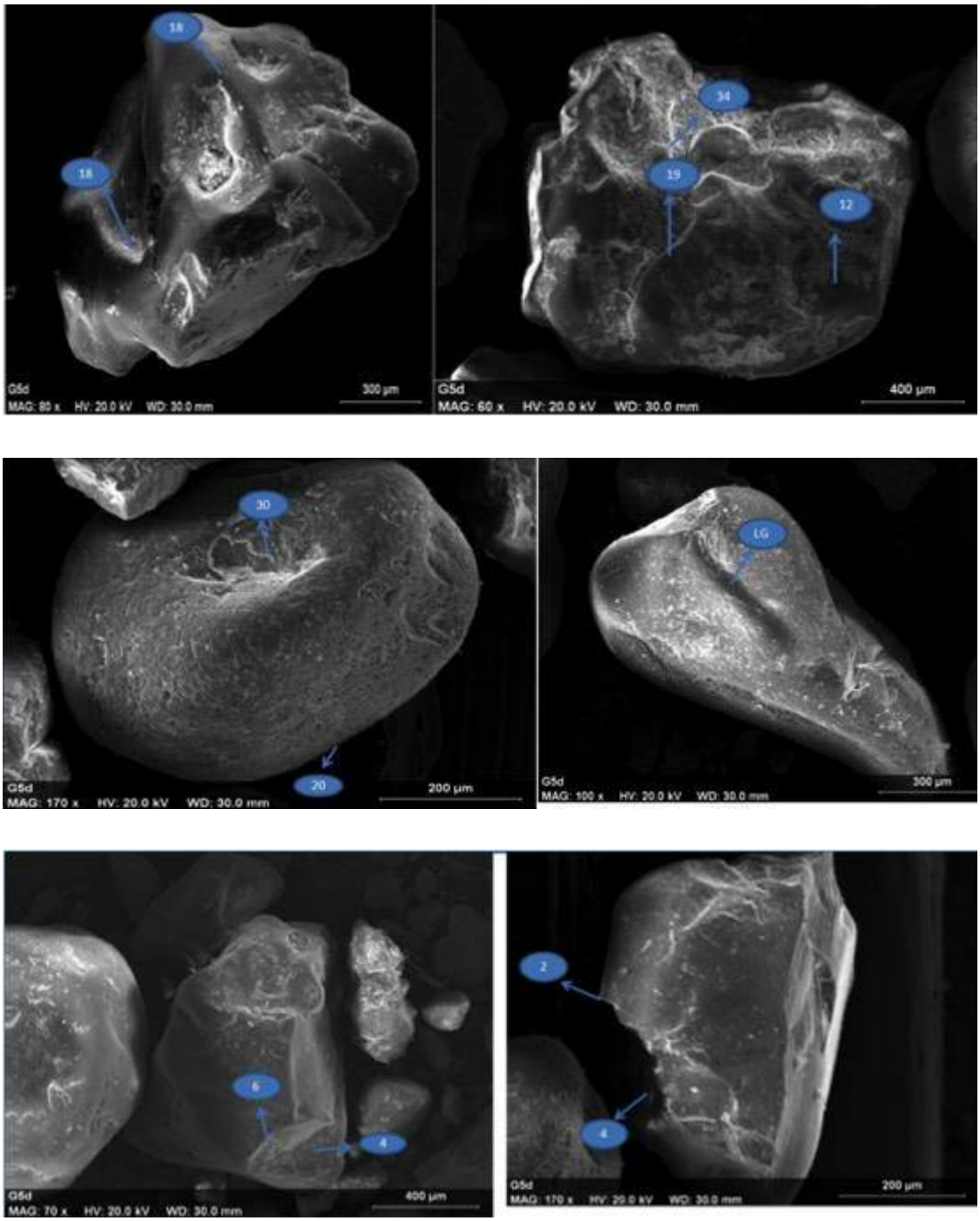


*Figure 4-41 Photomicrograph of sample A*

The above photomicrograph shows (18) mechanical V-pits (19) dish shape (12) irregular pits (20) Roundness (30) Solution pits (6) fresh conchoidal fractures (2) edge abrasion (31) solution crevasses.

Sample A: The grains from sample A predominantly from Figure 4-41 shows roundness, mechanical V shaped pits, and conchoidal fractures. Some other features observed contain solution pits, solution crevasses and significant amount of precipitation.

The presence of these features confirms the heavy transportation during the deposition process. The presence of abrasive edges further confirms the transpiration activity. Generation of roundness and V pits could be traced to sub aqueous collisions. Presence of precipitation on a sample may be a result of post depositional chemical reaction taking place between the grains.

#### 4.1.5.3.2 Sample B

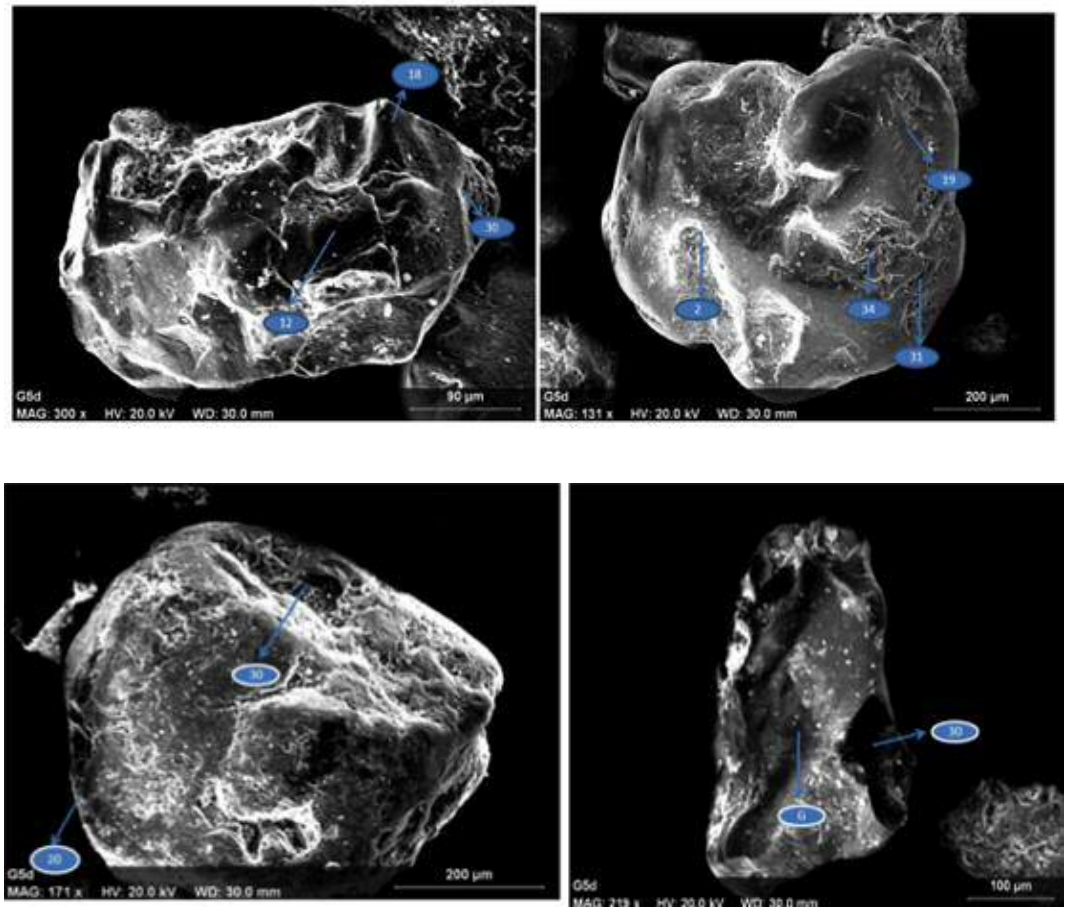


*Figure 4-42 Sample B SEM photomicrographs*

The above photomicrograph shows the different surface features observed in this depositional environment. Location (18) showing mechanical V-pits (19) showing

evidence of dish shape (12) irregular pit, (34) Amorphous precipitation (silica) (30) Roundness, G-grooves, (6) Smoothened conchoidal fracture (3) breakage blocks and (2) showing edge abrasion, (14) fractured plates, (20) solution pits, (31) solution crevasses and W- highly weathered grain.

As it may be seen from Figure 4-42 Figure 4-43 and graph in Figure 4-45 the predominant features observed in this sample are solution v- pits and irregular pits, solution crevasses and abundance of amorphous precipitation with mechanical v pits and irregular angularity. These features are good indicators of moderate amount of transportation and large amount of post depositional chemical reaction giving rise to the amorphous precipitation in various locations.

According to literature (Bell J. K., 2013) (Hein, Cotterill, & Rice, 2006) (Hein.F, Langberg.W, & Kidston, 2001)the grains occur from Estuarine depositional environment. The features observed do confirm the presence low velocity deposition and weathering activity.

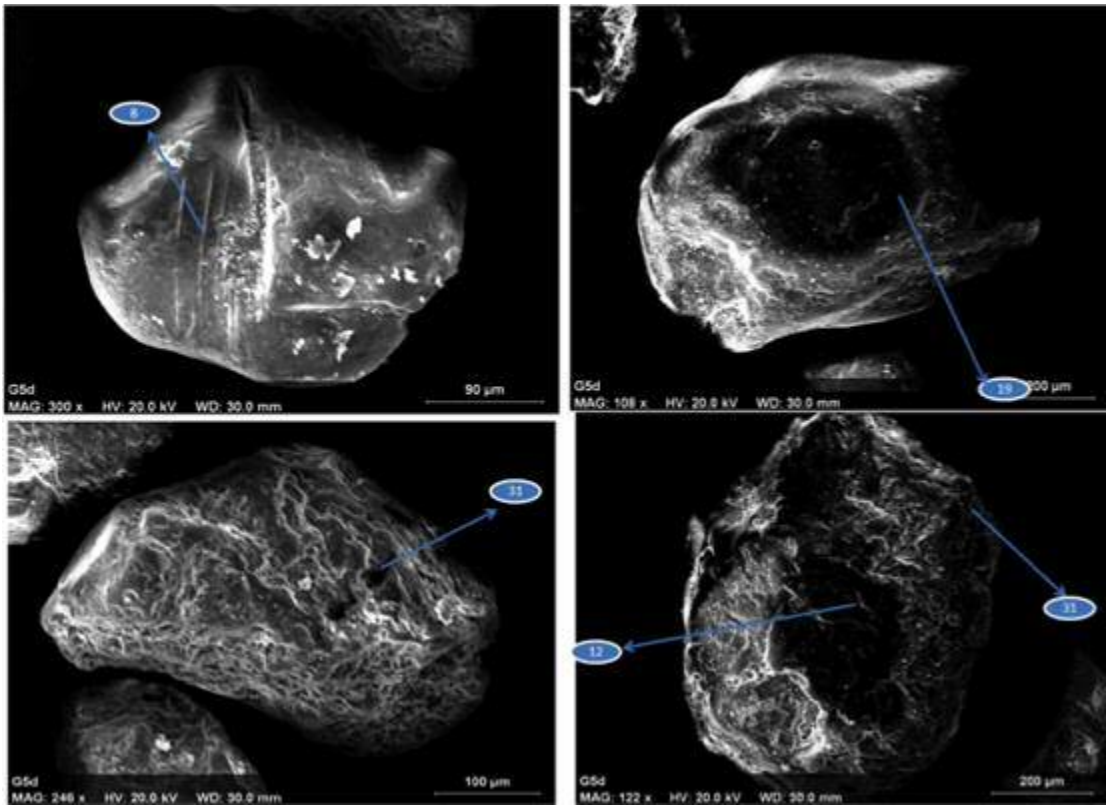

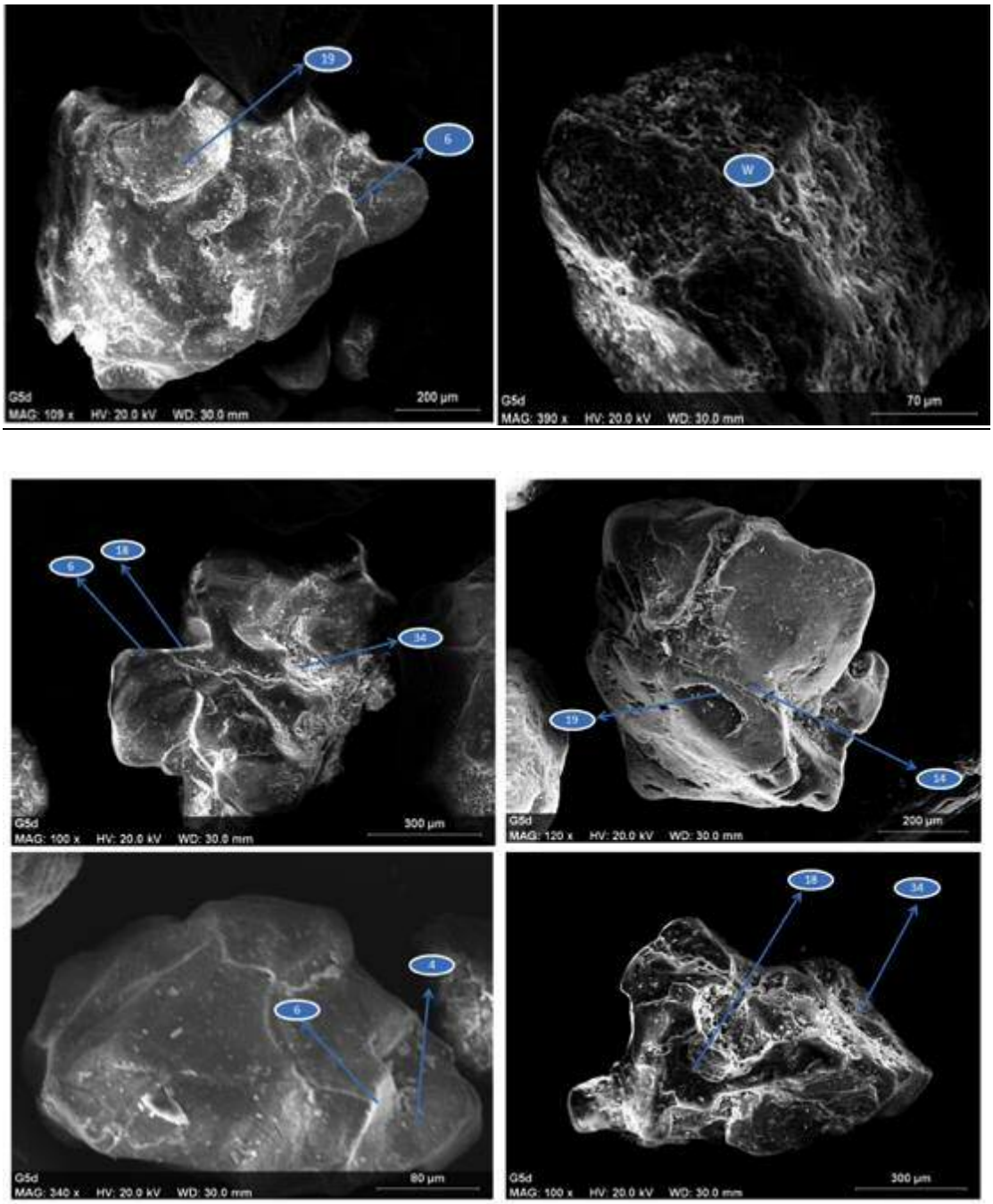


*Figure 4-43 SEM photomicrographs for sample B*

The above photomicrograph shows the different features observed from this depositional environment. Location (18) showing mechanical v-pit, (19) showing evidence of dish shape, (12) irregular pit, (34) Amorphous precipitation (silica), (30) Roundness, G-grooves, (6) smoothened conchoidal fracture, (3) breakage blocks and (2) showing edge abrasion, (14) fractured plates, 3.8 (20) solution Pits, (31) solution crevasses and W –highly weathered grain

4.1.5.3.3 Sample C

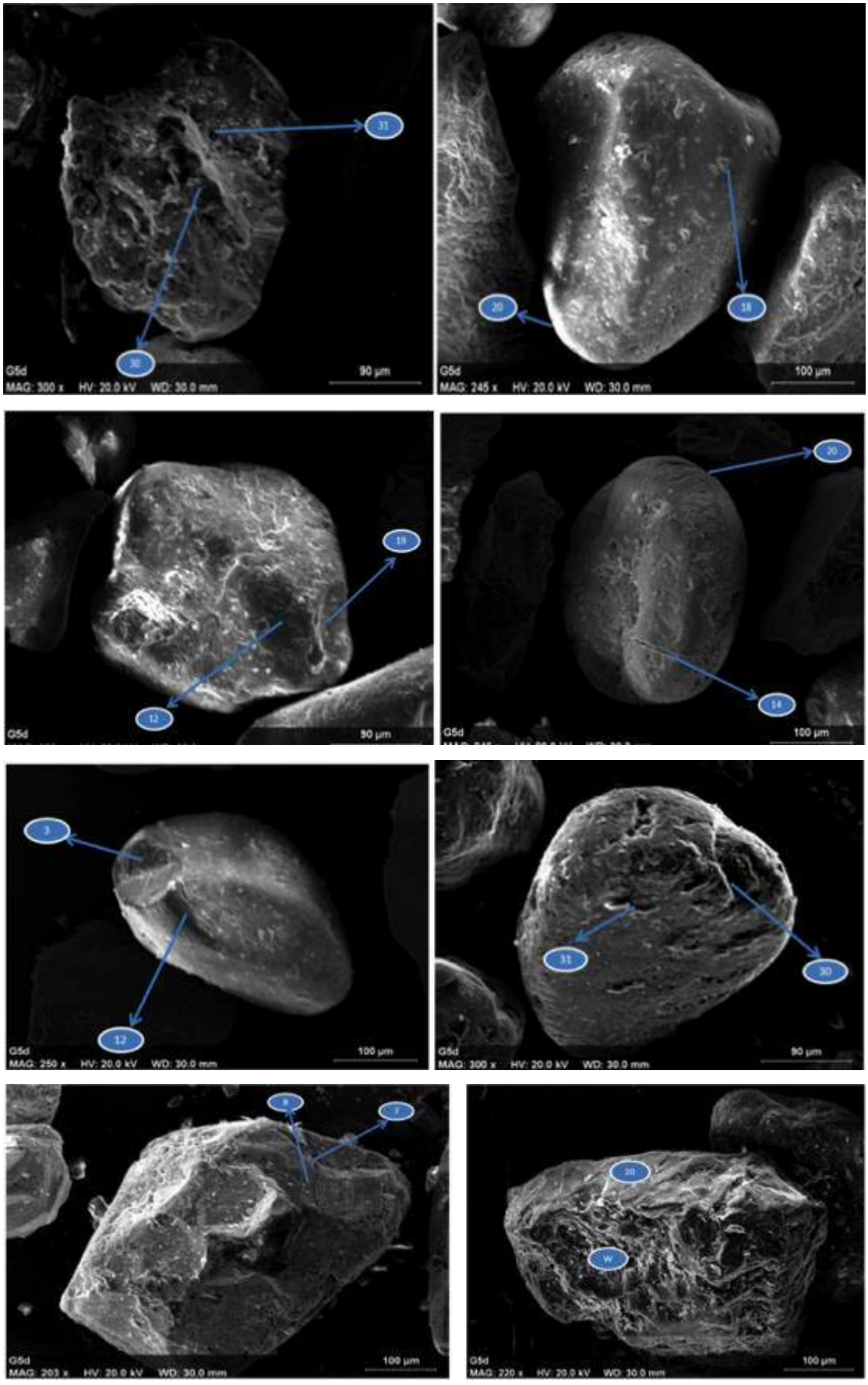

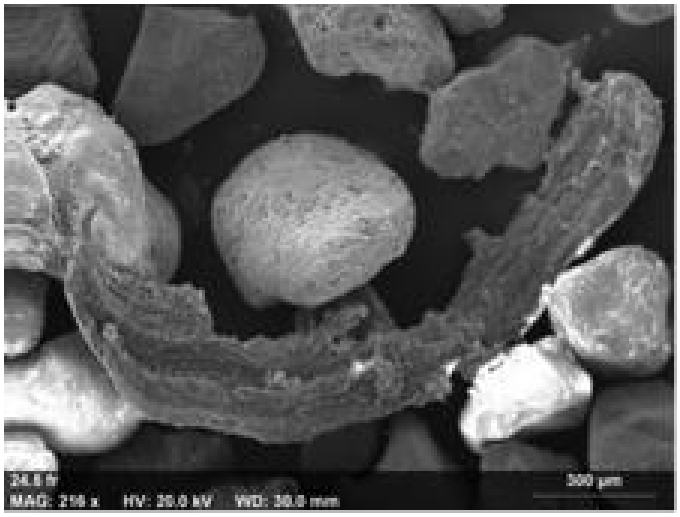

*Figure 4-44 SEM Photomicrographs for sample C*

The above photomicrograph for sample C shows the different surface features observed in this reservoir. Locations (18) showing mechanical v-pit, (19) showing evidence of dish shape, (12) irregular pit, (34) Amorphous precipitation (Silica), (30) Roundness, G-grooves, (7) fresh conchoidal fracture (3 and 4) breakage blocks, (14) fractured plates, (20) solution Pits, (31) solution crevasses, (8) straight Steps and presence of biological material.

Figure 4-44 shows the most abundant features observed from the grain from sample C. This sample shows an abundance of V pits mechanically etched, Solution V pits, step features, surface precipitation. This sample also indicates some fresh conchoidal fractures and presence of step fractures in the sample.

These features are indicators of significant amount of solution activity and presence of recent fracture development. This may be a result of post depositional activity or presence of high velocity deposition that may lead to the breakage of grains and generation of fractures in the grains.

The graph in Figure 4-45 indicates the presence of roundness mechanical and solution pits along with medium irregular pits and large conchoidal fractures again confirming the presence of higher velocity during the process of deposition.

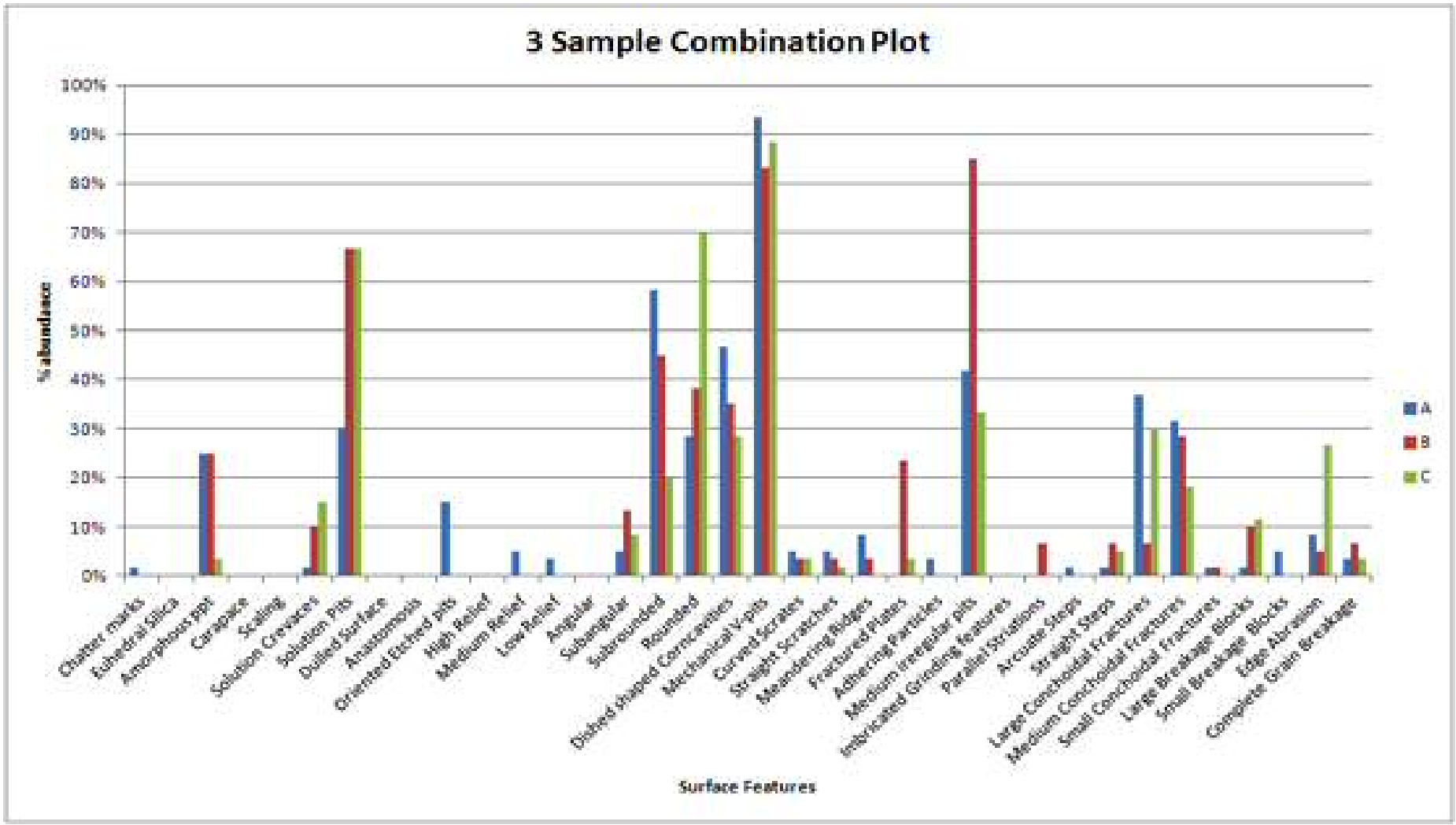


*Figure 4-45 Graph showing the comparative abundance of features in the grains of sample A, B and C respectively.*

## 4.2 Micro-CT Results

### 4.2.1 Visual comparison between Sample A, B and C

Observation of micro-CT images Figure 4-46,Figure 4-47 and Figure 4-48 provides immediate comparison of the three samples studied as part of this study. These three samples being integrated sections from core sample shows largely undisturbed host material with most properties intact.

Sample A: Contains coarser grains and micromass with few clay bridges being observed.

Sample B: Contains large abundance of fine grained material with few coarser grains being present

Sample C: Predominantly shows presence of finer grains.

Closer observation of Sample A Figure 4-46 shows presence of clay bridges and confirms observation made by (Bell, Eruteya, & Oono, 2012).

Sample A

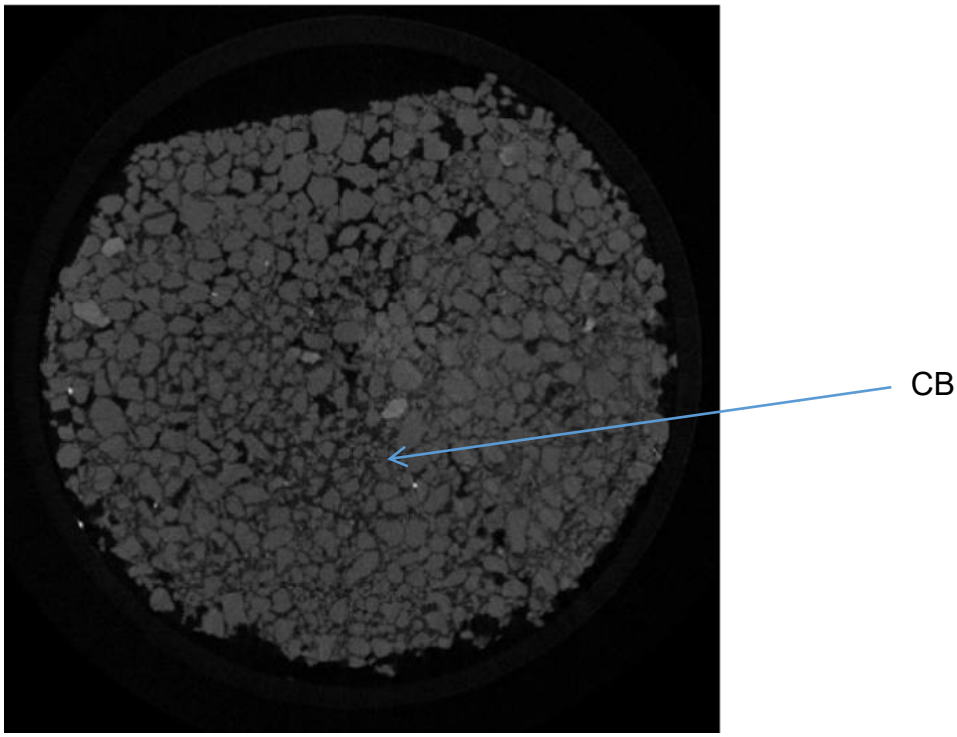


*Figure 4-46 micro-CT image of Sample A core sample*

## Sample B

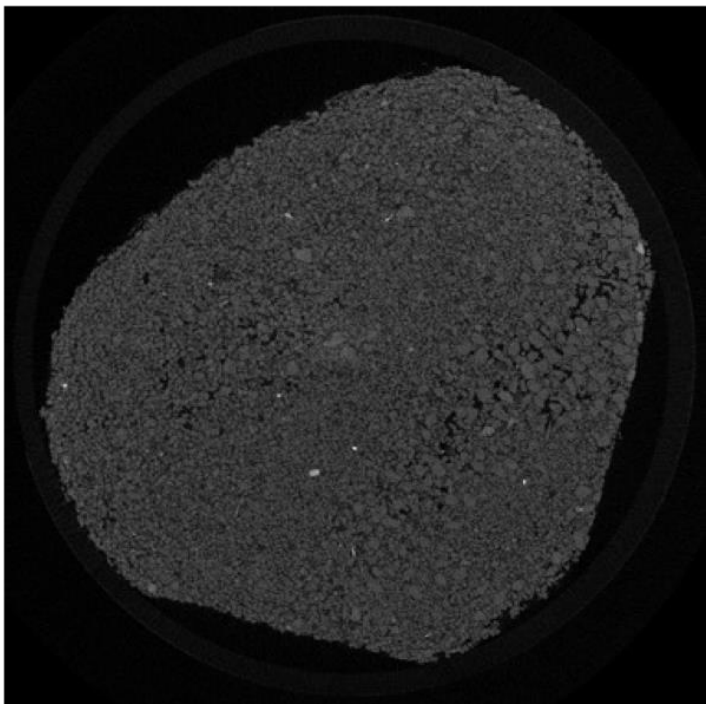

*Figure 4-47 micro -CT images of Sample B from core samples.*

## Sample C

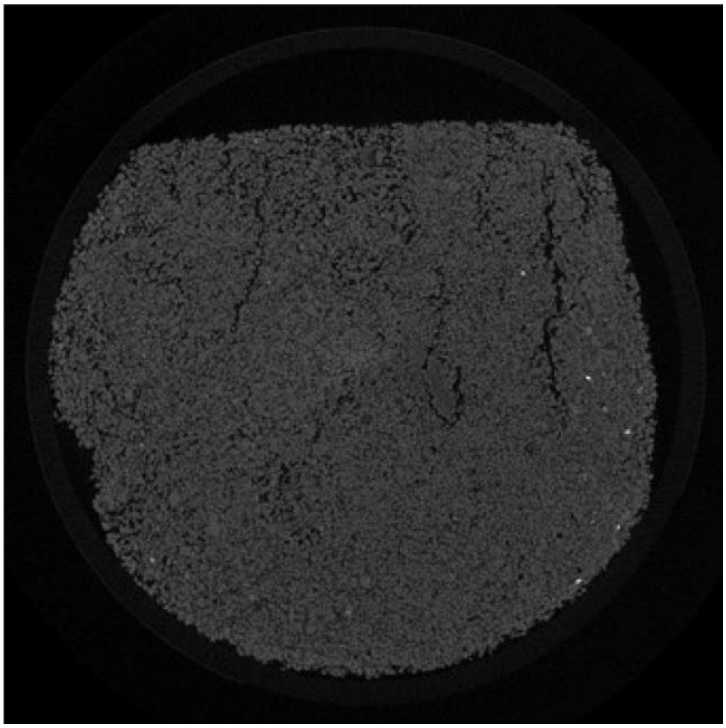

*Figure 4-48 micro -CT images of Sample C core sample.*

### 4.2.2 Statistical data analysis

This work has been quite extensive and covers following area, obtaining sorting for the three different samples provided, grain size, grain shape, skewness and kurtosis from the analysis carried out on the micro Ct data using Fiji. Similar statistical analysis as shown for Thin Sections and SEM are performed on micro-CT data.

#### *4.2.2.1 Grain Size distribution*

For sample A, total of 21,449 grains was analysed and classified using Wentworth size scale. The plot in Figure 4-49 shows significant presence of Medium sand, fine sands and very fine sands. the graphic mean is calculated at 2.52phi.

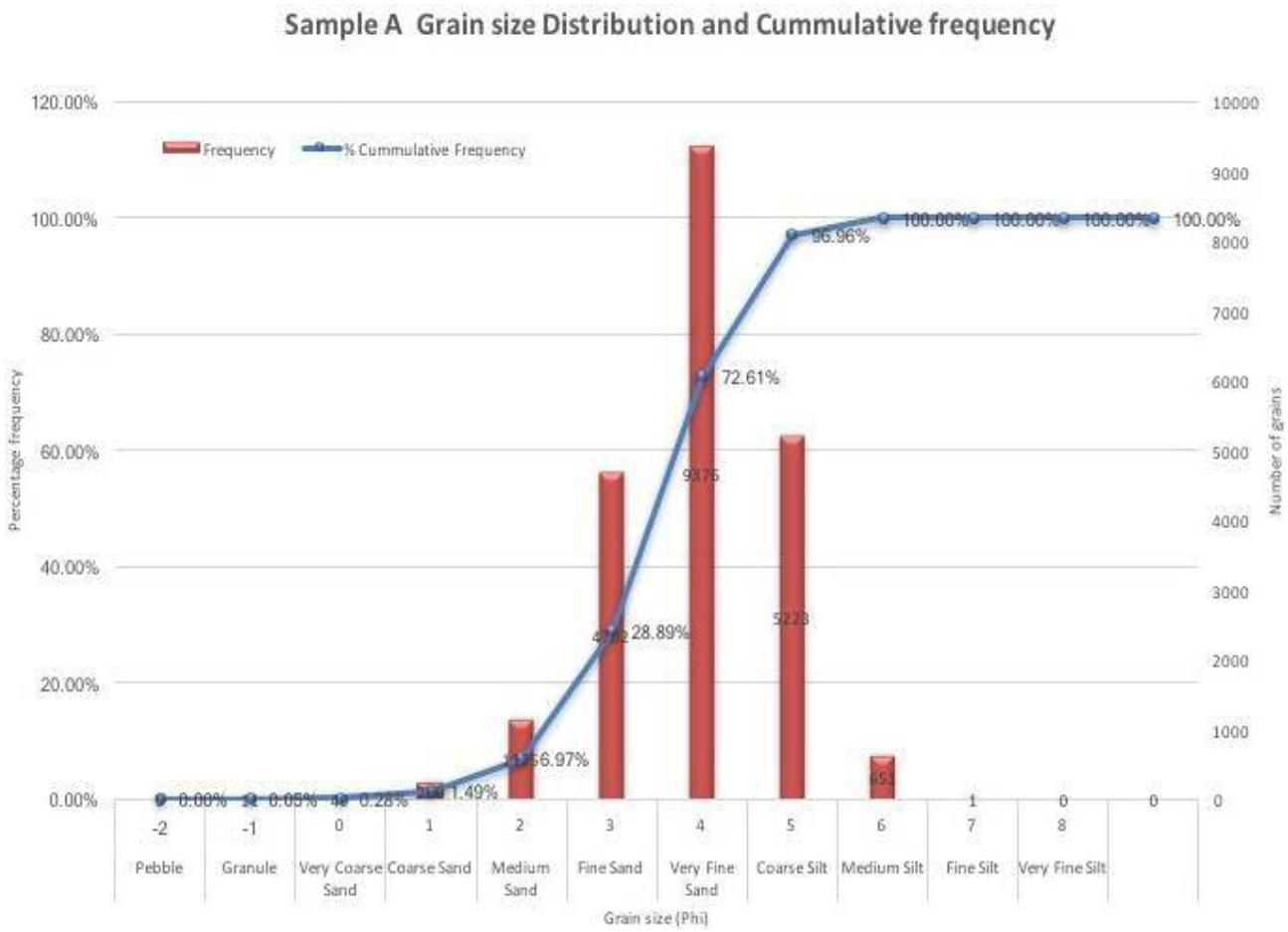


*Figure 4-49 Grain size distribution curve sample A*

For Sample B 28,865 were analysed and classified using the Wentworth scale. The plot in Figure 4-50 shows significant presence of fine sands to very fine sands. The calculated mean for the sample was at 2.81 phi.

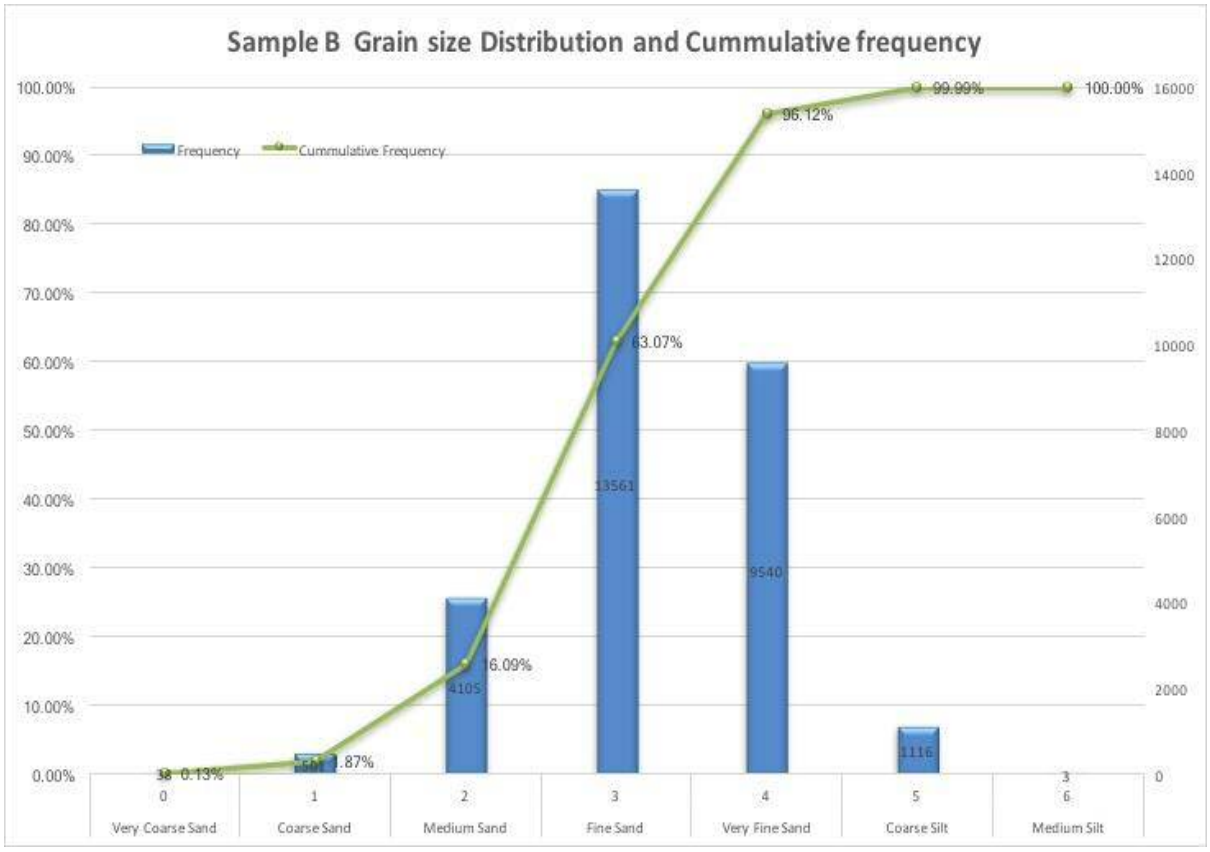


*Figure 4-50 Grain size distribution curve for sample B*

For Sample C 35,926 grains were analysed and classified using Wentworth scale. The plot in Figure 4-51 shows significant presence of fine sands to very fine sands with significant presence of finer elements as part of this sample that was absent from Sample A and B. The calculated mean for the sample was at 2.81 phi.

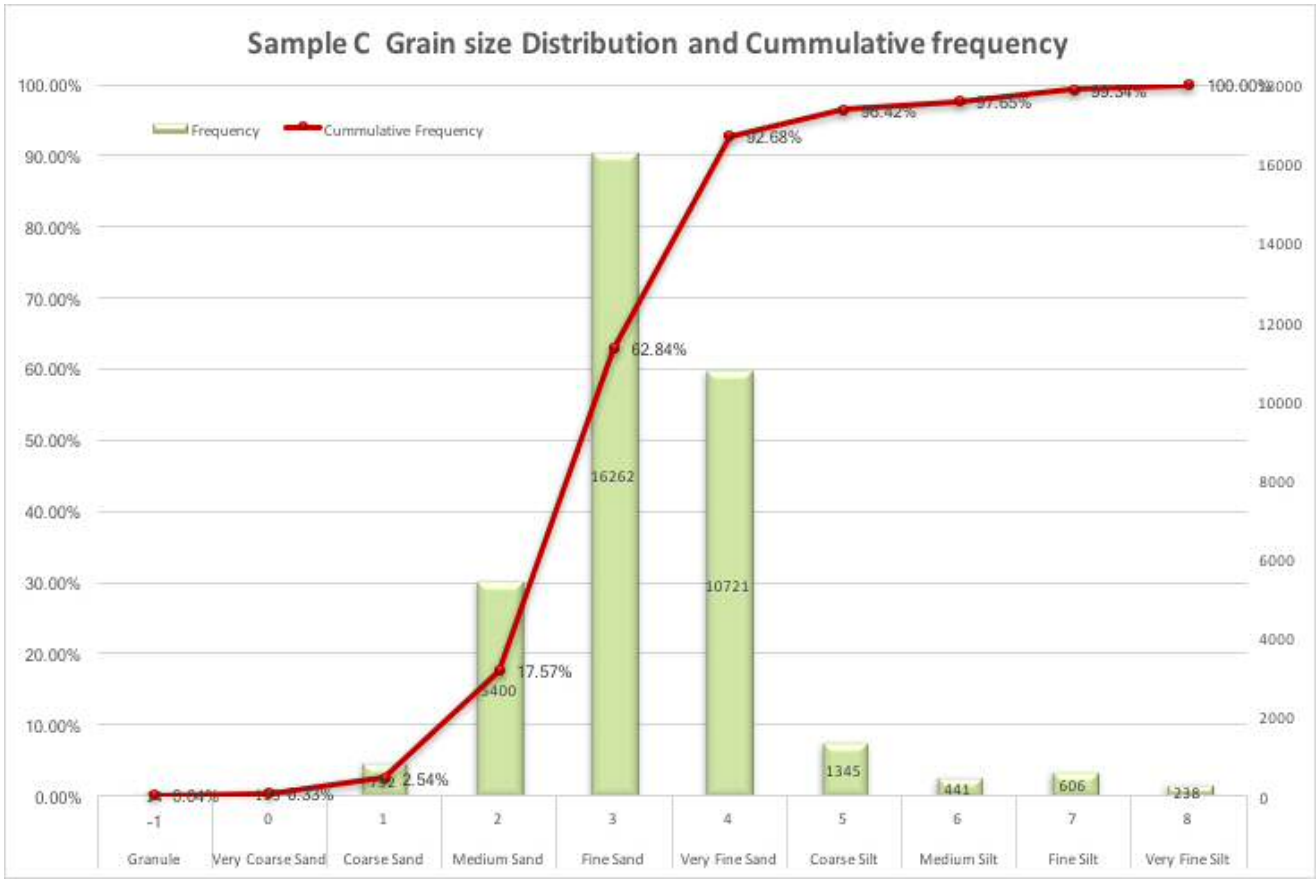


*Figure 4-51 Grain size distribution curve for sample C*

*Table 4-4 Summary of grain size distribution for sample A, B and C*

| Class of grain size (Wentworth grain scale) | Sample A | Sample B | Sample C |
|---|---|---|---|
| Granule | 0.00% | 0.00% | 0.00% |
| Very coarse sand | 0.05% | 0.00% | 0.00% |
| Coarse sand | 0.23% | 0.00% | 0.04% |
| Medium sand | 1.21% | 0.13% | 0.29% |
| Fine sand | 5.48% | 1.74% | 2.20% |
| Very fine sand | 21.92% | 14.22% | 15.03% |
| Coarse silt | 43.72% | 46.98% | 45.27% |
| Medium silt | 24.35% | 33.05% | 29.84% |
| Fine silt | 3.04% | 3.87% | 3.74% |
| Very fine silt | 0.00% | 0.01% | 1.23% |

#### *4.2.2.2 Grain Sorting*

Sorting for all three samples was calculated based on the inclusive graphic standard deviation introduced by Folk (1968). Table 3-2It shows the classification put forth following Folk's method used for classification of samples.

For sample A, values determined from the grain size cumulative frequency curve Figure 4-52 Cumulative Frequency curve Sample A are 0.65φ, 1.45φ, 3.6φand 4φ respectively.

As it may be observed based on the above calculations the sorting index for sample A was found to be 1.045 that lies in the (1.00 - 2.00) range that corresponds to "Poorly sorted".

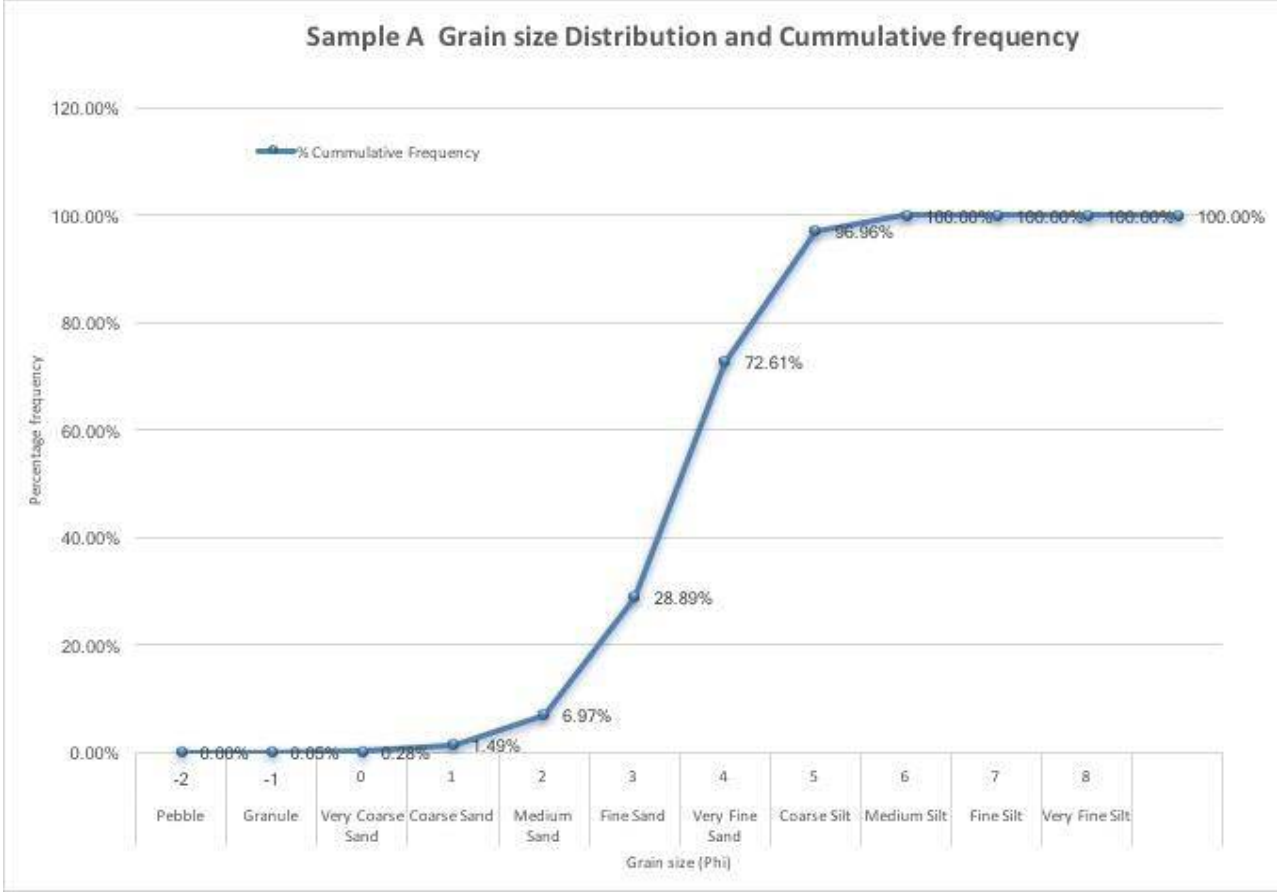


*Figure 4-52 Cumulative Frequency curve Sample A*

For sample B, values determined from the grain size cumulative frequency curve Figure 4-53 Cumulative frequency curve for sample B are 1.23φ, 2φ, 3.59φ and 3.81φ respectively.

As it may be observed based on the above calculations the sorting index for sample A was found to be 0.788 that lies in the (0.71 - 1.00) range that corresponds to “Moderately sorted”.

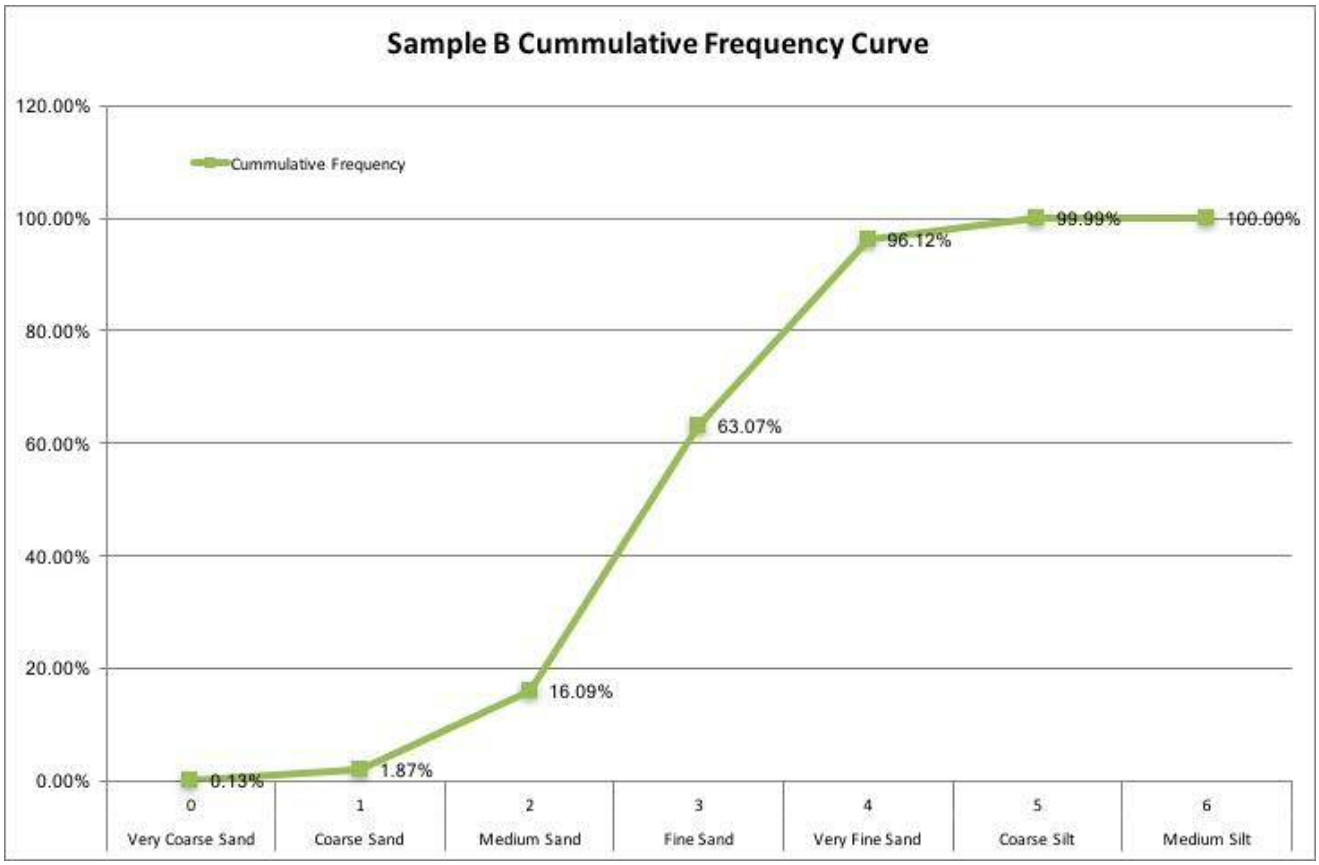


*Figure 4-53 Cumulative frequency curve for sample B*

For sample B, values determined from the grain size cumulative frequency curve Figure 4-54 Cumulative frequency curve for sample C are 1.2ϕ, 1.86φ, 3.53φand 4.5φ respectively.

As it may be observed based on the above calculations the sorting index for sample A was found to be 0.92 that lies in the (0.71 - 1.00) range that corresponds to “Moderately sorted”.

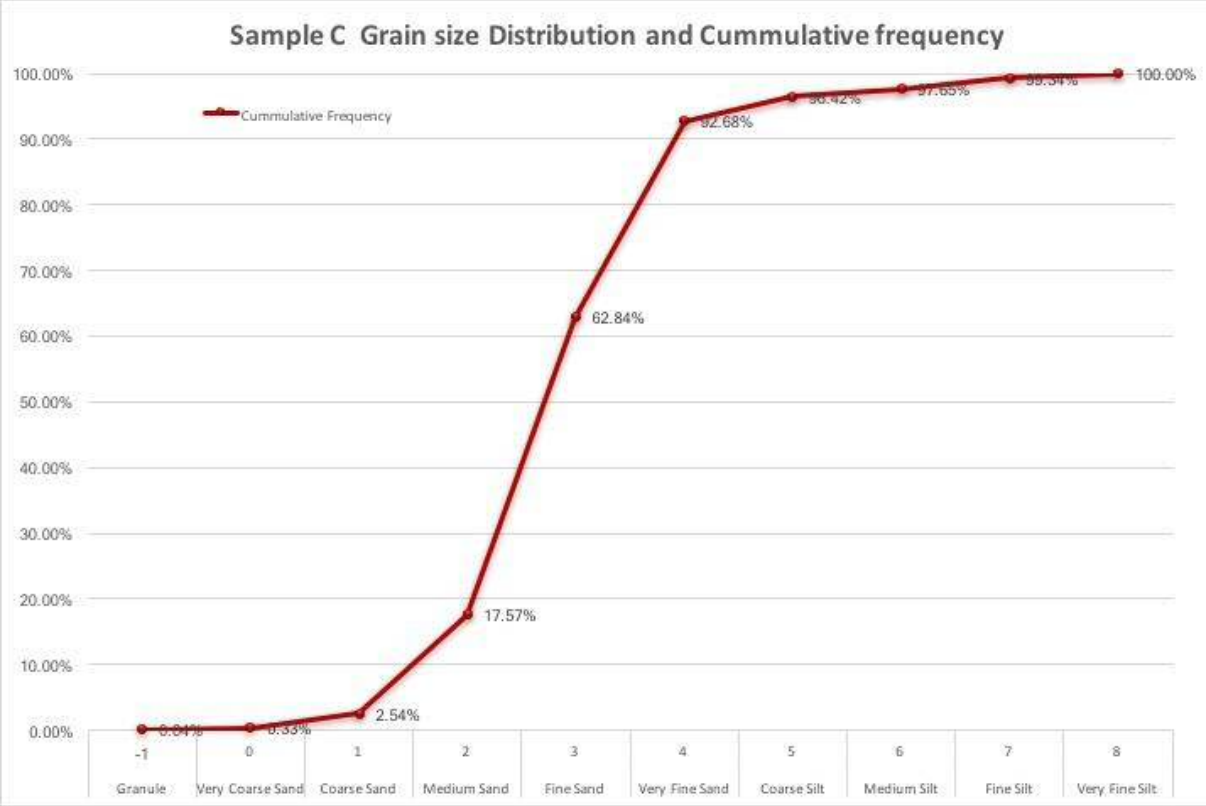


*Figure 4-54 Cumulative frequency curve for sample C*

*Table 4-5 Grain Sorting Summary*

| Phi (φ) | Sample A | Sample B | Sample C |
|---|---|---|---|
| Standard deviation | 1.045 | 0.788 | 0.9175 |
| 5 | 0.65 | 1.23 | 1.2 |
| 16 | 1.45 | 2 | 1.86 |
| 84 | 3.6 | 3.59 | 3.53 |
| 95 | 4 | 3.81 | 4.5 |

#### *4.2.2.3 Skewness and Kurtosis*

Skewness of the grain size distribution for the three samples was determined using the Folk (1968) graphic skewness formula.

For sample A, the skewness and kurtosis value of φ5, φ16, 25φ, φ50, φ75, φ84 and φ95 were obtained as 0.65φ, 1.45φ,1.9φ 2.5φ, 3φ, 3.6φ and 4φ.

The skewness is calculated at -0.041 which implies that the distribution is symmetrical. Kurtosis for sample A is Leptokurtic meaning that the central portion of the distribution curve has a better sorting.

For sample B, the skewness and kurtosis for this distribution is calculated at -0.1629 using skewness and kurtosis value of φ5, φ16, φ25, φ50, φ75, φ84 and φ95 were obtained at 1.2φ, 1.86φ, 2.2φ, 2.85φ, 3.4φ, 3.59φ and 3.81φ.

From the calculation, it shows that the cumulative curve for sample B is negatively skewed which implies that this particular sample mainly consists of coarse grains. And the Kurtosis for this distribution is platykurtic showing that the grains are well sorted in the tail portion of the curve.

Skewness for sample C is a positive value of 0.133 and kurtosis for sample c is leptokurtic. The skewness and kurtosis value of φ5, φ16, φ25, φ50, φ75, φ84 and φ95 were obtained at 1.5φ, 1.86φ, 2.2φ, 2.6φ, 3.2φ,3.53φ and 4.5φ.

From the calculation, it shows that the cumulative curve for sample B is positively skewed which implies that this particular sample mainly consists of coarse grains, and

the Kurtosis for this distribution is leptokurtic showing that the grains are well sorted in the tail portion of the curve.

*Table 4-6 Skewness and Kurtosis values summary table*

| Parameters( ) | Sample A | Sample B | Sample C |
|---|---|---|---|
| 5 | 0.65 | 1.2 | 1.5 |
| 16 | 1.45 | 1.86 | 1.86 |
| 25 | 1.9 | 2.2 | 2.2 |
| 50 | 2.5 | 2.85 | 2.6 |
| 75 | 3 | 3.4 | 3.2 |
| 84 | 3.6 | 3.59 | 3.53 |
| 95 | 4 | 3.81 | 4.5 |

*Table 4-7 Statistical calculation summary table*

| | | | |
|---|---|---|---|
| **Standard deviation ($б_1$)** | 1.045 | 0.788 | 0.9175 |
| **Class of sorting** | Poorly sorted | Moderately sorted | Moderately sorted |
| **Skewness ($sk_1$)** | -0.041 | -0.1629 | 0.133 |
| **Interpretation for Skewness** | symmetrical | Negative skewed | Positive skewed |
| **Kurtosis ($K_G$)** | 1.23 | 0.88 | 1.35 |
| **Interpretation for Kurtosis** | leptokurtic | platykurtic | leptokurtic |

#### *4.2.2.4 Grain shape (Roundness)*

Image analysis generated data for roundness and a range of 0.17-1 was used in determining the grain shape, where 0.17 represents very angular grains, 0.34 angular grains, 0.51 sub angular grains, 0.68 sub rounded, 0.85 rounded and 1 for perfectly well rounded grains.

From the graph in Figure 4-55, it shows that out of 21448 grains analysed by imageJ 1042 grains (4.86%) are well rounded, 4183 (19.50%) are rounded, 7034 (32.80%) are sub rounded grains, 7075 (32.99%) sub angular, 2099 (9.79%) angular grains and just 15 ( 0.07%) out of 21448 grains are very angular.

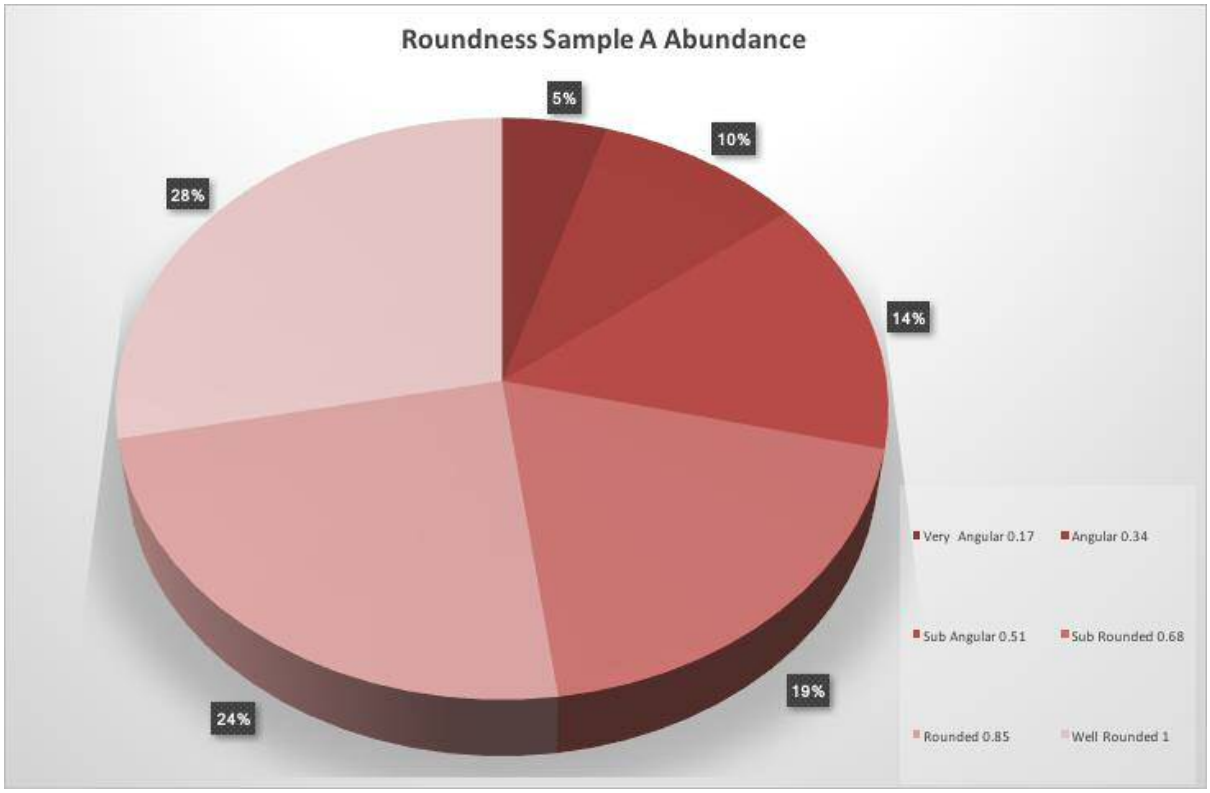


*Figure 4-55 Grain shape (Roundness Abundance) Sample A*

For sample B, the same range used in sample A was applied in determining the shape of the grains for sample B. The total number of grains analysed by images for sample B is 28864 and 11(0.04%) are very angular grains, 2444 (8.47%) angular grains, 9409 (32.60%) sub angular, 9721 (33.68%) sub rounded, 5861 (20.31%) rounded and 1418 (4.91%) for rounded grains. This is shown below in Figure 4-56.

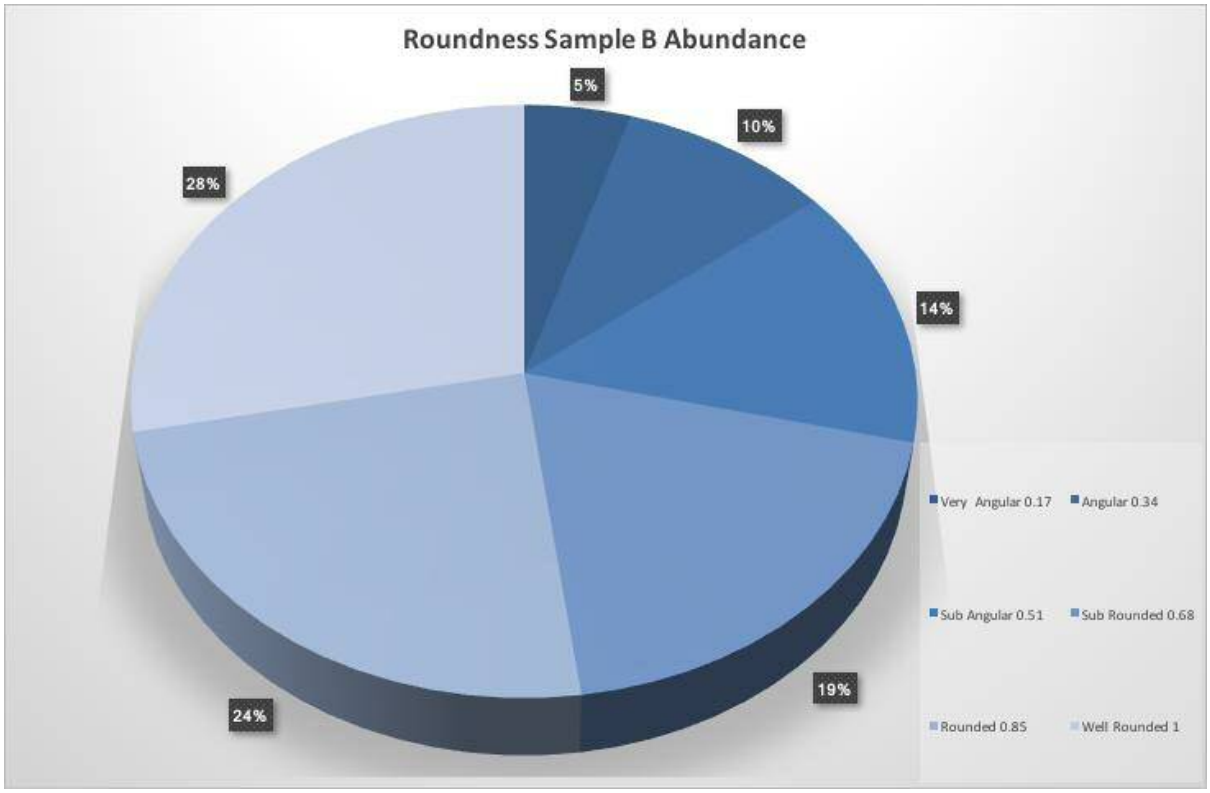


*Figure 4-56 Grain shape (Roundness Abundance) Sample B*

For sample C, a total of 35926 grains were analysed by image analysis and a range of 0.17-1 was used to determine the grain shape where 1 represents well rounded grains. 15(0.04%) very angular, 3101 (8.63%) angular, 11510 (32.04%) sub angular, 12219 (34.01%) sub rounded, 7213 (20.08%) rounded and 1868 (5.20%) for rounded grains. Figure 4-57 demonstrates the  abundance of grains in each of the sections of angular to well rounded.

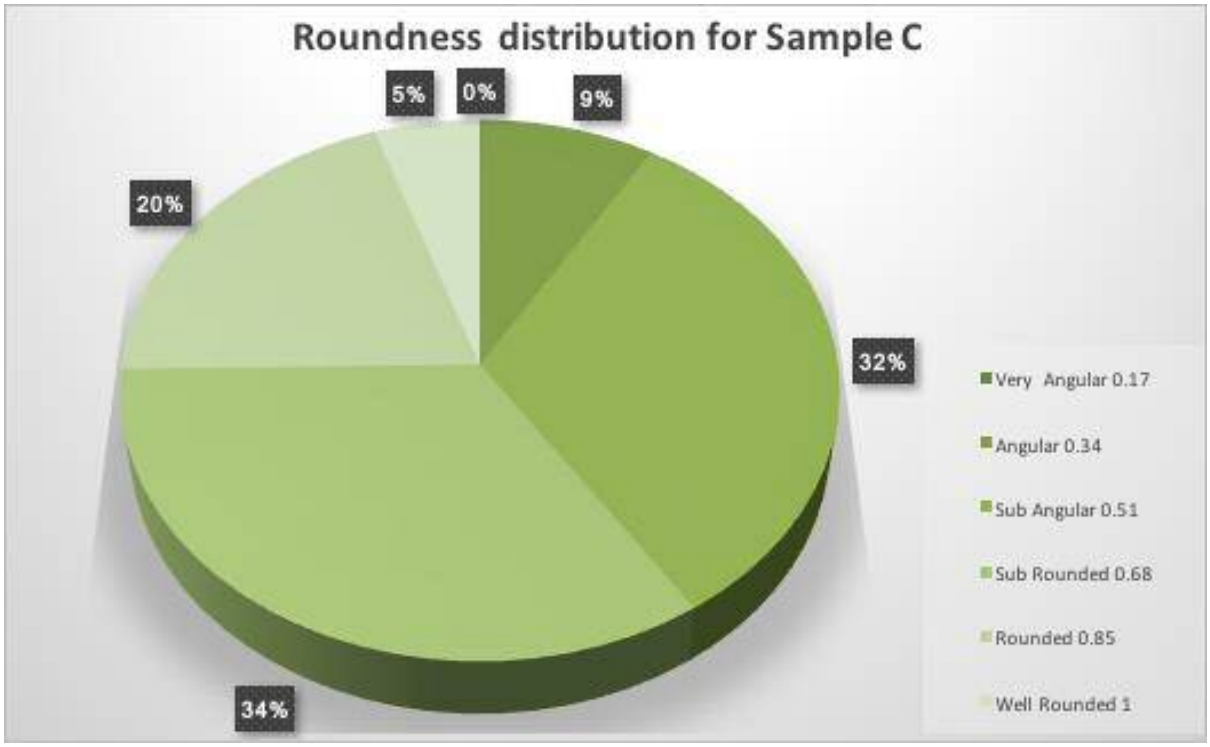


*Figure 4-57 Grain shape (Roundness Abundance) Sample C*

*Table 4-8 Grain Shape Abundance Summary*

| Grain shape | Sample A | Sample B | Sample A |
|---|---|---|---|
| **Very angular** | 0.07% | 0.04% | 0.04% |
| **Angular** | 9.79% | 8.47% | 8.63% |
| **Sub angular** | 32.99% | 33.60% | 32.04% |
| **Sub rounded** | 32.80% | 33.68% | 34.01% |
| **Rounded** | 19.50% | 20.31% | 20.08% |
| **Well rounded** | 4.86% | 4.91% | 5.20% |

### 4.2.3 Porosity determination

Binary image stacks for all the three samples were analysed using the Particle Size Distribution (PSD) and Pore Size Distribution, values for the total void and total grain area were generated so then the porosity can be calculated by using the E.q. 2-7

The resulting volumetric calculations for the three samples are provided in the following Table 4-9,

*Table 4-9. Volumetric porosity determination on Image analysis of 10 ROI*

| Images | Void area ($nm^3$) | Grain area ($nm^3$) | Porosity | Porosity % |
|---|---|---|---|---|
| **Sample A** | 117140 | 476450 | 0.245 | 24.5% |
| **Sample B** | 143751.0 | 482829 | 0.297 | 29.8% |
| **Sample C** | 208002 | 498829 | 0.416 | 41.6% |

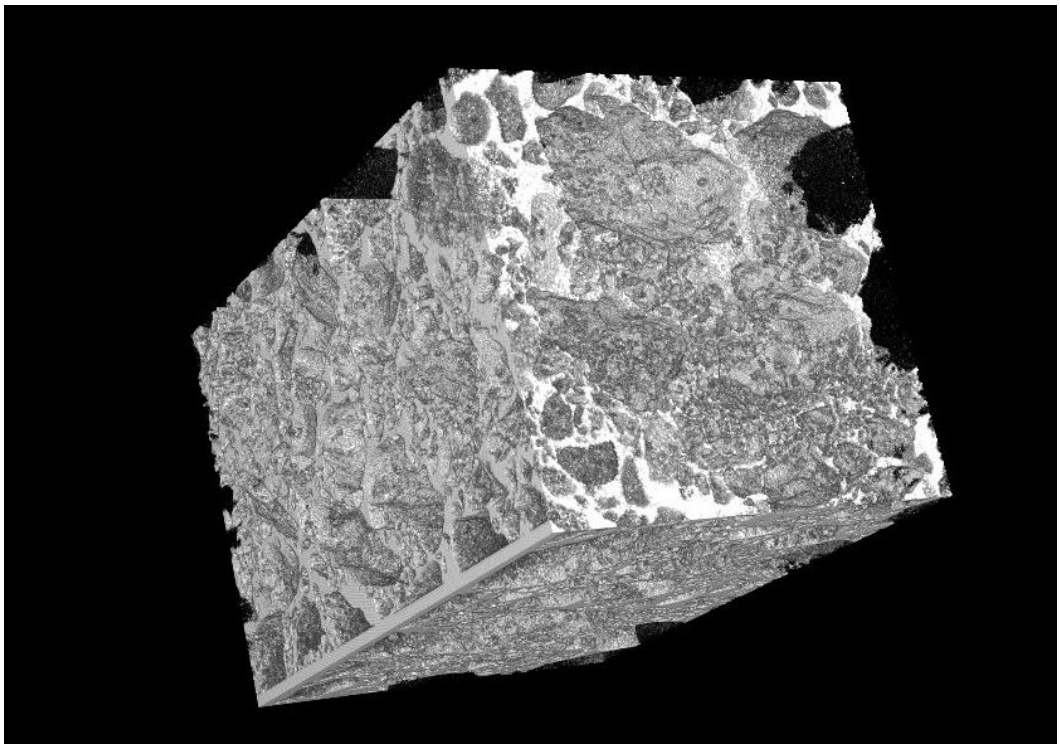

*Figure 4-58 3D representation of porosity calculation for Sample A.*

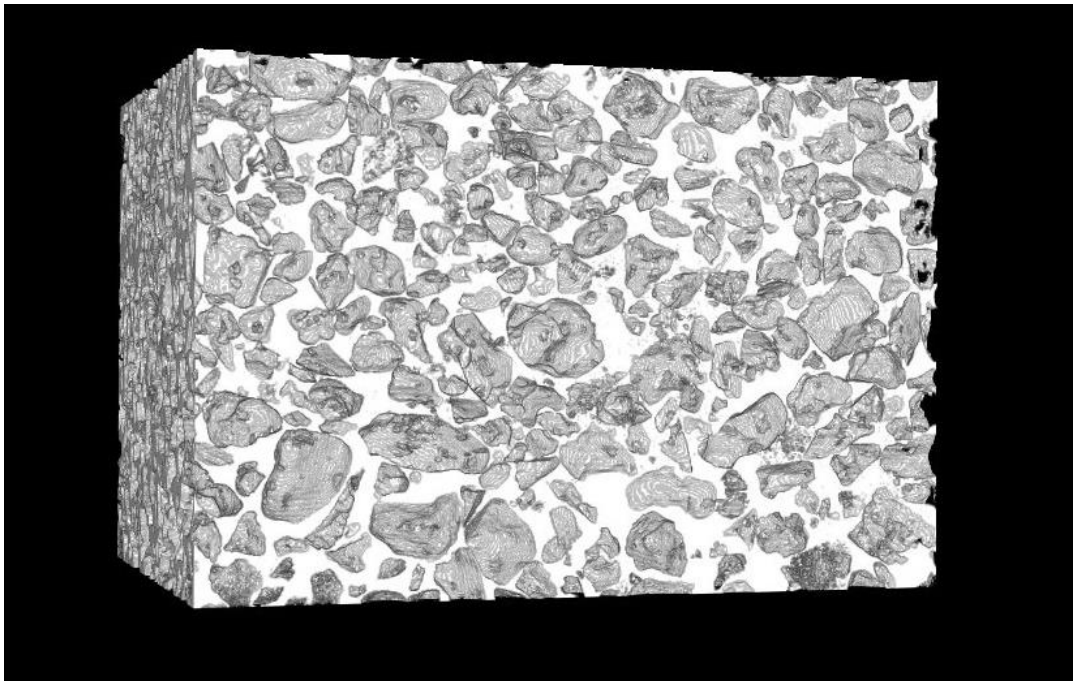

*Figure 4-59 3D representation of porosity calculation for Sample B.*

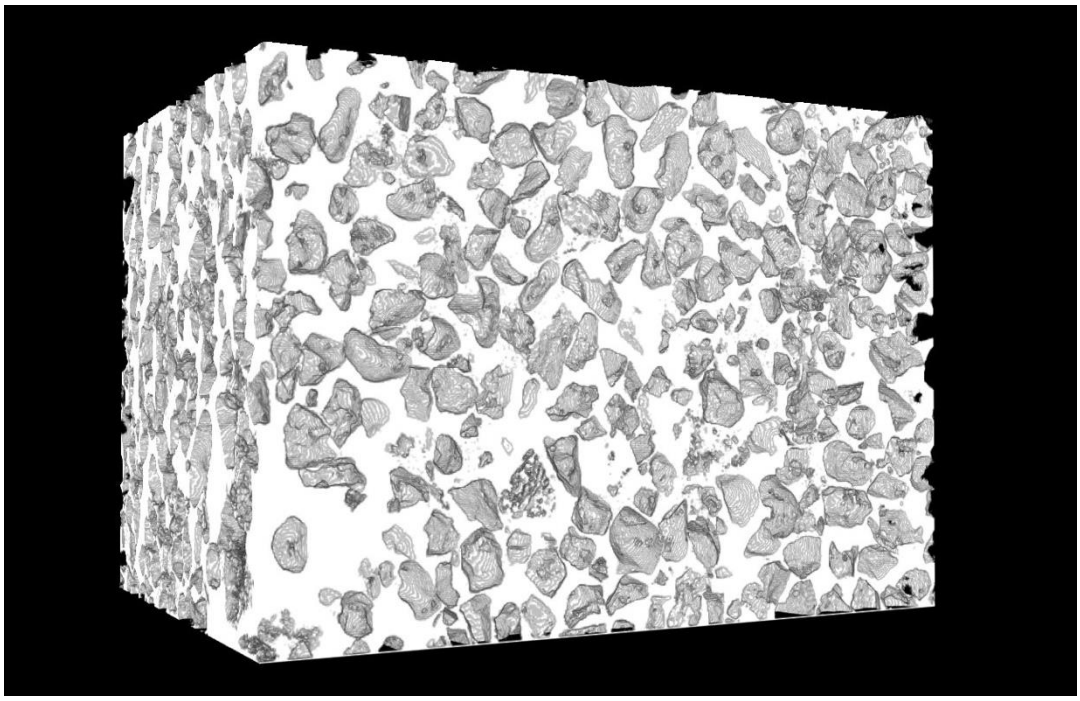

*Figure 4-60 3D representation of porosity calculation for Sample C.*

### 4.2.4 Permeability determination

Permeability was determined following VanBarren's Equation 2-15 as this equation compared to the Krumbien Monks equation and Berg's equation takes into account

the effect that grain morphology has on distribution, sorting and skewness of the grains which in turn affect the cementation index and porosity for the samples.

While performing calculations for VanBarren's equation there are two possible ways in which it can be performed. Either through the use of standardised parameters provided and used by Prison, 1958; Luo and Kantzas, 2008 or through the use of sorting, cementation factors and porosity, determined through image analysis as part of this study.

To determine permeability following parameters determined through this study (m) Cementation factor is determined as follows.

For

Sample A: ———

Sample B: ———

Sample C: ———

Determination of abundant grain size in μm is required for the purpose of calculation. since $D_d$ determined through image analysis is calculated in phi, conversion is performed on the basis of modified Krumbien's formula as stated below.

Where

= is the Krumbien phi scale.

D= diameter of the particle in milimeters

$D_0$= is a reference diameter, equal to nearest integer (e.g.=1mm)

Once this equation is rearranged it becomes possible to determine appropriate grainsize.

$D= D_0X$

Sample A: 3 X =443

Sample B: 3 X = 534

Sample C: 3 X =449

Since all parameters are available as stated in Table 4-10 calculations are performed as follows:.

Calculation for Permeability calculation:

Sample A:

Sample B

Sample C

*Table 4-10 Permeability based on research results*

| Images | D | | m | c | Permeability md |
|---|---|---|---|---|---|
| **Sample A** | 443 | 0.243 | 1.17 | 1.045 | 1886 |
| **Sample B** | 534 | 0.297 | 1.10 | 0.788 | 21853 |
| **Sample C** | 449 | 0.41 | 1.18 | 0.92 | 37146 |

Now, since the standardised values are available for (m) cementation factor and (c) sorting index, the following calculations are performed.

Sample A

Sample B

Sample C

*Table 4-11 Permeability based on standard parameters*

| Images | D | | m | c | Permeability md |
|---|---|---|---|---|---|
| **Sample A** | 443 | 0.243 | 1.6 | 1.0 | 1184 |
| **Sample B** | 534 | 0.297 | 1.6 | 0.91 | 7064 |
| **Sample C** | 449 | 0.41 | 1.6 | 0.91 | 26580 |

As you may observe from Table 4-10 and Table 4-11, results for sample B and C shows significant variation to the properties obtained by following standardized Van Barren's values and the values that have been obtained through this study. There could be two reasons that may explain variation. 1.The micro-CT scans used in this study were not able to distinguish between the grains and the micromass which will have an impact on porosity and permeability. The variation will occur primarily due the variation in the volume obtained during the process of binarisation. 2.As may be seen from the results obtained in thin section analysis, the bioturbation varies porosity and consequently permeability in this reservoir. These two reasons may have contributed to the variation in the results obtained. Secondly, the standardised table uses laboratory mixture of sands in ideal conditions whereas in this case core samples have been used which will influence the grain morphology. Secondly, as observed through the study of outcrop thin sections, this region has presence of bioturbation. The results from analysis of bioturbation thin sections in chapter 4 shows that there is significant change to porosity, permeability and morphological properties for that section. The increase in production may be as a result of bioturbation in the specified area.

### 4.2.5 Models in 3D

On receiving data from micro CT, Image stacks were imported in Drishti software package which is principally used for biological studies. An attempt was made to determine volumetric properties following this software package, though several issues with computer capacity were experienced.

Even though, volumetric calculations could not be performed on Drishti, the package was able to provide a 3D visualisation of all the three data sets by varying threshold limit within the visual region and observing different phases of samples in specified threshold bandwidths.

Sample A:

As you may observe from Figure 4-61 sample A is made up of coarse grains, fine grain and very fine grains. This has definitely lead to the poor sorting that was determined through image analysis and statistical calculations as previously stated in this chapter. The effect of such grain distribution can be observed on porous and permeable structure that can be seen in Figure 4-62. Wherein, as a result of large voids being occupied by finer grains the sample has less space available leading to the lower values of permeability that can be observed in calculations as afore mentioned in section 4.2.4.

#### 4.2.5.1 Sample A

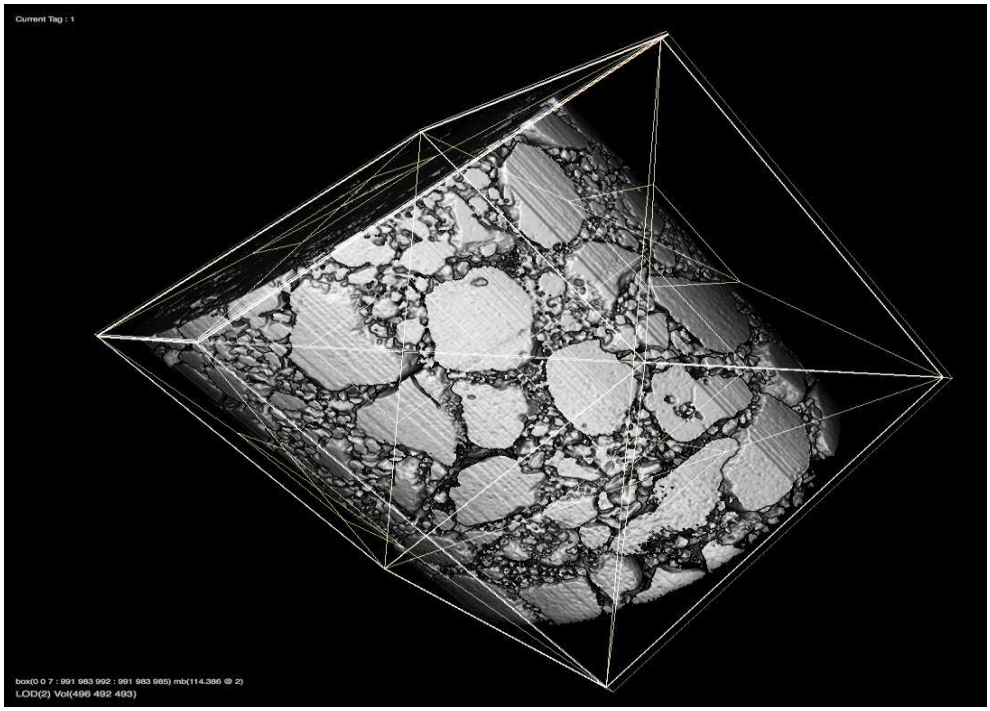


*Figure 4-61 Sample A 3D grain representation*

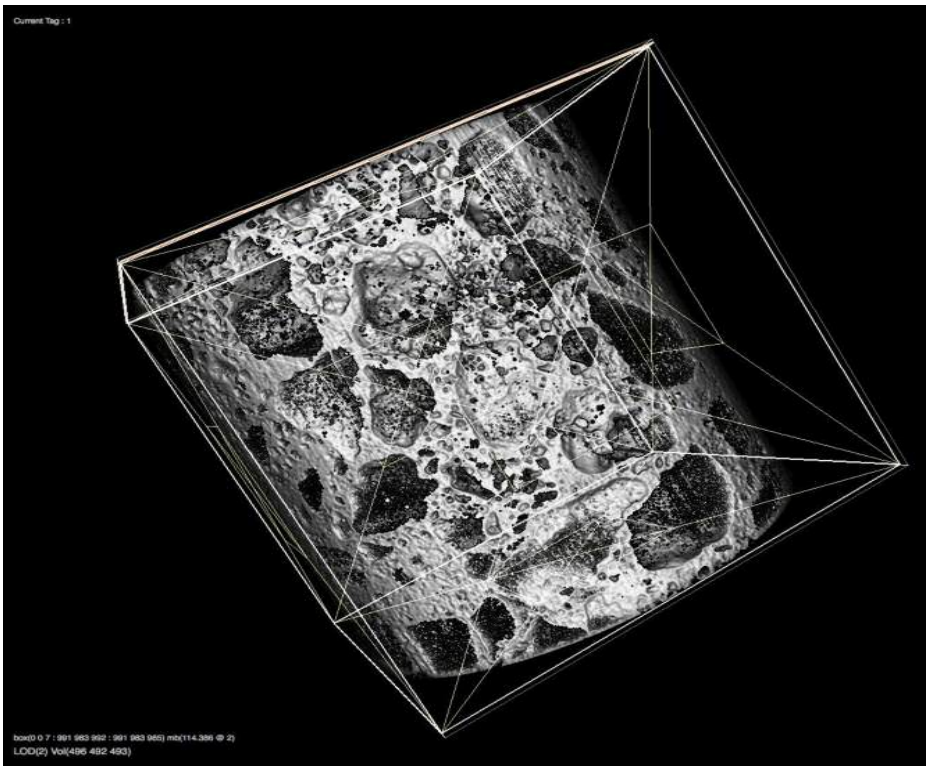


*Figure 4-62 Sample A 3D Grain representation*

#### *4.2.5.2 Sample B:*

As it may be observed from following Figure 4-63 sample B is primarily made up of medium, fine and very fine grains. As a result, it shows moderate sorting due to similar size being observed within grains. In addition, the presence of sub rounded, rounded and well-rounded grains as part of the sample contributes towards moderate sorting of the sample. This further contributes towards an increase in porosity and permeability as seen from calculated results in Table 4-9, Table 4-10 and Table 4-11. Figure 4-64 confirms the presence of higher volume of oil along with higher porosity within sample B.

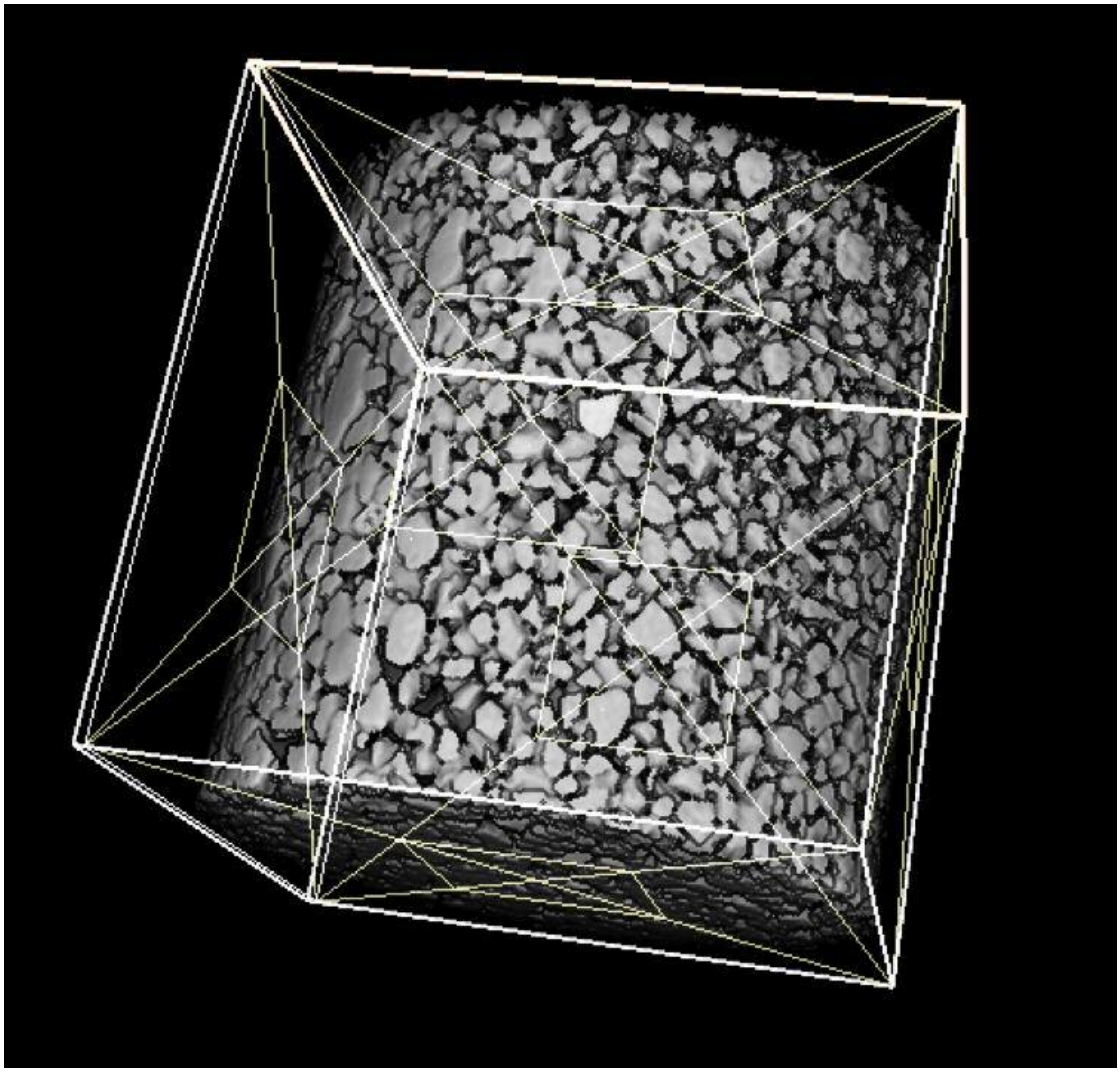

*Figure 4-63 Sample B 3D grain representation*

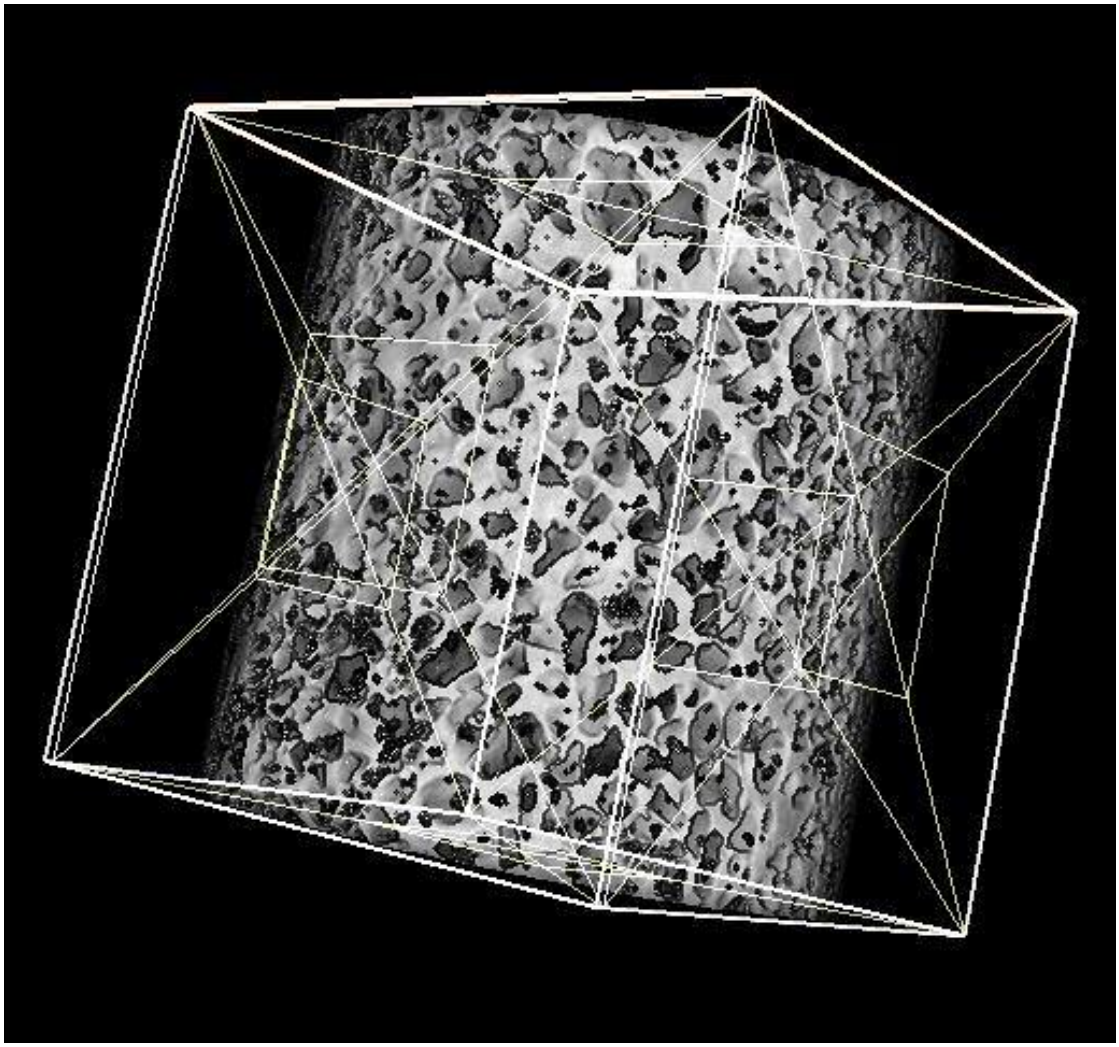

*Figure 4-64 Sample B 3D pore fluid representation*

### *4.2.5.3 Sample C*

*Similar to Sample B with regards to Sample C as it may be observed from Figure 4-65 this sample is predominantly made up of fine, very fine grains along with presence of micromass as it could be observed as part of image and statistical analysis. Presence of such grains has provided this sample with moderate sorting and has contributed to its porosity and permeability. Results displayed in*

Table 4-7, Table 4-9,Table 4-10 and Table 4-11, also points towards another factor which has provided this sample with large porosity and permeability. This may be due to the contribution of bioturbation or significant weathering that has been observed by this sample. Furthermore, few grains have shown that this sample has also been through some post depositional weathering leading to finer elements and fractured grains.

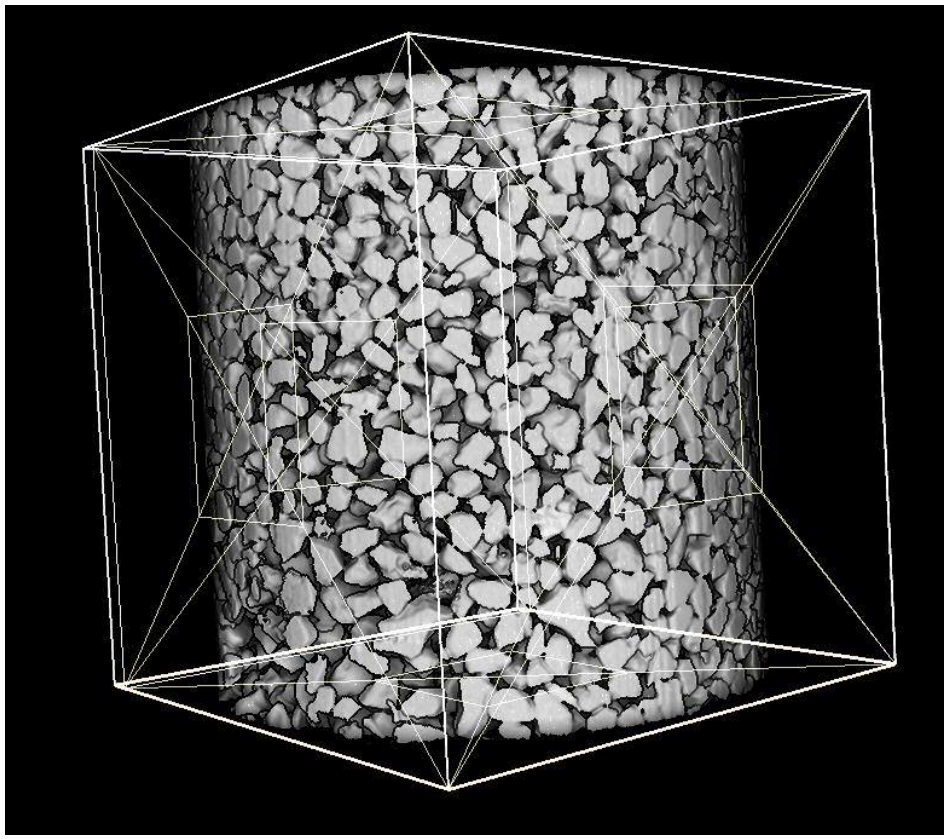

*Figure 4-65 Sample 3D Grain representation*

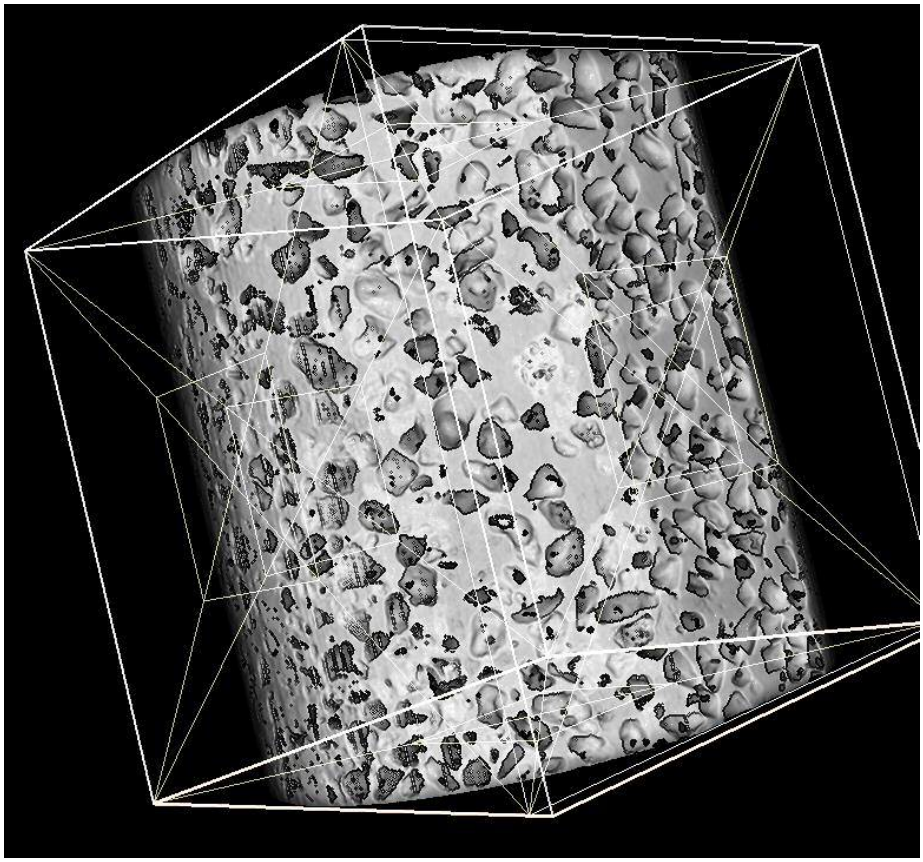

*Figure 4-66 Sample C 3D Pore Representation*

To conclude this chapter around 8 usable thin sections could be prepared to provide good quality images. This allowed for initial analysis of grain morphology showing oil coated grains, fractures, and presence of bioturbation which brings about variation to the properties at localised level. To overcome challenges from thin sections, SEM analysis was performed on subsurface core samples (Sample A, B & C) that were cleaned following soxhlet technique. The SEM analysis was able to demonstrate fining downward sequence through grain size distribution, Sub Rounded to well-rounded was observed in Sample A & Sample C respectively. This analysis provided a way to determine sorting of poorly sorted, moderately sorted and moderately sorted for Sample A, B & C respectively. High magnification scan of subsurface core samples revealed high transportation environment for sample A, moderate transportation for sample B and high transportation and predominant post depositional fracturing in sample C.

A Micro CT analysis performed to verify the results obtained through SEM analysis was able to demonstrate similar results and confirm findings. Though an additional analysis of porosity and permeability could be performed on core samples. This study

revealed good results. Permeability was calculated following two sets of values, that were obtained through this study and the values that were provided as standardised values. A variation was observed between the two values and further work will need to be performed to verify application of properties.

# 5 Simulation Studies

## 5.1 Case 1 Dead Oil SAGD

### 5.1.1 Case 1 Steam Injection Pressure Sensitivity Analysis:

The steam injection pressure was varied from 2500kPa up to 4500kPa. This allowed the study of increasing injection pressure and how it impacted upon the cumulative oil production and spread of the steam chamber.

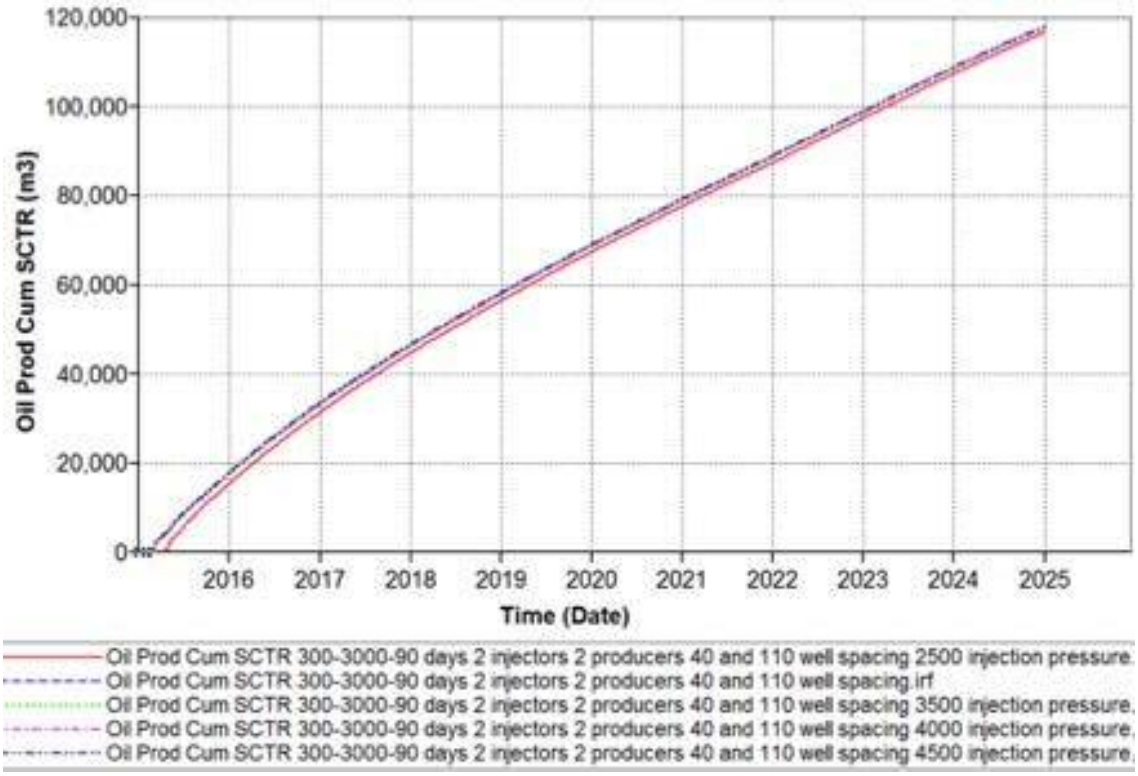


*Figure 5-1 Case 1 Injection pressure sensitivity analysis, cumulative oil graph*

*Table 5-1 Case 1 Injection pressure sensitivity analysis for cumulative oil values*

| Injection Pressure (kPa) | Cumulative Oil SC ($m^3$) |
|---|---|
| 2500 | 116,799.0 |
| 3000 | 117,475.2 |
| 3500 | 117,740.8 |
| 4000 | 117,939.2 |

| | |
|---|---|
| 4500 | 118,197.4 |

Increasing the injection pressure of the steam resulted in an increase in the cumulative oil produced. This increase was not large, but still showed a positive trend between the two parameters. The injection pressure of 4500 kPa was considered the best case and used in the following simulations.

### 5.1.2 Case 1 Steam Injection Rate Sensitivity Analysis:

On completion of injection pressure analysis, the injection rate was optimized by varying the injection rate from 100 m³/day to 500 m³/day. This allowed the analysis of injection rate on the production.

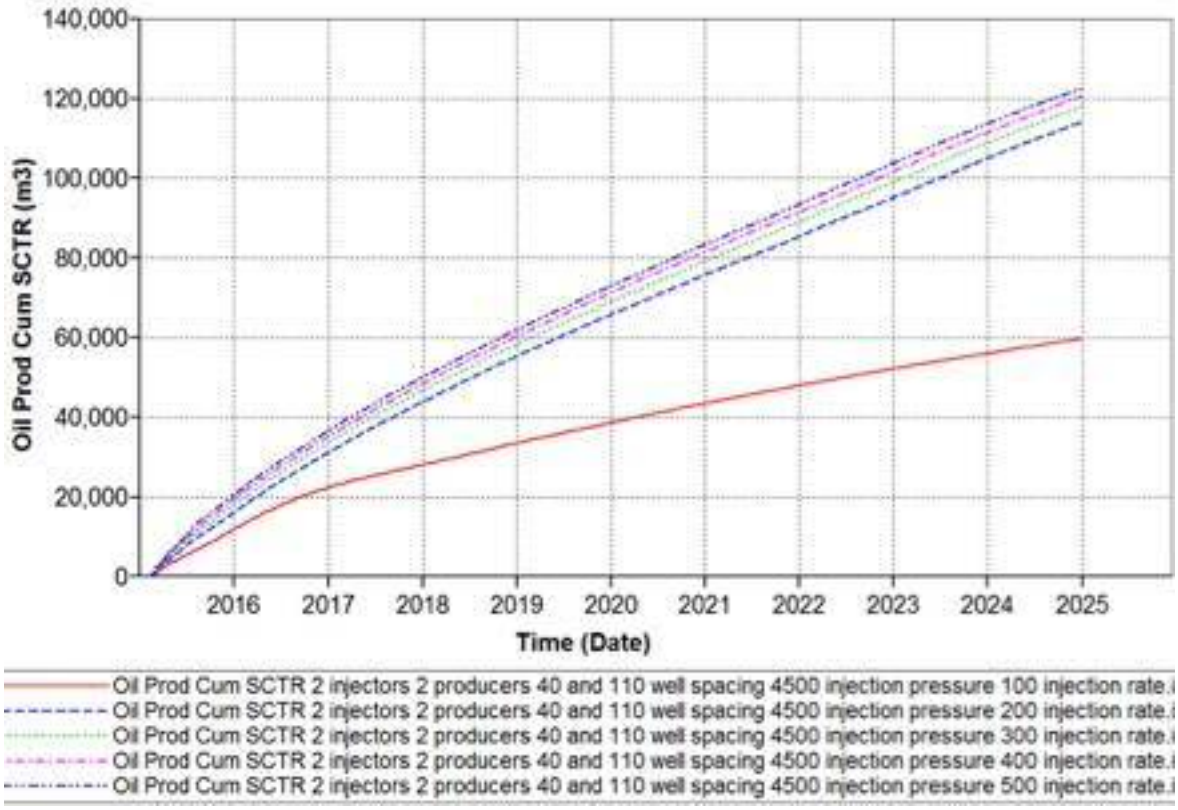


*Figure 5-2 Case 1 Injection rate sensitivity analysis, cumulative oil graph*

As can be observed in Figure 5-2, and Table 5-2 as the steam injection rate was increased the cumulative oil recovered also increased. This may primarily be achieved because the additional steam injected increased the heat transfer to the oil, thus reducing its viscosity and enabling it to flow.

*Table 5-2 Case 1 Injection rate sensitivity analysis for cumulative oil*

| Steam Injection Rate ($m^3$/day) | Cumulative Oil SC ($m^3$) |
|---|---|
| 100 | 59,693.2 |
| 200 | 114,310.2 |
| 300 | 118,197.4 |
| 400 | 120,731.0 |
| 500 | 122,776.6 |

At an injection of 100 $m^3$ over the 10 years provided significantly less oil production. This is primarily due to the quantity of steam injected being insufficient to overcome the reservoir temperature and provide necessary drive and heat to drive the chamber expansion thereby reducing the quantity of oil that could be produced. The optimum steam injection rate in this case is 500 $m^3$ per day, and this was the value used for the subsequent simulations.

### 5.1.3 Case 1 Pre Heating Period Sensitivity Analysis:

Upon confirming injection pressure and quantity of steam to be injected a study was performed to understand just how much time the steam chamber needs to be heated to achieve optimum production from the reservoir. This was performed by running simulations with varying pre-heating periods namely: 0, 1 ,2 ,3 and 4 months steam injection.

In the pre-heating analysis, the cumulative oil production for all cases showed no significant difference over the ten-year period. As a result, the daily oil rate was also plotted to observe how the pre-heating affected production on a daily basis. Figure 5-3 shows that the longer the pre heating period the higher the initial oil production. This can be contributed to the allowed time that can transfer heat to surrounding regions and providing larger quantities of mobile oil with lowered viscosity to produce.

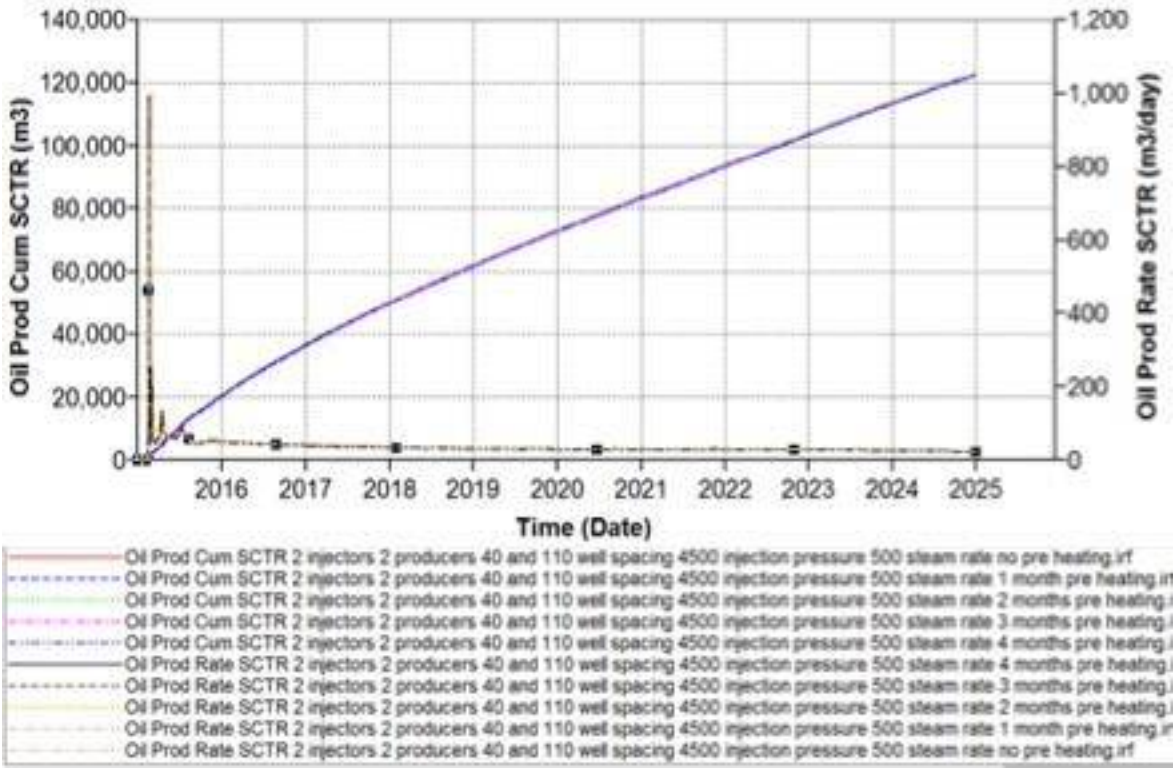


*Figure 5-3 Case 1 Pre heating period sensitivity analysis for cumulative oil graph*

### 5.1.4 Case 1 Steam Quality Sensitivity Analysis:

The steam quality was changed to 0.5, 0.6, 0.7, 0.8 and 0.9 to investigate the effect this had on the production.

*Table 5-3 Case 1 Steam Quality sensitivity analysis for cumulative oil*

| Steam Quality | Cumulative Oil SC ($m^3$) |
|---|---|
| 0.5 | 120,961.6 |
| 0.6 | 121,892.8 |
| 0.7 | 122,541.4 |
| 0.8 | 122,646.0 |
| 0.9 | 122,941.2 |

As seen in Table 5-3 when steam quality is increased the cumulative oil produced also increases, but only by a small margin. A steam quality of 0.9 gave the best production

of 122,941.2m³ which is around 2000m³ more oil when compared to the 0.5 steam quality case.

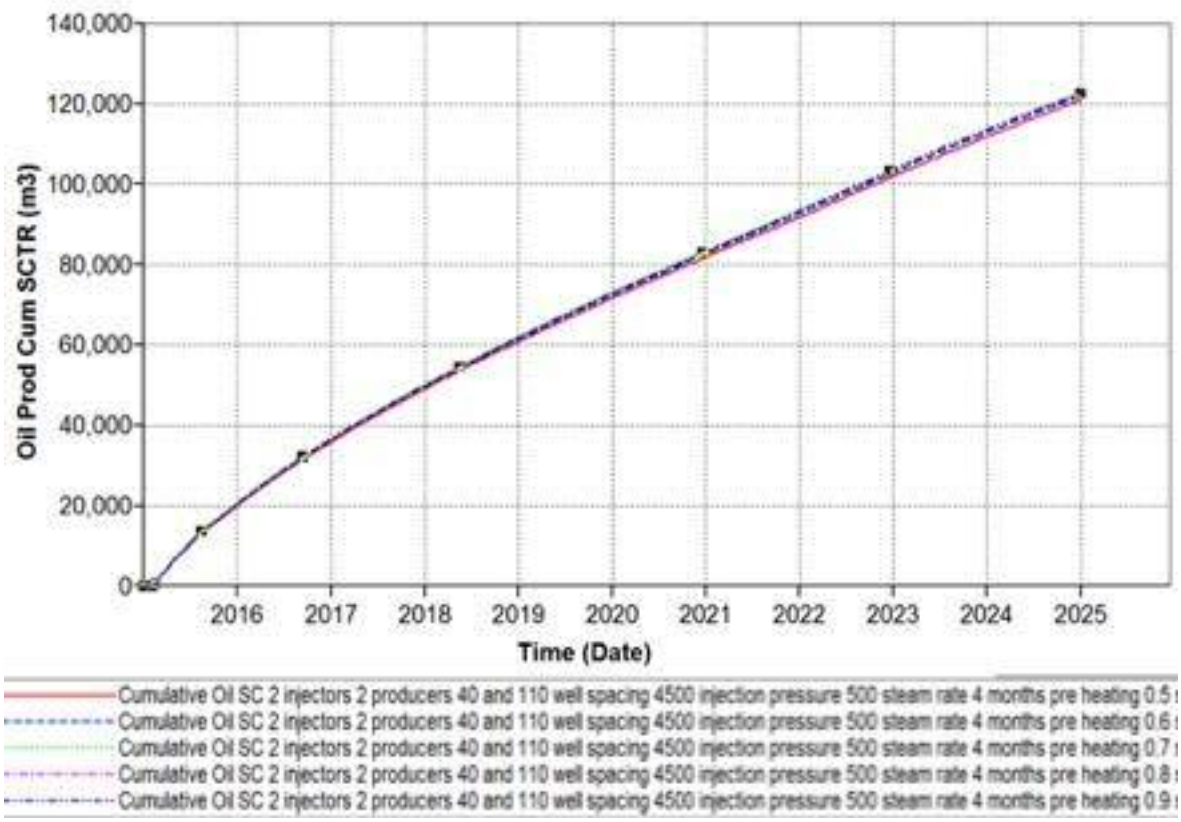


*Figure 5-4 Case 1 Steam quality sensitivity analysis for cumulative oil graph*

### 5.1.5 Case 1 Optimised Model

Case 1 simulation model is then run with aforementioned parameters of 4500 kPa for the injection pressure, 500 m³/day for the steam injection rate, 4 months for the pre-heating period and 0.9 for the steam quality. The resulting simulation is shown in

The models below show how the steam chamber spreads throughout the reservoir during stream injection. Figure 5-5 is at initial temperature conditions, Figure 5-6, Figure 5-7 and Figure 5-8 show the spread after 3, 6 and 10 years.

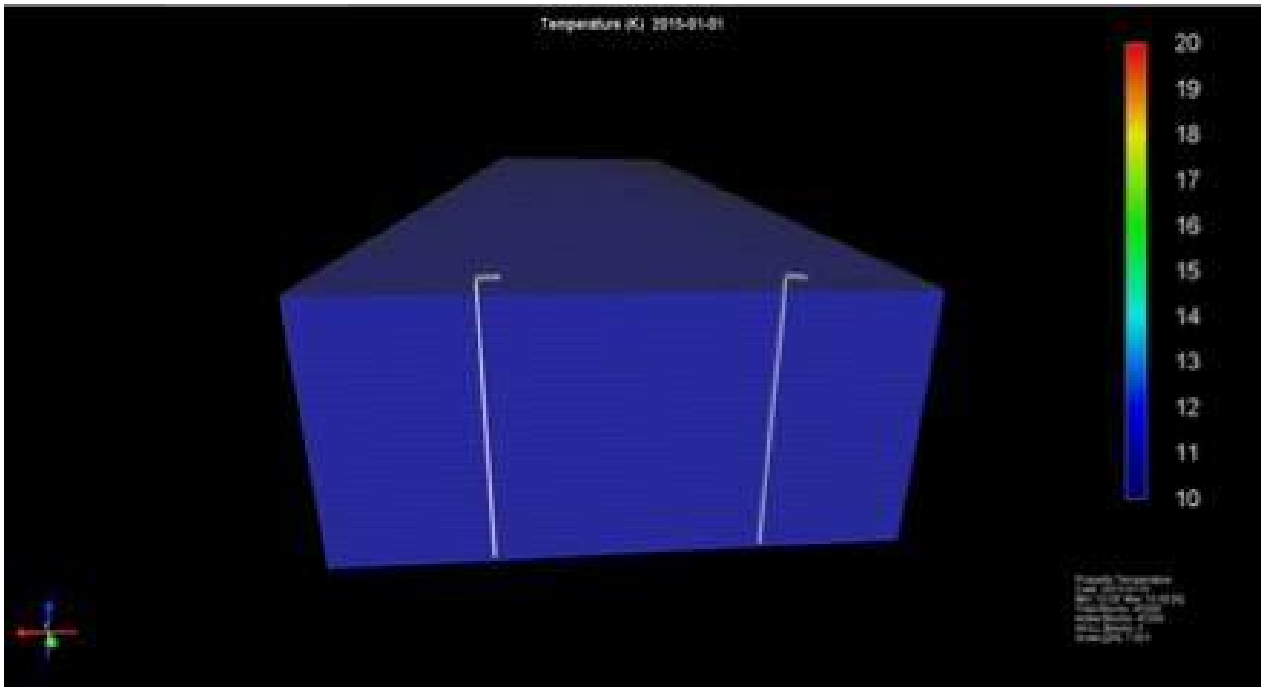


*Figure 5-5 Case 1 Steam chamber expansion initial conditions*

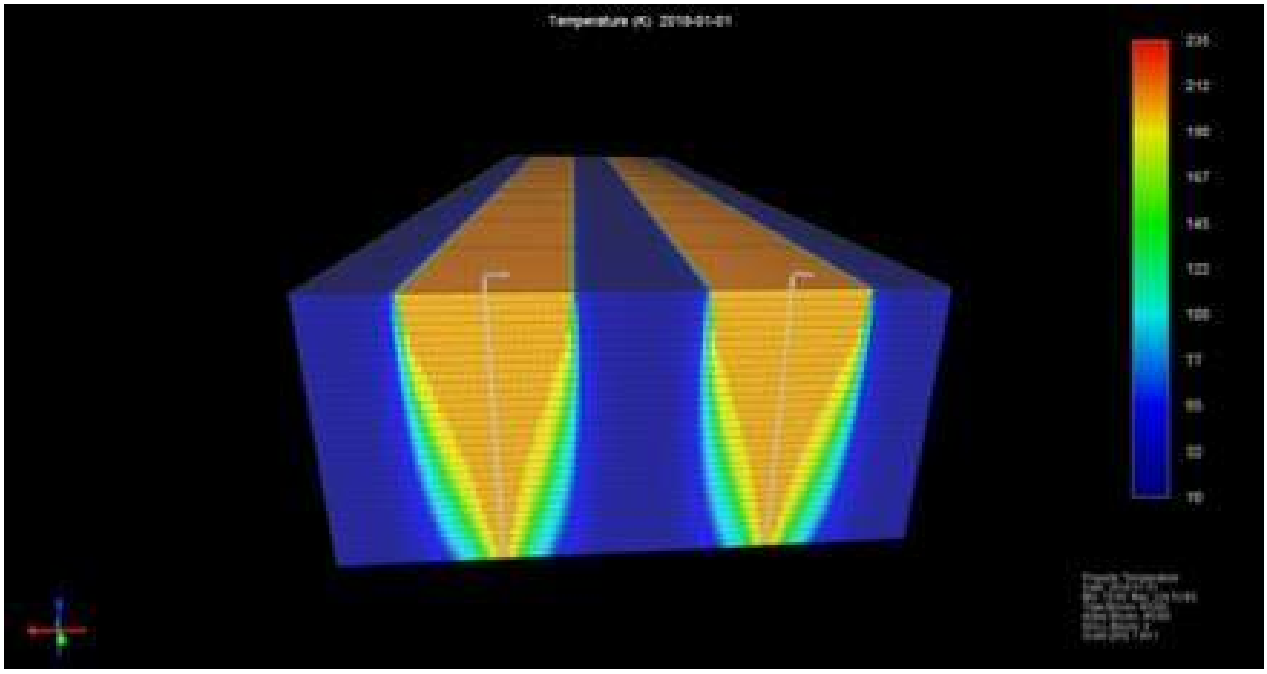


*Figure 5-6 Case 1 Steam chamber expansion after 3 years*

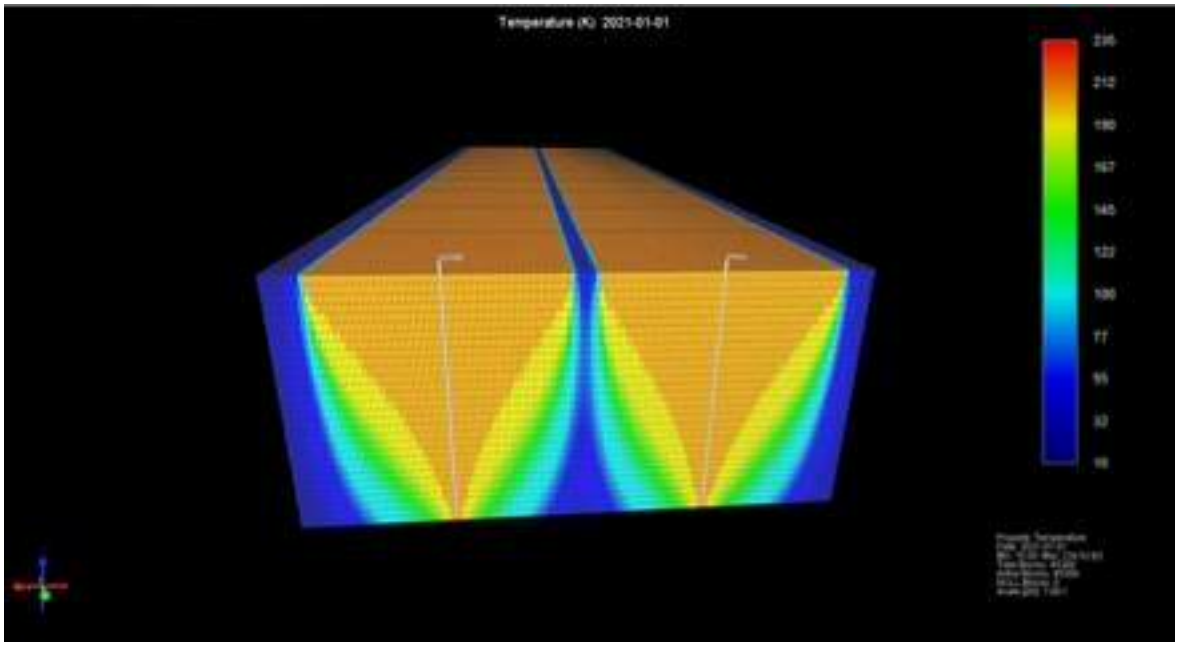


*Figure 5-7 Case 1 Steam chamber expansion after 6 years*

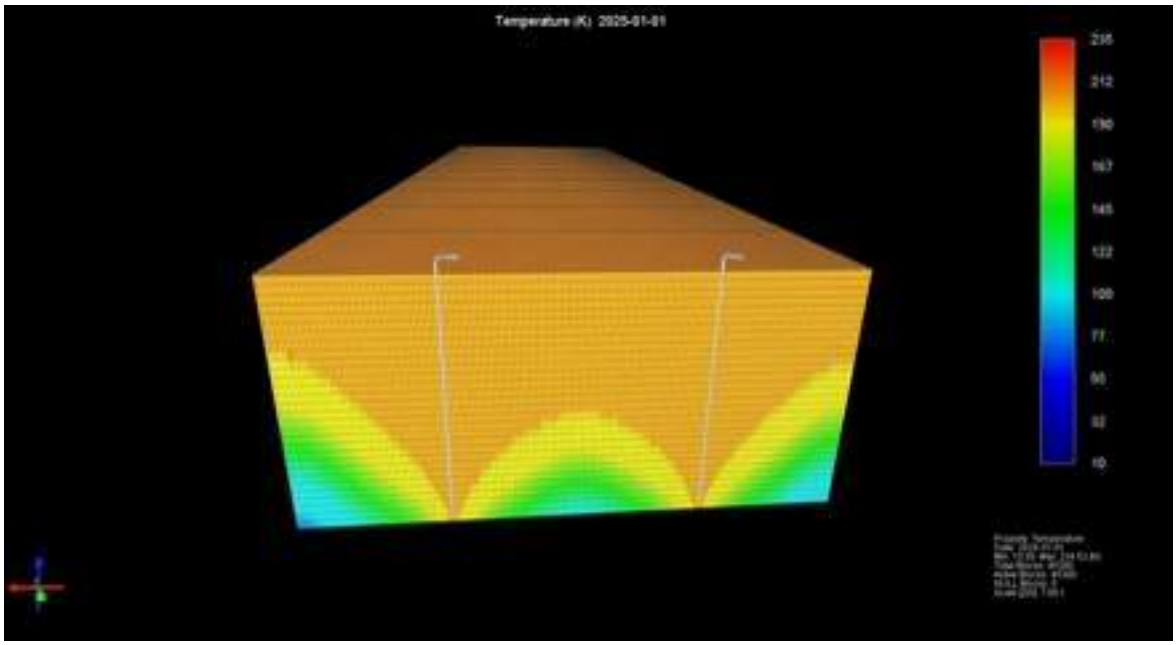


*Figure 5-8 Case 1 Steam chamber expansion after 10 years*

Figure 5-8 shows that the steam chamber (the orange area of the model) effectively reached the reservoir boundaries, although not completely sweeping the reservoir. The steams sweep efficiency in this instance can be classed as effective as most of the area of the reservoir has been heated, thus reducing the reservoir oil viscosity and enabling the production of the oil.

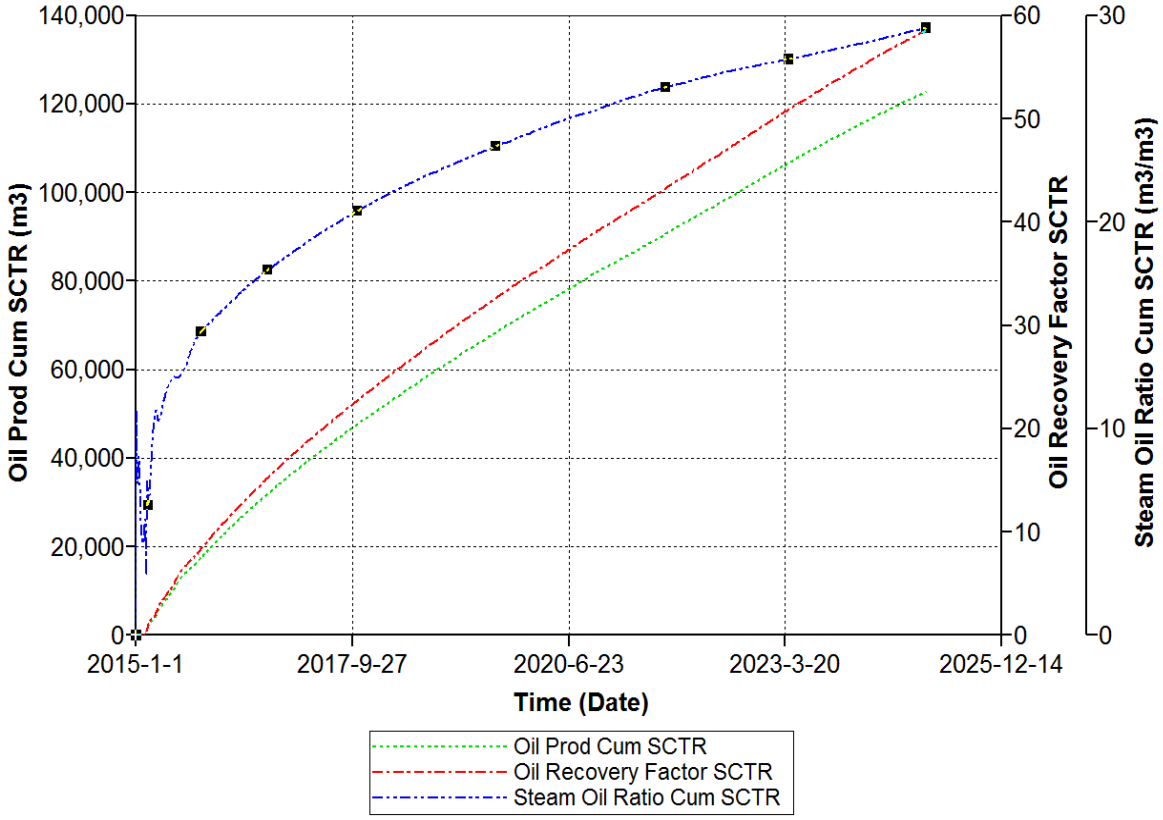


*Figure 5-9 Optimised Case 1 Model showing Cumulative oil production, recovery factor and steam oil ratio*

The graph in Figure 5-9 shows the comparative graph between Oil Production, Oil recovery factor and steam oil ration. Quantity wise a cumulative production from this field was achieved at 122,941.2 m³, with a recovery factor of 59% and a peak steam oil ratio 29 m³/m³. Even though, this recovery factor is at the top end of the potential for a SAGD project, it is most likely the result of the porosity and permeability being quite high. The SOR can be seen to give a value of about 29 m³/m³ which is not economical for production, however the maximum oil recovery is the aim of the study.

## 5.2 "Case 2": Property model with Dead Oil SAGD

### 5.2.1 Case 2 Steam Injection Pressure Sensitivity Analysis:

In 'Case 2' the porosity and permeability were changed in the three layers based on data obtained from Bell, Kulkarni, & Marge (2013) in Table 5-4. A sensitivity analysis was carried out on the same parameters as in 'Case 1', in order to investigate how the more accurate field data affected the cumulative production. As in 'Case 1' the injection pressure was varied from 2500 to 4500 kPa.

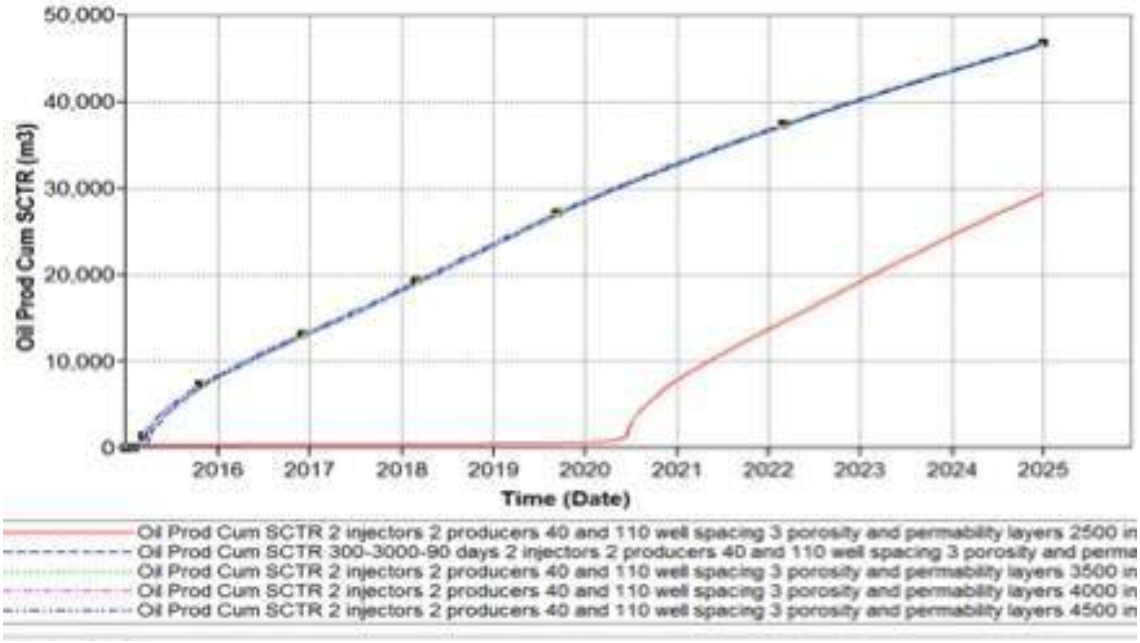


*Figure 5-10 Case 2 Injection pressure sensitivity analysis for cumulative oil graph*

*Table 5-4 Case 2 Injection pressure sensitivity analysis for cumulative oil values*

| Injection Pressure (kPa) | Cumulative Oil SC ($m^3$) |
|---|---|
| 2500 | 29,458.7 |
| 3000 | 46,628.8 |
| 3500 | 46,688.2 |
| 4000 | 46,776.6 |
| 4500 | 46,797.1 |

As seen in the Figure 5-10 there are some important variations that can be observed through this model. Firstly reduction in permeability has forced low pressure injection to start production at a later date compared to case 1, secondly, the defining data in case 2 has dropped the overall production almost by half as compared to case 1. This may be due to the presence of well-defined reservoir sections with lower reserves due to lower porosity and permeability values within three sections which is restricting the spread of steam front as well. Though injecting steam at pressures of 4500 kPa seems to have overcome the challenge and increased production.

### 5.2.2 Case 2 Steam Injection Rate Sensitivity Analysis:

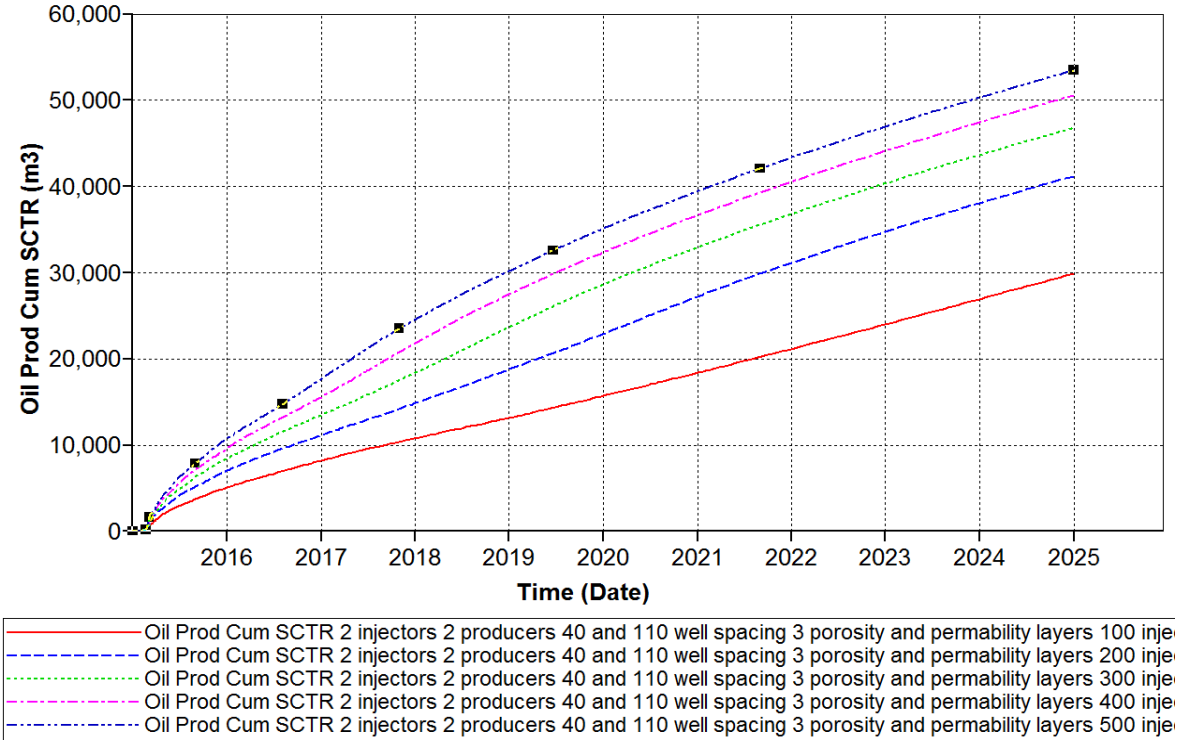


*Figure 5-11 Case 2 Injection rate sensitivity analysis graph for cumulative oil*

In 'Case 2', variation to the injection rate seems to have a much greater effect on the cumulative oil production compared to 'Case 1', as is evident from Figure 5-11 and Table 5-5. Although there is a greater spread of results the trend is still the same as in 'Case 1'. The highest production rate observed was 53,485 m³, at an injection rate of 500 m³/day. This is the same result as in 'Case 1' apart from the fact that it is lower probably due to the reduced permeability

*Table 5-5 Case 2 Injection rate sensitivity analysis for cumulative oil*

| Steam Injection Rate (m³/day) | Cumulative Oil SC (m³) |
|---|---|
| 100 | 29,906.1 |
| 200 | 41,206.8 |
| 300 | 46,797.1 |
| 400 | 50,581.7 |
| 500 | 53,485.0 |

### 5.2.3 Case 2 Pre Heating Period Sensitivity Analysis:

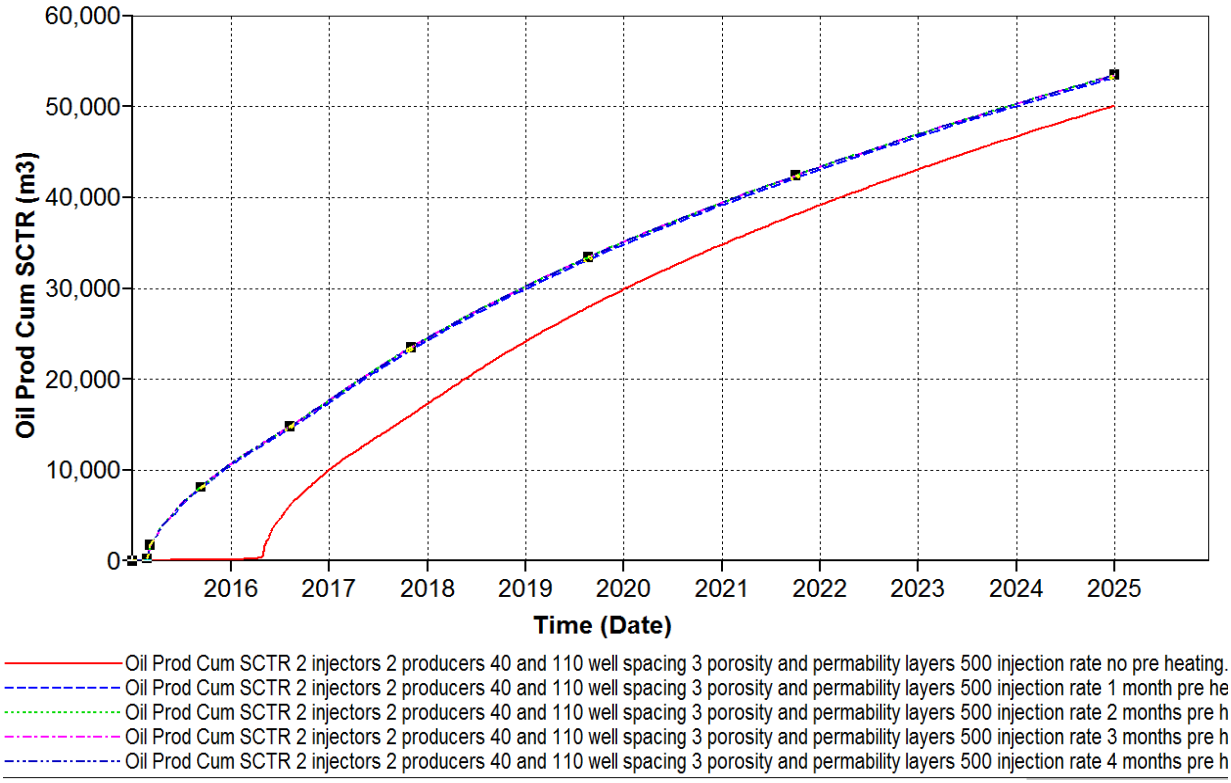


*Figure 5-12 Case 2 Pre heating period sensitivity analysis for cumulative oil production graph*

*Table 5-6 Case 2 Pre Heating Period sensitivity analysis for cumulative oil*

| Pre Heating Period (Months) | Cumulative Oil SC (m³) |
|---|---|
| No Pre Heating | 50,008.2 |
| 1 | 54,189.1 |
| 2 | 54,201.9 |
| 3 | 54,211.4 |
| 4 | 54,284.3 |

As can be observed from Figure 5-12 no pre heating caused the beginning of production to be delayed until just after 2016. This may be due to the fact that lack of preheating hindered steam fronts in advance delaying production. The rest of the cases showed no real significance apart from a pre heating period of 4 months producing over 70m³ more than the rest.

### 5.2.4 Case 2 Steam Quality Sensitivity Analysis

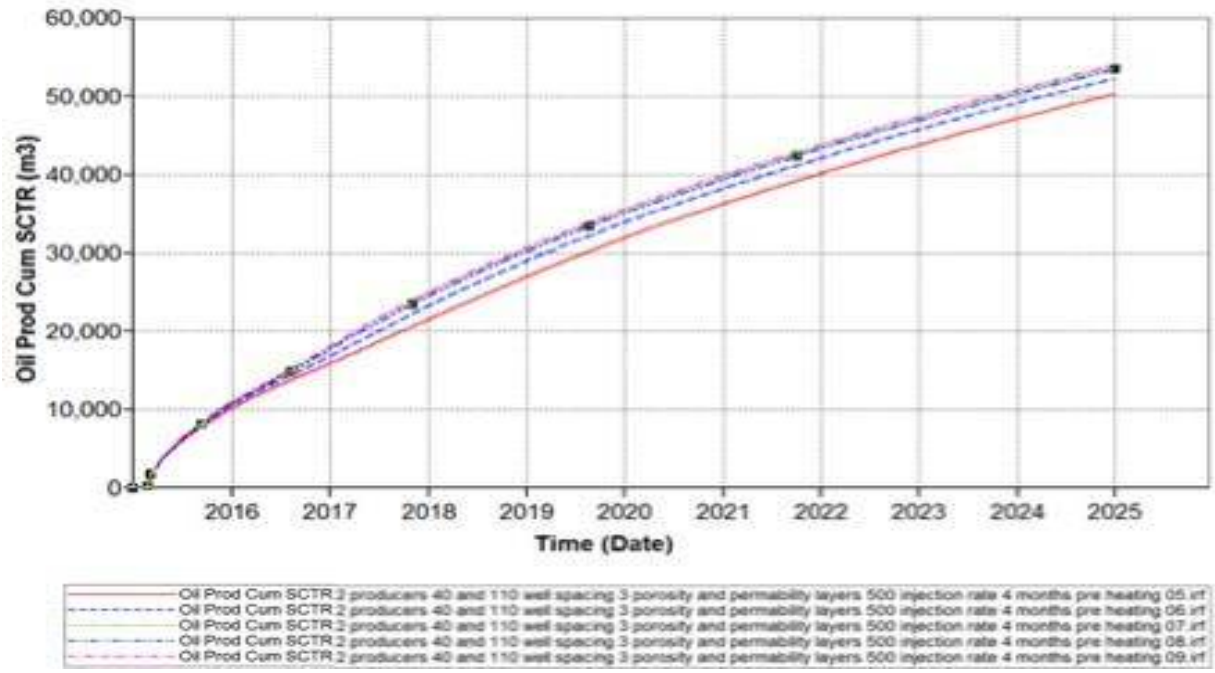


*Figure 5-13 Case 2 Steam Quality sensitivity analysis for cumulative oil production graph*

*Table 5-7 Case 2 Steam Quality sensitivity analysis for cumulative oil production*

| Steam Quality | Cumulative Oil SC ($m^3$) |
|---|---|
| 0.5 | 50,067.0 |
| 0.6 | 51,992,8 |
| 0.7 | 52,545.1 |
| 0.8 | 54,185.7 |
| 0.9 | 54,284.6 |

Considering steam quality we can observe the significant impact on production values from the reservoir. This is primarily due to the fact that with higher quality the steam is better able to transmit the heat to the reservoir fluid and mobilise a higher quantity of fluid. The optimum case of steam quality was 0.9, which resulted in a cumulative oil production of 54,284.6$m^3$. This result correlates with the steam quality in 'Case 1', again proving that the results are valid because of the correlation.

### 5.2.5 Case 2 Optimised Model

Case 2 optimised simulation model when run with simulation parameters of injection pressure at 4500 kPa, injection rate was 500 $m^3$/day, a 4 month pre heating period and 0.9 steam quality. Provided comparative results that can be seen from Figure 5-17. Though, consistency within parameters set for simulations means that both models can be compared with each other to observe variation within production that is brought about by inherent property change. This is a direct result of a well-defined finer reservoir model which will allow better analysis for any economic studies for this region.

Based on observations from Figure 5-14Figure 5-15Figure 5-16 The steam chamber in 'Case 2', has not spread to the reservoir boundary even after the 10 year period. Confirming that steam spread is slower even though the area surrounding the well is hotter as compared to case 1.

Case 1

Case 2

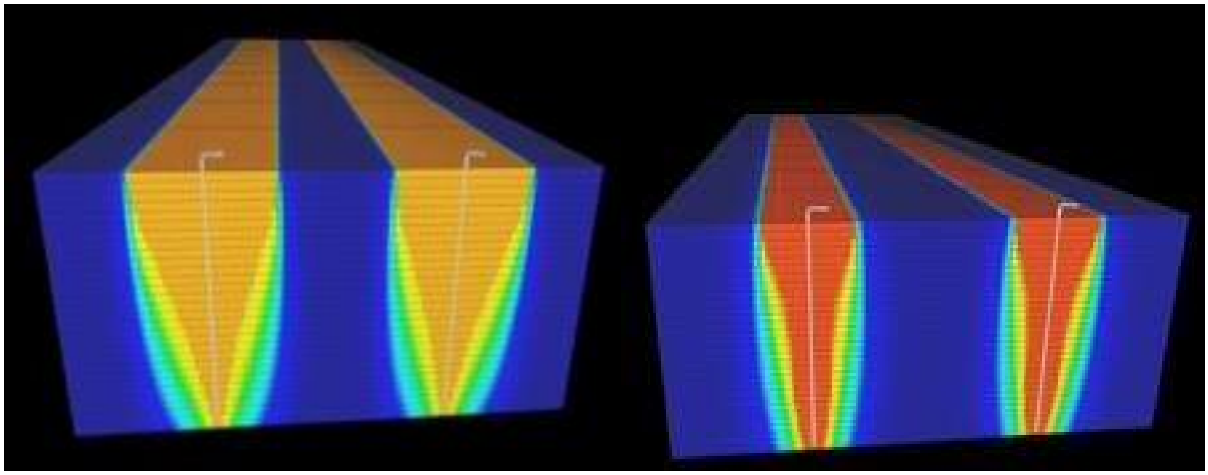

*Figure 5-14 Case 1 and 2 comparative steam chamber expansion in 3 years period*

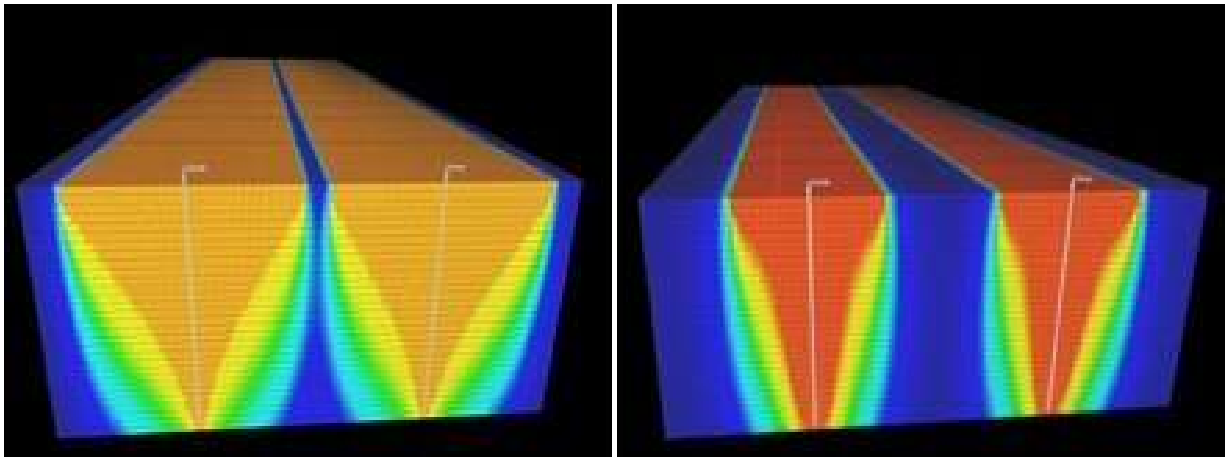

*Figure 5-15 Case 1 and 2 comparative steam chamber expansion in 3 years period*

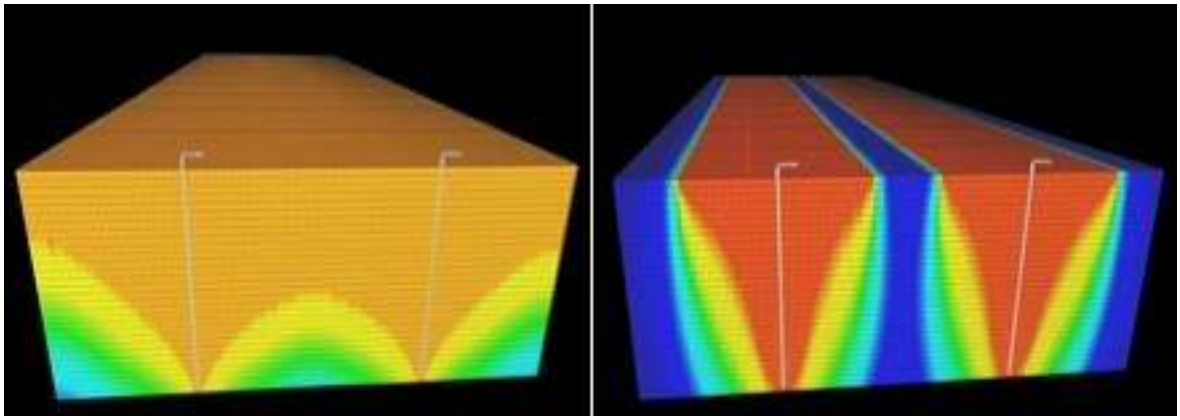

*Figure 5-16 Case 1 and 2 comparative steam chamber expansion in 3 years period*

This can be explained by the decreased permeability in the model, which causes the steam chamber not to spread as quickly through the reservoir so the heat is more concentrated around the well.

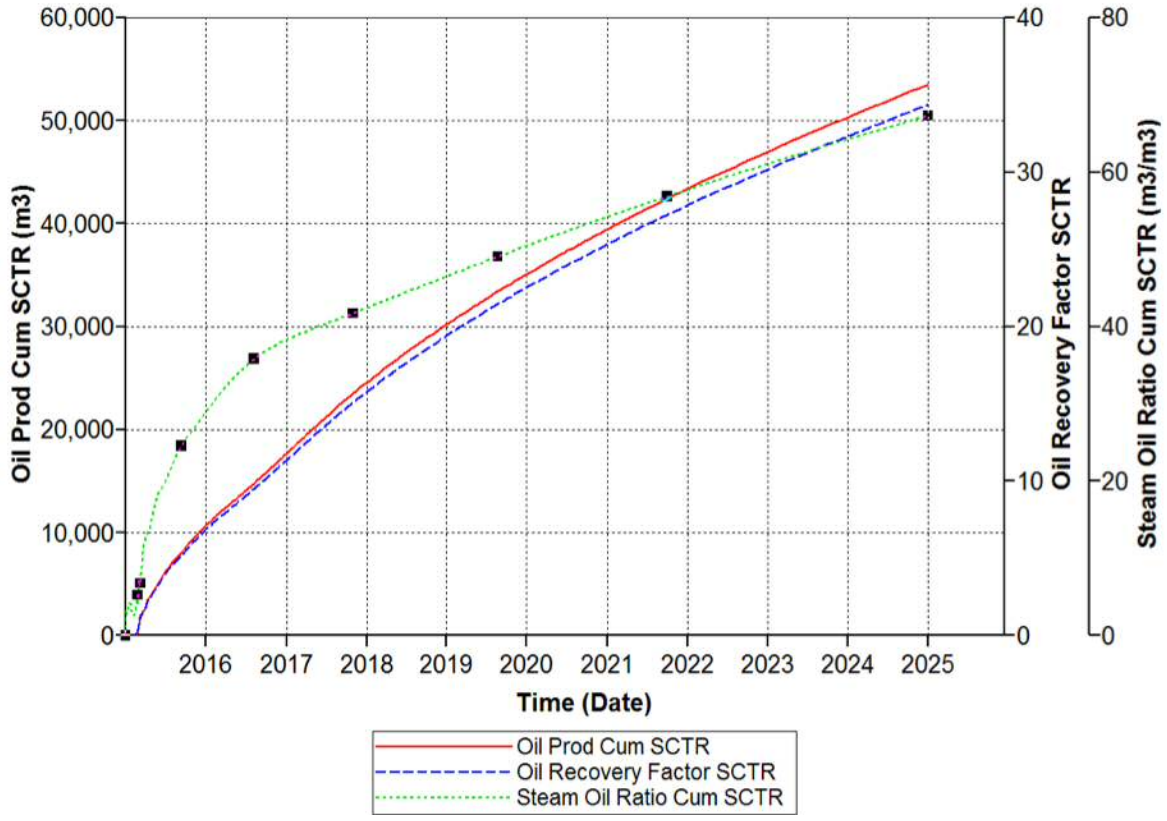


*Figure 5-17 Optimised Case 2 Model showing Cumulative oil production, recovery factor and steam oil ratio*

As seen in Figure 5-17 the total cumulative oil produced from 'Case 2' was 53,560 m³ which is around 50% lower compared to 'Case 1'. This is primarily caused by the reduction in the porosity and permeability, which makes it more difficult for the steam to spread through the reservoir, which reduces the contact of the steam to the oil and hence reduces production. This can also be observed from Figure 5-17 where the recovery factor has dropped from 59% to about 35%. The steam oil ratio in this case for one well peaked at 35 m³/m³ which was the most efficient amongst the models. In an area where a good water supply is available it is acceptable to have a higher SOR because it is not as expensive to acquire the water, whereas in an area with poor water supply a lower injection rate and steam quality may be considered to be more economical.

## 5.3 Case 3: Bioturbation models Dead Oil SAGD

For the 'Case 3' models, Bioturbation was added to see if this would affect the performance of the reservoir. A total of 5% bioturbation was added through all 10 layers of the model. The permeability and the porosity were both increased by 10% to take into account the bioturbation. As it can be observed from results in chapter four

Figure 4-14 and Figure 4-15**Error! Reference source not found.** which further needs to be modified to Table 4-11 as future work.

### 5.3.1 Case 3 Steam Injection Pressure Sensitivity Analysis:

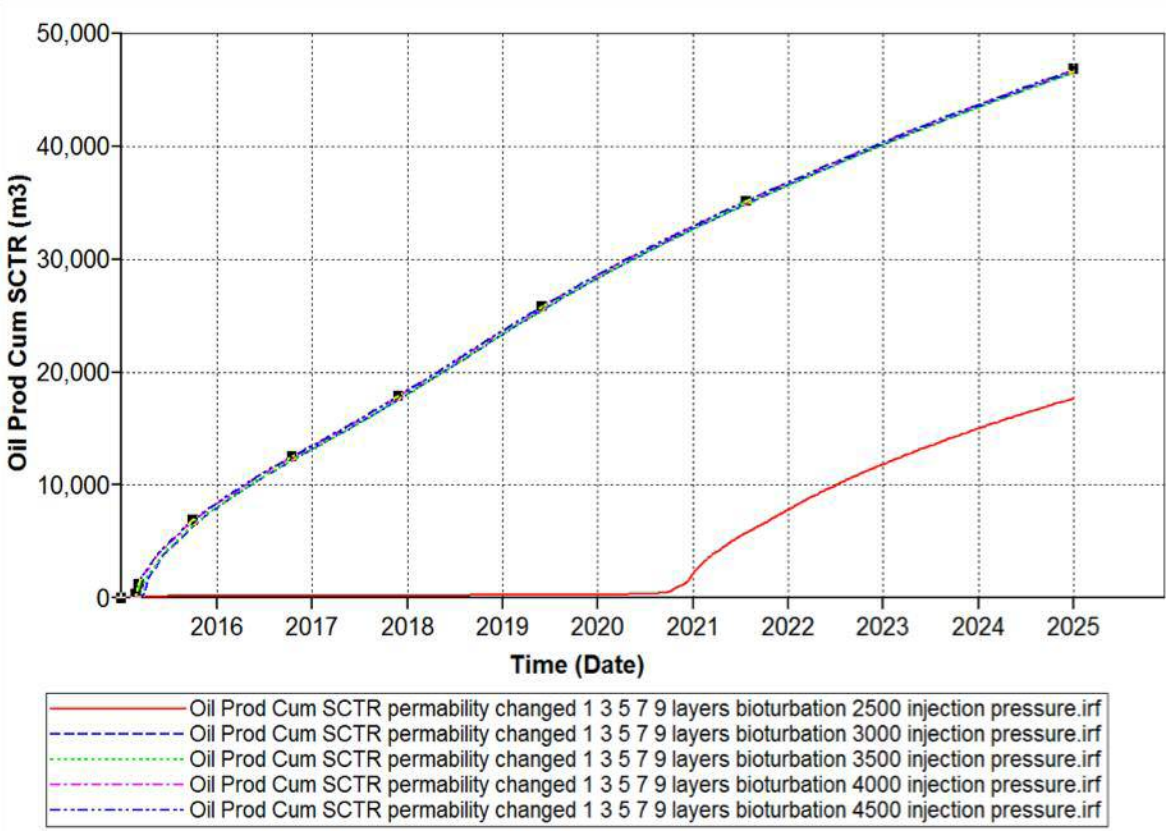


*Figure 5-18 Case 3 Injection pressure sensitivity analysis for cumulative oil graph*

In 'Case 3', the same general trend is shown for the cumulative oil production as in 'Case 2', with the 2500 kPa case only starting production just before the year 2021. This is caused by the lack of pressure for the steam chamber to propagate throughout the reservoir effectively. The bioturbation only slightly hinders the cumulative oil production as can be seen when comparing the cumulative oil produced from and Figure 5-26.

*Table 5-8 Case 3 Injection pressure sensitivity analysis for cumulative oil*

| Injection Pressure (kPa) | Cumulative Oil SC ($m^3$) |
|---|---|
| **2500** | 17,697.6 |
| **3000** | 46,614.9 |

| | |
|---|---|
| **3500** | 46,656.2 |
| **4000** | 46,756.7 |
| **4500** | 46,786.1 |

### 5.3.2 Case 3 Steam Injection Rate Sensitivity Analysis:

Injection rate was curiously studied as part of an optimisation process, as it was expected to have some effects on the overall production from the reservoir due to artificially generated high permeability channels within the reservoir.

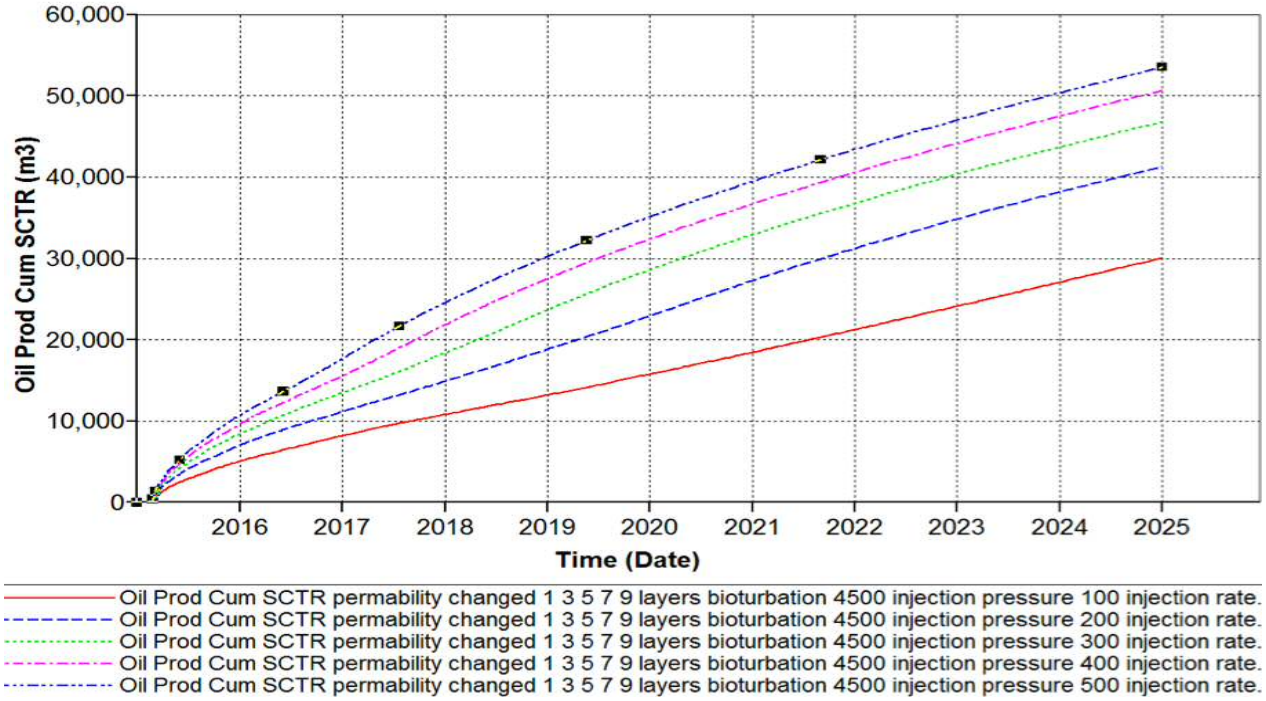


*Figure 5-19 Case 3 Injection rate sensitivity analysis graph for cumulative oil graph*

*Table 5-9 Case 3 Injection rate sensitivity analysis graph for cumulative oil*

| Steam Injection Rate ($m^3$/day) | Cumulative Oil SC ($m^3$) |
|---|---|
| 100 | 29,926.6 |

| | |
|---|---|
| 200 | 41,200.1 |
| 300 | 46,778.2 |
| 400 | 50,562.5 |
| 500 | 53,475.9 |

In ‘Case 3’, the injection rate produced almost identical results to the ones from ‘Case 2’. This proves that the injection rate along with other elements is one of the dominant parameters in the driving mechanisms in the reservoir. This is because even with an addition of the bioturbation, which from the sensitivity analysis on injection pressure can be seen to hinder the production, the cumulative oil rates are the same as in case. 2. Once again, an injection rate of 500m³/day produced the highest cumulative oil with a value of 53,475.9m³.

### 5.3.3 Case 3 Pre Heating Period Sensitivity Analysis:

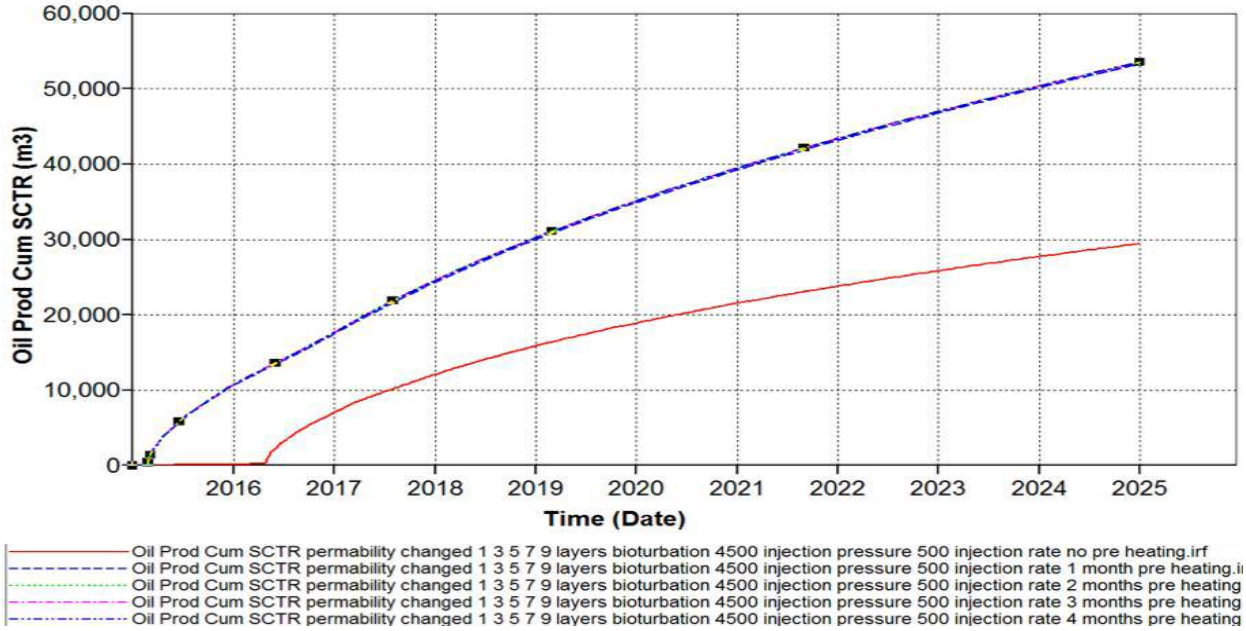


*Figure 5-20 Case 3 Pre heating period sensitivity analysis for cumulative oil production graph*

Similar to the injection rate the pre-heating period was expected to have an additional effect on the reservoir. This was primarily due to the higher permeability zones generated by bioturbation which may affect spread of heat through the reservoir.

*Table 5-10 Case 3 Pre heating period sensitivity analysis for cumulative oil production*

| Pre Heating Period (Months) | Cumulative Oil SC ($m^3$) |
|---|---|
| No Pre Heating | 29,910.5 |
| 1 | 54,158.1 |
| 2 | 54,191.6 |
| 3 | 54,209.9 |
| 4 | 54,275.0 |

Figure 5-20 shows the same principle trend as in 'Case 2', though with a drop in production for the no pre heating case because of the bioturbation. This may be providing a conduit for heat loss within the reservoir reducing an effectiveness of the steam front to spread through an entire reservoir. On the contrary, the presence of clays within these sections will create blockages to the steam spread and may also effectively reduce production from the reservoir.

### 5.3.4 Case 3 Steam Quality Sensitivity Analysis:

As can be seen from a graph in Figure 5-21 The results from the sensitivity analysis on 'Case 3', showed no significant difference to those produced from 'Case 2', apart from being marginally lower. This shows that the bioturbation in this model is not highly influenced by an improved steam quality. The bioturbation has consistently caused a lower result in production when compared with the results in 'Case 2' with no bioturbation.

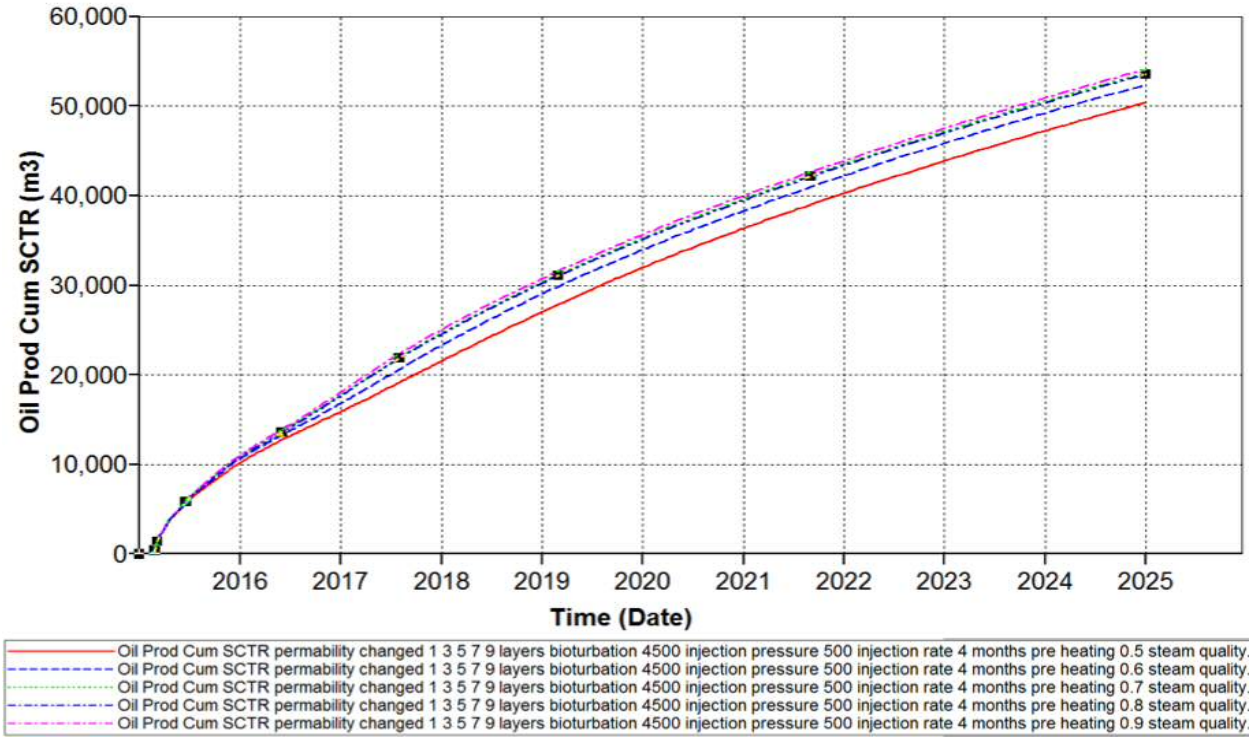


*Figure 5-21 Case 3 Steam Quality sensitivity analysis for cumulative oil production graph*

*Table 5-11 Case 3 Steam Quality sensitivity analysis for cumulative oil production*

| Steam Quality | Cumulative Oil SC (m³) |
|---|---|
| 0.5 | 50,068.1 |
| 0.6 | 51,896.6 |
| 0.7 | 52,976.0 |
| 0.8 | 53,122.9 |
| 0.9 | 53,479.5 |

### 5.3.5 Case 3 Optimised Model:

Similar to case 1 and case 2 optimised parameters of 4500 kPa, an injection rate of 500 m³/day, pre heating period of 4 months and a steam quality of 90% were applied

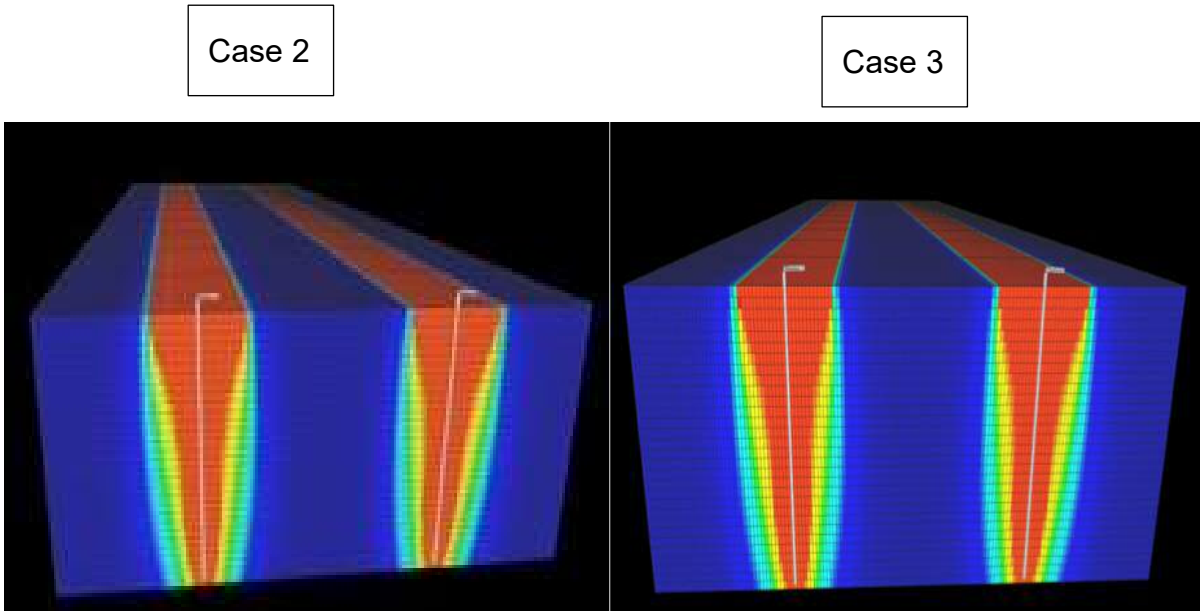


*Figure 5-22 Case 2 and Case 3 year 3 steam chamber expansion.*

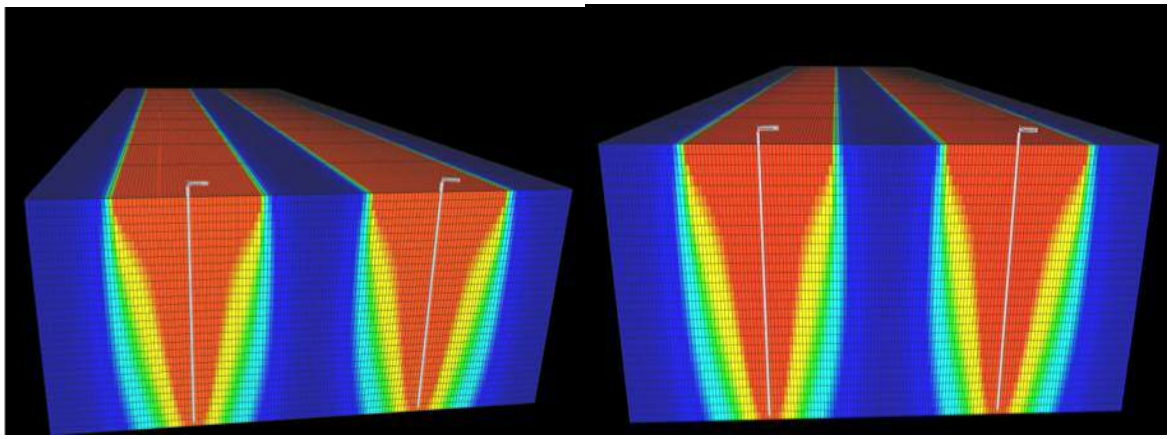

*Figure 5-23 Case 2 and Case 3 year 6 steam chamber expansion*

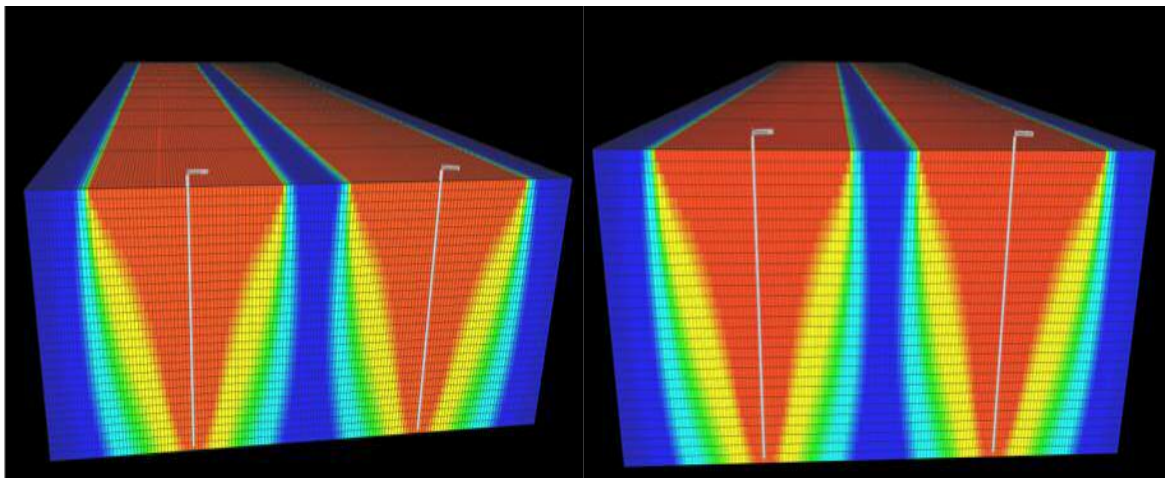

*Figure 5-24 Case 2 and Case 3 Year 10 Steam chamber expansion*

As may be seen from Figure 5-22,Figure 5-23 and Figure 5-24 case 2 and case 3 does not show significant difference to the production for an optimised model though this could easily vary if the quantity of bioturbation varies within the reservoir. The

optimised model used an injection pressure of As can be seen from the comparison graph of ‘Case 2’ and ‘Case 3’ in Figure 5-25 the bioturbation has very little effect on the production of the reservoir. From a numerical perspective ‘Case 2’ produced a cumulative oil total of 53,560 m³, whereas ‘Case 3’ produced a slightly lower total of 53,479.5 m³. This proves bioturbation hinders production in a reservoir even though the individual sections of bioturbated matrix have a higher porosity and permeability. This result confirms an earlier statement that bioturbation acts as a non-productive zone causing the slight drop in production either due to the escape of steam or due to the generation of impermeable sections within the reservoir.

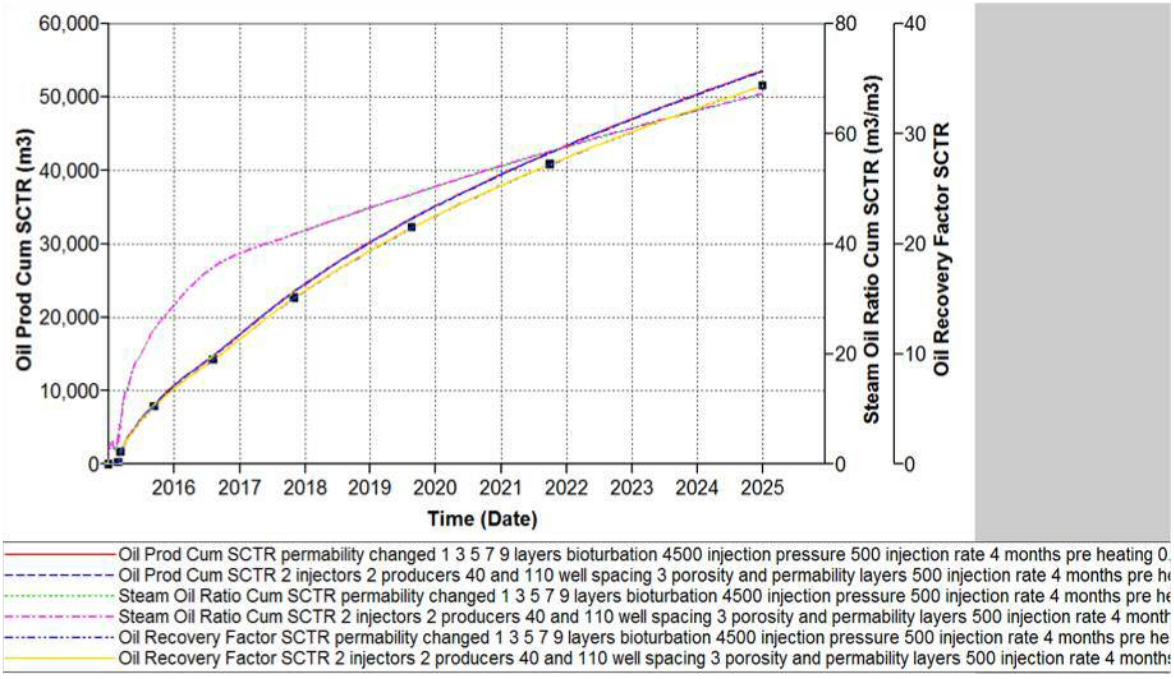


*Figure 5-25 Optimised Case 2/3 Model showing Cumulative oil production, recovery factor and steam oil ratio*

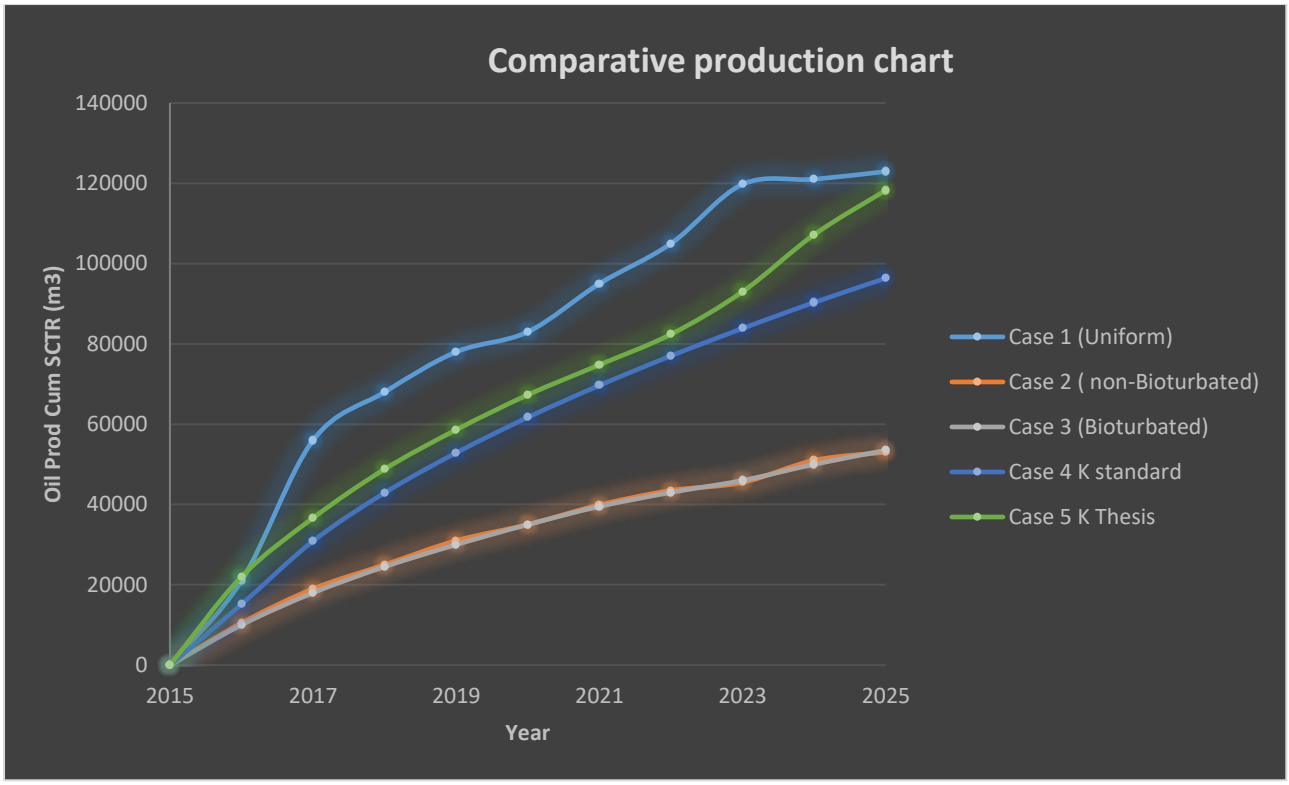


*Figure 5-26 Comparative production amongst three cases developed*

Figure 5-26 shows comparative cases run for the simulation work performed based on the data obtained through this thesis. Wherein, Case 1 is Shin and Polikar model, Case 2 (non-Biotubated) is on the basis of porosity and permeability determined through 2D image analysis, Case 3 (Bioturbated) simulation based on 2D bioturbation analysis in addition to porosity and permeability, Case 4 K standard represents 3D porosity and permeability demonstrated in Table 4-11 and finally Case 5 is 3D micro-CT based porosity and 3D permeability demonstrated in Table 4-10.

As shown from the graph using generalised properties will over predict production which may lead to inaccurate economic analysis and on the other hand relying on 2D image analysis may also provide very conservative results introducing inaccuracies. Following a workflow and determining properties through a combination of methods as set forth in this thesis provides more reliable porosity and permeability allowing better prediction of an unconsolidated reservoir. Though considering that work conducted as part of this thesis does not take into account presence of clays, it is likely that porosity and permeability values may decrease moderating simulation estimates observed.

# 6 Conclusion and Recommendations for future work

## 6.1 Concluding Remarks

This study was designed to 1. Perform a systematic investigation of an unconsolidated outcrop and reservoir samples. 2.Conduct a study following numerous methods of investigation namely: Thin Section Analysis, SEM analysis, micro-CT analysis followed by image analysis to understand applicability in an unconsolidated reservoir. 3.Based on the results obtained and applicability of aforementioned methods used to develop a workflow that could provide RCAL analysis with better reliability 4. Design and test geomodel against simulation studies published on Canadian Oil Sands reservoir.

## 6.2 Conclusion

1. Systematic investigation of an unconsolidated outcrop using thin sections is difficult as thin sections are difficult to develop. Though, the investigation of good thin sections revealed the effects of bioturbation on internal property variations within the sample.
2. Morphological properties could be determined confirming fining downward sequence, poor to moderate sorting, presence of clays and post depositional reworking & activity on few grains.
3. A systematic approach of following techniques set forth within objectives provided a useful workflow to investigate an unconsolidated reservoir and provide better accuracy results.
4. Geomodel designed and run with assistance of additional published data showed variation to the production depending on accuracy of property determination. Furthermore, effects of bioturbation could also be observed while analysing results from several runs.

## 6.3 Research Contribution

This thesis enhances knowledge on some of the issues faced while working with an unconsolidated reservoir samples. The outcome from this thesis demonstrates fundamental properties of the McMurray formation estuarine deposition and provides a reliable workflow which if applied carefully may provide more accurate results from an unconsolidated reservoir.

Looking at specific results obtained through methodologies followed within this research, Thin section preparation introduces a workable methodology which will provide usable thin sections of large size. The Image analysis provides an evidence of bioturbation and quantifies the variation within grain arrangements, porosity and permeability. As can be read through the results chapter, the entire process of thin section preparation and analysis thereof is presented. The initial study was able to provide interesting findings where arrangements within Canadian Oil Sands could be observed, showing mixed wettability and presence of bioturbation. Careful image analysis of selective workable thin sections quantified approximately at 10 % variation to the porosity within bioturbated region of thin section compared to the rest. The effect of bioturbation was further studied through simulation.

Considering a combined approach of SEM and micro-CT the analysis provided a means to determine grain morphology through multiple ways. This allowed verification of grain size distribution, roundness, weathering characteristics and post depositional activity that has taken place on this reservoir. The results show fining down sequence moderately to well-rounded grains with poor to moderate sorting index. Though care should be taken at this resolution, clays are not clearly distinguishable on 2D micro CT slices and neither could they be trapped during the soxhlet cleaning process. Heterogeneities have been observed within the cores studied. Furthermore, a weathering analysis has shown post depositional weathering and fracturing of grains as observed in Sample C.

The results point towards three different types of variations namely: poorly, moderately and well sorted for samples A,B and C.

- Fining downward trend was observed (from a comparison of the 3 different depths)
- Pre and post depositional weathering
- Porosity values of 29%, 23% and 26% for sample A, B and C respectively.

It is expected that the properties listed above and their variation will have a significant effect on the flow . The above observations and findings were published at various stages of this study. (Bell, Boateng, Olawale, & Roberts.D, 2011) (Bell J. , Kulkarni, Momoh, & Morris, 2015) (Bell, Eruteya, & Oono, 2012) (Bell J. K., 2013)

Aforementioned publications also allow me to say with confidence that host material governs the flow of fluids in the absence of a consolidating and/or cementing matrix). This will be further tested through reservoir simulation modelling.

The Micro CT section focused at determining grain morphology, Porosity and Permeability using 3D micro-CT analysis approach, samples were scanned at 5□m and were stacked to form a 3D representative image using a variety of software packages.

Considering the volume of data that was required to be constructed using the 3D imageJ software package, this was not successful. Hence, Drishti software package was utilised to reconstruct 3D. This software not only allowed to reconstruct them but also allowed the separation of two phases of grains and Oil from the core sample providing very useful visualisation.

The image stacks were then imported and analysed in Fiji (an ImageJ derivative) which provided meaningful information on grain sorting, packing, Tortuosity allowing me to calculate Porosity and Permeability of the sample following Van Barren's equation.

Porosity based on 3D analysis was observed to be 24%, 29% and 41% respectively.

Permeability of three samples using calculated values are 2693 mD ,15040mD and 37146md respectively for sample A, B and C

Permeability calculated from standard values are 1720mD, 4861mD and 26580mD respectively for sample A, B and C.

The variation to the properties could be the result of micro CT not being able to detect clay which results in lower grain volume in porosity and permeability determination.

Chapter 6 in this study talks about the development of the simulation model and comparing the results with already published work by Shin and Polikar. Properties obtained through this study were able to develop a simulation model though, additional properties such as relative permeability and oil composition for simulation.

The resulting simulation runs have shown significant variation to production depending on the properties considered and applied to the entire reservoir thickness.

The Property model and Bioturbation model, which used the more accurate porosity and permeability data obtained through SEM and micro CT, showed that the heterogeneities of the models resulted in decline of the cumulative oil production and the recovery factors.

Bioturbation has proved to inhibit production of a reservoir but only by 0.4% in terms of the recovery factor. This shows the disturbance by the organisms creating the bioturbation results in non-productive channels because of the bound clay in those regions.

Negative bioturbation in most cases hinders production and the recovery factor, with positive bioturbation in most cases improving production, and the recovery factor.

A higher steam temperature doesn't necessarily always result in a higher production, due to higher heat losses, resulting in a lower average reservoir temperature.

The average difference from the lowest bioturbation case to the highest, with the same parameters, caused an average difference in the recovery factor of around 0.35%, which equates to around a 1% difference, with this equating to a difference in cumulative oil of up to 2,200 m^3.

Overall this research will provide a means to significantly improve the modelling of unconsolidated Canadian Oil Sands reservoir modelling. Additionally, it further emphasises the importance of the fabric and its control on the production from the reservoirs in this region.

## 6.4 Future Work Recommendations

- To improve statistical validation this work should be repeated on more core samples.
- Clays play an important role in heterogeneities within reservoir especially where water/steam is used as a primary method of recovery. As certain clays have a tendency to swell once they are in contact with water. A detailed analysis of clays through X-ray diffraction studies will provide a means of identifying clay elements within these cores.
- Bioturbation may occur in a variety of ways, sometimes by occupying spaces within a sedimentary environment and other times by creating burrows and

pathways within sedimentary formation. A thorough study will assist in the identification of either types so that it could ultimately be replicated within reservoir simulation studies.

- To further the micro CT approach on an unconventional reservoir a detailed pore network model should be developed. This shall assist in quantifying void spaces within the reservoir. Furthermore, for Canadian Oil Sands it will enhance the understanding of heterogeneities and internal structure for McMurray formation where bitumen acts as a cementing matrix.
- A combined simulation development with understanding of clays, bioturbation and pore network modelling will provide an improved reservoir model to quantify production from this region.

# 7 References


Adams, J., Rostron, B., & Mendoza, C. (2004). Coupled fluid flow, heat and mass transport and erosion in the Alberta basin: Implication for the origin of the Athabasca oil sands. *Canadian Journal of Earth Science, 41*, 1077-1095.

Al-Bazzaz, W. H., & Al-Mehanna, Y. W. (2007). Porosity, Permeability and MHR Calculations Using SEM and Thin Section Images for Characterizing Complex Mauddud-Burgan Carbonate Reservoir. Paper Presented At the SPE Asia Pacific Oil And Gas Conference And Exhibition, Jakarta Indonesia. *Asia Pacific Oil and Gas Conference and Exhibition, 30 October-1 November 2007, Jakarta, Indonesia.* Jakarta: Society of Petroleum Engineers.

American Petroleum Institute. (1998). Recommended Practices for Core Analysis. Retrieved from http://w3.energistics.org/RP40/rp40.pdf

Aminu, M., & Kulkarni, K. (2015, April 7). *The influence of Grain Morphology on Reservoir Quality of Some Athabasca Oil Sands Samples.* Retrieved June 9, 2016, from Omicsgroup.org: http://www.omicsgroup.org/journals/the-influence-of-grain-morphology-on-reservoir-quality-of-some-athabasca-oilsands-samples-2329-6755-1000204.php?aid=54944

Aminu.M.D., & Kulkarni.K. (2015). *The Influence of Grain Morphology on Reservoir Quality of Some Athabasca Oil Sands Samples.* Creative Commons Attribution License.

Anfort, S., Bachu, S., & Bentley, L. (2001). Regional-scale hydrogeology of the Upper Devonian-Lower Cretaceous sedimentary succession southcentral Alberta basin, Canada. *AAPG Bulletin, 85*, 637-660.

Antonio, N., & Palacios Chun, A. (2014). *Assessment of Thermal Recovery: Steam Assisted Gravity Drainage (SAGD) to improve Recovery Effecienty in the Heavy- Oil Fields of the Peruvian Jungle.* Retrieved from Onepetro.org: https://www.onepetro.org/download/conference-paper/SPE-171108-MS?id=conference-paper%2FSPE-171108-MS

Ashrafi, M., Souraki, Y., & Torsaeter, O. (2012, October 14). Effect of Temperature on Athabasca Type Heavy Oil- Water Relative permeability curves in Glass Bead Packs. *Energy and Environment Research, 2*(2). doi:http://dx.doi.org/10.5539/eer.v2n2p113

Baker, H. (1976). Environmental sensitivity of submicroscopic surface textures on quartz sand grains – a statistical evaluation. *Journal of Sedimentary Petrology*(46), 871-880.

Bell, D. J., & Dawes, L. (2018, July 25). *Radipedia.org*. Retrieved from Ring Artifact: https://radiopaedia.org/articles/ring-artifact-1

Bell, J. K. (2013, November 14). *Novel Approach To Determining Unconsolidated Reservoir Properties: Fabric and Flow in Oil sands.* Retrieved November 14, 2013, from www.onepetro.org: http://www.onepetro.org/mslib/servlet/onepetropreview?id=SPE-168803-MS

Bell, J., Boateng, A., Olawale, O., & Roberts.D. (2011, October 24). *The Influence of Fabric Arrangement on Oil Sand Samples from the Estuarine Depositional Environment of the Upper McMurray Formation.* Milan: Search and Discovery *. Retrieved from http://www.searchanddiscovery.com/documents/2011/80197bell/ndx_bell.pdf

Bell, J., Eruteya, O., & Oono, O. (2012). Application of Petrographic Image Analysis and Multivariate Statistical Techniques for Textural Studies of Oil Sand Samples. Paper 80212 Presented At The AAPG Annual Conference And Exhibition, Long Beach California. [Online] Available At: Http://www.Searchanddiscovery.Com [Accessed On 28 August, 2013]. *Presented At The AAPG Annual Conference And Exhibition,.* Long Beach California.: AAPG, www.search and discovery.com. Retrieved Dec 20, 2012, from Http://www.searchanddiscovery.com

Bell, J., Kulkarni, K., & Marge , M. (2013). *Novel Approach to Determining Unconsolidated Reservoir Properties: Fabric and Flow in Oil Sands.* Denver: Unconventional Resources Technology Conference.

Bell, J., Kulkarni, K., Momoh, A., & Morris, L. (2015, June 3). Oil Sands Fabric: the Grain Component and Influences on Reservoir Properties. *Search and Discovery*. Denver, Colarado, United States: AAPG Search and Discovery.

Blott, S., & Pye, K. (2008, February). Particle shape: a review and new methods of characterization and classification. *55*, 31-63.

Bozzola, J., & Russell, L. (1998). Electron Microscopy. In J. Bozzola, L. Russell, & M. A. Jones (Ed.), *Electron Microscopy* (p. 670). Bartlett Publishers.

Brewer, R., & Sleeman, J. (1960). Soil Structure and Fabric : Their Definition and Description. *Journal of Soil Science*, 75-87.

Bull, P. ( 1978 ). A quantitative approach to scanning electron microscope analysis of cave sediments. In W. Whalley (Ed.), *Scanning Electron Microscopy in the Study of Sediments* (pp. 821-828). Norwich: Geobooks.

Bull, P., & Morgan, R. (2006). Sediment Fingerprints: A forensic technique using quartz sand grains. *Science & Justice, 46*, 107 – 124.

Butler, R. (1997). Thermal Recovery of Oil and Bitumen. In R. Butler, *Thermal Recovery of Oil and Bitumen* (p. 528).

Carrigy, M. (1959). Geology of McMurray Formation, pt. 3,General Geology of the Mcmurray Formation. *Research Council of Alberta Memoir, 1*, 130.

Chen, Q. (2009). Retrieved from https://pangea.stanford.edu/ERE/pdf/pereports/PhD/ChenQing09.pdf

Cheung, K. L. (2013). *SAGD Well Pair Spacing Evaluation with Consideration of Central Processing Facility Constraints.* Calgary: Society of Petroleum Engineers.

CMG. (2013). Modelling SAGD in STARS . *Tutorial for SAGD* . CMG.

Coskun, S. a. (1996, August). Image Analysis for Estimating Ultimate Oil Recovery Efficiency by Water flooding For Two Sandstone Reservoirs. *Journal Of Petroleum science and Engineering, 15*(2-4), 237-250.

DeepwellOil. (2018, July 25). *Deep Well Oil -Oil Sand Recovery Technology.* Retrieved from http://www.deepwelloil.com/Oil%20Sands%20Recovery%20Technologies.pdf

Demianov, A., Dinariev., O., & Evseev., N. (2014). *Introduction to the density functional method in hydrodynamics.* Moscow: FIZMATLIT.

Diwan, U., & Kovscek, A. R. (1999). *An Analytical Model for Simulating Heavy-Oil Recovery by Cyclic Steam Injection Using Horizontal Wells.* U.S. Department of Energy, Bartlesville.

Dress, L., & Ulery, A. (2008). *Methods of soil Analysis - Part 5: Mineralogical Methods.* American Society of Agronomy.

Felipussi, S. C., & Roque, W. L. (2002). Identifying 3D Pores Connectivity from 2D Thin Section Image Analysis. *17th World Petroleum Congress.* Rio de Janeiro , Brazil: World Petroleum Congress.

FitzPatrick, E. (1984). *Micromorphology of soils.* New York, USA: Chapman & Hall.

Flach, P. (1984). Oil sand Geology-Athabasca deposit north . *Alberta Research Council Buletin, 46*, 31.

Folk, R. (1951). Stages of textural maturity in sedimentary rocks. *Journal of Sedimentary Petrology, 21*, 127-130.

Folk, R. (1966). *A review of Grain-Size Parameters* (Vol. 6). doi:https://doi.org/10.1111/j.1365-3091.1966.tb01572.x

Fowler, M., Stasiuk, L., & Hearn, M. (1999). Devonian hydrocarbon source rock and their derived oil in the western Canada Sedimentary Basin. *Bulletin of Canadian Petroleum Geology, 47*, 43-62.

Gingras, M., Maceachern, J. A., Dashtgard, S. E., Pemberton, G., & Rangers, M. (2016, September). The Significance of trace fossils in the McMurray Formation, Alberta, Canada. *Bulletin of Canadian Petroleum Geology, 64*, 233-250.

Government of Canada. (2015, May 15). *Oil Sands - Water Management*. (ISBN 978-0-660-02150-8) Retrieved May 2016, from Natural resource of Canada: https://www.nrcan.gc.ca/sites/www.nrcan.gc.ca/files/energy/pdf/oilsands-sablesbitumineux/14-0704%20Oil%20Sands%20-%20Water%20Management_e.pdf

Hein, F., Cotterill, D., & Rice, R. (2006). *Subsurface Geology of the Athabasca Wabiskaw-McMurray Succession: Lewis-Fort McMurray Area, Northeastern Alberta.* Alberta: Earth Science Report.

Hein.F, Langberg.W, & Kidston, C. (2001). *A comprehensive field guide for Facies Characterization of the Athabasca Oil Sands, Northeast Alberta.* Alberta Energy and Utilities Board, Alberta Geological Survey. Alberta: Alberta Energy and Utilities Board.

Higgs, R. (1979). Quartz grain surface features of Mesozoic- Cenozoic sands from the Labrador and Western Greenland continental margins. *Journal of Sedimentary Petrology*(49), 599-610.

Hilfer.R. (1991, July). Geometric and dielectric characterization of porous media. *PHY.Rev.B., 44*(1), 60-75.

Hossain, Z. (2011). Relative Permeability Prediction from Image Analysis of Thin Sections. *SPE EUROPEC/EAGE Annual Conference and Exhibition.* Vienna, Austria: Society of Petroleum Engineers.

Jardine, D. (1974). Cretacious Oil of Western Canada. *Canadian Society of Petroleum Geologist Memoir , 3*, 50-67.

Jongerius, A. a. (1963). *The preparation of mammoth-sized thin sections. .* Paper, Netherlands Soil Survey Institute, Wageningen., Netherlands Soil Survery Institute, Wageningen.

Kasper-Zubillaga, J., & Faustinos-Morales, R. (2007). Scanning electron microscopy análisis of quartz grains in desert and coastal dune sands (Altar Desert, NW Mexico). *Ciencias Marina, 11-22*(33).

Kiasari, H. H., Sola, S., & Naderif, A. (2010). Investigation On The Effect Of The Reservoir Variables And Operational Parameters On SAGD Performance. *Brazilian Journal Of Petroleum And Gas*. Retrieved 12 06, 2016

Krinsley, D. H., & Doornkamp, J. C. (1973). *Atlas of Quartz Sand Surface Texture.* London: Cambridge University Press .

Li, P., Chan, M. Y., & Froehlich, W. (2009). *Steam Injection Pressure and the SAGD Ramp-Up Process.*

Mahaney, W. (2002 ). In *Atlas of Sand Grain Surface Textures and Applications.* (p. 237). Oxford: Oxford University Press.

Masters, J. (1984). Lower Cretaceous oil and gas in WesternCanada. In masters J.A (ed.), Elmworth-case study of a deep basin gas field. *Association of Petroleum Geology Memoir, 38*, 1-33.

Mattax, C., McKinley, R., & Clothier, A. (1975, December 10). Core Analysis of Unconsolidated and Friable Sands. *Journal of Petroleum Technology, 27*(12), 1423-1432. Retrieved from http://www.pe.tamu.edu/wattenbarger/public_html/Selected_papers/--Geomechanics/SPE%2004986%20Mattax.pdf

Mazzullo, J., & Magenheimer, S. (1987). The original shape of quartz sand grains. *Sedimentary Petrology*, 57,479,487.

Mazzulo, J., Sims, D., & Cunningham., D. (1986). The effects of Eolian Sorting and Abrasion upon the shapes of fine quartz sand grains. *Sedimentary Petrology*, 56, 45, 56.

Mele.G, M. T. (2011, July 8-14). Pore characterization of oil sands by X-ray Micro-CT and 3D image analysis. Austin, Texas, USA.

Micro Photonics Inc. (2015, May 12). *How does amicro_CT scanner work?* Retrieved from https://www.microphotonics.com/how-does-a-microct-scanner-work/

Morrow, N., Huppler, J., & and Simmons, A. I. (1969). Porosity and Permeability of Unconsolidated, Upper Miocene Sands From Grain-Size Analysis. *Journal of Sedimentary Petrology 39 (1)*, 312-321.

Mortensen, J., Engstrøm.F, & Lind.I. (1998). The relation among porosity, permeability, and specific surface of chalk from the Gorm field, Danish North Sea:. *SPE Reservoir Evaluation & Engineering,, 1*(3), 245-251.

Moshier, S., & Waples, D. (1985). Quantitative Evaluation of Lower Cretaceous Mannville Group as source rock for Alberta's oil sands. *American Association of Petroleum Geologists Bulletin, 69*, 161-172.

Mossop, G. (1980). Geology of the Athabasca Oil Sand . *Science, 207*, 145-152.

Nanoscience Technology. (2018, July 24). *Nanoscience.com*. Retrieved from How an SEM works: https://www.nanoscience.com/technology/sem-technology/how-sem-works/

Nejad, K. S., Berg, E., & Ringen, J. (2011). Effect of Oil Viscosity on Water/Oil Relative permeability. *International Symposium of the Society of Core Analyst .* Austin. Retrieved July 23, 2018, from http://jgmaas.com/SCA/2011/SCA2011-12.pdf

Nelson, P. (1994). Permeability-porosity relationships in sedimentary rocks. *The Log Analyst 35(3)*, 38-62.

Okhravi, R., & Amini, A. (2001). Characteristics and provenanace of the loess Deposits of the Gharatikan watershed on Northeast Iran . *Global and Planeary changes, 28*, 11, 22.

Oren, P., Bakke, S., & Arntzen, O. (1998, December). Extending Predictive Capabilities to Network Models . *SPE Journal, 3*(04).

Pasu, M., & Gautheyrou, J. (2006). *Handbook of Soil Analysis : Mineralogical, Organic and Inorganic Methods.* Netherlands: Springer.

Pemberton, S., Mossop, P., & Flach, G. (1982). Trace fossil from the Athabasca oil sand, Alberta, Canada. *Science, 217*, 825-827.

PetroWiki Porosity Vs Permeability for Morrow paper. (n.d.). Porosity Vs Permeability Corelation. PetroWiki. Retrieved July 23, 2018, from https://petrowiki.org/File:Vol1_Page_690_Image_0001.png#file

Plumely, W. (1948). Black Hills terrace gravels: A study of Sediment transport . *Journal of Geology , 48*, 526-577.

Pye, K., & Mazullo, J. (1994). Effect of tropical weatering on quartz Grain shape: an example from North Eaatern Austarlia. *Sedimentary Research*, 507.

Raymond, M. S., & Leffler, W. (2006). *Oil and Gas Production in Nontechnical Language.* (M. Patterson, & R. Hensley, Eds.) Tulsa, Oklahoma, USA: PennWell Corporation.

Reidiger, C., Fowler, M., & Snowdon, L. (1999). Origin and alteration of Lower Cretaceous Mannville Group oil from the Provost oil field east central Alberta, Canada. *Bulletin of Canadian Petroleum Geology , 47*, 43-62.

Richa, Mukerji, T., & Keehm, Y. (2006). Image Analysis And Pattern Recognition For Porosity Estimation From Thin Sections. *2006 SEG Annual Meeting, 1-6 October,.* New Orleans: Society of Exploration Geophysicists.

Romanova.U.G, Ma.T, Piwowar.M, Storm.R, & J., S. (2018, February 8). *Thermal Formation Damage and Relative Permeability of Oil Sands of the Lower Creataceous Formations in Western Canada.* Retrieved from One Petro.org: https://www.onepetro.org/download/conference-paper/SPE-174449-MS?id=conference-paper%2FSPE-174449-MS

Sarker, M., & Siddiqui, S. (2009). Advances in Micro-CT Based Evaluation of Reservoir Rocks. *SPE Saudi Arabia Section Technical Symposium and Exhibition* (pp. 2-9). Alkhobar: Society of Petroleum Engineers .

Shafer.J, M, G., J, R., D, R., Pairoys.F, T, B., . . . Longo.J. (2013, December). Recent Advances in Core Analysis. *Society of Petrophysicists and Well- Log Analysts, 54(6)*, 554-579. (S. John, Ed., & onepetro.org, Compiler) onepetro.org.

Shin, H. (2012). *A simple parameter to optomize SAGD operating conditions .* Incheon: Department of Energy Resources Engineering.

shin, H., & Polikar, M. (2005). Optimizing SAGD in three major canadian oil-sands areas. *ATCE .* Society of Petroleum Engineers.

Shin, H., & Polikar, M. (2005). Optimizing the SAGD Process in Three Major Canadian Oil-Sands Areas. *Annual Technical Conference and Exhibition.* Dallas, Texas: Society of Petroleum Engineers.

Solymar, I., & Fabricius.M. (1999). Image Analysis and Estimation of Porosity and Permeability of Arnager Greensand, Upper Cretaceous, Denmark. *Physics and Chemistry of the Earth., 24*(7), 587-591.

Souraki, Y., Ashrafi, M., Karimaie, H., & Torsaeter, O. (2012). *Experiemental Analyses of Athabasca Bitumen Properties and Field Scale Numerical Simulation Study of Effective Parameters on SAGD Performance.* Trondheim: Norwegian Unoversity of Science and Technology (NTNU).

Vigrass, L. (1968). Geology of Canadian Heavy oil Sands. *American Association of Petroleum Geologist Bulletin, 52*, 1984-1999.

Wang, J., Dong, M., & Asghari, K. (2006). Effect of Oil Viscosity on Heavy -Oil/ Water Relative Permeability Curves. *SPE/DOE Symposium on Improved Oil Recovery.* Tulsa: Society of Petroleum Engineers.

Washburn, E. (1921, February 12). Note on a method of determining the distribution of pore sizes in a porous material. *7*, 115. Retrieved July 23, 2018, from https://www.ncbi.nlm.nih.gov/pmc/articles/PMC1084764/pdf/pnas01901-0009.pdf

Weerakkody, Y., & Murphy, A. (2018, July 25). *Beam Hardening*. Retrieved from Radiopedia.org: https://radiopaedia.org/articles/beam-hardening

Wightman, D., & Pemberton, S. (1997). Lower Cretaceous (Aptian) McMurray Formation: an overview of the Fort McMurray area, northeastern Alberta. In Petroleum Geology of the Cretaceous Mannville Group, Western Canada. S.G Pemberton and D.P James (eds.). *Canadian Society of Petroleum Geologists, Memoir, 18*, 312-344.

Wightman, D., MacGillivray, J., McPhee, D., & Berezniuk, H. B. (1991). McMurray Formation and Wabiskaw Member (Clearwater Formation): regional perspectives dervied from north primrose area, Alberta, Canada. *fifth UNITAR International Conference on Heavy Crude and Tar Sand., 1*, 285-320.

Wright, G. N., McMechan, M. E., & Porter, D. E. (1994). Structure and achitecture of the Western Canada Sedimentary Basin. *Geological Atlas of the Western Canada Sedimentary Basin*.

X.Garcia, L.T., A., Martin, B. J., Matthai, Stephan, K., Latham, & John, P. (2009, August). Numerical study of the effects of particle shape and polydispersity on permeability. *Phy. Rev.E., 80*(2), 021304.

Yuan, J.-Y., & McFarlane, R. (2009). Evaluation of Steam Circulation Strategies for SAGD start-up. *Canadian International Confernce .* calgary .

Zainudin, B. W., S., W. N., Md Zain, Z., & Riepe, L. (2014). Application of Digital Core Analysis (DCA) and Pore Network Modeling (PNM) Based on 3D Micro-CT Images for an EOR Project in a Mature Oil Field in East Malaysia. *Offshore Technology Conference.* Kuala Lumpur.

# FORM UPR16

## Research Ethics Review Checklist

**Please include this completed form as an appendix to your thesis (see the Research Degrees Operational Handbook for more information**

UNIVERSITY OF PORTSMOUTH

| **Postgraduate Research Student (PGRS) Information** | | | | **Student ID:** | 836515 |
|---|---|---|---|---|---|
| **PGRS Name:** | Kanad Sadashiv Kulkarni | | | | |
| **Department:** | Technology | **First Supervisor:** | Dr. Mohamed Hassan | | |
| **Start Date:** (or progression date for Prof Doc students) | **21/10/2016** | | | | |
| **Study Mode and Route:** | Part-time ☒ | MPhil ☐ | MD ☐ | | |
| | Full-time ☐ | PhD ☒ | Professional Doctorate ☐ | | |

| | |
|---|---|
| **Title of Thesis:** | Reservoir quality determinationa nd modelling of unconsolidated Canadian Oil Sands reservoir following analytical techniques |
| **Thesis Word Count:** (excluding ancillary data) | 38443 |

If you are unsure about any of the following, please contact the local representative on your Faculty Ethics Committee for advice. Please note that it is your responsibility to follow the University's Ethics Policy and any relevant University, academic or professional guidelines in the conduct of your study

Although the Ethics Committee may have given your study a favourable opinion, the final responsibility for the ethical conduct of this work lies with the researcher(s).

**UKRIO Finished Research Checklist:**
(If you would like to know more about the checklist, please see your Faculty or Departmental Ethics Committee rep or see the online version of the full checklist at: http://www.ukrio.org/what-we-do/code-of-practice-for-research/)

| | |
|---|---|
| a) Have all of your research and findings been reported accurately, honestly and within a reasonable time frame? | YES ☒ NO ☐ |
| b) Have all contributions to knowledge been acknowledged? | YES ☒ NO ☐ |
| c) Have you complied with all agreements relating to intellectual property, publication and authorship? | YES ☒ NO ☐ |
| d) Has your research data been retained in a secure and accessible form and will it remain so for the required duration? | YES ☒ NO ☐ |
| e) Does your research comply with all legal, ethical, and contractual requirements? | YES ☒ NO ☐ |

**Candidate Statement:**

I have considered the ethical dimensions of the above named research project, and have successfully obtained the necessary ethical approval(s)

| | |
|---|---|
| **Ethical review number(s) from Faculty Ethics Committee (or from NRES/SCREC):** | 8CC0-948A-82D1-EFBB-FEED-8043-1B0B-009D |

If you have *not* submitted your work for ethical review, and/or you have answered 'No' to one or more of questions a) to e), please explain below why this is so:

| | | |
|---|---|---|
| **Signed *(PGRS)*:** |  | **Date:** 04/12/2018 |